Dissertation zur Erlangung des Doktorgrades der
Fakultät für Chemie und Pharmazie der
Ludwig-Maximilians-Universität München

Extruded lipid implants for intravitreal use – protein stability, release kinetics and process design

Moritz Vollrath

aus Erfurt, Deutschland

2017

Erklärung

Diese Dissertation wurde im Sinne von § 7 der Promotionsordnung vom 28. November 2011 von Frau PD Dr. habil. Julia Engert betreut.

Eidesstattliche Versicherung

Diese Dissertation wurde eigenständig und ohne unerlaubte Hilfe erarbeitet.

München, den 04.07.2017

Moritz Vollrath

Dissertation eingereicht am: 04.07.2017

1. Gutachter: PD Dr. habil. Julia Engert

2. Gutachter: Prof. Dr. Gerhard Winter

Mündliche Prüfung am: 28.07.2017

FOR ILONA

ACKNOWLEDGEMENTS

The present thesis was prepared between March 2013 and August 2016 at the Department of Pharmacy, Pharmaceutical Technology and Biopharmaceutics at the Ludwig-Maximilians-University in Munich under the supervision of PD Dr. habil. Julia Engert and Prof. Dr. Gerhard Winter.

First and foremost, I am deeply grateful to PD Dr. habil. Julia Engert for being my doctoral supervisor. I am grateful for her valuable scientific and personal support, the excellent guidance in the scientific daily routine and for all the helpful and fruitful discussions. Julia is gratefully thanked for always being available for direct contact of all research issues. The success of this thesis is closely connected with her person.

I would like to express my deepest gratitude to Prof. Dr. Gerhard Winter for being a member of his research group. During that time, he guided me through all phases of the PhD program with his excellent and continuous scientific input as well as personal advice. I want to highlight his ambition to support my scientific and my personal development. Moreover, he facilitated the contribution to several research conferences in Europe and the United States.

I have to thank Prof. Dr. Wolfgang Friess for all helpful and interesting discussions in the past years. Thank you for creating the pleasant working conditions together with Prof. Dr. Gerhard Winter in your labs.

I highly appreciate the collaboration with Dr. Balamurali Ambati and Randon Michael Burr from the Moran Eye Center (Salt Lake City, Utah, USA). I would like to thank them for supporting us with material and for performing the *in-vivo* study. Mike, thanks for the visit in Munich and all the fruitful discussions we had during this time.

Dr. Christoph Schmidt from the University of Ulm is thanked for the material support of mini-FH for the experimental work of this thesis.

Many thanks are expressed to my students Sophie Scholze, who did her bachelor thesis under my supervision, and my research scholar David Hernandez.

It is all about people. I warmly thank my lab mates Dr. Christian Neuhofer, Michaela Breitsamer and Weiwei Liu for the great and trustful time we had together in lab B1.029. I have to thank all my colleagues from the Winter and Friess labs for creating a comfort zone that enabled the productive working atmosphere. The social events and all other coming togethers were great fun. It is difficult to mention someone in particular, but I am most grateful to Randy Wanner, Kay Strüver, Dr. Matthias Lucke, Dr. Marie-Paule Even, Laura Engelke, Benjamin Werner, Katharina Geh, Leticia Rodiguez, Dr. Christoph Korpus, Simon Eisele, Corinna Dürr, Ellen Köpf, Ayla Tekbudak, Dr. Alexandra Partenhauser and last but not least Alice Hirschmann.

Thanks are extended to Coriolis Pharma for the possibility to use the XRPD. Dr. Riccardo Torosantucci is thanked for performing the iCE analysis for me.

I also want to thank Christian Minke for taking uncounted numbers of SEM micrographs and Dr. Jaroslava Obel for performing ICP-AES. Special thanks go to the entire team of the workshop who really did a great job in manufacturing our custom-made parts of the extruders.

I deeply thank my parents, my parents-in-law and my siblings Constanze and Florian as well as Michi and Johanna for the support they gave me over all the years and for simply being my family. Finally, I would like to thank my wife Ilona for her continuous encouragement, for her appreciative patience and for her love.

TABLE OF CONTENT

I. GENERAL INTRODUCTION

I.1 INTRODUCTION

Years of intensive research in pharmaceutical industry and academic have resulted in about 300 biotechnology products which are approved in the US, thereby covering 16 medical areas and about 250 indications [1, 2]. Most protein based drugs are used in therapy of serious diseases such as diabetes, cancer or autoimmune diseases [3]. Especially a combination with conventional low molecular weight drugs results in a better treatment compared to the administration of one single therapeutic protein drug [4].

The key obstacle of any drug delivery system - especially in delivering proteins - is accurately defined by van de Weert *et al.* [4]: «The main aim […] is to deliver the drug to the active site at the right time, at a therapeutically effective concentration, at the highest patient convenience/compliance, with the lowest possible side effects and at the lowest possible costs». The key to a successful protein formulation and its delivery is therefore the knowledge of chemical, physical and biological properties of the protein, including immunogenicity, stability and pharmacokinetic properties. For example, the chemical and physical stability is influenced by pH, ionic strength, temperature and surface interactions [5].

All these factors can be influenced by different formulation strategies. One may differentiate between formulation stabilisation using stabilisers or the direct modification of the protein structure. Stabilisation of proteins in the liquid and dry state (freeze-dried) is implemented using excipients, e.g. hydroxypropyl-beta-cyclodextrine (HP-β-CD) [6-8], sucrose [9-11], or by using surfactants. For instance, a well-known representative of this class are polysorbates [12-14]. Modifying the protein structure itself to improve its properties represents another strategy [5]. This includes the use of protein analogues with more promising properties, e.g. insulin lispro for type 2 diabetes or aldesleukin (IL-2 analogues) for therapy of renal cell carcinoma. Another approach is the attachment of fatty acids to the protein structure (acylation) which can increase

the half-life or the affinity to blood protein albumin. This principle has been applied for proteins like interferon-α [15] or desmopressin [16]. Likewise, the attachment of polyethylene glycol (PEGylation) or hydroxyethyl starch (HESylation) increases the half-life of proteins [5]. Additionally, these modifications improve the safety profile by shielding antigenic epitopes [17]. For example, a commercial product is PEG-interferon-α with an improved pharmacokinetic profile compared to native interferon-α [18]. To quote just one example, HESylation of Anakinra has been investigated by Liebner *et al.* [19, 20].

For protein and peptide based drugs, oral administration is still not possible (except for cyclosporine) since proteins and peptides are degraded by enzymes of the gastrointestinal tract, which results in poor bioavailability of the drugs [4, 21]. Furthermore, most proteins have a short half-life within the body due to hydrolysis and denaturation within the stomach. The intestinal mucosa of the small intestine is poorly permeable for larger molecules being an additional factor for poor bioavailability [22].

Alternative routes for protein administration have been studied such as buccal [23], rectal [24] nasal [25, 26], or pulmonary [27, 28] delivery. There is a need to develop a delivery system for proteins and peptides to the human body which show higher bioavailability and a longer half-life, which consequently results in lower doses and fewer side effects.

I.2 CONTROLLED PROTEIN DELIVERY

I.2.1 CURRENTLY MARKETED PEPTIDE AND PROTEIN DEPOTS

So far, parenteral application of pharmaceutical proteins and peptides is indispensable due to their instability in the gastrointestinal tract and/or bioavailability limitations. To circumvent these problems, parenteral application of protein drugs including subcutaneous injection and intravenous infusion is common practice. As most proteins exhibit short half-lives compared to small molecule drugs [29], frequent administration is required which is associated with high costs in the health care system [30]. Therefore, depots have been investigated for parenteral administration to minimise dosing frequency and improve patients' convenience.

In 1990, Zoladex® was approved, which is a depot system containing the peptide Goserelin, a gonadotropin releasing hormone (GnRH) super agonist for the treatment of prostate cancer and breast cancer [31]. Zoladex® is available as a one-month or three-months depot formulation and is formulated within a poly-lactic-co-glycolic acid (PLGA) and poly-lactic acid (PLA) matrix. The approval of Zoladex® was the initial impulse for other GnRH analoga formulated within a PLGA/PLA matrix: Lupron Depot®, which is composed of a microparticulate system (PLA and leuprorelin acetate), was approved in 1993 for the treatment of prostate cancer, endometriosis, fibroids, and central precocious puberty (CPP) for children [32-35]. Also, Profact Depot® containing a GnRH analogon (buserelin acetate) is formulated in a PLA/PLGA matrix. The *in-situ* forming depot Eligard® was launched in 2002 and contains leuprorelin acetate for treatment of prostate cancer [36, 37]. It is formulated in PLGA and N-methyl-2-pyrrolidon (NMP) and forms a depot once administered subcutaneously. So far, all depots described have in common that there are releasing peptides from a PLGA/PLA matrix.

Also formulated as an injectable suspension of PLGA microparticles is Nutropin Depot®, which represents the only marketed product delivering the protein drug somatropin, a recombinant human growth hormone. It was approved by the FDA in 1999 for the treatment of growth failure due to a lack of adequate endogenous GH secretion [38]. Nutropin Depot® was intended to

release somatropin over a period of one month, but was withdrawn in 2004 which was explained by «significant resources required by both companies (Alkmers Inc. and Genentech Inc.) to continue manufacturing and commercializing the product». Sandostatin LAR® represents a further depot based on PLGA microparticles for the treatment of acromegaly or tumors of the gastroenteropancreatic endocrine system. It contains octreotide acetate and is administered monthly.

In 2011, the last approved depot for sustained delivery of a peptide was Bydureon®, which represents a further development of Byetta® (approved in 2007). Bydureon® contains the glucagon-like-peptide-1 (GLP-1) analoga exenatide and is encapsulated within PLGA microspheres [39]. Bydureon® is administered once a week for the treatment of diabetes type 2 [40-42].

In summary, all marketed products in which a protein drug is encapsulated within a matrix (without further direct modification) are based on PLGA/PLA matrices. Protein drugs encapsulated within such depots are rather small, ranging from approximately 1.2 kDa for the GnRH analoga to up to 22 kDa for somatropin, meaning that depots for monoclonal antibodies or other protein formats are not yet commercially available.

I.2.2 MATRIX MATERIALS FOR CONTROLLED RELEASE OF PROTEINS AND PEPTIDES

For sustained release of peptides and proteins, a wide variety of matrix materials has been described in literature, including a broad variation of synthetic (HEMA, PVA, EVA, PLGA/PLA, PEG) and natural polymers (alginate, chitosan, silk, casein, zein, cellulose derivates, collagen, triglycerides, phospholipids, cholesterol) forming implants, gels, micro- and nanospheres or films. In the following, the most recently used materials are briefly described with a special focus on PLA/PLGA matrices as they represent the most commonly used material and had been used

within this study as well. Lipids have also been investigated as parenteral sustained release depots and will be discussed separately (I.2.3).

I.2.2.1 PLA/PLGA & PLGA COMPOSITES

Although PLA/PLGA can be categorised as synthetic materials (which will be discussed in I.2.2.3), this paragraph is dedicated due to its intensive use. This polymer had been approved by regulatory agencies and is the only one being in use for marketed products (described above). Thus, research groups along the globe have investigated this matrix since decades. Between 1998 and 2008, predominantly the preparation of PLGA based microparticles for the sustained release of model proteins like bovine serum albumin (BSA) [43] but also pharmaceutical proteins such as erythropoietin [44-46] human growth hormone [47, 48], insulin [49], insulin-like growth factor-I [50], or bone morphogenetic protein-2 (BMP-2) [51] have been described. PLGA based implants [52, 53] and *in-situ* forming gels [54, 55] have been investigated as well.

Along the preparation of PLGA based depots, the use of organic solvents is problematic in terms of protein stability as proteins tend to aggregate within a hydrophobic environment and at interfaces [56, 57]. The erosion of the matrix has negative effects on protein stability because degradation of PLA and PLGA results in an acidic microclimate, inducing a pH drop within the depot [58, 59]. Thus, chemical degradation, e.g. deamidation [60] and acylation [61], of the proteins has been observed.

To overcome these drawbacks, two strategies had been pursued: the addition of excipients or the modification of the matrix itself. To prevent protein degradation, excipients like PEG [62, 63], HP-β-CD [64] or basic salts [53, 65] have been added. The modification of the matrix has been followed since 2007 as more and more literature can be found describing PLA/PLGA-composites to overcome protein instability issues and to improve release kinetics. This includes conjugates with amino cyclodextrins [66], copolymers with monomethoxy-PEG [67], histidine [68], oligo(vinyl sulfadimethoxine) [69], or chitosan-graft-PLA micelles [70]. In addition, new

preparation methods like electrostatic adsorption of proteins onto PLGA nanoparticles have been investigated as described by Pakulska *et al.* [71] in 2016. Chang *et al.* investigated PLGA-triacetin depots for sustained release applications of a f_{ab}-fragment [72] reporting on a sustained release of 80 days.

In conclusion, it can be stated that PLGA based depots have been improved including both protein stability and release behaviour. Nevertheless, still major problems need to be addressed as protein instabilities [72] and incomplete release profiles [73] can still be found.

I.2.2.2 NATURAL POLYMERS

Natural polymers occur in nature and are often water-based. Examples of naturally occurring polymers are for example chitosan, collagen, silk, or cellulose.

Chitosan have been extensively investigated within the last 10 years. Especially the preparation of particulate systems is reported, for instance nanoparticles and microparticles [74, 75]. Chitosan based depots have been described for tissue engineering applications of bone and cartilage. Hou *et al.* and Zhang *et al.* investigated the controlled release of NEL-like molecule-1 (NELL-1) from chitosan nanoparticles [76] or chitosan/hydroxyapatite particles [76, 77] whereas BMP-6 was formulated within chitosan scaffolds [78]. In addition, the controlled release of insulin from chitosan microspheres [79], thermoresponsive chitosan hydrogels [80], chitosan-zinc copolymers [81], or chitosan composite hydrogels [82] has been described. However, chitosan has not yet been approved by regulatory agencies for parenteral applications.

Alginate based depots are a further representative of natural polymers. Especially in recent publications, alginate composites rather than pure alginate based depots have been described. As already reported for chitosan depots, bone remodeling applications represent the major research field for alginate based systems. For instance, NELL-1 was encapsulated into apatite coated alginate/chitosan microparticles and was delivered for up to 30 days [83]. A thermoresponsive chitosan/dextran-polylactide/glycerophosphate hydrogel and selected alginate microspheres for the controlled release of BMP-2 for up to 42 days has been described

by Zhu *et al.* [84]. Likewise, Zuo *et al.* reported on heparin-conjugated alginate microspheres for the delivery of basic fibroblast growth factor (bFGF) addressing bone remodeling [85]. However, about a broader possible use of alginate scaffolds for sustained protein delivery has been reported as well [86]. Despite the application orientated research, research is still on-going towards a fundamental understanding of the underlying interaction mechanisms between proteins and alginate matrices as reported by Schweizer *et al.* [87]. They observed that ionic interactions between polyanions of the matrix and monoclonal antibodies occur which can be exploited for sustained release delivery. In 2016, Bazban-Shotorbani *et al.* reported on a new technology to synthesise alginate nanogels with tunable pore size for controlled protein delivery [88].

Another representative of the class of natural polymers is collagen. In the early 1990s, Marks *et al.* has already reported on dermal wound healing applications using fibroblasts seeded onto collagen matrices [89]. More recently, collagen and collagen composites have been described for tissue engineering applications. For instance, Friess *et al.* investigated the delivery of BMP-2 from collagen sponges [90, 91]. The controlled release of BMP-2 from collagen fibers [92], collagen-hydroxyapatite scaffolds [93], and conjugated collagen scaffolds [94] have been utilised and show the potential of collagen in the field of bone regeneration.

Beyond the «classical» polymers used for controlled release applications, silk represents a new and promising natural polymer and has been extensively studied within the last years. It should be stated that silk based depots can be divided into recombinant spider silk based systems and systems containing of the silk from the cocoons of *Bombyx mori*. Recombinant spider silk particles have been described by Hofer *et al.* releasing lysozyme for up to 28 days [28]. Furthermore, recombinant spider silk was used to produce films for controlled release applications. Agostini *et al.* studied the release of BSA from differently coated spider silk films that could deliver the protein in a close to zero order kinetic for 90 days. The other type of silk can be extracted from the cocoons of *Bombyx mori* as described by Hayden *et al.* [95]. A broad variety of depots has been described using this type of silk including hydrogels for intraocular

delivery of Bevacizumab [96], the sustained release of cytokines from films [97] or systemic investigations on monoclonal antibody stabilisation by silk biomaterials [98].

I.2.2.3 SYNTHETIC POLYMERS

As an alternative to PLA/PLGA and natural polymers, synthetic materials have been studied as matrix material for controlled protein delivery.

Among others, this includes polyanhydrides comprising fatty acids and sebacic acid, thereby enabling better controllable polymer properties. Polyanhydrides have been already studied since the early 1990s for controlled protein applications using model proteins such as BSA, ovalbumin or lysozyme [99-101]. Still, further research needs to be carried out addressing the molecular structure descriptors which appear to have the greatest impact on the release kinetics in order to optimise release behaviour [102].

The class of poly(ε-caprolactone) (PCL) represents a further synthetic polymer. PCL is a widely-used polymer and has been approved by the FDA. It is a biocompatible and biodegradable polymer, which is non-toxic. PCL degradation does not create an acidic environment which could possibly negatively affect the integrity of encapsulated protein drug [103]. With PCL as matrix material, versatile depots can be produced including nanoparticles, fiber meshes or implants. For example, electrospun fiber meshes composed of PCL and polyethylene oxide (PEO) have been described for the controlled release of lysozyme for up to 300 hours. It was demonstrated that the initial burst can be reduced by adjusting the PCL/PEO ratio [104]. Within another publication, Rayaprolu *et al*. reported on BSA loaded PCL nanoparticles using D-α-tocopheryl polyethylene glycol 1000 as an emulsifier [105]. By this, a sustained BSA release of 5 days was achieved. Stanković *et al.* described long-term release of up to 170 days of various proteins and peptides including goserelin, lysozyme and carbonic anhydrase from hot melt extruded poly(ε-caprolactone-PEG)-*b*-poly(ε-caprolactone) multiblock-copolymer implants [106]. The structurally related polymer dihydroxyacetone-based poly(carbonate ester) has also been described for controlled release applications of BSA and lysozyme [107].

Beyond the already known and established polymers (EVA, PVA, polyanhydrides, PCL), more and more very specific and unique polymers can be found in literature. As an example, the use of trimethylopropane ethoxylated-ethyl 2-mercaptoproprionate (TMPE-TL) or trimethylo-propane ethoxylated ethyl thioglycolate (TMPE-TG) hydrogels has been described for the controlled delivery of bioactive horseradish peroxidase (HRP) for up to 16 days [108]. Furthermore, thermosensitive hydrogels consisting of multi-block Pluronic copolymers linked by lactide oligomers has been investigated delivering hGH over 13 days [109].

Generally, within the last few years, more and more sophisticated and highly complex release systems have been described in literature. This suggests that the «classical materials» have been replaced by completely new platform technologies or new composites with well-known materials. This opens entirely new research fields with innumerable possibilities. Just to name a few, within recent years it has been reported on glycidyl methacrylated dextran/gelatin hydrogel scaffolds [110], Diels-Alder hydrogels [111-113], nanogels made of hybrid hydroxyapatite nanoparticles with chitosan/polyacrylic acid [114], PEGylated fibrin gels [115], calcium phosphate based nanorods and nanowires for intracellular protein delivery [116], or photoactivated depots for the controlled release of insulin [117, 118].

It should be further mentioned that protein crystals for controlled release applications represent a very interesting and challenging research field at once [119-122].

I.2.3 LIPID VEHICLES FOR CONTROLLED RELEASE OF PROTEINS AND PEPTIDES

The Oxford Dictionary of Biochemistry and Molecular Biology defines lipids as biological substances that are generally hydrophobic in nature and in many cases soluble in organic solvents [123] such as fatty acids, phospholipids, sterols, sphingolipids, terpenes and others [124]. Other references divide this group of elements into different categories based on their chemistry, containing classes and subclasses of molecules, e.g. fatty acyls, glycerolipids, glycerophospholipids, sphingolipids, sterol lipids, prenol lipids, saccharolipids and polyketides

[125]. All definitions have one thing in common: lipids are predominantly hydrophobic but partly also have a hydrophilic component. Various types of lipids, many of them physiological substances such as triglycerides, cholesterol or phospholipids, have been investigated for lipid based implants [126].

As already mentioned before (I.1), oral application of proteins and peptides is in most cases not possible due to their degradation by the harsh conditions within the stomach and gastro-intestinal tract [21]. Thus, efforts have been made to explore alternative administration routes for protein drugs for lipid-based carriers covering the pulmonary, transdermal or parenteral route [127-130].

I.2.3.1 SOLID LIPID NANOPARTICLES

Solid lipid nanoparticles (SLNs) have attracted increasing attention as carrier for protein and peptide drugs. Mostly, SLNs are composed of physiological lipids, which make them an interesting alternative to synthetic polymers. Synthetic polymers have been used as common pharmaceutical excipient but also in food and cosmetic industry and thus considered to be save [131-133]. To prepare SLNs, the lipid raw material, emulsifier and water or solvent are needed. Commonly used lipids are triglycerides (e.g. Compritol® 888 ATO, Dynasan® 114), partial glycerides, steroids (cholesterol), fatty acids (trilaurin, trimyristin, tripalmitin), and waxes (cetyl palmitate) [134]. Various preparation methods are described in literature, e.g. ultrasonication, micro emulsion based technologies, solvent emulsification/evaporation, double emulsion methods, or spray drying methods. However, two main production techniques (high-pressure homogenisation and microemulsion-based techniques) are prevailed [135]. These techniques do not require potentially toxic organic solvents, which may also have deleterious effects on the protein drugs.

Since the early 1990s, SLNs have been used as drug delivery system (DDS) for proteins and peptides including topical, oral, pulmonary and parenteral administration routes [136]. The use

of this vector as depot for protein drugs has been addressed within several publications, e.g. for yak interferon-α [137], insulin [138], or human recombinant epidermal growth factor [139].

Within recent years, SLNs have gained more and more interest as DDS for peptides and nucleic acids. For instance, Sacchetti *et al.* described the use of SLNs to deliver the octapeptide LSCQLYQR for the treatment of resistant ovarian carcinoma. SLNs were formulated by a double emulsion method using stearic acid or Compritol® 888 ATO and different surfactants which resulted in SLNs being 130 nm to 1140 nm in size, all with a negative zeta potential [140]. However, SLNs showed substantial cytotoxic effect on ovarian carcinoma cells indicating that SLNs could carry efficiently the peptide to its target. In the course of an increased interest in the delivery of nucleic acids, SLNs have been used for RNA delivery [141]. For this purpose, usually cationic SLNs are needed due to the electrostatic interactions between negatively charged nucleic acids and positively charged lipids, which enables the formation of so-called lipoplexes [142-144]. As an example, it was demonstrated that cationic SLNs are capable to form complexes with DNA plasmids [143]. Jin *et al.* developed SLNs able to delivery siRNA to glioblastoma by overcoming the blood-brain-barrier with no apparent systemic toxicity [145]. Successful RNA delivery has also been described by Montana *et al.* using cationic SLNs as non-viral vectors for gene delivery [146]. Furthermore, lipid composites for nucleic acid delivery have been described as well [147, 148].

I.2.3.2 SOLID LIPID IMPLANTS

Within first publications describing solid lipid implants (SLIs) as DDS, SLIs were produced by compression or casting methods and were focused on fundamental questions, e.g. drug release mechanisms or solid-state behaviour of the lipids using exclusively small non-proteinaceous molecules. Then, model proteins have been encapsulated and *in-vitro* release behaviour was described followed by first *in-vivo* applications. Consequently, the composition of SLIs was optimised to prolong release periods ending up with the introduction of release modifiers, precipitating agents and pore formers. Compression as standard manufacturing technique was replaced by twin-screw (tsc)-extrusion, which has become the leading manufacturing technique

for SLIs so far. Applying tsc-extrusion to manufacture SLIs, research was carried out to prolong the release of proteins up to 240 days. Further, protein-lipid-interactions (which has been neglected up to now) has gained more and more interest because this aspect might play a major role in controlled protein release form lipid based DDS. Most recent, the field of possible applications was spread including vaccination, tumour therapy or intraocular applications.

This «evolution» of SLIs within the last 20 years will be spotlighted more in detail in the following section. At this point it should be briefly mentioned that quite a significant number on publications is available addressing the «fundamental research» in the field of SLIs. This includes dissolution aspects [149-152], mathematical modeling [153-156], elucidation of underlying release mechanisms [157-159], solid-state behaviour of triglycerides [160-163], or casting as preparation method [164-166]. However, since all these publications used small molecules as model drugs rather than proteins and peptides, they are not enclosed within the following text.

COMPRESSED SOLID LIPID IMPLANTS FOR PROTEIN AND PEPTIDE DELIVERY

Compression represents a very fast, easy and inexpensive manufacturing technique and was the method of choice in the early stages of SLI manufacturing. Versatile lipids have been used to prepare compressed SLIs by applying hydraulic presses. Direct compression has been used by different research groups for approximately 20 to 25 years for controlled release applications of proteins and peptides [126, 167-170].

In 1987, Wang *et al.* incorporated insulin in lipidic matrices consisting of different fatty acids, anhydrides of fatty acids, triglycerides and cholesterol [171]. SLIs were administered subcutaneously and controlled release of insulin was measured for approximately 1 month, as measured by the blood glucose level of diabetic Wistar rats. Moreover, the authors already reported on erosion of the SLI once administered subcutaneously, thereby already underlining the potential as biodegradable DDS [126].

On the sustained release of labelled BSA and hyaluronidase was reported by Vogelhuber *et al*. in 2003 using a compressed glycerol trimyristate matrix. *In-vitro* investigations revealed a high initial burst and incomplete protein release, which was explained by insufficient amounts of pore-forming agents. In addition to *in-vitro* testing, the implants were tested under *in-vivo* conditions by subcutaneous implantation in mice showing a good *in-vivo* stability after 15 days [170, 172].

The biocompatibility of lipid implants was addressed by Guse *et al.* [173] in 2006. The authors observed that a blend of glycerol tripalmitate with either lecithin or cholesterol showed good biocompatibility after subcutaneous implantation in mice while an increasing amount of lecithin led to increased inflammatory reactions at the site of administration. The incorporation of lecithin led to clearly visible signs of degradation which was not the case for cholesterol.

Also published in 2006, Appel *et al.* investigated insulin loaded implants with the background of cartilage engineering [169]. Lipid matrix cylinders with dimensions of 2 mm x 2 mm were manufactured from glycerol tripalmitate by compression without further additives. SLIs were loaded with different concentrations of insulin (0.2 % to 2 %) and the bioactivity of released insulin was measured for up to 4 weeks. The authors reported that the bioactivity of encapsulated and released insulin was preserved as the weights of cartilaginous cell-polymer constructs increased compared to the control [169].

Compression as manufacturing technique was also used for the controlled release of interleukin-18 (IL-18), reported by Koennings *et al.* [174]. A cell culture assay was established for the bioactivity determination of released IL-18 showing a continuous release of 10 ng to 100 ng IL-18 per day for up to 12 days. An incomplete release (< 35 %) of IL-18 from the matrices was explained by insufficient amounts of pore-forming agents (as stabiliser and pore forming agent, PEG was used). Furthermore, it was reported on an integrity loss with ongoing release, which would be related to protein degradation during incubation. Within a second publication, Koennings *et al.* addressed the sustained release of brain-derived neurotrophic factor (BDNF) with an additional focus on different manufacturing strategies [175]. Four different manufacturing techniques performed with the model protein lysozyme (all counting to

compression based approaches) were applied: (i) direct mixing of lyophilised lysozyme with lipid powder, (ii) a solid-in-oil dispersion of lyophilised lysozyme in tetrahydrofuran mixed with a solution of the triglycerides, (iii) a water-in-oil emulsion (the protein was dissolved in the aqueous phase and the lipid in dichloromethane), and (iv) a co-lyophilisation of lysozyme with PEG 6000 prior to compression. Slowest release was observed for more than 60 days applying the water-in-oil emulsion technique and the co-lyophilisation approach. Interestingly, the water-in-oil emulsion technique induced higher levels of aggregates, thus the co-lyophilisation technique was found to be most appropriate. Consequently, this technique was used for the preparation of BDNF loaded SLIs. *In-vitro* release studies revealed a sustained release of BDNF for up to 30 days, although total amount of released protein was only 60 % [175].

Starting in 2004 with the publication «Continuous release of rh-interferon a-2a from triglyceride matrices» by Mohl *et al.* [167], the research group of Prof. Winter addressed the topic of lipid based depots for controlled protein release. Mohl *et al.* described compressed SLIs consisting of glycerol tristearin, PEG 6000 and lyophilised rh-interferon α-2a. In contrast to Koennings *et al.*, Mohl *et al.* reported on an almost complete release of incorporated rh-interferon α-2a (more than 90 %) over a period of 1 month. The authors further stated, that the release rate was controlled by the amount of PEG 6000, which was added to the formulation acting as a pore-forming agent. In addition, compressed SLIs were stored for 6 months prior to *in-vitro* release in order to investigate the storage stability of the SLIs including protein stability and release [176]. After a 6-month storage, the release patterns were comparable to those from non-stored SLIs. Furthermore, rh-interferon α-2a was released in its monomeric form when HP-β-CD was used as stabiliser even after storage of the implants at room temperature. It turned out that the use of trehalose as excipient resulted in increased levels of aggregated and oxidized species after storage and release [176].

The role of PEG as release modifier was investigated by Herrmann *et al.* [177]. The release of rh-interferon α-2a was monitored as a function of different PEG percentages within the formulation. For this, SLIs were prepared by compression comprising 0 to 20 % PEG. The

addition of PEG substantially changed both the protein release rate and the underlying mass transport mechanisms [177]. If no PEG was added, the release of rh-interferon α-2a was purely diffusion controlled. Contrarily, in PEG-containing SLIs the release rate remained constant over prolonged periods of time pointing into the direction that also other release mechanisms (which were not observed before) were involved. Interestingly, the release of PEG itself from SLIs persisted purely diffusion controlled, irrespective of the amount of PEG added. Herrmann *et al.* concluded that different mass transport mechanisms govern the release of rh-interferon α-2a out of the lipidic implant. Further work showed that at a physiological pH rh-interferon α-2a tends to precipitate in the presence of PEG which was reflected in the release kinetics [156, 178]. By this, it was shown for the first time that the release of pharmaceutical proteins can be controlled by an *in-situ* precipitation.

The *in-vivo* rh-interferon α-2a release from compressed SLIs was studied by Schwab *et al.* [168]. SLIs were implanted subcutaneously in rabbits and sustained protein release was measured over 9 days. A modelling of the data revealed that the *in-vivo* release correlated closely with the *in-vitro* release. The lipase induced degradation of lipid implants was also investigated by Schwab *et al.* to obtain information about degradation time frames of SLIs once administered. SLIs were compressed from either 100 % of a single triglyceride or a blend of two of the following lipids: Dynasan® D112 (trilaurin), D114 (trimyristin), D116 (tripalmitin) or D118 (tristearin). The authors stated that the triglyceride D112 seems to play a major role in the degradation and erosion processes of the implants [179]. This is due to the melting point of D112, which is below the human body temperature leading to disintegration and loss of physical integration, which is also of special interest of the present work.

Jensen *et al.* reported on the *in-vitro* release of insulin from compressed lipid implants being the first author after nearly 10 years using again compression as preparation technique [180]. The work described the investigation of UV imaging-based *in-vitro* methods to enable the visualisation of released drug to mimic the subcutis. Jensen *et al.* stated that «Insulin release from 10 % (w/w) implants into agitated solution was faster as compared to release into agarose

hydrogel. This was ascribed to the additional mass transfer resistance provided by the agarose hydrogel. » [180].

TWIN-SCREW EXTRUDED SOLID LIPID IMPLANTS FOR PROTEIN AND PEPTIDE DELIVERY

Schulze *et al.* [181] introduced tsc-extrusion as manufacturing technique for lipid implants which meanwhile became one of our standard manufacturing techniques besides the direct compression technique described above [168, 175, 177].

Lipid implants consisted of 10 % rh-interferon α-2a co-lyophilised with HP-β-CD and 10 % PEG 6000 incorporated into a lipid matrix. The lipid matrix consisted of D118 with either H12 or E85 both low melting lipids. Extrusion was performed at 40°C with a screw speed of 40 rpm. The authors stated that sustained release occurred in a sustained manner over 15, 40, or 60 days as a function of the composition [181]. Moreover, the preparation process did not affect the stability of rh-interferon α-2a which was studied by FT-IR and SDS-PAGE.

Tsc-extrusion was systematically investigated by Sax *et al.* approaching the influence of melting events on the *in-vitro* release of lysozyme [182]. For this purpose, D118 was admixed with different low melting lipids (having slightly different melting points) and PEG 4000 or PEG 6000 was added as pore forming agent. A more sustained release (for up to 240 days) of lysozyme was achieved when the amount of PEG was reduced. Interestingly, the inner structure of the implant changed during release as measured by DSC and XRPD. The authors explained that phenomenon by a partial melting of the lipid matrix. Thus, Sax *et al.* concluded that partial melting of the implants during *in-vitro* release was found to be a major factor for the controlled protein release being a useful tool to trigger release. To study this phenomenon more in detail, single molecule fluorescence microscopy revealed that two release pathways were present. Surprisingly, it was observed that «proteins were not only released via water-filled pores (created by dissolution of the pore-former), but surprisingly also through diffusion in a phase of molten lipid.» [183]. This represented a completely new finding which is crucial for the future development of lipid-based depots also being important for this thesis.

The *in-vivo* biodegradation was described in a rabbit model by Sax *et al.* [184]. Different formulated SLIs were implanted subcutaneously in rabbits and implant mass was measured for 6 months. After 6 months, recovered implant mass was only 24 % in average. Furthermore, biodegradation was a function of formulation: the presence of pore forming agent resulted in higher mass loss and an accelerated degradation rate. The unique composition of a low melting and a high melting lipid was claimed to be responsible for the good biodegradability due to a partial melting of the implant at physiological temperatures.

Neuhofer used this formulation investigated by Schulze *et al.* and Sax *et al.* for the encapsulation of the hydrophobic protein native interferon-β-1b (nIFN-β-1b) [185]. The sustained release of nIFN-β-1b was described for up to 10 days when surfactants (0.1 % SDS or 0.15 % laureth-12) were added to the release medium. Since almost no release was observed when no surfactants were added (approximately 5 % after 7 days), it was assumed that the high hydrophobicity and solubility effects might play a role for triggering the release of proteins. This hypothesis was strengthened by the more complete release of more hydrophilic PEGylated interferon-β-1b (60 % within 7 days). Thus, Neuhofer was the first studying possible interactions between the proteins and the matrix materials by adsorption experiments and QCM studies. QCM studies revealed a tendency to fewer protein adsorption of PEG-IFN-β-1b to a tristearin surface than nIFN-β-1b. This indicates a stronger affinity of nIFN-β-1b to hydrophobic surfaces [185].

Interactions between triglycerides and peptides were studied by Even focussing on interactions between peptides (being different in charge and hydrophobicity) and the lipids D114 (trimyristin), soybean lecithin and cholesterol [186]. Even found that adsorption to D114 was a function of hydrophobicity of the peptide.

Moreover, Even *et al.* explored new application fields for SLIs. The authors described the *in-vivo* investigation of SLIs as depot for vaccines [186] using the model antigen Quil-A in a mice model. Quil-A was released for 14 days and the overall immune response ($CD4^+$ and $CD8^+$ T-cell proliferation, IgG production, cytokine secretion) revealed a successful proof of concept.

Addressing the field of immunotherapies, the peptide tyrosinase-related protein-2 (TRP-2), being an antigen in tumour therapy approaches, was successfully incorporated into SLIs and tested in mice. The *in-vivo* study showed that mice which received TRP-2 loaded implants had delayed tumour growth for 3 days compared to groups having received no TRP-2 [187]. Within this publication, Even *et al.* was the first one using the ZE-5 mini-extruder from Three-Tec for the production of tsc-extruded implants. They stated that «The type of extruder used to produce the implants had a major influence on implant properties and the release behaviour, demonstrating that extrusion parameters and lipid formulations have to be individually adapted to each extrusion device.» [187]. These aspects are of special interest of the present work since the ZE-5 mini-extruder was intensively used.

I.2.4 INTRAOCULAR DELIVERY

The treatment of several serious eye diseases, e.g. age related macular degeneration (AMD), is up to now associated with significant side effects due the penetration of the posterior segment of the eye by a needle [30, 96]. AMD is the leading cause of blindness in industrialised nations for people over 50 years [188]. The wet AMD accounts for only 15 % of all AMDs, but causes about 90 % of blindness [189]. The pathology is based on weak blood vessels underneath the macula and retina affecting a leakage of fluids (e.g. blood) into the eye and finally causing macular damage [190]. This causes the distribution of inflammatory markers (cytokines or VEGF) generating ischemia and inflammation, which leads to choroidal neovascularisation (CNV) [191]. New blood vessels grow irregular under the macula supporting rapid central vision loss. Furthermore, CNV has a strong link to increased expression of the VEGF gene [192]. Currently, the management with anti-VEGF drugs such as Bevacizumab (Avastin®), Ranibizumab (Lucentis®) and Aflibercept (Eylea®) are representing the state of the art therapy [193-197]. Besides the stress for the patient, the required monthly injections into the vitreous causes injection-related adverse effects like endophthalmitis [96]. Hence, it would be preferable to prolong the period between two intravitreal injections by using sustained release devices to

improve patient convenience, safety, and efficacy. With these limitations, efforts are being made to develop ocular inserts releasing therapeutic drugs over a long time to reduce application intervals.

I.2.4.1 MARKETED PRODUCTS FOR INTRAOCULAR ADMINISTRATION

Currently, there are four commercially available ocular implants providing long-term release from either biodegradable or non-biodegradable polymeric systems over several months to years.

Vitrasert®, the first non-biodegradable intravitreal implant approved by the FDA in 1996, contains ganciclovir for the therapy of cytomegalovirus retinitis. It is consisting of a drug pellet, coated with PVA allowing drug release of 5 to 8 months [198]. The outer and inner permeable PVA layers sandwiching a discontinuous layer of impermeable EVA controlling the release. Other intravitreal devices based on this technology are on the market such as Retisert® from Bausch and Lomb which contains fluocinolone acetonide and is approved for the treatment of chronic non-infectious uveitis [199]. Iluvien™ is another injectable intravitreal insert which delivers a very low dose of the corticosteroid fluocinolone acetonide (0.5 µg to 0.2 µg/day) to the retina over a period of about 3 years [200]. The implant consists also of a drug-loaded core coated with a PVA layer and has a release opening. All these implants are non-biodegradable and need to be surgically removed.

Ozurdex® is commercially available since June 2009 and was approved by the FDA for the treatment of macular edema [201]. The implant consists of a PLGA matrix, which degrades slowly to lactic acid and glycolic acid allowing the long-term release of dexamethasone of up to 6 months [202-204].

In summary, it can be concluded that an ocular insert loaded with a therapeutic protein or peptide has not yet reached the market.

I.2.4.2 VEHICLES FOR INTRAOCULAR DELIVERY OF PROTEINS AND PEPTIDES

The development of intravitreal inserts for the sustained release of therapeutic proteins and peptides is currently in the focus of research. Delivery platforms described in literature are multifaceted including implants, hydrogels and particulate systems affirming the efforts, which had been made within the last years. Interestingly, irrespective of the depot used within those studies, it is noteworthy that in most (but not all) cases Bevacizumab was used.

In 1999, the first intravitreal controlled release application of a monoclonal antibody was described by Mordenti *et al.* [205]. Trastuzumab was encapsulated into PLGA microspheres and injected into rabbit eyes. The depot was well tolerated in the eye and suitable for ocular applications as no relevant side effects were reported. However, the total cumulative release of Trastuzumab was only 32 %, thereby indicating large portions of non-released and/or nonnative antibody [29].

The most represented dosage form are hydrogels and semisolid depots including thermo-responsive hydrogels [206], Diels-Alder hydrogels [111], or silk hydrogels [96]. As an example, thermoresponsive hydrogels consisting of poly(N-isopropyl acrylamide) were cross-linked with PEG-diacrylate and Bevacizumab and Ranibizumab were encapsulated within this matrix. A sustained release for approximately 3 weeks was observed whereby the release rate was controllable by varying the cross-linking degree [206]. Bevacizumab had also been encapsulated within silk hydrogels, which were administered into rabbit eyes. Release concentrations were achieved after 90 days equivalent than those achieved at 30 days with the positive standard dose control (a single injection of 50 µl Bevacizumab intravitreally administered). Thus, a comparable therapeutic threshold based on a dosage administration schedule of one injection/month was achieved [96].

The sustained-release of a f_{ab}-fragment has been described by Asmus *et al.* Here, the authors considered the use of a hydrophobic polyester hexylsubstituted PLA (hexPLA) as matrix. The f_{ab}-fragment exhibited an excellent compatibility with the matrix and the protein was released for

6 to 14 weeks [207]. Furthermore, the antibody fragment structure remained intact during incorporation and release.

A representative of particulate systems is described by Chen *et al.* where the encapsulation of connexin43 mimetic peptide into PLGA micro- and nanoparticles is broached for treatment of retinal ischaemia [208]. The use of PLGA based nano- and microspheres for Bevacizumab delivery was shown by Li *et al.* showing a sustained release for over 90 days [209].

Another interesting approach is the use of nanostructured mesoporous silica films loaded with Bevacizumab. By this technique an *in-vitro* release of bioactive Bevacizumab over one month has been observed [210]. A fascinating but completely different technology has been described by Gooch *et al.* and Molokhia *et al.*, the so-called capsule drug ring (CDR). The CDR is designed to serve as refillable reservoir and being placed within the capsular bag during cataract surgery with the ability to release Bevacizumab close to zero order kinetic [211, 212].

I.2.4.3 LIPID BASED VEHICLES FOR INTRAOCULAR USE

Only a few publications are available regarding the intraocular delivery of proteins from lipid based systems. The study of Abrishami *et al.* is one of the few describing the *in-vivo* performance of Bevacizumab encapsulated within a nanoliposomal formulation [213]. Liposomes were prepared by the dehydration-rehydration method and were scaled to nano size even though the exact diameter is not mentioned. However, the Bevacizumab containing liposomal formulation was tested in rabbit eyes and Bevacizumab concentration was monitored for 42 days. The depot was well tolerated over 42 days and Bevacizumab clearance was slower for the liposomal formulation compared to the soluble form.

A single publication is available addressing the *in-vivo* performance of SLIs for intravitreal purposes. In 2014, Tamaddon *et al.* reported on SLIs consisting of a glyceride tripalmitate matrix. The implants had a diameter of 0.4 mm and were fabricated via a hot melt extrusion method. *In-vitro* release of clindamycin was up to 10 days and *in-vivo* biocompatibility was tested in rabbit eyes showing no abnormalities up to 2 months after implantation into the rabbit

eye [214]. Even though the SLIs did not contained a protein drug, the similarity to the SLIs described within this thesis is noteworthy.

It is apparent, that lipid based intravitreal depots are in the early stages and that much more research should be done. On the other hand, this highlights that the work presented here is intended to exactly address this gap considering it as an incentive for further research.

I.2.5 PROTEIN STABILITY CONSIDERATIONS FOR CONTROLLED RELEASE SYSTEMS

The controlled release of pharmaceutical protein drugs is a key strategy to reduce both systemic side effects and the frequency of drug administration [71]. However, developing protein delivery systems which ensure both suitable release and at the same time maintaining the stability of the protein drug represents the major challenge [215]. Jiskoot *et al.* already underlined the importance of knowledge on possible protein instability and immunogenicity even before considering it for a sustained release depot. [216].

During a «life time» of a DDS, the proteins are exposed to multiple unfavorable conditions, e.g. during the manufacturing process, storage of the DDS prior to use and during release. Considering the great diversity and number of DDS for protein and peptide drugs, it is surprising that numerous publications do not pay any or not sufficient attention to this important topic.

Generally, each single protein – even among the same subclass – has its own unique physicochemical «fingerprint» which needs to be taken into consideration when developing a DDS. For instance, each protein is unique by its isoelectric point (pI), surface charge distribution, hydrophobic patches or buffer capacity dedicated by its primary structure [29]. Moreover, when considering different protein formats such as bispecific antibodies, f_{ab}-fragments, PEGylated proteins or fusion proteins, these differences become even more enhanced.

A protein encapsulated within a DDS is even more exposed to additional stress conditions than a protein administered intravenous. These additional stresses can occur during encapsulation/manufacturing, storage, and *in-vivo* release.

Harsh conditions can arise during encapsulation/manufacturing of the DDS and can be exemplarily illustrated by the production of PLGA particles where vigorous stirring and emulsification of a protein solution into a polymer solution is obligatory [60]. Moreover, proteins are exposed to organic solvents and interfaces and the high hydrophobicity of PLGA favours interactions [217]. Of course, these issues can also be encountered when other technology platforms than PLGA are used. For instance, in case of particular lipid-based DDS including the preparation of liposomes [218].

Once administered, e.g. subcutaneously, the protein need to retain its integrity at the administration site at the conditions prevailing *in-vivo*. In the case of subcutaneously administered DDS (e.g. *in-situ* forming gels), the depot retains the drug for long time periods at the administration site often exceeding their endogenous half-life [219]. This is because under *in-vivo* conditions, proteins tend to degrade much faster than under *in-vitro* storage conditions (2°C to 8°C). Additionally, after administration the protein is exposed to 37°C and the present of matrix degradation products, interstitial fluid, proteolytic enzymes, various cells and cellular by-products (reactive oxygen species) which could result in adverse side effects [216, 220]. Moreover, «stabilizers present within the original formulation rapidly dissipate and are usually not available to protect the drug during drug release inside the matrix» as stated by Schweizer *et al.* [29].

Despite protein instability considerations, also the immunogenicity aspects should be considered since a number of immunological risks are associated with the application of DDS including hypersensitivity reactions [221]. Moreover, pharmacokinetics, biodistribution and targeting capability can be negatively affected [220]. The highest risk are anti-drug-antibodies against the protein drug itself [222], its aggregates [223-226], the matrix material or targeting

ligands associated with the DDS. This could cause reactions and formation of membrane attack complexes or accelerated clearance as stated by Rojko *et al.* [227].

Jiskoot *et al.* perfectly summarised this topic and formulated three approaches for the adequate characterisation of proteins in DDS to «obtain as complete a picture as possible of the quality of the drug product»: (i) characterisation of the protein encapsulated within the DDS, (ii) characterisation of released protein and (iii) characterisation of protein which remained within the depot [216].

During this work, it was intended to take these approaches into consideration.

II. OBJECTIVES OF THE THESIS

The applicability of parenteral depots has been studied intensively within the last two decades. Besides the thoroughly investigated PLA/PLGA depots [48, 73], those depots include PLGA-composites [68, 70, 72], alginate [84], chitosan [76, 77, 80], silk [28, 96, 98], or casein [228], just to name a few. Due to the drawbacks of PLA/PLGA materials in terms of protein stability [49, 72, 229], lipid based depots have gained more and more importance as material for long term delivery of proteinaceous drugs. Preserving the integrity of incorporated proteins [176, 181] is the most valuable benefit over commonly used PLA/PLGA polymers.

Previous works on triglyceride based implants have already demonstrated the suitability of such depots to maintain stability of both encapsulated and released protein [176, 181]. Furthermore, the long-term release of protein drugs from triglyceride implants was demonstrated by a rather simple and straightforward compression technique [167, 177]. Within our group, tsc-extrusion was established and meanwhile became one of the standard manufacturing techniques. It was shown that tsc-extruded SLIs exhibit a more sustained release and a more homogenous drug distribution compared to SLIs manufactured by direct compression [230]. For instance, long-term release of protein drugs was successfully demonstrated for interferon α-2a, which was delivered for more than 60 days [181] and for lysozyme, for which a release of more than 200 days was described [182]. Also, it has already been demonstrated that SLIs are a promising platform for various applications, e.g. vaccination [231], tumour therapy [187], subcutaneous administration [184], or intraocular use (data not published).

The starting point of the present work was an established extrusion process on the MiniLab® Micro Rheology Compounder which was used for the sustained long-term release of different model proteins and therapeutic proteins [232]. Also, *in-vivo* investigations had revealed excellent biocompatibility after subcutaneous [184] and intravitreal administration (data not

published). Within those works, sustained release of different commercially available protein formats has not yet been reported. Also, protein stability and biological activity aspects had not been investigated systematically with regards to tsc-extrusion as manufacturing technique. Furthermore, the impact of different extrusion parameters (e.g. extrusion temperature, screw speed) on implant characteristics and release patterns had not been investigated systematically [182, 186, 233, 234].

Consequently, the present work was aimed to address the following objectives:

(i) further optimisation of the manufacturing process (extrusion parameters, formulation) with a focus on intraocular use is described in **chapter IV**. For this, a new extruder (ZE-5 mini extruder) was acquired allowing to manufacture small batches. In a first step, the established process was transferred from a MiniLab® Micro Rheology Compounder to a ZE-5 mini extruder. It was aimed to optimise the process to reach delivery time frames of at least 3 months. Second, as a potential intraocular use was considered, reducing implant dimensions and increasing the protein load while ensuring release patterns and storage stability was intended. To study the impact of the incorporated protein on release patterns, different protein formats were used including three commercially available products: Ranibizumab (Lucentis®), Bevacizumab (Avastin®) and Aflibercept (Eylea®). Additionally, another model mAb was used. To further tailor the release, triglycerides were pre-melted prior to extrusion to intentionally change their thermal and physicochemical properties.

(ii) A 3-month *in-vivo* study in rabbit eyes using Ranibizumab loaded SLIs was executed to evaluate the *in-vitro-in-vivo* release correlation and pharmacodynamic effects within a choroidal neovascularisation (CNV) model (**chapter V**).

(iii) Within **chapter VI**, the bioactivity of fractions released from SLIs of the natural complement regulator Factor H (mini-FH) was studied to obtain information on its biological activity once released.

(iv) Further work included the systematic investigation on stability of released protein over the complete release duration covering colloidal, chemical and conformational stability (**chapter VII**). Comparison of stability profiles delivered from SLIs to PLGA-based implants was performed.

(v) Recent work pointed into the direction that not only the manufacturing settings influence release patterns but also the properties of the protein itself [185, 186]. Consequently, the influence of possible triglyceride-protein-interactions on protein stability was investigated within **chapter VIII**.

(vi) Solid lipid extrusion (SLE) has been used previously within different works [162, 163, 235-237]. However, the extrusion process itself and its impact on the lipid matrix and release patterns has not yet been described. It was therefore the aim of **chapter IX** to characterise the SLE process with regards to how changing process parameters affect the properties of the lipid matrix and the release patterns of the model mAb. Therefore, the impact of process parameters such as extrusion speed, temperature, and lipid composition on implant properties was investigated systematically.

III. MATERIALS AND METHODS

III.1 MATERIALS

III.1.1 PROTEINS

In this thesis, the following proteins were utilised for the preparation of long-term release lipid depot systems:

A monoclonal IgG_1 antibody (mAb) formulated in a 10.5 mM sodium phosphate buffer at pH 6.4 at a concentration of 17.3 mg/ml was utilised.

Bevacizumab (Avastin®) is a recombinant humanised monoclonal IgG_1 antibody that binds to human vascular endothelial growth factor (VEGF) [195, 238, 239] and has an approximate molecular weight of 149 kDa. Bevacizumab is formulated at a concentration of 25 mg/ml in a 50 mM sodium phosphate buffer containing 60 mg/ml α, α-trehalose and 0.04 % polysorbate 20 at a pH of 6.2.

Ranibizumab (Lucentis®) is a recombinant humanised IgG_1 monoclonal antibody fragment from Bevacizumab (Avastin®), inhibiting the biologic activity of VEGF [193, 196]. Ranibizumab has a molecular weight of approximately 48 kDa and is formulated in 10 mM histidine-HCl, 10 % α, α-trehalose dihydrate and 0.01 % polysorbate 20 at pH 5.5.

The recombinant fusion protein Aflibercept (Eylea®) consists of portions of human VEGF receptors and extracellular domains fused to the F_c portion of human IgG_1 [191, 197]. It is a dimeric glycoprotein with a molecular weight of 97 kDa containing 15 % glycosylation which results in an overall molecular weight of 115 kDa. Aflibercept is formulated in 10 mM sodium phosphate at a concentration of 40 mg/ml, also containing 40 mM sodium chloride, 5 % sucrose and 0.03 % polysorbate 20 at pH 6.2.

Bevacizumab (Avastin®), Ranibizumab (Lucentis®) and Aflibercept (Eylea®) were kindly provided by the Moran Eye Center (Salt Lake City, Utah, USA).

The C3-opsonin targeted complement inhibitor mini-FH having a molecular weight of 43.3 kDa [240, 241] was available as freeze-dried powder without further stabilisers. It was provided by the group of Dr. Christoph Schmidt from the Institute of Pharmacology and Natural Products and Clinical Pharmacology, Ulm University, Germany.

III.1.2 TRIGLYCERIDES

The triglycerides Dynasan® D118, Witepsol H12, H12 and H12A were a kind gift from Cremer Oleo (Hamburg, Germany). The high melting lipid D118 consists of nearly 100% tristearin, whereas the low melting lipids Witepsol H12, H12 and H12A are a mixture of trilaurin, trimyristin and tripalmitin (Table III-1).

Table III-1: Properties of the triglycerides H12, H12A, Witepsol H12 and D118.

	H12	**H12A**	**Witepsol H12**	**D118**
Hydroxyl value [mg KOH/g)	0.0	0.0	5.0	2.4
C12 fatty acid (trilaurin) [%]	70.2	74.2	70.8	0.0
C14 fatty acid (trimyristin) [%]	27.1	25.3	26.0	0.0
C16 fatty acid (tripalmitin) [%]	2.3	0.2	2.4	0.0
C18 fatty acid (tristearin) [%]	0.0	0.0	0.0	98.2
Triglyceride content [%]	99.7	99.9	96.5	99.9
T_{onset} [°C]	36.8	37.4	32.0	70.0
$T_{melting}$ [°C]	43.1	42.4	39.9	72.7

III.1.3 POLY(D,L-LACTIC-CO-GLYCOLIC)

The Poly(D, L-lactic-co-glycolic) (PLGA) Resomer® RG 502, Resomer® RG 502 H and Resomer® RG 755 S were purchased from Evonik Industries (Essen, Germany). Based on the different ratios of lactide to glycolide acid and different end groups, properties of PLGAs varied in their molecular weight, degradation time and chemical end groups (Table III-2).

Table III-2: Properties of the Resomer® polymers RG 502, RG 502 H and RG 755 S.

Type of Resomer®	Molecular weight	Ratio Poly(D,L-lactic-co glycolic)	Degradation time frame	End group
RG 502	7.000 to 17.000 Da	50:50	< 3 months	alkyl ester
RG 502 H	7.000 to 17.000 Da	50:50	< 3 months	free COOH
RG 755 S	76.000 to 116.000 Da	75:25	< 6 months	ester

III.1.4 CHEMICALS AND SALTS

All reagents and chemicals used within this work are listed in Table III-3. All chemicals and salts were of analytical grade.

Table III-3: List of chemicals and salts used within this work.

Substance	Abbreviation	purchased from
4,4′-Dianilino-1,1′-binaphthyl-5,5′-disulfonic acid dipotassium salt	Bis-ANS	Sigma-Aldrich Chemie GmbH, Steinheim, Germany
Ammonium sulfate	$(NH_4)_2SO_4$	Sigma-Aldrich Chemie GmbH, Steinheim, Germany
di-Sodium hydrogen phosphate dihydrate p.A.	$Na_2HPO_4*2H_2O$	AppliChem GmbH & Co. KG, Darmstadt, Germany
Hydroxypropyl-β-cyclodextrine	HP-β-CD	Wacker Chemie AG, Burghausen, Germany
Imidazole	-	Sigma-Aldrich Chemie GmbH, Steinheim, Germany

n-Hexane	-	Sigma-Aldrich Chemie GmbH, Steinheim, Germany
Piperazine	-	Sigma-Aldrich Chemie GmbH, Steinheim, Germany
Polyethylene glycol 6000 PF	PEG 6000	Clariant GmbH, Frankfurt am Main, Germany
Potassium chloride	KCl	AppliChem GmbH & Co. KG, Darmstadt, Germany
Potassium dihydrogen phosphate	KH_2PO_4	Merck KGaA, Darmstadt, Germany
Sodium azide	NaN_3	Merck KGaA, Darmstadt, Germany
Sodium chloride	NaCl	Prolabo, Leuven, Belgium
Sodium dihydrogen phosphate dihydrate	$NaH_2PO_4*2H_2O$	AppliChem GmbH & Co. KG, Darmstadt, Germany
Tris(hydroxymethyl)aminomethane	Tris	Sigma-Aldrich Chemie GmbH, Steinheim, Germany

III.2 METHODS

III.2.1 PREPARATORY STEPS

III.2.1.1 DIALYSIS

Dialysis of the protein formulations was performed to deplete the formulations of buffer salts and stabilisers and to substitute them with hydroxypropyl-β-cyclodextrine (HP-β-CD). HP-β-CD was used as lyoprotectant to assure protein stabilisation during freeze drying and storage as reported previously for rh-interferon α-2a [176] and erythropoietin [242]. The protein bulk materials were dialysed against 50 mM sodium phosphate buffer pH 6.2 at 4°C by complete buffer exchange thrice resulting in 20 liters total buffer volume. The theoretical dilution factor was calculated with 1200. Dialyses was performed in a CelluSep® T1 tube from Orange

Scientific (Braine-l'Alleud, Belgium) with a molecular weight cut off (MWCO) of 3.5 kDa. After dialysis, the protein concentration was determined spectrophotometrically by applying an UV-VIS spectrometer Agilent 8452 (Böblingen, Germany). The protein concentration was set to 10 mg/ml and HP-β-CD was added to obtain a ratio of 1:1 [w/w], 2:1 [w/w] or 3:1 [w/w].

III.2.1.2 LYOPHILISATION PROCESS

Aliquots of 2.0 ml of the formulations were filled into 10R vials and lyophilised using an Epsilon 2-6D freeze dryer from Christ (Osterode, Germany) (Figure III-1). In brief, the solution was frozen to -50°C at a rate of 1°C/min and the temperature was held for 30 min. Primary drying was performed at a shelf temperature of -10°C and a pressure of 0.09 mbar for 24 h. Afterwards, the temperature was increased to 25°C within 4 h. Secondary drying was then performed at 25°C for 7 h. After the cycle was finished, freeze dried samples were held at 5°C at 0.09 mbar. Product temperature was monitored with thermocouples placed at the edges and in the middle of the shelf. Finally, the freeze dryer was vented with filtered nitrogen gas to approximately 800 mbar. Vials were stoppered and crimped after unloading.

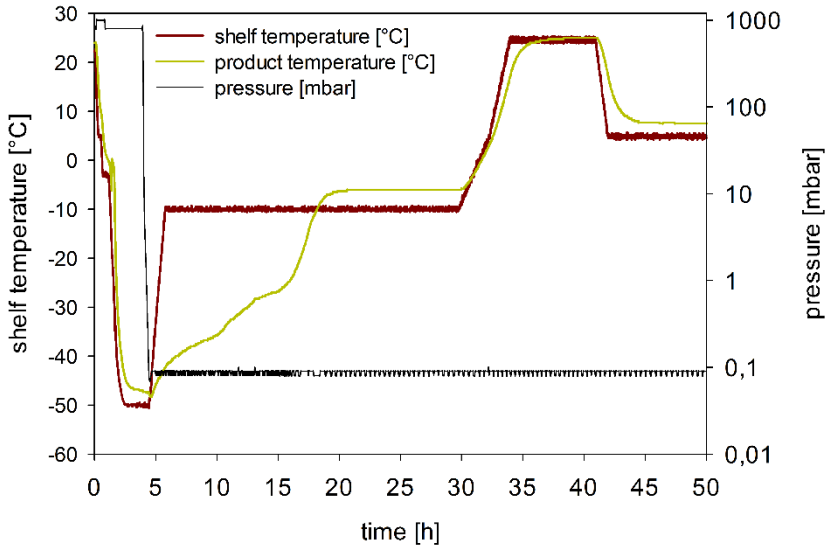

Figure III-1: Shelf temperature and pressure traces of an examplary freeze-drying run. Thermocouples were placed in the formulations to monitor the product temperature.

III.2.1.3 PRE-MELTING OF LIPIDS

For specific experiments, lipids were pre-melted prior to extrusion by simultaneous melting of the high and low melting lipid at 80°C to obtain a homogenous molten mass. The molten mass was not further stirred. The melt was allowed to cool down to room temperature at approximately 23°C. The solidified melt was ground using mortar and pestle, sieved (< 180 µm) and stored at 4°C.

III.2.2 PREPARATION OF IMPLANTS

III.2.2.1 TSC-EXTRUSION OF SLIS ON A MINILAB® MICRO RHEOLOGY COMPOUNDER

Applying the MiniLab® Micro Rheology Compounder (Thermo Haake GmbH Karlsruhe, Germany) the composition listed below was extruded according to the formulation described by Sax *et al.* [182]. Tsc-extrudates were prepared from a powder mixture comprising 10 % protein lyophilisate, 10 % PEG 6000 lyophilisate, 24 % H12 and 56 % D118. Equal masses of lyophilisates and triglycerides were weighed into a mortar and mixed to create a uniform powder mixture. Afterwards, remaining H12 and D118 was added to ensure a homogenous distribution of the single components. Extrusion was performed at 41°C with closed bypass channel, screw speed was adjusted to 40 rpm and the extruder outlet was set to 1.9 mm. Approximately 5 g of the material was fed into the barrel by compressing it manually. The obtained lipid strand was cut into pieces of approximately 20 mm resulting in an average weight of 67 mg per implant.

III.2.2.2 TSC-EXTRUSION OF SLIS ON A ZE-5 MINI-EXTRUDER

Formulations consisting of 10 % to 20 % protein lyophilisate and different ratios of the low melting lipid H12 and the high melting lipid D118 were extruded on a ZE-5 mini extruder. H12, D118 and lyophilised protein were weighed into a mortar and admixed by hand to create a uniform powder mixture. When extrusion was performed with pre-melted lipids, protein

lyophilisate was added to the sieved (< 180 µm) cooled down solidified melt and the powder mixture was homogenised manually using pestle and mortar. Tsc-extrusion was performed using a ZE-5 mini-extruder from Three-Tec (Seon, Switzerland) comprising three heating zones. Approximately 1 g of the powder mixture was fed manually into the barrel of the ZE-5 mini-extruder and extrusion was performed between 33°C to 42°C. The rotation speed of the screws was set between 20 rpm to 80 rpm. The implant diameters were adjusted by applying outlet plates with 0.8 mm, 1.5 mm, 1.7 mm and 2.0 mm diameter, respectively. Extruded implants were cut into a length of 15 mm resulting in an implant weight of around 30.7 mg ±0.78 mg (1.5 mm diameter) and 39.3 mg ±0.96 mg (1.7 mm diameter).

III.2.2.3 TSC-EXTRUSION OF SLIS ON ZE-5 MINI-EXTRUDER USING A FEEDING TUBE

The inlet die to the ZE-5 mini-extruder barrel was equipped with a custom-made feeding tube of 22 cm length and 0.9 cm diameter and a custom-made pestle to feed the material into the barrel. The material was filled into the feeding tube (3 g) and the powder mixture was fed into the barrel by applying a constant weight on the pestle. Extrusion of various formulations (30 % to 70 % H12) was performed at extrusion temperatures ranging from 33°C to 42°C at different screw speeds (40 rpm to 80 rpm).

III.2.2.4 DOUBLE EXTRUSION OF SLIS ON ZE-5 MINI-EXTRUDER WITH FEEDING TUBE

In a first approach, extrudates with 10 % lyophilisate were produced using a lipid matrix consisting of 50 % H12 and 50 % D118 extruded at 35°C and 40 rpm. The lipid strand was ground, sieved (< 180 µm) and extruded a second time at 33°C, 35°C or 37°C.

In a second approach, a formulation comprising 20 % protein lyophilisate and 80 % D118 was first extruded at 65°C. Afterwards, the extrudates were ground and sieved (< 180 µm), H12 was added to get a lipid matrix composed again of 50 % H12 and 50 % D118. Second extrusion was then performed at 35°C.

In a third approach, 20 % protein lyophilisate and 80 % H12 were extruded at 35°C within the first extrusion run. D118 was added to the ground and sieved (< 180 µm) extrudate to obtain a 50:50 lipid matrix of H12 and D118 which was then extruded at 35°C a second time. During all double extrusion runs, rotation speed was set to 40 rpm.

III.2.2.5 PREPARATION OF PLGA BASED IMPLANTS

PLGA implants were prepared by mixing 10 % protein lyophilisate (1:1 [w/w] protein to HP-β-CD) with 90 % Resomer® RG 502, Resomer® RG 502 H or Resomer® RG 755 S, respectively, in a mortar to obtain a homogenous powder blend. The powder mixture (approximately 1.5 g) was fed manually to the ZE-5 mini-extruder and extrusion was performed at 70°C at a screw speed of 60 rpm. Extruded PLGA rods with a diameter of 1.5 mm were cut into a length of 15 mm resulting in a weight of 52.9 mg (±4.15 mg) and a protein load of 2.66 mg (±0.21 mg).

III.2.3 PROTEIN RELEASE TESTS

Extrudates (n=4) were cut into a length of 15 mm and were placed in 2.0 ml micro-centrifuge tubes (VWR, Radnor, PA, USA) and incubated at 37°C in a Certomat® IS (Sartorius BBI, Göttingen, Germany) horizontal shaker at 40 rpm in 1.0 ml PBS buffer pH 7.4 comprising 10 mM sodium phosphate, 137 mM NaCl and 2.7 mM KCl. At predetermined time points, the release medium was exchanged completely and tempered incubation medium was added. Protein concentration was analysed spectrophotometrically at 280 nm applying an UV-VIS spectrometer (Agilent 8453, Böblingen, Germany). For all proteins, linearity of measurements was established for a concentration range of 0.001 mg/ml to 1.0 mg/ml.

III.2.4 DETERMINATION OF IMPLANT PROPERTIES

III.2.4.1 DYNAMIC SCANNING CALORIMETRY (DSC)

Thermal properties of lipid raw material and implants were measured using a Netzsch DSC 204 (Selb, Germany). Approximately 15 mg sample (accurately weighed) was weighed into aluminium sample pans and crimped before heating from 0°C to 90°C with a heating rate of 5 K/min. T_{onset}, $T_{melting}$ and the melting energy of the lipids were assessed.

III.2.4.2 X-RAY POWDER DIFFRACTION (XRPD)

To determine lipid modifications and crystallisation events, XRPD was performed using an Empyrean powder diffractometer (PANalytical, Almelo, The Netherlands) equipped with a copper anode (45 kV, 40 mA, Kα1 emission at a wavelength of 0.154 nm) and a PIXcel3D detector. Approximately 100 mg of finely sieved sample material were placed onto the sample holder and analysed in the range of 0° to 50° 2-theta with steps of 0.05° 2-theta.

III.2.4.3 SCANNING ELECTRON MICROSCOPY (SEM)

The morphology of extrudate surfaces and cross sections were analysed either using a JSM6500F Field Emission Electron Microscope (Jeol, Eching, Germany) or a FEI Helios G3 UC (Hillsboro, Oregon, USA) without any further processing or coating. SEM micrographs were taken at an operating voltage of 2.0 kV at a magnification of 40x, 300x and 2500x (JSM6500F) or at a voltage of 1.5 kV at a magnification of 80x, 300x and 2000x (FEI Helios G3 UC).

III.2.4.4 MECHANICAL PROPERTIES

Mechanical properties of extrudates were analysed using a Texture Analyser TA XT2i (Stable Microsystems, Godalming, UK). Compressive strength was assessed by compressing the samples with a cylindrical piston having a diameter of 13 mm (Figure III-2 A). Settings were adjusted to a pre-test speed of 1.0 mm/s, test speed of 0.1 mm/s, post-test speed of 10 mm/s

and a trigger force of 0.05 N. The maximal force at the point of breakage was defined to be the compressive strength.

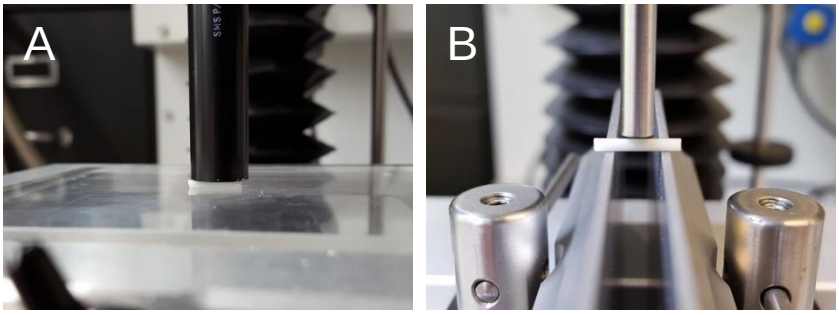

Figure III-2: Experimental setup of (A) compressive strength and (B) bending strength.

For analysis of bending strength, the sample was located on two holders being 10 mm apart from each other (Figure III-2 B). The sample was levitating were the piston touched the extrudate. Bending strength was measured by pressing a piston (4 mm in diameter) with a speed of 0.1 mm/s until the sample broke. The maximal force measured before the sample broke was defined as bending strength. Trigger force was set to 0.05 N. Per batch, experiments were performed six times at room temperature.

III.2.4.5 TRUE DENSITY MEASUREMENTS

Samples were cut into pieces with a length of approximately 5 mm, transferred to a measuring insert and weighed accurately before placing the insert into a helium pycnometer AccuPyc® 1330 (Micromeritics, Norcross, USA). After the chamber was flushed ten times with helium, the replaced volume was measured six times. For each sample, triplicates were measured resulting in eighteen single measurements per sample. Based on these volumes and with the exact mass, true density was calculated.

III.2.5 METHODS USED FOR THE *IN-VIVO* STUDY IN RABBIT EYES

III.2.5.1 MATERIALS

The f_{ab}-fragment Ranibizumab (Lucentis®) was dialysed as described above (III.2.1.1). After dialysis, the protein concentration was determined spectrophotometrically by applying an UV-VIS spectrometer Agilent 8452 (Böblingen, Germany). The protein concentration was set to 10 mg/ml and HP-β-CD was added to obtain a ratio of 1:1 [w/w]. Afterwards, the solution was filtered into sterile 50 ml tubes (Sarstedt, Nürnbrecht, Germany) using a 0.22 µm sterile syringe filter (VWR, Radnor, PA, USA). The sieved (< 180 µm) triglycerides H12 and D118 were gamma irradiated with 30.5 kGy (Synergy Health, Allershausen, Germany).

III.2.5.2 LYOPHILISATION PROCESS

Samples of 2.0 ml of the sterile protein solution were filled into autoclaved 10R vials under aseptic conditions. Lyophilisation was performed using an Epsilon 2-12D freeze dryer from Christ (Osterode, Germany) following the lyophilisation protocol described in III.2.1.2. After the cycle was finished, freeze dried samples were held at 5°C at 0.09 mbar. Finally, the freeze dryer was vented with filtered nitrogen gas (0.22 µm) to approximately 800 mbar. Vials were stoppered and crimped after unloading.

III.2.5.3 IMPLANT PREPARATION

Parts of the ZE-5 mini-extruder that could potentially be in contact with the product were autoclaved, glass ware and further equipment was heat sterilised applying a GTA 50 heat steriliser (Medizin- und Labortechnik KG, Hamburg, Germany). Extrusion was performed as described above (III.2.2.2) at an extrusion temperature of 35°C and a screw speed of 40 rpm. To prevent any contamination of Ranibizumab loaded implants before, during or after the preparation process, extrusion was performed in a laminar air flow cabinet (Hera Safe, Kendro Laboratory Products GmbH, Germany) under aseptic conditions.

Figure III-3: Semicircle shaped Ranibizumab loaded implants manufactured under aseptic conditions.

The lipid strand was formed manually with the aid of a sterile glass rod (9.4 mm in diameter) to obtain semicircle shaped rods fitting into a rabbit eye (Figure III-3). Finally, implants were placed into sterile 2.0 ml micro-centrifuge tubes (VWR, Radnor, PA, USA).

III.2.5.4 CHOROIDAL NEOVASCULARISATION MODEL

Neovascularisation was induced by an adeno-associated virus (AAV) mediated expression of vascular endothelial growth factor (VEGF) as previously described [243]. Recombinant AAV vector was chosen because it was extensively used in retina and other systems to deliver transgenes with little toxicity and inflammation [244]. To induce this into dutch-belted rabbit eyes, AAV-VEGF was injected subretinally. The AAV vector transfected the retinal pigmented epithelium to induct VEGF expression. Disease model induction was examined by fluorescein angiography. A fluorescein solution with 100 mg/ml was injected (100 µl) into the vitreous, enabling an imaging for up to 30 minutes. Although it was intended to induce choroidal neovascularisation, evidence suggested it was only retinal neovascularisation.

III.2.5.5 IMPLANT INCISION AND RANIBIZUMAB PHARMACOKINETIC STUDY

Semicircle shaped SLIs were inserted into dutch-belted rabbit eyes by a small incision. The rabbits were sacrificed after 14, 28, 42 and 84 days and Ranibizumab amounts were measured

in different compartments namely cornea, vitreous, lens, iris, retina/choroid, aqueous humor, conjunctiva, and sclera. Ranibizumab concentrations were measured using an enzyme-linked immunosorbent assay (ELISA) as already described [245, 246]. In brief, samples were diluted to be within the linear range of the assay (0.375 ng/ml to 12 ng/ml) using StabilCoat reagent (Surmodics Inc., Eden-Prairie, MN, USA) and 100 µl were aliquoted onto VEGF coated 96-well plates. The 96-well plates were incubated for 2 h at room temperature with agitation. To remove unbound Ranibizumab, plates were washed with 0.05 % Tween 20 in PBS pH 7.4. Bound Ranibizumab was detected using an antihuman IgG antibody labelled with horseradish peroxidase (HRP) (Pierce Biotechnology Inc., Rockford, IL, USA). The labeled antihuman IgG antibody was diluted 1:20.000 in StabilCoat reagent. Aliquots of 100 µl of the diluted antihuman IgG antibody were pipetted onto 96-well plates and incubated for 45 min at room temperature with agitation. Unbound IgG was removed by washing the plates 3 times with 0.05 % Tween 20 in PBS pH 7.4. Chemiluminescence was triggered by the SuperSignal ELISA Pico Chemiluminescent Substrate (Pierce Biotechnology Inc., Rockford, IL, USA) and measured using a PHERAstar Microplate Reader (BMG Labtech, Durham, NC). Ranibizumab concentration of the samples was calculated from the standard curve.

The induction of choroidal neovascularisation and the pharmacokinetic studies were performed by the Moran Eye Center, Salt Lake City, Utah, USA.

III.2.6 PROTEIN STABILITY DETERMINATION

III.2.6.1 DETERMINATION OF THE CONCENTRATION OF RELEASED PROTEIN FRACTIONS

Vivaspin® 20 Ultrafiltration Tubes equipped with a PES membrane (Sartorius Stedim Biotech, Goettingen, Germany) with a MWCO of 50.000 Da for mAb and Bevacizumab, a MWCO of 30.000 Da for Aflibercept or a MWCO of 10.000 Da for Ranibizumab were used to concentrate the released protein fractions. Tubes were filled with collected release medium and centrifuged

at 8000 x g for 20 min at 20°C using a Sigma® 4K-15 centrifuge (Sigma, Osterode, Germany). Protein concentration was determined using a NanoDrop 2000 UV-VIS Spectrophotometer (Thermo Scientific, Wilmington, USA), and protein concentration was adjusted to 1.0 mg/ml with PBS pH 7.4 for further analysis.

III.2.6.2 LIGHT OBSCURATION (LO)

Subvisible particles were counted and allocated cumulative in a range of 1 µm to 200 µm by using a SVSS (PAMAS, Rutesheim, Germany). The system is equipped with an HCB-LD-25/25 sensor which allows a detection of maximal 120,000 particles > 1 µm/ml. Before measurements, the system was rinsed with highly purified water until total particle count was less than 30 particles per ml. For analysis, the system was rinsed with 0.5 ml sample followed by three measurements of 0.3 ml sample. Between each sample measurement, the system was flushed with 10 ml of highly purified water. If necessary, 250 µl of sample were diluted to 3.00 ml with highly purified water to not exceed the total particle count of 120,000. Data analysis was performed using the PAMAS PMA software and particle diameters in a range of > 1 µm to 200 µm were assessed. If not otherwise noted, all results are given in cumulative particle count per ml of non-diluted sample.

III.2.6.3 TURBIDITY

Turbidity was measured using a Hach Lange Nephla nephelometer (Hach Lange GmbH, Düsseldorf, Germany). For measurements, 1.0 ml sample were pipetted in turbidity glass cuvettes with flat bottom. Each measurement was performed three times. The measured scattered light (wavelength = 860 nm) is given in FNU (formazine nephelometric units), detected in an angle of 90°.

III.2.6.4 SIZE EXCLUSION HIGH PERFORMANCE LIQUID CHROMATOGRAPHY (SE-HPLC)

Protein monomer content, fragments and high molecular weight (HMW) soluble aggregates were determined via SE-HPLC using a Waters 2695 Separations Module with a Waters 2487 Dual λ Absorbance Detector (Waters, Milford, USA). Linearity of measurements was established for a concentration range of 0.01 mg/ml to 1.0 mg/ml. For separation, the flow rate was adjusted to 0.5 ml/min. A sample volume of 25 µl with a concentration of 1.0 mg/ml were injected onto a TSKgel $G3000_{SWXL}$ size exclusion column (300 mm x 7.8 mm; Tosoh Bioscience, Tokyo, Japan). The running buffer consisted of 50 mM sodium phosphate containing 300 mM NaCl and was adjusted to pH 7.0.

III.2.6.5 ION EXCHANGE CHROMATOGRAPHY (IEX)

For charge variant separation of the mAb and Bevacizumab, IEX was used according to a method previously described by Farnan *et al.* [247]. IEX was performed on a Waters 2695 Separations Module with a Waters 2487 Dual λ Absorbance Detector (Waters, Milford, USA). For separation, 50 µl of sample (1.0 mg/ml) was injected onto a 4 mm x 50 mm Dionex ProPac® WCX-10G guard column coupled to an analytical 4 mm x 250 mm Dionex ProPac® WCX-10 column. Mobile phases A and B consisted of 2.4 mM Trizma® Base, 1.5 mM imidazole and 11.6 mM piperazine at a pH of 6.0 (mobile phase A) and 9.5 (mobile phase B), respectively. For separation of the different charge variants of mAb and Bevacizumab, the gradient of mobile phase B was adjusted for each protein (Figure III-4). The column was washed with 100 % eluent B for 5 minutes before it was equilibrated with 100 % eluent A for 5 minutes prior to the next injection. The flow rate was set to 1.0 ml/min. Eluted protein was monitored spectrophotometrically at 280 nm.

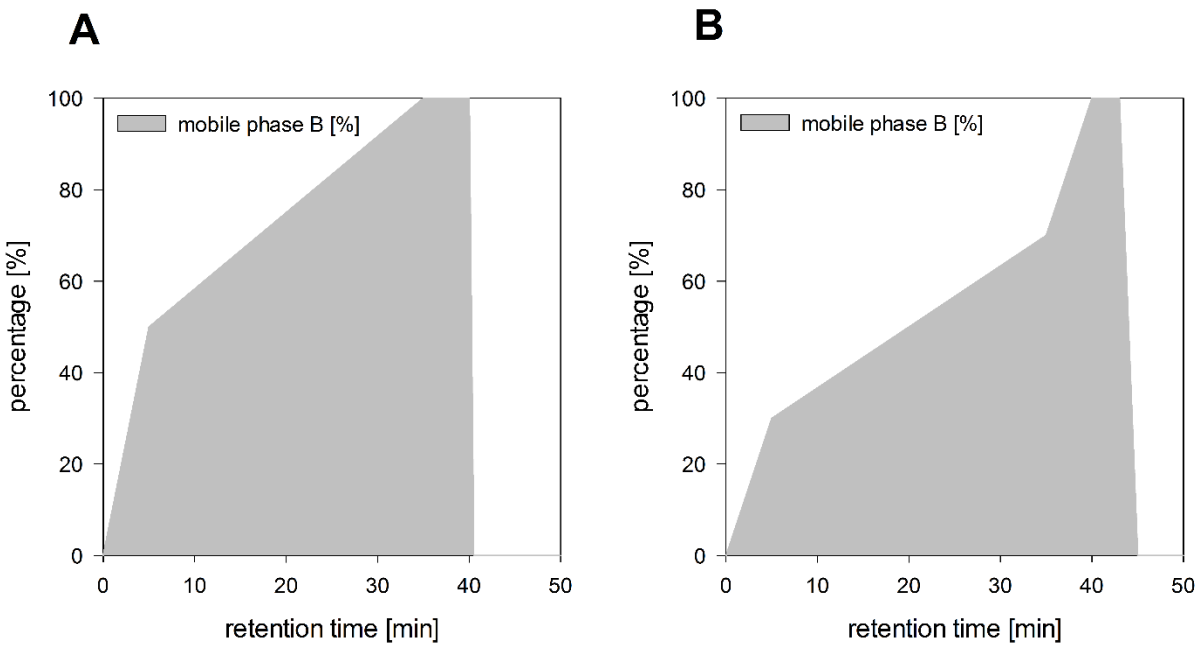

Figure III-4: Gradient of mobile phase B for charge variant separation of (A) mAb and (B) Bevacizumab.

III.2.6.6 HYDROPHOBIC INTERACTION CHROMATOGRAPHY (HIC)

For charge variant separation of Ranibizumab and Aflibercept, HIC was performed using a Waters 2695 Separations Module with a Waters 2487 Dual λ Absorbance Detector (Waters, Milford, USA). A sample volume of 50 µl with a concentration of 1.0 mg/ml was injected onto an analytical 4.6 mm x 250 mm Dionex MAbPac™ HIC-10 column for separation. Flow rate was adjusted to 1.0 ml/min and eluted protein was detected at 280 nm. Mobile phase A consisted of 1.5 M ammonium sulfate and 50 mM sodium phosphate. Mobile phase B consisted of 50 mM sodium phosphate. Mobile phases were adjusted to pH 7.0. Prior to sample injection, the column was allowed to equilibrate with eluent A. For separation of the different charge variants of Ranibizumab and Aflibercept, for each protein the gradient of mobile phase B was adjusted (Figure III-5). Post-gradient, the column was washed with 100 % eluent B for 3 min before the composition was returned to 100 % A for 5 min in preparation for the next injection.

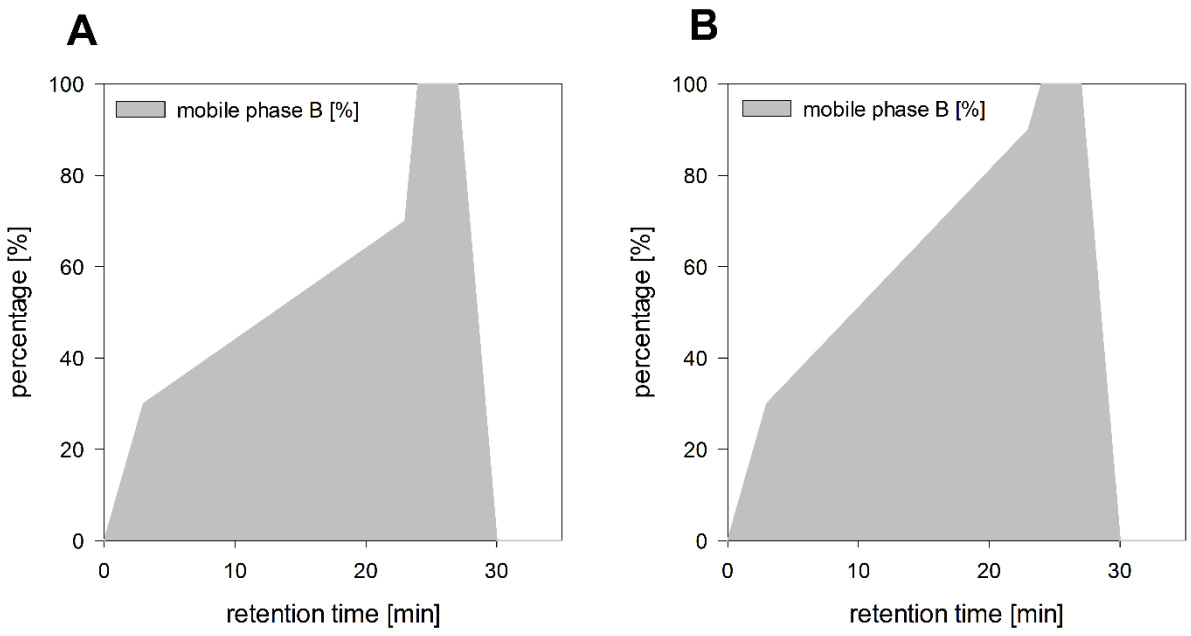

Figure III-5: Gradient of mobile phase B for charge variant separation of (A) Ranibizumab and (B) Aflibercept.

III.2.6.7 NON-REDUCING DENATURATING SODIUM DODECYL SULFATE – POLYACRYLAMIDE GEL ELECTROPHORESIS (SDS-PAGE)

Non-reducing denaturating SDS-PAGE was used to monitor aggregation and fragmentation of the proteins. Analysis was performed using a XCell SureLock™ Mini-Cell Electrophoresis System (Novex by Life Technologies, Carlsbad, CA, USA). For separation and resolution of the mAb, Bevacizumab and Aflibercept, NuPAGE® Novex® 3-8 % Tris Acetate Protein Gels 1.0 mm x 10 wells and NuPAGE® Tris-Acetate SDS Running Buffer were used. Separation was accomplished at a constant voltage of 150 V and a running time of 50 to 55 min using a Bio Rad PowerPac 200 (Bio-Rad Laboratories, Hercules, CA, USA).

Ranibizumab was analysed using NuPAGE® Novex® 4-12 % Bis-Tris Protein Gels 1.0 mm x 12 wells and NuPAGE® MOPS SDS Running Buffer. For separation, a constant voltage of 200 V for approximately 50 min was applied.

All samples were diluted with NuPAGE® LDS Sample Buffer to an initial concentration of 37.5 µg/ml and were denatured at 90°C for 5 min. Each well was loaded with 12 µl sample resulting in a total mass of 0.45 µg protein per well. Gels were stained with the SilverXPress® Silver Staining Kit according to the manufacturer's recommendations. The performance of the system was monitored by a BSA sensitivity control. Each gel was loaded with 1.80 ng and 0.36 ng BSA, respectively. Gels were stained until both bands became visible before staining was stopped by adding the stopping solution. Molecular weight of protein bands was calculated using a molecular weight marker on each gel. For the mAb, Bevacizumab and Aflibercept the HiMark™ Pre-stained Protein Standard was used, while for Ranibizumab the Mark12™ Unstained Standard was used.

III.2.6.8 CAPILLARY GEL ELECTROPHORESIS

As an orthogonal method to classical non-reducing denaturating SDS-PAGE, capillary gel electrophoresis applying an Agilent 2100 Bioanalyzer system (Agilent, Santa Clara, CA, USA) was carried out for Ranibizumab. The system offers a fast and reliable separation, sizing and quantification of proteins in a range of 14 kDa to 230 kDa. Due to these limitations, analysis of mAb, Bevacizumab and Aflibercept was not performed. Ranibizumab samples were analysed under non-reducing conditions using a Protein 230 Kit (Agilent, Santa Clara, CA, USA). According to the Agilent Protein 230 Assay Protocol, 4 µl of sample (1.0 mg/ml) and 2 µl of sample buffer were admixed and incubated at 95°C for 5 min. After samples were allowed to cool down, 84 µl highly purified water were added and 6 µl were then pipetted into the sample wells of the protein chip. The protein chip was prepared by loading it with the gel-dye mix, destaining solution und molecular weight marker according to the protocol provided by the manufacturer. The chip was then placed into the system and analysis was started immediately.

In addition, capillary gel electrophoresis was performed under reducing denaturating conditions for all proteins. Analysis was performed as described above except one adjustment: before

adding 2 µl of sample buffer to 4 µl sample, the sample buffer was spiked with 1 M Dithiothreitol (DTT) solution resulting in 4.83 mM/µl DTT.

III.2.6.9 CAPILLARY ISOELECTRIC FOCUSING (CIEF)

Imaged capillary isoelectric focusing (cIEF) was conducted using an iCE280 instrument coupled with a PrinCE Microinjector (ProteinSimple, San Jose, CA, USA), where the molecules are detected across the whole IEF column (capillary). UV light at a wavelength of 280 nm was focused on the UV-transparent capillary and images were captured at regular intervals by aid of a charge-coupled device (CCD) camera. Prior to analysis, the fused, silica-coated (FC) cartridge was installed according to the provider's instructions. Reservoirs for the anode were filled with 0.08 M phosphoric acid (in 0.1 % methylcellulose, electrolyte kit, ProteinSimple, San Jose, CA, USA) and for the cathode with 0.1 M sodium hydroxide (in 0.1 % methylcellulose, electrolyte kit, ProteinSimple).

During analysis of Ranibizumab and Bevacizumab (0.5 mg/ml), isoelectric focusing of the samples took place by pre-focusing for 1 min at 1500 V followed by focusing for 5 min at 3000 V. The focusing process was monitored while images were captured every 30 sec. The UV absorption image was analysed using the software ChromPerfect (Version 5.5.6). Protein sample was mixed with carrier ampholytes, methyl cellulose, and water as reported in Table III-4. The sample mixtures were vortexed and spun using a bench top centrifuge (Espresso, Thermo Fisher Scientific, Waltham, MA, USA) for 3 min at 10.000 rpm. An aliquot of 150 µl of the supernatant was transferred into an iCE280 glass vial insert (300 µl, ProteinSimple, San Jose, CA, USA). Finally, the glass vial insert was spun for 1 min at 7.500 rpm to remove air bubbles (potentially causing "spikes" in the electropherogram). Glass vial inserts were then loaded into a sample holder and placed into the temperature-controlled auto sampler.

Table III-4: Overview of experimental conditions and composition of Ranibizumab and Bevacizumab samples used for cIEF.

	Servalytes pH 2-9 [µl]	Low pI marker 5.85 [µl]	High pI marker 10.1 [µl]	MC 1 % [µl]	MQ [µl]	Sample [µl]	Final volume [µl]
Ranibi-zumab	4.0	1.0	1.0	50.0	94.0	50.0	200.0
Bevaci-zumab	4.0	1.0	1.0	50.0	94.0	50.0	200.0

III.2.6.10 FOURIER TRANSFORM INFRARED SPECTROSCOPY (FT-IR)

To determine the conformation of proteins, a Bruker Tensor 27 FT-IR Spectrometer (Bruker Optics, Ettlingen, Germany) equipped with a BIO ATR II cell was used. The mercury cadmium telluride detector was allowed to cool down prior to each measurement by cooling it with liquid nitrogen for one hour. The beam path was purged with nitrogen and the temperature was kept constant at 25°C. Sample concentration was 1.0 mg/ml and 30 µl of sample was used for each determination. Each spectrum was recorded in 100 scans between 1000 cm^{-1} to 4000 cm^{-1} whereat a blank spectrum was subtracted. The collected spectra were Fourier transformed using the Opus software (Version 6.8, Bruker Optics, Ettlingen, Germany). The spectra were further normalised and the second derivative was calculated using the smoothing algorithm with 17 smoothing points. Each sample was recorded in triplicates and mean spectrum was calculated.

III.2.6.11 EXTRINSIC FLUORESCENCE

Extrinsic fluorescence was measured using a Cary Eclipse Spectrofluorimeter (Varian, Santa Clara, CA, USA). Samples were diluted with PBS pH 7.4 to an initial concentration of 100 µg/ml and 50 µl of a 2 mM Bis-ANS solution were added. For measurements, 50 µl were transferred into a submicro fluorescence glass cuvette (Hellma Analytics, Müllheim, Germany). Each

sample was scanned in triplicates in steps of 5 nm with an excitation wavelength of 390 nm and an emission wavelength of 400 nm to 600 nm.

III.2.6.12 INDUCTIVELY COUPLED PLASMA ATOMIC EMISSION SPECTROSCOPY (ICP-AES)

To test the raw materials and implants towards metal impurities, ICP-AES was performed using a ICP AES VISTA RL radial equipped with a CCD dual detector and a SPS 5 auto sampler (Varian, Santa Clara, CA, USA). Prior to analysis, the samples were stored in 10R vials at 4°C. For analysis, approximately 2 mg of sample (accurately weighed) was dissolved in 1.5 ml concentrated HNO_3 at 110°C and was diluted with highly purified water to a final concentration of 3 % [v/v]. Each sample was measured ten times at two different wavelengths to identify possible impurities with aluminium (Al), cobalt (Co), chrome (Cr), copper (Cu), iron (Fe), manganese (Mn), nickel (Ni), lead (Pb) and tin (Zn) against standard solutions of known concentrations. Plasma temperature was set to 10.000 K and flow rate was adjusted to 1.0 ml/min.

III.2.7 ONLINE PRESSURE MEASUREMENT DURING EXTRUSION

To monitor the pressure within the extruder barrel during an extrusion run, the outlet plate was equipped with a custom-made resistance strain gauge (nanoFaktur GmbH, Ettlingen, Germany), which was inserted into the outlet plate (Figure III-6). Thus, it was ensured that the sensor did not change the dimensions of the barrel and had no influence on extrusion performance. It was possible to measure directly the force in real time when the material was pressed against the outlet plate by the rotating screws. The signal of the resistance strain gauge was amplified using a data logger SensorData Easy (Soemer Messtechnik GmbH, Lennestadt, Germany) and was recorded with the software H&B DOP 4P (Hauch & Bach, Lynge, Denmark).

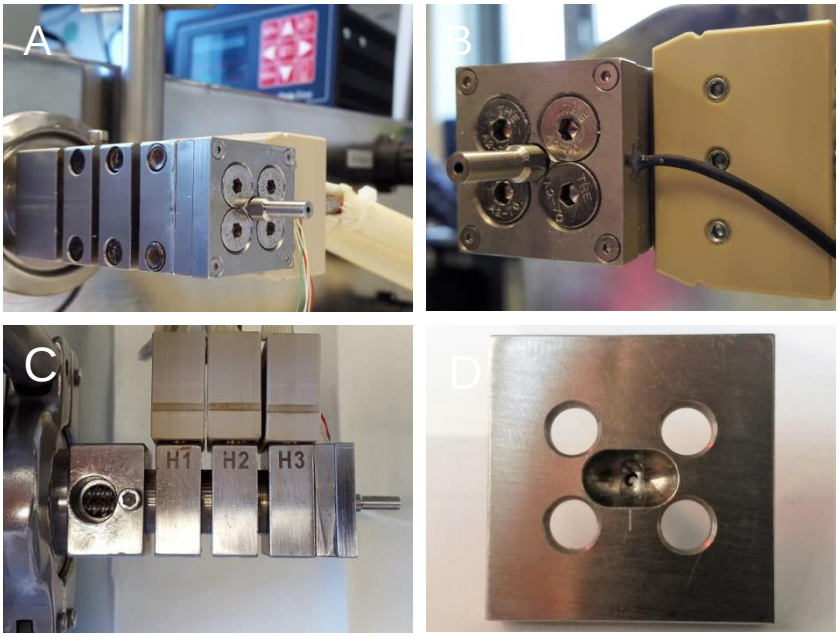

Figure III-6: Images of the barrel of the ZE-5 mini-extruder equipped with the custom-made resistance strain gauge manufactured by nanoFaktur GmbH, Ettlingen, Germany.

For calibration of the sensor, defined weights ranging from 0.5 kg to 50 kg were attached (weights were hanging downwards) to the outlet plate. The correlation between applied weight and read out of the data logger was found to be linear (R^2 = 0.9987) and was converted into extrusion pressure in kPa by dividing the force (in Newton) by the area the material was compressed to ($6.127*10^{-5}$ m^2) shown on Figure III-6 D. For all experiments, extrusion runs were performed in triplicates.

III.2.8 RABBIT ERYTHROCYTE HEMOLYSIS ASSAY

The rabbit erythrocyte hemolysis assay was performed to determine the biological activity of the mini-FH released from SLIs. The protein mini-FH is a C3-opsonin targeted complement inhibitor with a molecular weight of 43.3 kDa [240]. The assay was performed by the group of Dr. Christoph Schmidt from the Institute of Pharmacology and Natural Products and Clinical Pharmacology, Ulm University, Germany, as previously described [241]. In brief, 10 µl human

serum containing Mg-EDTA was mixed with 20 µl sample in PBS pH 7.4 and 10 µl of a rabbit erythrocyte suspension in PBS/Mg-EDTA. The final serum concentration was 25 %. The mixture was incubated for 30 min at 37°C before it was stopped by adding 120 µl PBS/EDTA with a concentration of 5 mM on an ice bath. Hemolysis was determined via optical density measurement of 100 µl of the supernatant at 405 nm using a spectrophotometer.

IV. *IN-VITRO* RELEASE STUDIES FROM LIPID AND PLGA IMPLANTS

PARTS OF THIS CHAPTER HAVE BEEN PUBLISHED IN THE *EUROPEAN JOURNAL OF PHARMACEUTICS AND BIOPHARMACEUTICS* AS:

Moritz Vollrath, Julia Engert, Gerhard Winter

Long-term release and stability of pharmaceutical proteins delivered from solid lipid implants, European Journal of Pharmaceutics and Biopharmaceutics 117 (2017) 244-255

IV.1 INTRODUCTION

Within the last years, controlled release of pharmaceutical proteins from implantable/insertable devices has received more and more attention. The need for such devices can easily be illustrated using the example of intraocular treatment of AMD with anti-VEGF drugs such as Ranibizumab (Lucentis®), Bevacizumab (Avastin®), or Aflibercept (Eylea®). To date, anti-VEGF drugs are the standard treatment for AMD [248], but their frequent application causes high costs on the health care system [30]. Besides the stress for the patient, the required monthly injections - for example of Lucentis® - into the vitreous causes injection-related adverse effects like endophthalmitis [96]. Hence, it would be preferable to prolong the period between two intravitreal injections by using sustained release devices to improve patient convenience, safety, and efficacy. For this study, anti-VEGF drugs were used, namely the recombinant humanised monoclonal IgG_1 antibody Bevacizumab (Avastin®), the f_{ab}-fragment Ranibizumab (Lucentis®) and the recombinant fusion protein Aflibercept (Eylea®). Furthermore, another IgG_1 antibody (model mAb) was used as well.

Since the early 2000s, lipid based drug delivery systems have gained more and more interest as platform for sustained release of proteins [167, 173, 174, 249, 250]. Lipid implants were shown to have excellent properties for *in-vivo* applications as demonstrated by good biodegradability and biocompatibility [184]. Moreover, long-term release of protein drugs was successfully demonstrated: interferon α-2a was delivered for more than 60 days [181], and sustained release of lysozyme was described for more than 200 days [182]. To date, several research groups are working on lipid based depots including implants for sustained erythropoietin release as described by Appel *et al.* [169] and Jensen *et al.* [180], or the intravitreal use of clindamycin phosphate loaded lipidic implants as published by Tamaddon *et al.* or using solid lipid nanoparticles (SLNs) for an immense variety of application possibilities [134, 141, 214, 251, 252].

Preserving the integrity of incorporated proteins such as interferon α-2a [176, 181] or brain-derived neurotropic factor (BDNF) [175], is the most valuable benefit over the commonly used and well investigated PLA/PLGA polymers. Indeed, these polymers provide a biodegradable system as well, but erosion/degradation of the polymer creates difficulties associated with the biodegradation process: a drop in pH and an increase in osmotic pressure, particularly inside the matrix, often results in degradation products caused by acylation, deamidation or aggregation [49, 253, 254], and incomplete release [54, 68, 242, 255].

Within our group, Schulze *et al.* [181] introduced tsc-extrusion as manufacturing technique for lipid implants, which meanwhile became our standard manufacturing technique besides direct compression or casting methods described in early studies [168, 175, 177]. Compared to release profiles of compressed implants, we observed a more sustained release of extruded implants in addition to a more homogenous drug distribution [256]. Tsc-extrusion was already used in several of our studies [182, 183, 233], allowing the manufacturing of triglyceride blends of a low melting and a high melting lipid at comparatively low temperatures of 42°C [181, 183].

The overall aim of the present chapter was to establish formulation and extrusion settings which result in an implant that ensures a long-term release of at least 3 months and is sufficiently small for intravitreal use. To reach this goal, the following steps were performed:

(i) reproduction: Reproduction of existing data [232] as a proof of concept using a MiniLab® Micro Rheology Compounder.

(ii) transfer: A transfer from a MiniLab® Micro Rheology Compounder to a ZE-5 mini-extruder to reduce the batch size was carried out.

(iii) optimisation: As the release profile was not identical for the same formulation extruded on different extruders, the formulation and extrusion settings were adapted to the ZE-5 mini-extruder.

(iv) increase of protein load: Since an adequate amount of drug substance should be provided when release time frames of several months are considered,

increasing protein load was attempted by three different approaches. The increase of the protein lyophilisate percentage, the change of protein lyophilisate composition, and the change of implant diameter were tested.

(v) Storage stability: storage stability of extruded SLIs was determined to ensure that implants guarantee comparable release characteristics particularly after storage. Therefore, lipid implants were stored for 4 and 12 weeks after production at 4°C prior to *in-vitro* release. Due to potential changes in lipid modifications occurring upon storage, lipid characteristics were also assessed. Protein stability of released protein of stored and non-stored was analysed as well and will be presented in chapter VII.

(vi) Pre-melting of lipids: The effect of melting point, melting energy and lipid modifications on release patterns and storage stability of SLIs was studied. For this, H12 and D118 were simultaneously molten at 80°C, the molten mass was allowed to cool down before it was ground and sieved (< 180 µm) prior to extrusion.

Additionally, PLGA based extrudates were produced using different polymers (Resomer® RG 502, RG 502 H and RG 755 S) in order to compare those data with release profiles obtained from SLIs. PLGAs with different degradation time frames were used for two reasons: first, to evaluate the impact of depot erosion in addition to diffusion and second, to determine the impact of different end groups on release profiles. Protein stability aspects of protein released from lipid and PLGA matrices will be addressed within chapter VII.

IV.2 Results and Discussion

IV.2.1 Lyophilisate stability study

SLIs were produced via tsc-extrusion where the protein was embedded within the lipid matrix as a lyophilisate. HP-β-CD was used as lyoprotectant to assure protein stabilisation during freeze drying and storage as reported previously for rh-interferon α-2a [176] and erythropoietin [242]. Furthermore, it was described by Ressing *et al*. that HP-β-CD increased stability and activity of IgG antibodies compared to samples which were formulated with dextran or sucrose [257]. The stability of the proteins within the freeze-dried matrix was determined to ensure sufficient protein stability at the point of SLI production. The stability of freeze-dried protein was investigated over 24 weeks since stability of released protein was extensively studied within this work (chapter VII). However, produced lyophilisates were used within 8 weeks.

IV.2.1.1 Dialysis and lyophilisation

The protein bulk was dialysed as described above (III.2.1.1) to deplete the formulations of buffer salts and stabilisers and to substitute them with 50 mM sodium phosphate pH 6.2.

Table IV-1: Monomer content of the protein bulk (mAb), marketed formulation and after dialysis.

	Monomer content before dialysis [%]	Monomer content after dialysis [%]
mAb	97.74 (±0.15)	97.42 (±0.19)
Ranibizumab	99.97 (±0.01)	100.00 (±0.00)
Bevacizumab	96.10 (±0.56)	95.37 (±0.06)
Aflibercept	98.62 (±0.06)	98.56 (±0.01)

This was essential because all proteins were formulated with different stabilisers (III.1.1) which could potentially have an impact on release behaviour, for instance trehalose, sodium chloride, or sucrose.

After dialysis, the monomer content was measured by SE-HPLC showing no negative impact caused by the dialysing procedure (Table IV-1). The protein concentration within the dialysed formulations was adjusted to 10 mg/ml and HP-β-CD was added to obtain a ratio of 1:1 [w/w], 2:1 [w/w] or 3:1 [w/w].

IV.2.1.2 PHYSICAL STABILITY OF PROTEINS

Freeze-dried samples were stored at 4°C for 24 weeks and samples were taken at pre-determined time points after 2, 4, 8, 12 and 24 weeks. Lyophilisates were reconstituted with highly purified water (0.2 µm filtered) to obtain a protein concentration of 1.0 mg/ml.

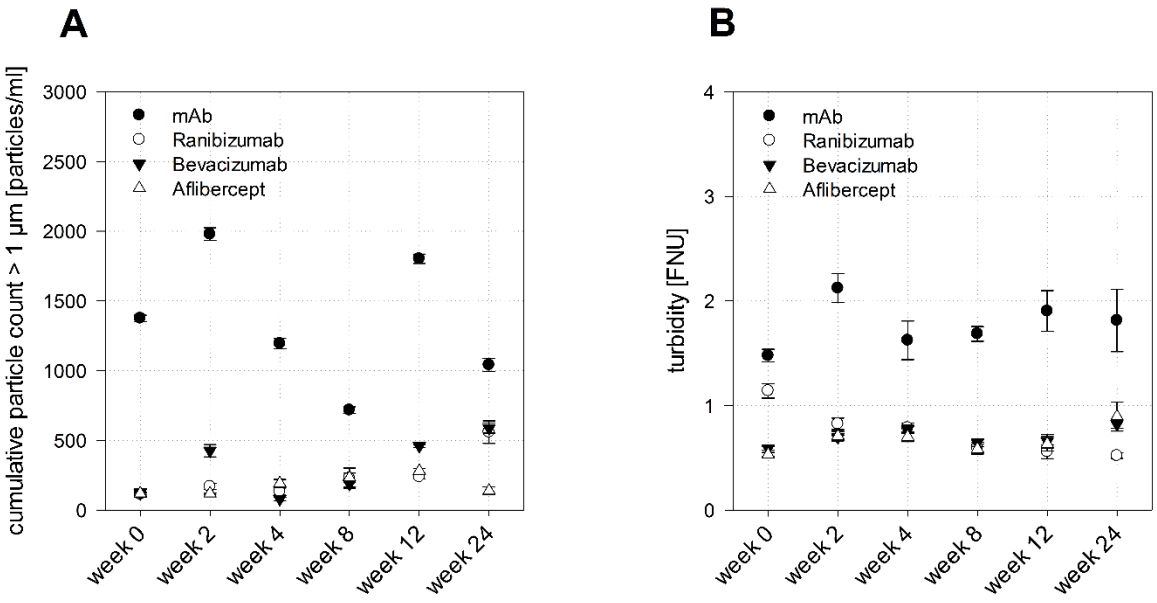

Figure IV-1: (A) Light obscuration measurements and (B) turbidity measurements of reconstituted samples measured after 0, 2, 4, 8, 12 and 24 weeks of storage at 4°C.

The formation of subvisible particles upon storage was measured using LO and turbidity (Figure IV-1). The samples were not diluted prior to measurements. For mAb, cumulative particle count and turbidity was found to have the highest values ranging between 716 (±24) and 1979 (±46) cumulative particle count per ml and 1.47 FNU (±0.06 FNU) and 2.12 FNU (±0.14 FNU) turbidity over the observation period. An increase in cumulative particle count and turbidity upon storage

was not observed. This also applies to Aflibercept, where no increase of both cumulative particle count and turbidity was observed. LO results for Ranibizumab and Bevacizumab showed a continuous increase, starting after approximately 8 weeks of storage and a final maximal particle count of 559 (±81) for Ranibizumab and 587 (±36) for Bevacizumab after 24 weeks of storage. The corresponding turbidity measurements after 24 weeks where measured at 0.52 FNU (±0.03 FNU) and 0.89 FNU (±0.14 FNU). Turbidity measurements did not show a continuous increase over the storage period.

Table IV-2: Monomer content before lyophilisation and after reconstitution of the lyophilisates with highly purified water (0.22 µm filtered) at week 0 and week 24.

	Monomer content before lyophilisation [%]	**Monomer content at week 0 after lyophilisation [%]**	**Monomer content at week 24 after lyophilisation [%]**
mAb	97.74 (±0.15)	97.55 (±0.06)	96.01 (±0.05)
Ranibizumab	99.97 (±0.01)	100.00 (±0.00)	100.00 (±0.00)
Bevacizumab	96.10 (±0.56)	95.45 (±0.04)	94.26 (±0.69)
Aflibercept	98.62 (±0.06)	98.33 (±0.02)	97.89 (±0.29)

Table IV-2 illustrates the monomer content of samples before lyophilisation and after reconstitution directly after the freeze-drying run (week 0) and after a storage of 24 weeks at 4°C. There is no major difference in monomer content before and after lyophilisation, meaning that the lyophilisation process did not negatively impacted protein stability. Upon storage of the freeze-dried product, the monomer content decreased maximally by 1.54 % for mAb. Ranibizumabs` monomer content stayed constantly at 100 %. In addition to SE-HPLC, non-reducing SDS-PAGE was performed to determine possible aggregates and fragments which were not detected by SE-HPLC. For mAb, the loss of 1.54 % monomer upon storage was most likely caused by aggregation rather than fragmentation, as aggregates having a size of approximately 250 kDa were observed (Appendix, Figure XII-1). The same trend was observed for Bevacizumab and Aflibercept. For both proteins, aggregates with an approximate size of

260 kDa (Bevacizumab) and 224 kDa (Aflibercept) were detected directly after lyophilisation (Appendix, Figure XII-3 and Figure XII-4). In contrast, for Ranibizumab mainly fragments with a size of about 25 kDa were detected (Appendix, Figure XII-2) but no aggregation occurred over the storage period. However, for all proteins degradation was found to be negligible.

Based on the results for physical stability assessed by LO, turbidity, SE-HPLC and SDS-PAGE, it can be concluded that all proteins were physically stable over the storage period of 24 weeks. Slightly elevated particle counts were observed for Ranibizumab and Bevacizumab as well as minor degradation products for all proteins obtained by SDS-PAGE. Since the lyophilisates were further processed within 8 weeks, physical stability was considered as sufficient.

IV.2.1.3 Chemical stability of proteins

In addition to physical stability, lyophilisates were further analysed towards chemical stability. After reconstitution with 0.22 µm filtrated highly purified water to a concentration of 1.0 mg/ml, chemical stability was measured by IEX (mAb and Bevacizumab) and HIC (Ranibizumab and Aflibercept) and the change of main charge variant percentage was determined. Samples were analysed directly after lyophilisation and after a 24-week storage showing a small decrease of main charge variant percentage for all proteins.

Table IV-3: Percentage of main charge variant after reconstitution of the lyophilisates with highly purified water (0.22 µm filtered) at week 0 and week 24.

	Percentage of main charge variant at week 0 [%]	**Percentage of main charge variant at week 24 [%]**
mAb	43.79 (±0.61)	41.37 (±0.05)
Ranibizumab	99.37 (±0.02)	96.22 (±0.20)
Bevacizumab	70.83 (±1.24)	68.12 (±0.95)
Aflibercept	95.91 (±0.35)	95.02 (±0.30)

Table IV-3 illustrates that Ranibizumab samples showed highest loss after 24 weeks (3.15 % ±0.20 %), whereas the main charge variant of Aflibercept decreased only by 0.89 % (±0.30 %). The chemical stability was considered as sufficient because the lyophilisates were further processed within 8 weeks.

IV.2.2 EXTRUDER TRANSFER

The sustained long-term release of a mAb was already described by Sax over a period of approximately 150 days [232]. First, an experiment was carried out to reproduce these data. All formulation and extrusion parameters were adjusted exactly to those used within the previous experiments. SLIs consisted of 10 % protein lyophilisate, 10 % PEG 6000 lyophilisate, 24 % H12 and 56 % D118. Extrusion temperature was set to 41°C at a screw speed of 40 rpm using a MiniLab® Micro Rheology Compounder (Thermo Haake GmbH Karlsruhe, Germany). *In-vitro* release was executed at 37°C.

Sax reported on a sustained release of mAb over 150 days in a linear fashion without any burst events [232]. Figure IV-2 A represents the release profile obtained by the reproduction experiment. The mAb was released in an almost linear manner over approximately 170 days. An initial burst release was not observed. Both release curves of mAb - reported in 2012 by Sax and described within the present work - are comparable to each other, leading to the conclusion that tsc-extrusion as preparation method can be considered as reliable and reproducible.

The main drawback of the MiniLab® Micro Rheology Compounder is a minimal batch size of approximately 5 g. To reduce the batch size from 5 g to 1 g, the identical formulation was extruded using a ZE-5 mini-extruder from Three-Tec (Seon, Switzerland), to test if the developed formulation was transferable to a different extruder ensuring the same release patterns.

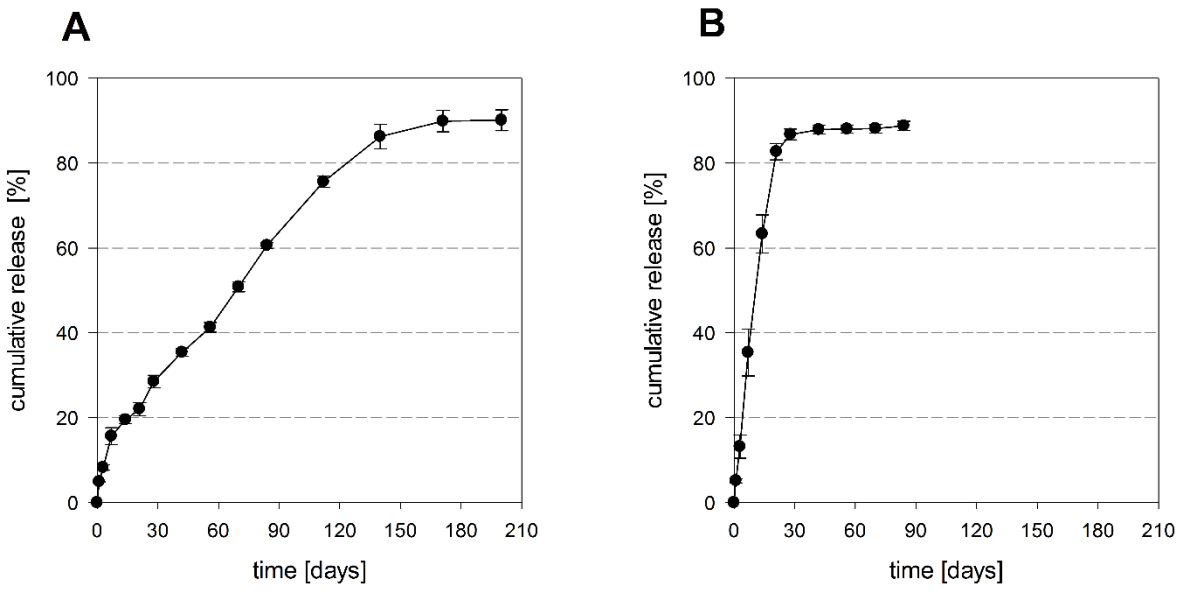

Figure IV-2: *In-vitro* release of mAb from SLIs extruded using a (A) MiniLab® Micro Rheology Compounder and a (B) ZE-5 mini-extruder from Three-Tec. Formulation of SLIs and extrusion settings were identical.

Therefore, the exact formulation listed above was extruded with identical settings used before. The release profile of mAb is illustrated in Figure IV-2 B. A linear release over the first 28 days delivering approximately 85 % of total incorporated protein can be observed, followed by a phase where no more protein was delivered. Comparable release profiles using both extruders were not achieved. To clarify why release rates were so dramatically different, SLIs were further investigated towards mechanical properties and optical appearance.

Compressive strength and true density of implants were determined. The results are depicted in Table IV-4, showing that both compressive strength and true density were lower for SLIs manufactured with the ZE-5 mini-extruder. This points into the direction that implants were compressed less with the ZE-5 mini-extruder compared to the MiniLab® Micro Rheology Compounder (for further details on considerations about extrusion pressure and its impact on release patterns, please see chapter IX). This allows the incubation medium to penetrate faster into the lipid matrix and may be one explanation for the accelerated release.

Table IV-4: Compressive strength and true density of SLIs manufactured with both extruders. Formulation and extrusion parameters were identical.

	Compressive strength [N]	True density [g/cm^3]
MiniLab® Micro Rheology Compounder	1.75 (±0.072)	1.085 (±0.005)
ZE-5 mini-extruder	1.42 (±0.015)	1.069 (±0.002)

To prove this hypothesis, SEM micrographs of freshly extruded SLIs were acquired (Figure IV-3). The surface of SLIs manufactured with the MiniLab® Micro Rheology Compounder were characterised by a non-porous and smooth surface without obvious irregularities (the irregularities which can be seen in the right lower part of Figure IV-3 A are due to breakage caused by handling).

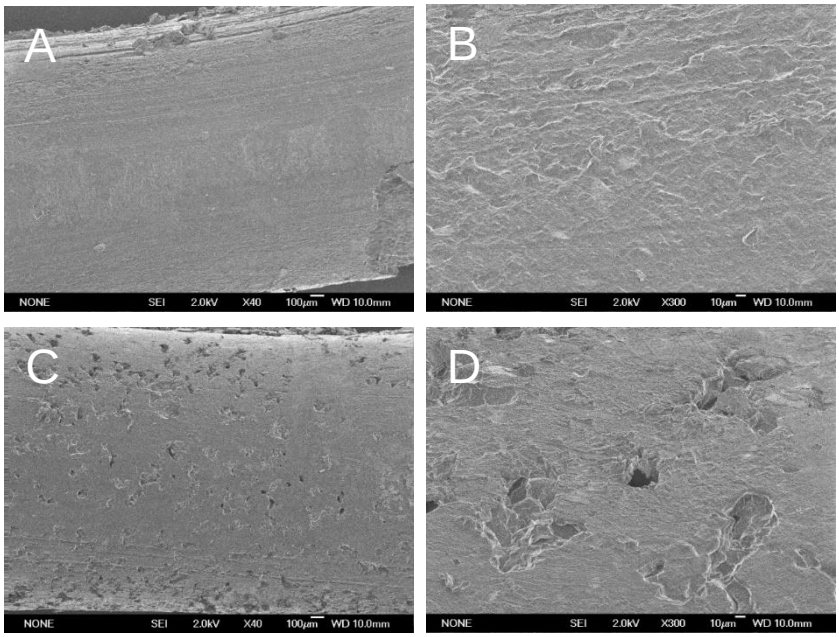

Figure IV-3: SEM micrographs of SLIs extruded with a (A and B) MiniLab® Micro Rheology Compounder and (C and D) a ZE-5 mini-extruder from Three-Tec. Displayed are implants` surfaces at a magnification of 40x and 300x.

Only at a magnification of 300x, the surface appeared slightly rough and uneven; the platelet-like structures are non-molten lipids (Figure IV-3 B). In contrast, SLIs produced with the ZE-5

mini-extruder exhibited a surface with numerous pores and channel-like structures. Looking more closely on surface morphology, pores with a size of approximately 20 µm were present as well as irregularities with a diameter of up to 80 µm (Figure IV-3 D).

IV.2.3 SETUP OPTIMISATION ON ZE-5 MINI-EXTRUDER

Since the release of mAb was accelerated and implant properties were found to be different when extruding the identical formulation on different extruders, optimisation was necessary.

It was aimed to increase the pressure within the extruder barrel by the following approaches: (i) elongating the outlet die, (ii) using a smaller outlet die and (iii) increasing the screw speed. Release experiments were performed with mAb only and were discontinued after 28 days because difference in release was already noticeable after this time.

IV.2.3.1 ELONGATION OF OUTLET DIE

In a first approach, the outlet die of the barrel was elongated (Figure IV-4). With respect to fluid mechanics, it is understood that an elongation should lead to an increase in pressure within the barrel and therefore generating a denser lipid matrix releasing the mAb in a slower fashion.

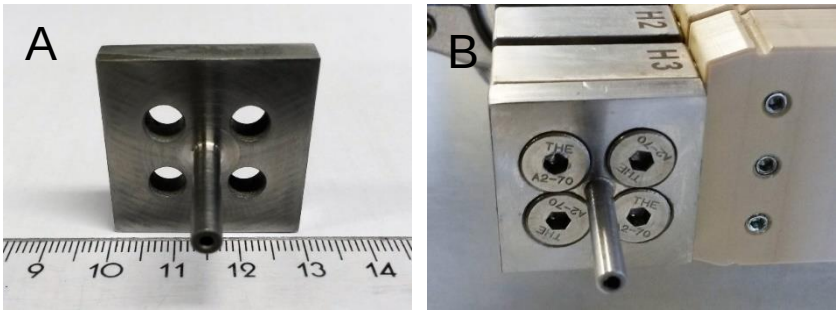

Figure IV-4: Pictures of the outlet plate of the ZE-5 mini-extruder with elongated outlet die. The elongated outlet die was custom-made and was produced by the LMU workshop.

The formulation and extrusion parameters were kept as before: 10 % protein lyophilisate, a lipid matrix of 30 % H12 and 70 % D118. Extrusion was performed at 41°C at 40 rpm. Importantly, already at this early stage of setup optimisation, PEG 6000 was avoided, as it can promote protein degradation [258, 259]. This represents one of the major advantages of the lipid implants described here.

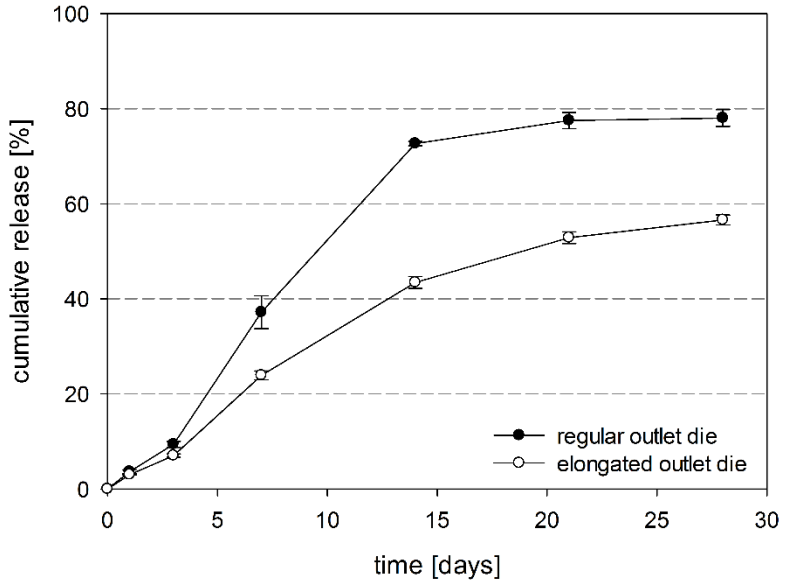

Figure IV-5: Cumulative release of mAb delivered from SLIs with a diameter of 2.0 mm. The extruder barrel was either equipped with or without an additional elongation of the outlet die.

As Figure IV-5 indicates, release rate of mAb was slowed down by equipping the outlet plate with an additional elongated outlet die, especially within the first days. For instance, after 7 days, 37.2 % mAb was liberated compared to 23.9 % when the extruder was equipped with the elongated outlet die. Although it was possible to slow down the release, it was intended to tailor release further. Therefore, the implant diameter was reduced to increase pressure within the barrel even more.

IV.2.3.2 REDUCTION OF IMPLANT DIAMETER

The implant diameter was reduced from initially 2.0 mm to 0.8 mm for two reasons: first, by increasing the pressure within the barrel, a further slowdown was intended and second, to obtain implant dimensions suitable for intraocular use.

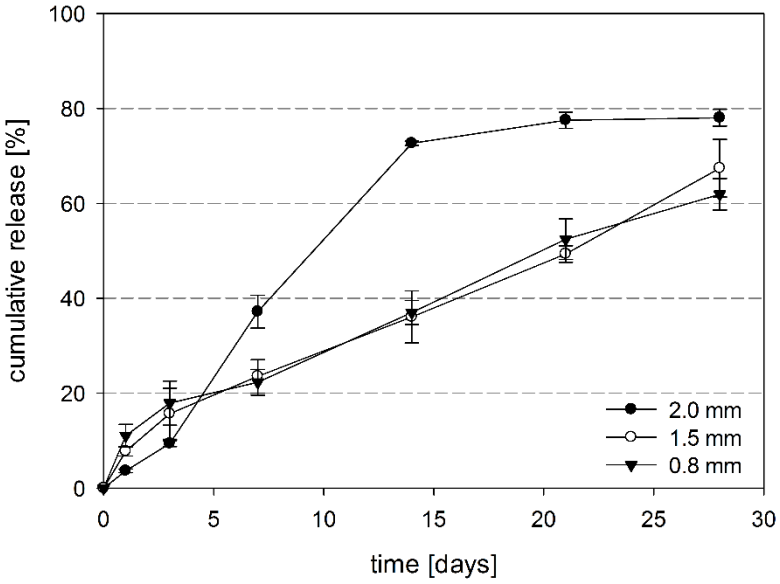

Figure IV-6: Cumulative release of mAb delivered from SLIs with different diameters ranging from 2.0 mm to 0.8 mm. The outlet plate was equipped with an additional elongation of the outlet die.

By reducing the implant diameter, it was possible to reduce the release further and additionally linearise it. For both implant diameters, 1.5 mm and 0.8 mm, a linear release over the first 28 days was observed. However, because the cumulative percentage of mAb released was only reduced by 14 % (78.0 % for 2.0 mm compared to 61.9 % for 0.8 mm) after 28 days, optimisation of extrusion settings was further continued.

IV.2.3.3 ADJUSTMENT OF SCREW SPEED

Adjustment of screw speed was performed with 1.5 mm implant diameter because protein load was too low for 0.8 mm diameter, especially when considering long-term release of several months.

The screw speed was varied from 10 rpm to 80 rpm, meanwhile all other extrusion parameters were not changed. Figure IV-7 illustrates the impact on the release of mAb: the slowest release can be observed for 40 rpm (22.3 % after 7 days). After 7 days, 72.5 % mAb was released at 80 rpm and 39.8 % at 10 rpm. Thus, it can be concluded that for this specific formulation using the ZE-5 mini-extruder the optimal extrusion settings were so far identified. The reason for the faster *in-vitro* release from implants extruded at 60 rpm and 80 rpm was most likely that implants were more porous comparing to slower screw speeds. This aspect is described within chapter IX.3.3.2.

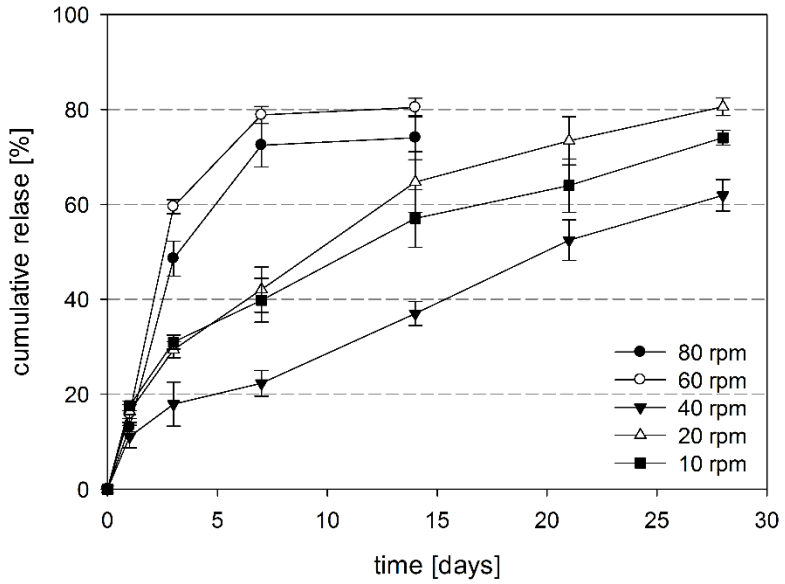

Figure IV-7: Cumulative release of mAb delivered from SLIs using different screw speeds ranging from 10 rpm to 80 rpm. The outlet plate was equipped with an additional elongation of the outlet die.

As an interim summary, it can be stated that all adjustments improved the release profile of mAb as the release rate was slowed down and release was linearised. However, since the release

rate was still too fast and far away from the desired 3 months, it was decided to change the system more profoundly by changing the lipid composition.

IV.2.3.4 CHANGE OF LIPID COMPOSITION

While changing the lipid composition of the extrudates, the percentage of protein lyophilisate was kept constant at 10 % and screw speed was adjusted to 40 rpm. First, lipid composition was changed from 30 % H12 stepwise to 50 % H12 (reduction of D118 from 70 % to 50 %) at a constant extrusion temperature of 41°C (Figure IV-8 A). Then, at a lipid composition of 50:50, the extrusion temperature was reduced from 39°C to 37°C and 35°C (Figure IV-8 B). For this experiment, release of mAb was monitored over 14 days.

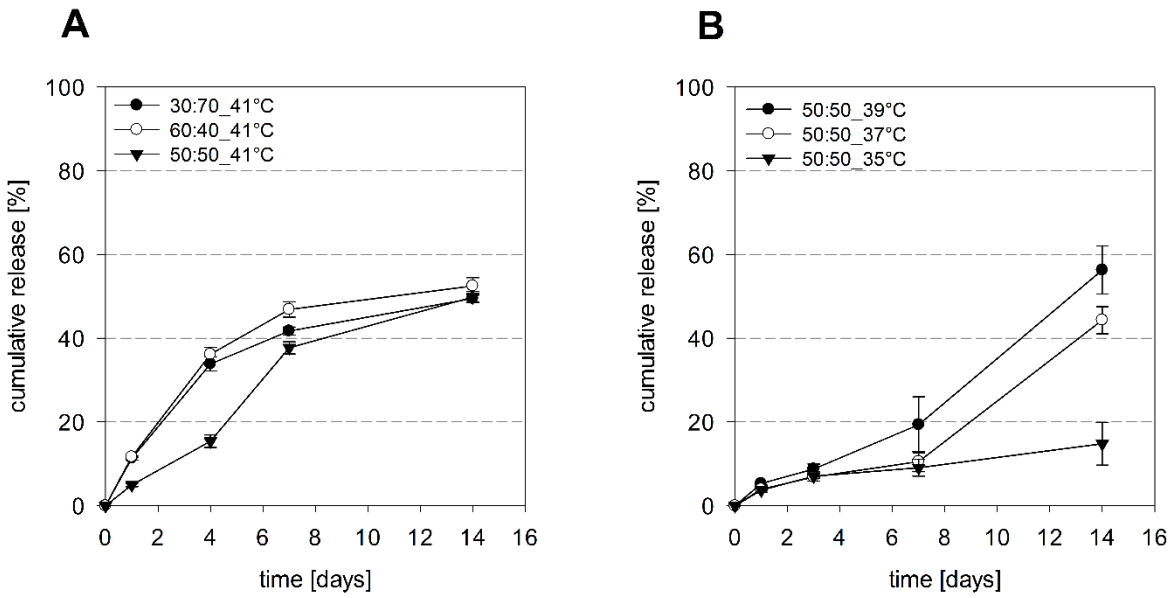

Figure IV-8: Cumulative release of mAb from SLIs consisting either of (A) different lipid compositions applying the same extrusion temperature or (B) a 50:50 lipid blend extruded at 39°C, 37°C or 35°C.

In Figure IV-8 A the release profiles of mAb delivered from SLIs consisting of different lipid matrices are depicted. The most promising release was observed for the 50:50 formulation, as especially during the initial phase a very slow release was observed. The overall release after

14 days was comparable, but due to the very slow release within the first days, the 50:50 formulation was chosen for further investigations.

The 50:50 formulation was therefore extruded at different temperatures ranging from 35°C to 39°C. A lower extrusion temperature was not feasible, as no continuous and homogenous lipid strand was formed. Higher extrusion temperatures than 41°C resulted in a molten lipid mass not forming a solid matrix. Slowest release of mAb was detected for an extrusion temperature of 35°C: after 14 days, only 14.8 % mAb were released compared to 56.3 % when 37°C were applied.

It was also tested if the H12 percentage could be increased even more (up to 90 %), but it turned out that a too high percentage of H12 leads to a disintegration of SLIs at the incubation temperature of 37°C, resulting in burst release (data not shown). Therefore, the optimal formulation and extrusion settings were identified as: 10 % protein lyophilisate, 45 % H12, 45 % D118 extruded at 35°C and 40 rpm.

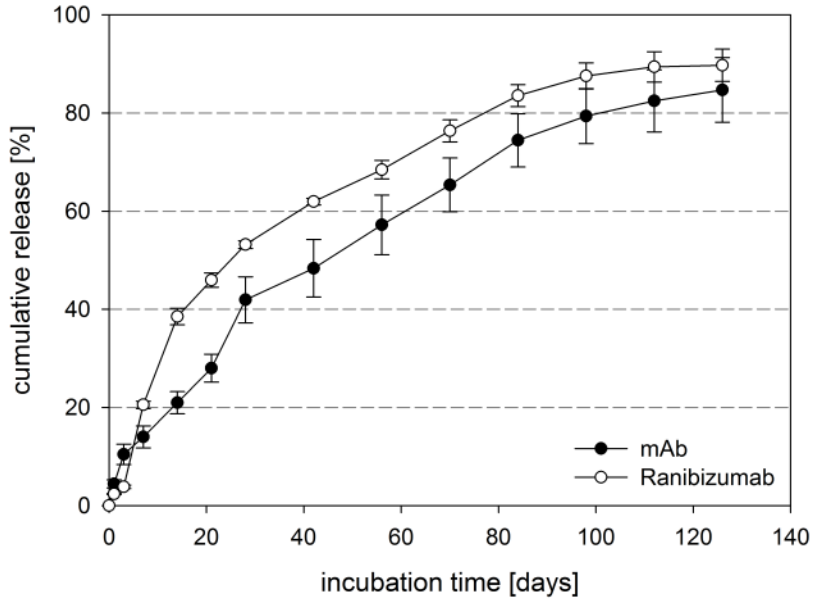

Figure IV-9: Cumulative release of mAb and Ranibizumab from SLIs consisting of a 50:50 lipid blend. Extrusion temperature was set to 35°C and screw speed was 40 rpm. The protein load was set to 5 % resulting in 1.53 mg (±0.06 mg) protein per implant.

This setup was also tested incorporating Ranibizumab into SLIs (Figure IV-9). Appropriate release profiles over 126 days for both tested proteins were obtained from a formulation consisting of 45 % H12 and 45 % D118 with 10 % protein lyophilisate (1:1 [w/w]), resulting in a protein load of 1.53 mg (±0.06 mg) per implant. The release profile of mAb is characterised by triphasic release behaviour without any initial burst release. An initial phase for the first 28 days, releasing approximately 22.9 µg protein per day, is followed by a phase lasting from day 28 to day 100 where in average 8.2 µg/day protein was released. During the last phase, (lasting from day 100 until day 126) only small amounts of protein were released (approximately 5 %; 2.7 µg/day). In total, approximately 85 % of incorporated protein was released.

Results from the Ranibizumab release study showed qualitatively the same triphasic release behaviour (Figure IV-9). During the first phase lasting for 4 weeks, 53 % of incorporated protein was released (28.9 µg/day) followed by an almost linear phase lasting from day 28 to day 110 in which approximately 34% of incorporated protein (equivalent to 6.5 µg protein per day) was liberated. In general, Ranibizumab release was faster compared to mAb and discontinued after 110 days at approximately 90 % of total protein amount. For both proteins, no burst release occurred.

Lipid implants were intentionally formulated without any pore forming agents. This, however, raises the question how proteins were set free. Even if the lipid matrix was strongly compressed, compacted and molten together by the extrusion process and applied temperature, micro-channels and tiny pores were still present, allowing the incubation medium to penetrate into the matrix as observed by SEM (Figure IV-10). Micrographs of the surface, taken with a magnification of 40x, showed a dense and smooth surface (Figure IV-10 A). Small pores having a size of 5 µm to 10 µm can be observed at 300x as displayed in Figure IV-10 C. Slightly larger pores and channels ranging between 10 µm to 25 µm can be found in the cross-section micrographs (Figure IV-10 D). Based on these observations, it can be assumed that the lipid implants contained an interconnected pore network, even if no pore forming agents were

incorporated. The protein lyophilisate itself will generate channels and pores *in-situ* due to its water solubility.

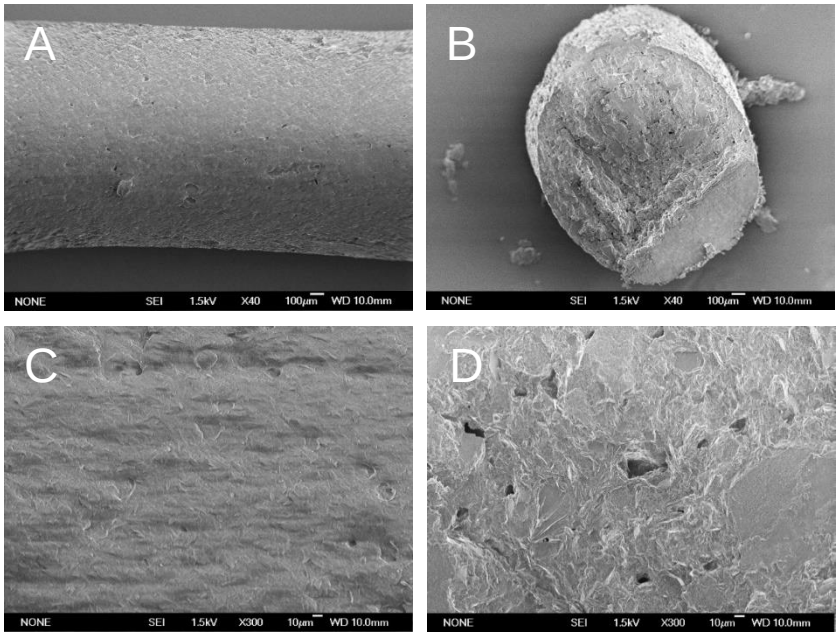

Figure IV-10: SEM micrographs of the surface and cross-section of lipid implants after extrusion and prior to incubation are shown. Micrographs (A) and (C) displaying the surface of the implant at magnifications of 40x and 300x, (B) and (D) are the corresponding micrographs of the cross sections, also taken at 40x and 300x.

IV.2.3.5 DISCUSSION OF PROPERTIES OF THE LEAD FORMULATION

In previous studies, a matrix with a protein load of 10 % protein lyophilisate, 10 % PEG 6000, 24 % H12 and 56 % D118 [181, 182] was extruded at 41°C and showed promising long-term release of lysozyme [182] and a monoclonal antibody [232] and was therefore the starting point for our study. Based on this formulation, screening studies were performed to identify the most promising formulation and settings on the ZE-5 mini-extruder. The most appropriate formulation for the ZE mini-extruder comprised 10 % protein lyophilisate and a lipid matrix consisting of 50 % H12 and 50 % D118; no PEG was added. An adequate extrusion temperature was determined at 35°C. Thus, a manufacturing setup was established to ensure the production of

SLIs which provide a constant and almost complete release (up to 95 %) of incorporated protein without any burst effects.

The intentional absence of PEG as a precipitant represents one of the major features of the developed formulation. It has been reported that PEG can slow down the release and minimise the initial burst due to precipitating events [177]. Sax *et al.* [182] already demonstrated that long-term release of proteins from SLIs without addition of PEG is feasible. The controlled release of lysozyme was reported for 230 days in which 80 % of protein was released. This study was performed with the rather small and robust protein lysozyme. Now, we demonstrated that SLIs can be produced without any further excipients showing no initial burst and ensuring long-term release of more complex and sensitive molecules such as monoclonal antibodies. Furthermore, as PEG can promote protein degradation [258, 259], avoiding PEG is favorable concerning protein stability, especially when release time frames of several months are considered. Furthermore, a reduction of the extrusion temperature to 35°C is beneficial as it reduces thermal stress on the protein.

The observed release curves of the proteins are a result of different release mechanisms complementing each other. It is well known that release from lipid matrices is mainly controlled by diffusion, (see Guse *et al.* and Koennings *et al.* [158, 260]). Furthermore, release can be influenced by the addition of hydrophilic pore forming agents, e.g. PEG [160, 177, 178] or trehalose [216] to modify release patterns. Once the implant is placed into the incubation medium, hydrophilic components dissolve quickly and are released through an interconnected pore-network. In 2012, Sax *et al.* described an additional release pathway of proteins from a lipid matrix which relies on a partial melting of the low melting lipid within the matrix [182]; the molecules diffuse in a phase of molten lipid [234]. It was shown, that both melting points (T_{onset} and $T_{melting}$) of the low melting lipid are very important parameters playing a major role in triggering protein release. Due to the similarity of our lipid matrix described here with the system Sax *et al.* characterised, we assume that also in our study T_{onset} and $T_{melting}$ of the low melting lipid are crucial parameters affecting release patterns. Therefore, the obtained long-term

release profiles for mAb and Ranibizumab are most likely an interplay of different release mechanisms mentioned above.

IV.2.4 INCREASE OF PROTEIN LOAD

Since an adequate amount of drug substance should be provided when release time frames of several months are considered, an increase of protein amount per implant was intended. Increasing protein load was attempted by three different approaches: (i) increase of the protein lyophilisate percentage, (ii) change of protein lyophilisate composition and (iii) change of implant diameter.

IV.2.4.1 PROTEIN RELEASE FROM IMPLANTS WITH INCREASING AMOUNTS OF PROTEIN LYOPHILISATE

With a protein load of 5 % and the minimal dimensions of the implants, total protein content of one single implant was on average approximately 1.53 mg. The percentage of protein was increased stepwise from initially 5 % to 7.5 % and 10 % to encapsulate more protein per implant. Lyophilisates comprised a mixture of protein and HP-β-CD in a ratio of 1:1 [w/w]. Consequently, the amount of lipids was reduced from 90 % to 80 %, while the lipid composition and extrusion settings were kept constant.

With increasing amounts of protein lyophilisate, the release of proteins was accelerated. For mAb, a substantial burst release was seen for the formulations containing 7.5 % and 10 % protein, respectively: after 1 day, 22.0 % mAb was released from the formulation comprising 7.5 % protein, whereas 23.1 % protein was quantified released from the formulation with 10 % mAb (Figure IV-11 A). For comparison, after 1 day only 4.4 % mAb was released from the lead formulation. Release stopped after 56 days of incubation for the formulations with 7.5 % and 10 % protein content between 85 % to 87 % of total protein load.

Ranibizumab release from the different formulations is illustrated in Figure IV-11 B. The release profiles for the formulations with 7.5 % and 10 % protein load were characterised by a high initial burst release: 12.8 % (7.5 % protein load) and 17.9 % (10 % protein load) were already released after 1 day compared to the lead formulation with 5 % protein content (2.3 % after 1 day). Additionally, release stopped 6 weeks earlier when protein content was increased.

Bevacizumab release was also accelerated with increasing lyophilisate percentage as illustrated in Figure IV-11 C. The comparatively short release duration of approximately 21 days for the lead formulation was even accelerated, especially during the first days of release. After 1 day, 38.8 % and 47.5 % were released from the formulations containing increased lyophilisate percentages compared to 11.8 % released from the lead formulation. Additionally, release stopped already after 14 days (7.5 % protein load) and 7 days (10 % protein load).

Qualitatively, similar observations were made for Aflibercept release, showing a faster release with increasing percentage of protein lyophilisate (Figure IV-11 D).

In summary, for all proteins release was observed to be faster, especially during the initial phase. Therefore, this attempt was not further pursued. The more water soluble lyophilisate generated a larger pore-network *in-situ* by dissolution leading to faster release rates. This is in accordance with previous results described by Mohl *et al.* for interferon α-2a [167]. Up to 20 % of PEG 6000 was added to the lipid matrix before lipid implants were manufactured by compression. The same phenomena was also observed by Sax *et al.* for lysozyme [182] where a higher proportion of PEG 4000 resulted in faster release rates. However, care must be taken when considering pore-forming effects of excipients, especially in terms of PEGs. The addition of PEG can lead to either an *in-situ* precipitation of the protein [178] or a larger pore-network [177] depending on the protein. The increase of lyophilisate exclusively generates a larger pore-network.

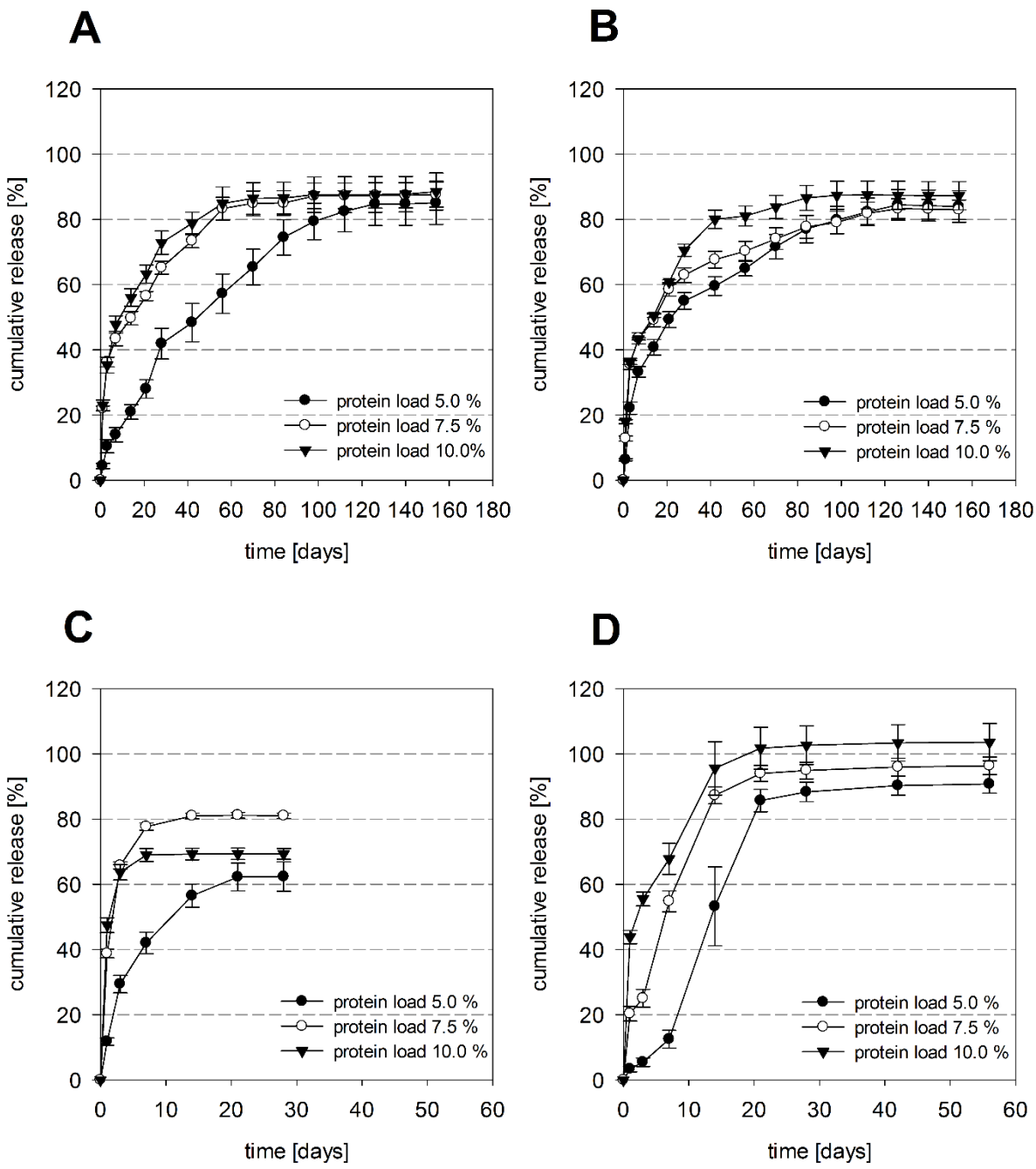

Figure IV-11: Cumulative release of (A) mAb, (B) Ranibizumab, (C) Bevacizumab and (D) Aflibercept from SLIs. Lipid implants were produced with different percentages of protein lyophilisate in a 1:1 [w/w] formulation with HP-β-CD resulting in a final protein load of 5 %, 7.5 % and 10 % per implant. Please note that the x-axis is scaled differently.

IV.2.4.2 PROTEIN RELEASE FROM LIPID IMPLANTS WITH DIFFERENT LYOPHILISATE COMPOSITIONS

In a next attempt, the composition of the protein lyophilisate was changed to increase protein load per implant. The protein ratio within the lyophilisate was increased from 50 % to 75 %, whereas the percentage of lipid portion was retained constant at 90 %. Due to the poor release patterns of Bevacizumab and Aflibercept, the following experiments were carried out with mAb and Ranibizumab only.

Figure IV-12 A and Figure IV-12 B display the release of mAb and Ranibizumab with lyophilisate formulations 1:1 [w/w] and 3:1 [w/w]. This time, the sustained release profiles were not significantly altered (no burst observed), and sustained release lasted equally long as for the low dose lead formulation. By changing the lyophilisate composition, 50 % more protein could be incorporated into the lipid implant without negatively affecting the release patterns.

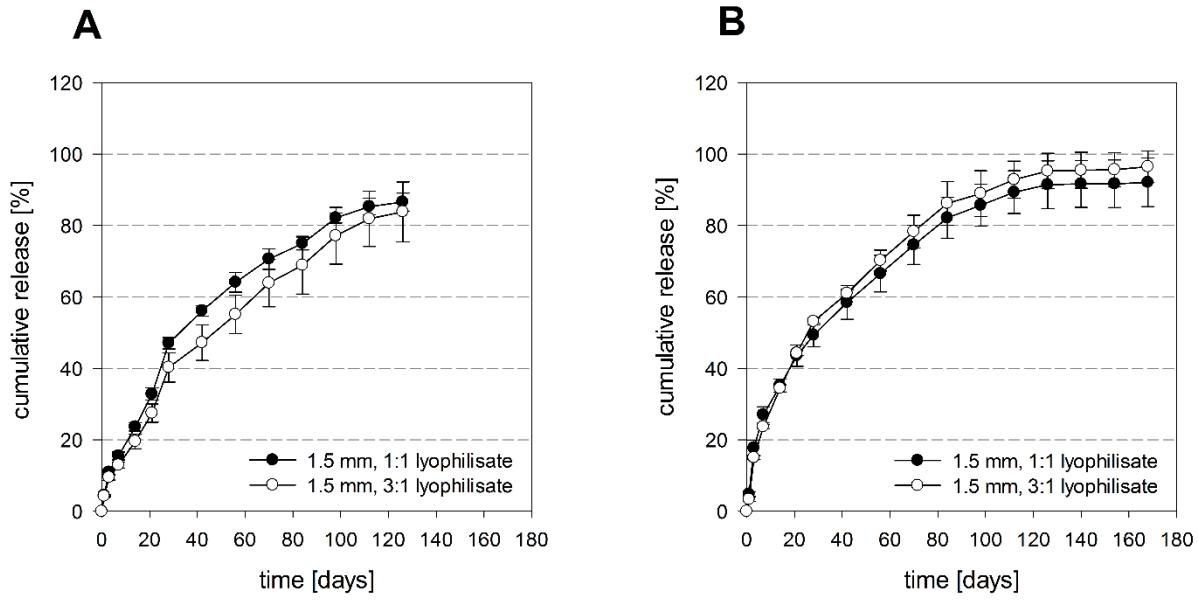

Figure IV-12: Cumulative release profiles of (A) mAb and (B) Ranibizumab from lipid implants. Protein lyophilisate percentage was kept at 10 % while the lyophilisate formulation was changed from 1:1 [w/w] protein:cyclodextrine ratio to 3:1 [w/w]. Protein load per implant was thus increased from 1.53 mg (±0.06 mg) to 2.40 mg (±0.23 mg).

The ratio of water-soluble (lyophilisate) to water insoluble (lipids) components stayed constant. Consequently, the micro structure of the lipid implant (pores and interconnected channels) of the implant was retained better. Figure IV-13 shows that both formulations, either comprising the 1:1 [w/w] protein lyophilisate (Figure IV-13 A) or the 3:1 [w/w] protein lyophilisate (Figure IV-13 B) have a comparable appearance of the micro structure in the cross sections. Due to a reduction of the stabilising agent, protein stability must be studied with care.

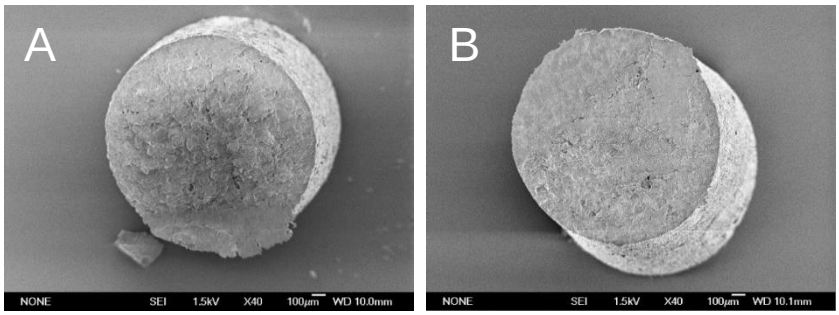

Figure IV-13: SEM micrographs of lipid implants after extrusion and prior to incubation. Micrographs displaying the cross section of SLIs manufactured with (A) 1:1 [w/w] protein lyophilisate and (B) 3:1 [w/w] protein lyophilisate at magnifications of 40x.

IV.2.4.3 PROTEIN RELEASE FROM IMPLANTS WITH DIFFERENT DIAMETERS

Another aspect towards increasing protein load was to change implant dimensions rather than varying the composition. The diameter was increased from 1.5 mm to 1.7 mm. Thus, the surface area was increased by 14 % and the implant volume by 25 %, resulting in an increased (approximately 25 %) protein mass per implant.

A diameter of 1.7 mm is still suitable for potential intravitreal incision and was realised by changing the outlet die of the ZE-5 mini-extruder. A further decrease of release rates was expected, based on the hypothesis that an increase in implant diameter increases diffusion path lengths.

Figure IV-14 indicates that both proteins were released within the same time frame and fashion from implants being 1.5 mm or 1.7 mm in diameter. For mAb, a biphasic release behaviour

comprising an initial phase of 4 weeks followed by a phase lasting from day 28 to day 100 was noticeable. The cumulative release of mAb released from 1.7 mm implant was slightly faster compared to 1.5 mm even though approximately 85 % to 90 % of total incorporated protein was released in both cases (Figure IV-14 A). Ranibizumab release was monitored over 154 days, showing that from both diameters release discontinued nearly after 120 days at 90 % to 95 % of total protein load (Figure IV-14 B).

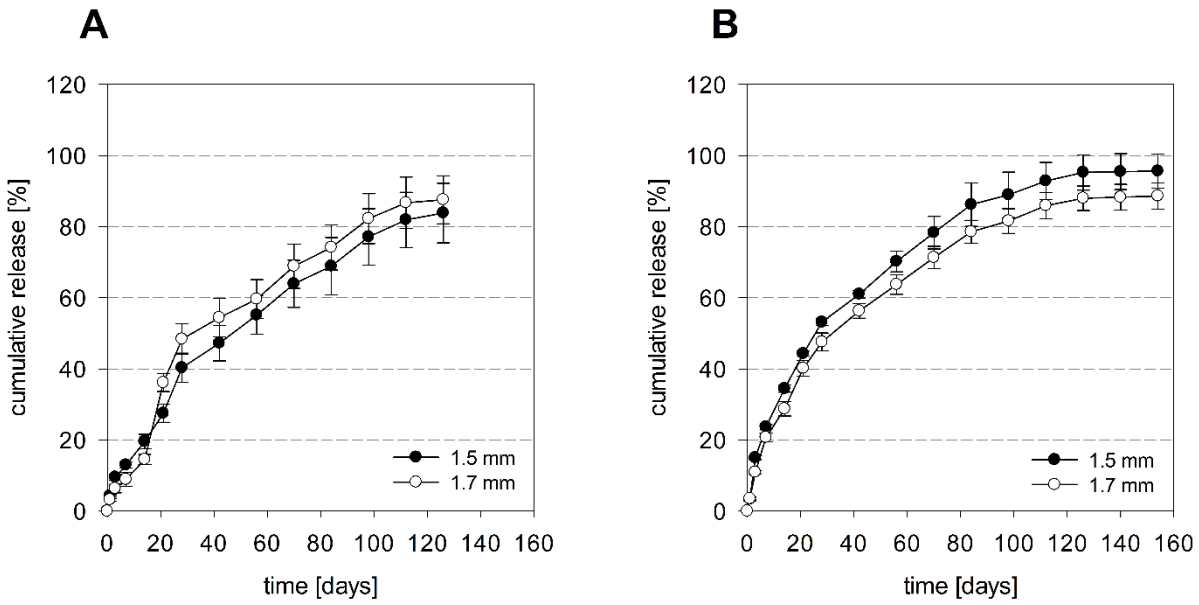

Figure IV-14: (A) displays the cumulative release profile of mAb, (B) shows cumulative Ranibizumab release. Implant diameter was increased from 1.5 mm to 1.7 mm comprising the 3:1 [w/w] lyophilisate formulation.

Release of both proteins from the larger diameter was faster than expected. Due to larger diffusion pathways of molecules diffusing out of the matrix, release was expected to be prolonged. In contrast to hot melt extrusion (HME), triglycerides were not completely molten during extrusion. Applying an extrusion temperature of 35°C induced merely a softening and sintering of the lipids, especially of the low melting lipid H12. Because of the semisolid state of the material, compression and compacting were the major mechanisms of implant formation. It can be speculated that during extrusion of SLIs with 1.7 mm diameter, the material was less compacted than at 1.5 mm which overcompensated the impact of larger diffusion pathways. However, this aspect requires further investigations.

IV.2.4.4 SUMMARY ON ATTEMPTS TOWARDS PROTEIN INCREASE

Overall, it was successfully demonstrated that protein load can be increased without negatively impacting the desired release time frame of 4 months. As illustrated in Table IV-5, protein load was increased from initially 1.53 mg to 3.00 mg per implant by changing the lyophilisate composition and implant diameter. This results in an increase of protein load by nearly 100 %. The desired release kinetic was not influenced by that. Assuming a sustained release of 120 days, the daily delivery rate was increased from approximately 11 µg/day to 23 µg/day.

Table IV-5: Protein load per implant and average released protein per day in dependency of the different formulations and settings. A release time frame of 120 days and 90 % of total released protein was basis for calculations.

Diameter	**1:1 [w/w] lyophilisate formulation**		**3:1 [w/w] lyophilisate formulation**	
	Total protein load per implant	**Average released protein per day**	**Total protein load per implant**	**Average released protein per day**
1.5 mm	1.53 mg (±0.06 mg)	10.93 µg	2.40 mg (±0.23 mg)	18.23 µg
1.7 mm	2.00 mg (±0.05 mg)	14.93 µg	3.00 mg (±0.08 mg)	22.58 µg

IV.2.5 IMPACT OF IMPLANT STORAGE

IV.2.5.1 *IN-VITRO* RELEASE PATTERNS

A major aspect concerning lipid based drug delivery matrices is their stability regarding properties and release patterns upon storage. It is well known that triglycerides exist in different modifications [261], such as α-, β- or β'-modifications which have an impact on properties like melting behaviour or crystallinity/amorphous state [181, 261]. Additionally, triglycerides can undergo an aging process upon storage, namely the conversation from the thermodynamically unstable α-modification to the more stable β-modification. These conversions can be prevented by curing of the implants at defined temperatures [233]. The system described here, consisted

of a binary triglyceride blend. Therefore, those aspects were of special interest as they can possibly change release patterns.

Lipid implants consisted of 45 % D118, 45 % H12 and 10 % protein lyophilisate with both 1:1 [w/w] and 3:1 [w/w] formulations resulting in a final protein load of 5.0 % and 7.5 %, respectively. For the following experiments, mAb and Ranibizumab were used only.

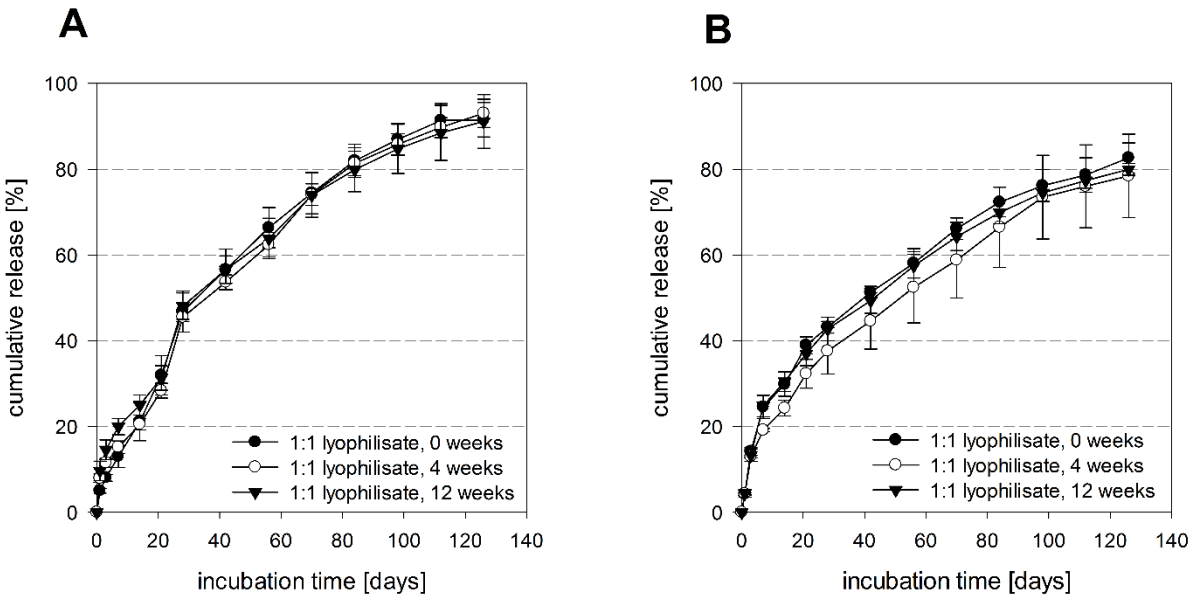

Figure IV-15: Cumulative release profiles of (A) mAb and (B) Ranibizumab directly after production (week 0) and after storage of 4 and 12 weeks at 4°C prior to *in-vitro* release.

Release studies were performed either directly after production (week 0) or after storage for 4 weeks or 12 weeks at 4°C in micro-centrifuge tubes. Release profile was then monitored over 126 days for both proteins (Figure IV-15). Displayed are the results for the formulation with 1:1 [w/w] lyophilisates, illustrating that release patterns were not affected by the storage; both proteins retained their characteristic release profiles. Comparable release curves were obtained for the 3:1 [w/w] lyophilisate formulation for both proteins (data not shown). Consequently, it can be concluded that SLIs can be stored for at least 3 months at 4°C prior to use ensuring same release properties. These observations are in line with results from a previous storage study of lipid implants described by Mohl *et al*. [176].

IV.2.5.2 STABILITY OF TRIGLYCERIDES IN THE LIPID MATRIX UPON STORAGE

DSC was performed to identify possible alterations in melting points and/or melting energy indicating changes in lipid modifications or crystal growth.

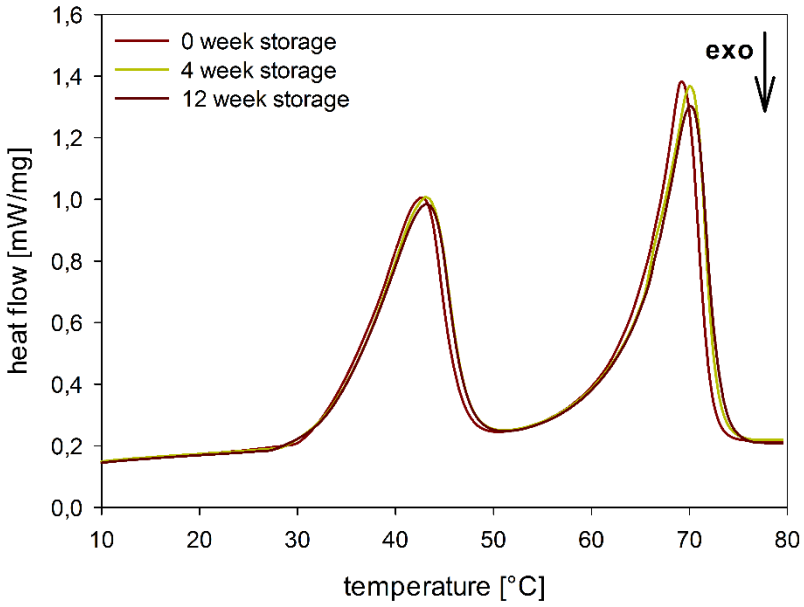

Figure IV-16: Melting curves of lipid implants consisting of 10 % protein lyophilisate, 45 % H12 and 45 % D118 after storage for 0, 4 and 12 weeks at 4°C.

Thermograms (Figure IV-16) obtained after 0, 4 and 12 weeks did not show differences in the course of the melting curves. The maximum melting points ($T_{melting}$) are summarised in Table IV-6. $T_{melting}$ of H12 was measured between 42.70°C and 43.23°C; the same was observed for D118. Melting energy was assessed as it is an indicator for the presence of amorphous lipids [233]. The melting energies for H12 and D118 remained constant upon storage, meaning no shifts in amorphous/crystallinity status of both triglycerides occurred (Table IV-6). No changes in $T_{melting}$ and melting energy values occurred, signifying that both triglycerides remained in their thermodynamically stable modifications.

Table IV-6: $T_{melting}$ and melting energy of H12 and D118 upon storage for 0, 4 and 12 weeks at 4°C.

Time point	$T_{melting}$ H12 [°C]	$T_{melting}$ D118 [°C]	Melting energy H12 [J/g]	Melting energy D118 [J/g]
week 0	42.70 (±0.46)	69.43 (±0.42)	75.74 (±3.21)	86.64 (±3.85)
week 4	43.10 (±0.46)	70.10 (±0.26)	76.19 (±1.68)	89.95 (±1.51)
week 12	43.23 (±0.42)	70.17 (±0.29)	74.40 (±0.65)	90.27 (±1.59)

Figure IV-17 A shows the XRPD patterns of H12 bulk material revealing two strong reflections at 2θ=20.9° d=0.42 nm and at 2θ=23.2° d=0.38 nm which are typical for orthorhombic chain packaging of the β'-modification [181]. The D118 bulk material diffraction patterns were characterised by three main reflection peaks at 2θ=19.4°, 2θ=23.2° and 2θ=24.3° (Figure IV-17 B) typical for the β-modification [167] with the corresponding short spacings at 0.46 nm, 0.38 nm and 0.37 nm. The reflection peak at 2θ=21.0° d=0.42 nm represents a small percentage of α-modification.

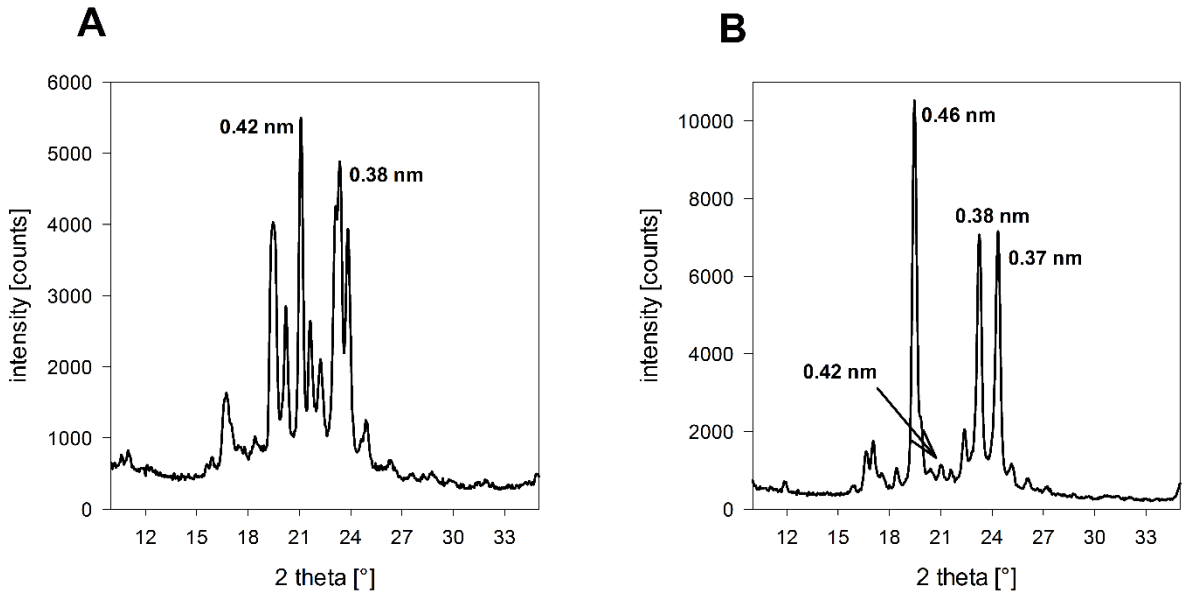

Figure IV-17: (A) shows diffraction patterns of H12 bulk material, (B) represents D118 bulk material diffraction patterns.

As displayed in Figure IV-18, the reflections of extruded SLIs are intermediates from those of pure H12 and D118, respectively [181]. The distinct diffraction lines at 2θ=19.6°, 23.4° and 24.5° match to the crystal spacings of the β-modification of D118 discussed above. At an angle of 2θ=23.4° d=0.38 nm, an overlay of the H12 β'-modification and the β-modification of D118 can be observed due to similar appearance at this angle. However, the XRPD patterns of the stored implants and the non-stored ones were identical.

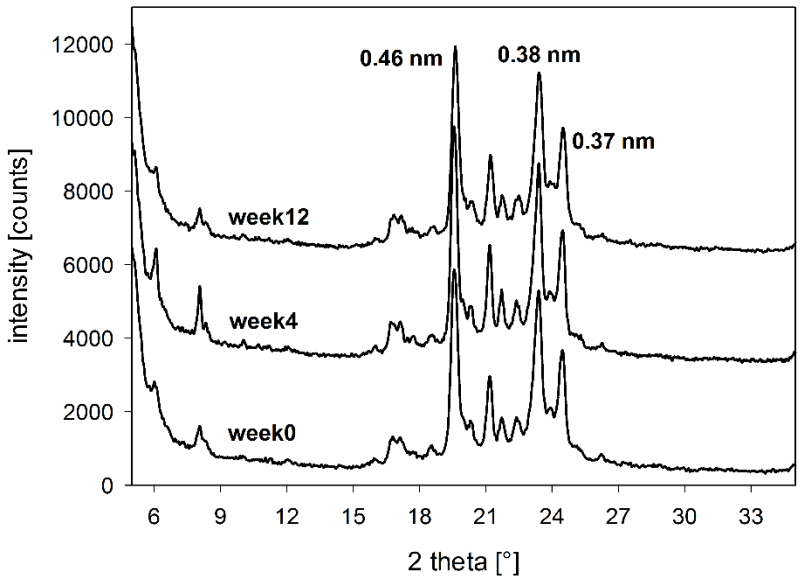

Figure IV-18: Patterns of lipid implants after storage for 0, 4 and 12 weeks at 4°C. For a better visualisation, the plots are displayed vertically.

Identical XRPD patterns of stored and non-stored implants (Figure IV-18) indicate that the same modifications were present. Due to comparable diffraction patterns observed before and after storage it can be concluded that H12 stayed in its β'-modification whereas D118 was present in the β-modification, also previously observed by Schulze *et al.* for implants containing interferon-α and PEG [181].

IV.2.6 PRE-MELTING OF TRIGLYCERIDES

The impact of storage on SLI characteristics has already been described in chapter IV.2.5 showing no aging of the triglycerides and therefore no changes in release patterns and thermal characteristics.

The present chapter is aimed to investigate the effect of different lipid modifications (coming along with different thermal characteristics of the lipids) on release patterns. For this, H12 and D118 were simultaneously molten at 80°C intentionally inducing unstable lipid modifications. Then, the molten mass was allowed to cool down before it was ground and sieved (< 180 µm) prior to extrusion. It was systematically investigated if the «pre-melting» has an impact on properties of lipid raw material and of extruded implants including thermal and physical properties as well as release patterns. In the following, the standard extrusion technique already described will be named as «conventional extrusion».

SLIs were manufactured with both extrusion techniques (conventional extrusion and extrusion with pre-melted lipids) using the established settings (50:50 lipid blend, 35°C extrusion temperature, 40 rpm, 1.5 mm x 15 mm). First, the characteristics of pre-melted lipid itself were investigated followed by investigating the impact on release patterns. Then, SLIs were stored for 0, 4 and 12 weeks at 4°C and thermal properties and release patterns were monitored.

IV.2.6.1 IMPACT OF PRE-MELTING ON LIPID CHARACTERISTICS

The pre-melted lipid raw material was prepared according to III.2.1.3. As a benchmark, thermal characteristics from SLIs extruded with the standard settings for conventional extrusion were studied.

Table IV-7: T_{onset} and $T_{melting}$ of H12 and D118 of freshly pre-melted raw material and after extrusion using pre-melted lipids. As a comparison, T_{onset} and $T_{melting}$ of H12 and D118 applying the conventional extrusion technique are listed.

	Pre-melting	Pre-melting and extrusion	Conventional extrusion
$H12_{onset}$ [°C]	32.55 (±0.71)	32.56 (±0.21)	34.10 (±0.99)
$H12_{melting}$ [°C]	39.05 (±0.92)	41.00 (±0.14)	42.80 (±0.70)
$D118_{onset}$ [°C]	64.53 (±1.14)	65.83 (±0.76)	63.93 (±1.12)
$D118_{melting}$ [°C]	71.33 (±1.46)	71.60 (±0.20)	69.43 (±0.42)

In Table IV-7, the values for T_{onset} and $T_{melting}$ for H12 and D118 are summarised. The pre-melting reduced T_{onset} of H12 by 1.6°C from 34.1°C to 32.6°C. Also, $T_{melting}$ of H12 was shifted from 42.8°C to 39.1°C. Equally, T_{onset} and $T_{melting}$ for D118 were slightly higher after pre-melting (approximately 1.5°C). Since the extrusion and the incubation temperatures are very close to the melting points of H12, they are of special interest. Therefore, pre-melting might substantially influence the release patterns since the melting point of the low melting lipid is a crucial parameter in terms of controlled release [183]. It is also worth to note, that $T_{melting}$ of pre-melted material was impacted by the extrusion process: $T_{melting}$ was 2°C higher than before extrusion. This means, that the applied temperature of 35°C (which is about 2.5°C higher than the T_{onset} of H12) already impacted the thermal characteristics of the pre-melted lipids. To study the impact of pre-melting not only on melting points but also on release patterns, SLIs were manufactured using both extrusion techniques (see IV.2.6.2).

XRPD was used to analyse lipid modifications. Diffraction patterns of extruded SLIs using both extrusion techniques and of the pre-melted lipids prior to extrusion are shown in Figure IV-19. The diffractograms of pre-melted lipid raw material (trace 1) and SLIs manufactured with those (trace 2) show no qualitative differences indicating that extrusion itself did not alter lipid characteristics, e.g. crystallinity. However, for SLIs produced with conventional extrusion (trace 3), patterns changed signifying that the pre-melting step altered lipid modifications.

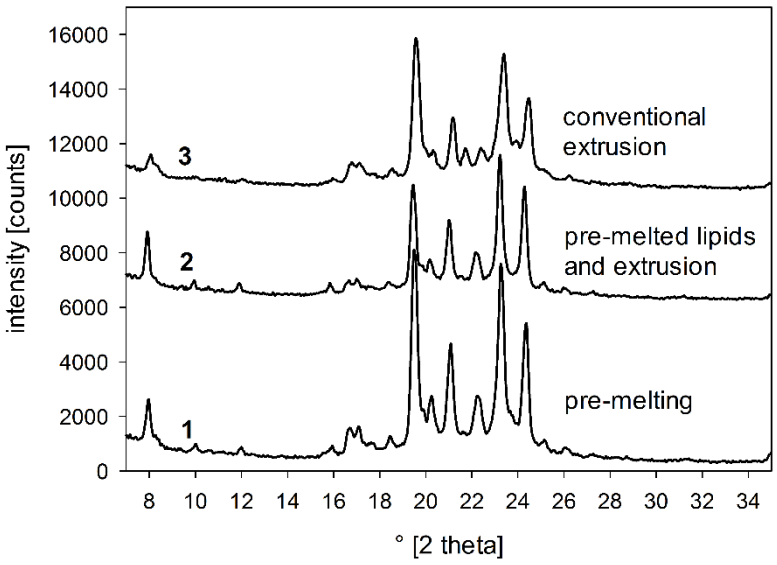

Figure IV-19: Diffraction patterns of pre-melted lipids prior to extrusion and of extruded SLIs produced with both conventional extrusion and extrusion with pre-melted lipids.

IV.2.6.2 IMPACT OF PRE-MELTING ON *IN-VITRO* RELEASE

SLIs were manufactured with freshly prepared pre-melted lipids to eliminate possible aging effects of the raw material on release patterns. Both extrusion techniques, conventional extrusion and extrusion with pre-melted lipids (Figure IV-20), were used. The extrusion settings and the composition of the lead formulation was used.

Figure IV-20 illustrates the cumulative release of mAb from SLIs using both extrusion techniques. Release was slowed down using pre-melted lipids. The triphasic release behaviour for the conventional extrusion technique was not observed anymore, instead the release was more linear over a longer period. A sustained and almost linear release can be described lasting from the very first day to day 140; an initial burst was not noticed. Between day 140 and day 200, little amounts of mAb were still released. An overall biphasic rather than a triphasic release behaviour was observed. Therefore, the release time frame could be extended from approximately 120 days to 200 days without changing the overall composition.

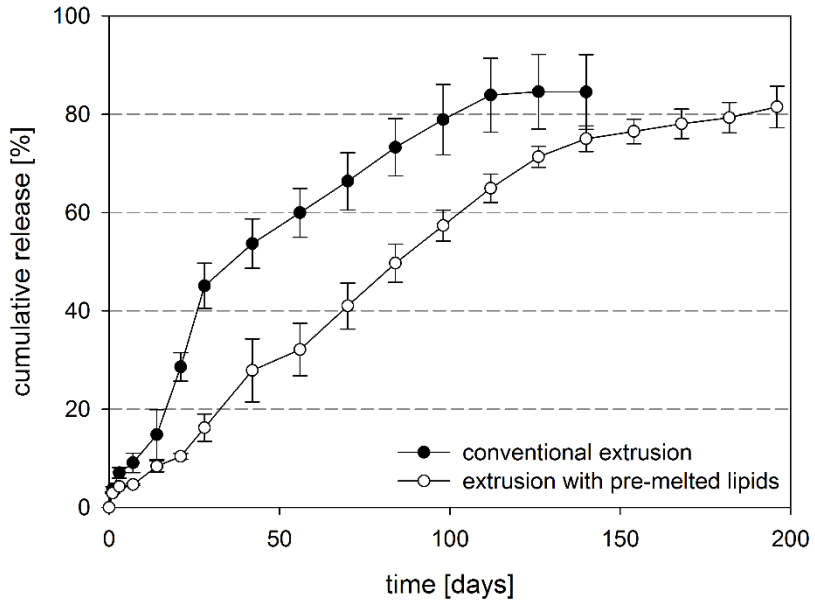

Figure IV-20: Cumulative release of mAb released from SLIs manufactured using the (●) conventional extrusion technique and (○) extrusion with pre-melted lipids.

In 2012, Sax *et al.* described a release pathway of proteins from a lipid matrix which relies on a partial melting of the low melting lipid within the matrix [182]; the molecules diffuse in a phase of molten lipid [234]. It was shown, that T_{onset} and $T_{melting}$ of the low melting lipid are very important parameters playing a major role in triggering protein release. A nearby explanation of the prolonged release in our case could be that at the incubation temperature of 37°C the H12 is already partially molten due to the low T_{onset} (Table IV-7) and thereby «closing» the pores and interconnected pores within the lipid matrix *in-situ*. Thereby, the molecules are hindered to diffuse out of the depot which results in prolonged release periods. The pre-melted lipids were exposed twice to a thermal input, which reduced the melting point of H12 and thereby softened and changed the flowability of the material. Measurements of the extrusion pressure supposedly favours that hypothesis: within the extruder barrel a pressure of 975 kPa (±74 kPa) for conventional extrusion was measured and 556 kPa (±41 kPa) were measured when pre-melted lipids were manufactured (see chapter IX).

INCREASE OF PROTEIN LOAD OF SLIS EXTRUDED WITH PRE-MELTED LIPIDS

By pre-melting of the lipids, it was possible to prolong and linearise the sustained release profile of mAb from 120 days to almost 200 days. Due to the very promising results, it was further investigated, if the protein load could be increased as previously described for SLIs produced with the conventional extrusion technique (IV.2.4) and if this technique is also applicable for the other proteins used.

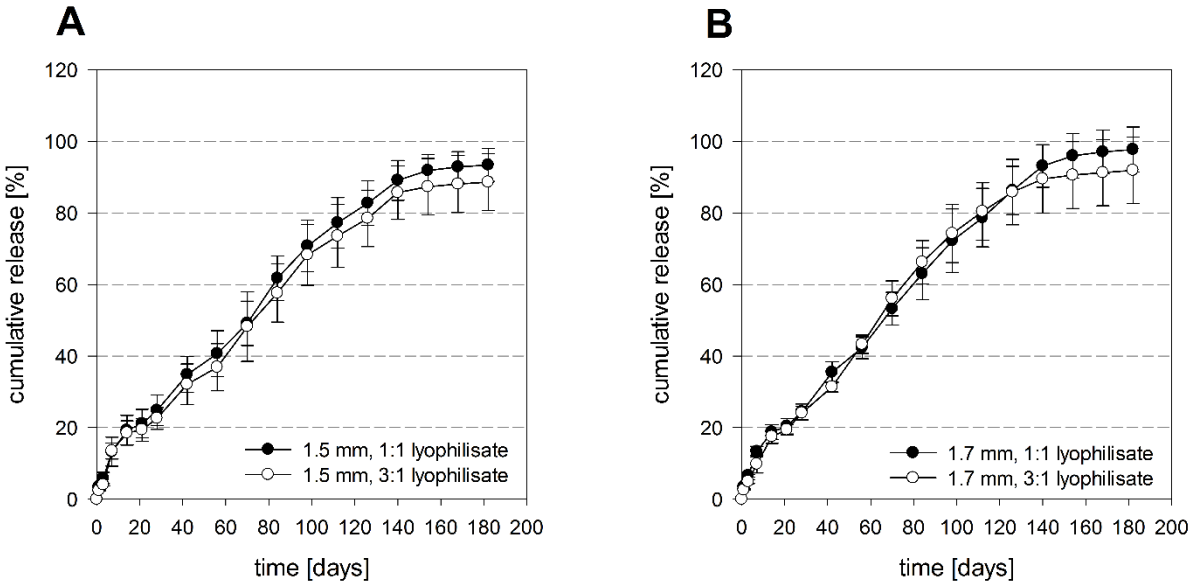

Figure IV-21: Cumulative release profiles of mAb from implants being (A) 1.5 mm and (B) 1.7 mm in diameter. Protein lyophilisate percentage was kept at 10 % while the lyophilisate formulation was changed from 1:1 [w/w] protein:cyclodextrine ratio to 3:1 [w/w]. SLIs were prepared with pre-melted lipids.

The approach to increase the percentage of lyophilisate was not successful (Appendix, Figure XII-5) since accelerated release rates were observed for all proteins with increasing percentage of lyophilisate. Simultaneously to the approaches already discussed in IV.2.4 for SLIs produced with conventional extrusion technique, the lyophilisate composition was changed from 1:1 [w/w] to 3:1 [w/w] to encapsulate 50 % more protein within the same amount of lyophilisate. The implant diameter was increased from 1.5 mm to 1.7 mm as well. Both approaches were performed with mAb and Ranibizumab. Release patterns for both proteins were not negatively influenced by the attempts (Figure IV-21 and Figure IV-22). It was therefore possible to

encapsulate 3 mg mAb and Ranibizumab into an SLI and deliver it over approximately 200 days using pre-melted lipids.

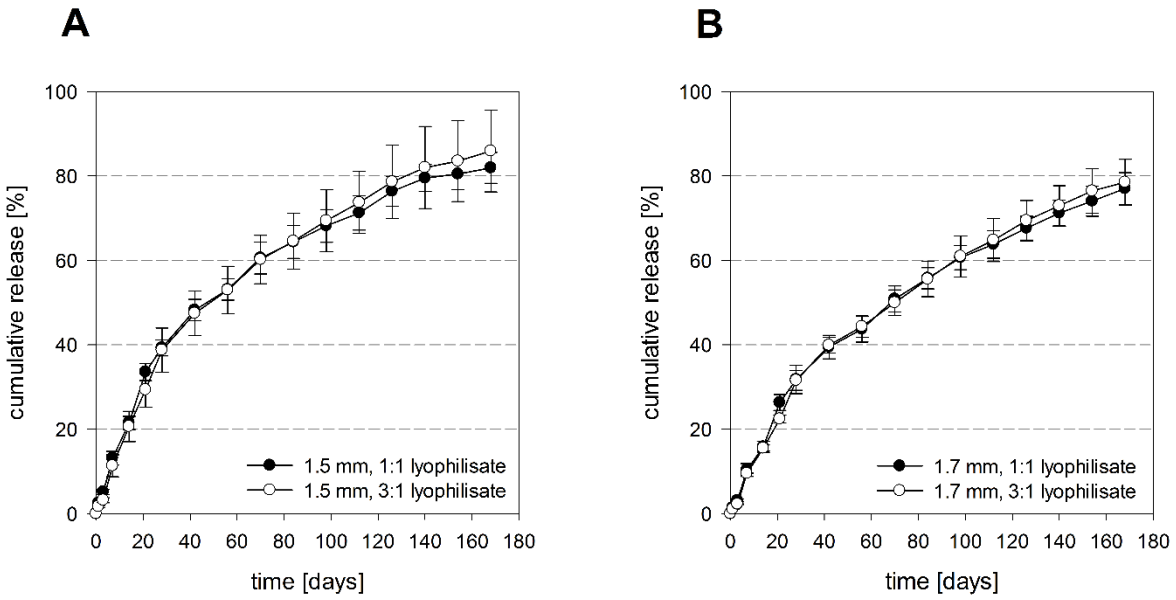

Figure IV-22: Cumulative release profiles of Ranibizumab from implants being (A) 1.5 mm and (B) 1.7 mm in diameter. Protein lyophilisate percentage was kept at 10 % while the lyophilisate formulation was changed from 1:1 [w/w] protein:cyclodextrine ratio to 3:1 [w/w]. SLIs were prepared with pre-melted lipids.

IV.2.6.3 IMPACT OF PRE-MELTING ON STORAGE STABILITY OF SLIS

As pre-melting had a strong impact on thermal characteristics (Table IV-7), lipid modifications (Figure IV-19) and the associated prolonged release, it was tested if triglycerides underwent an aging process upon storage. Since possibly unstable lipid modifications were induced (and therefore a change of crystallinity/amorphous status was induced), aging of triglycerides also affecting release patterns may be possible.

To systematically investigate the storage effect, SLIs were manufactured with both extrusion techniques (conventional extrusion and extrusion with pre-melted lipids) using the established settings (50:50 lipid blend, 35°C extrusion temperature, 40 rpm, 1.5 mm x 15 mm). SLIs were stored for 1, 2, 4 and 12 weeks at 4°C and were analysed towards thermal characteristics and release patterns.

IMPACT OF STORAGE ON THERMAL CHARACTERISTICS OF SLIS

After a storage of 1, 2, 4 and 12 weeks, SLIs were analysed towards T_{onset} and $T_{melting}$ of both lipids (Figure IV-23). Figure IV-23 A represents the melting points of H12 measured over 12 weeks upon incubation of SLIs produced with both extrusion techniques.

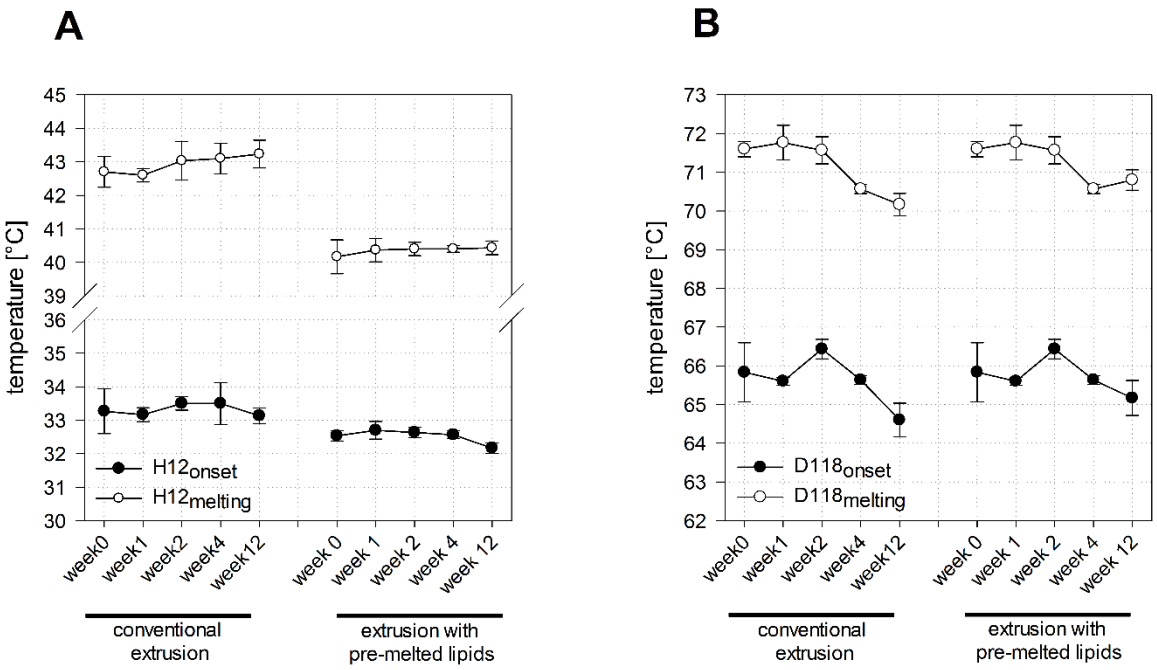

Figure IV-23: Overview of T_{onset} and $T_{melting}$ of both lipids (A) H12 and (B) D118. Implants were manufactured using both extrusion techniques, conventional extrusion and extrusion with pre-melted lipids.

For conventional extrusion, both values remained rather constant over time (T_{onset}: 33.2°C to 33.5°C; $T_{melting}$: 42.7°C to 43.2°C). This is also valid for SLIs produced with pre-melted lipids because $T_{melting}$ values stayed constantly at 40.2°C over time. The value for T_{onset} decreased from 32.5°C (week 0) to 32.1°C (week 12). Generally, changes of melting points as a function of the different extrusion techniques were not apparent for H12 melting points.

T_{onset} and $T_{melting}$ of D118 incorporated into the SLIs was also monitored over 12 weeks (Figure IV-23 B). Applying conventional extrusion, T_{onset} and $T_{melting}$ of D118 decreased by approximately 2°C during incubation time. Due to no obvious differences in release profiles after storing SLIs produced with conventional extrusion (Figure IV-15), a change in melting points was not

expected raising the question if the melting points of D118 (and H12) are affecting the release at all. The same trend was also observed for extrusion with pre-melted lipids: both melting points dropped by approximately 1°C within 12 weeks. The thermal characteristics of D118 changed more than those of H12 even though H12 is the low melting lipid and its melting points are very close to the extrusion and incubation temperature. It seems that a correlation between melting points and release patterns is not present probably due to the complexity of the system where other parameters are affecting the release (extrusion temperature, extrusion pressure, screw speed).

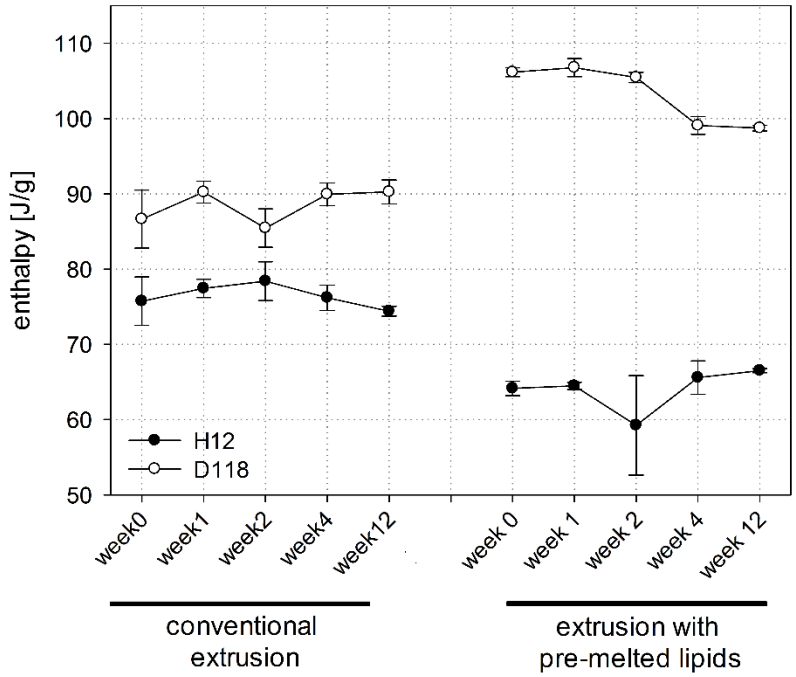

Figure IV-24: Overview of melting energies of both lipids manufactured within SLIs. Implants were manufactured using both extrusion techniques, conventional extrusion and extrusion with pre-melted lipids.

In addition to melting points, the melting energy was assessed as it is an indicator for the presence of amorphous lipids [233]. In Figure IV-24 the melting energies of H12 and D118, manufactured with both extrusion techniques and stored over 12 weeks, are displayed. Regarding conventional extrusion, melting energies of H12 and D118 demonstrated rather

constant values (H12: 75 J/g to 78 J/g; D118: 85 J/g to 90 J/g). Contrarily, for pre-melted lipids ΔH increased by 10 J/g (from 63 J/g to 72 J/g) for H12 and decreased from 105 J/g to 95 J/g concerning D118. The melting energies of both lipid components changed due to the pre-melting procedure. In general, a change in melting energy indicates a change in amorphous state of the lipids while a decrease designates an increase in amorphous amounts [233].

The crystallinity status of stored and non-stored SLIs was evaluated as well but results did not show any changes in XRPD patterns for both extrusion techniques (Appendix Figure XII-6 and Figure XII-7).

IMPACT OF STORAGE ON RELEASE PATTERNS OF SLIS

In addition to thermal characteristics, release patterns of stored and non-stored SLIs were evaluated to determine if the changes in melting points, melting energy and lipid modification have an impact on release patterns. SLIs extruded with conventional extrusion technique did not show any differences in release behaviour upon storage (Figure IV-15).

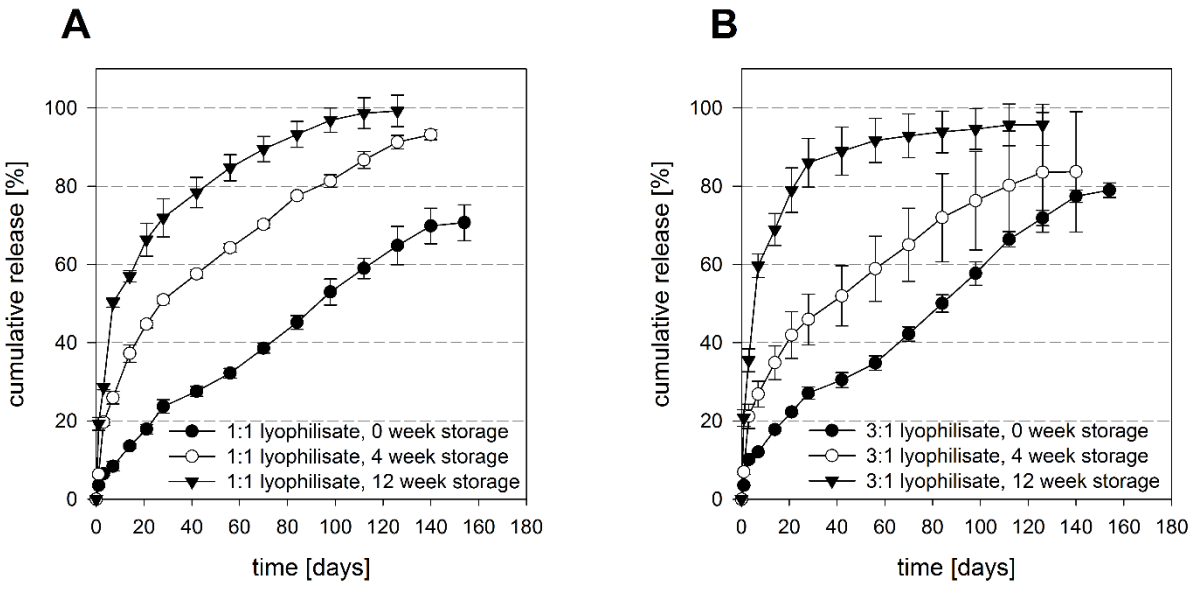

Figure IV-25: Cumulative release of mAb from SLIs extruded with pre-melted lipids and after a storage of 0, 4 and 12 weeks at 4°C. Lipid implants were produced with different protein lyophilisate compositions: either in a ratio of (A) 1:1 [w/w] or (B) 3:1 [w/w].

Figure IV-25 displays the release of mAb from SLIs stored for 0, 4 and 12 weeks at 4°C prior to release. SLIs were extruded with pre-melted lipids. Compared to the release profile obtained from non-stored SLIs (week 0), release was accelerated after a 4-week storage. Especially during the initial phase, substantially higher release rates were observed. For instance, after 7 days, 8.4 % mAb was released from non-stored SLIs but 25.9 % and 50.3 % from SLIs stored for 4 weeks and 12 weeks, respectively (Figure IV-25 A). These accelerated release rates are present over the complete release time of 160 days. Observations made for the 1:1 [w/w] lyophilisate hold also true for the 3:1 [w/w] lyophilisate (Figure IV-25 B).

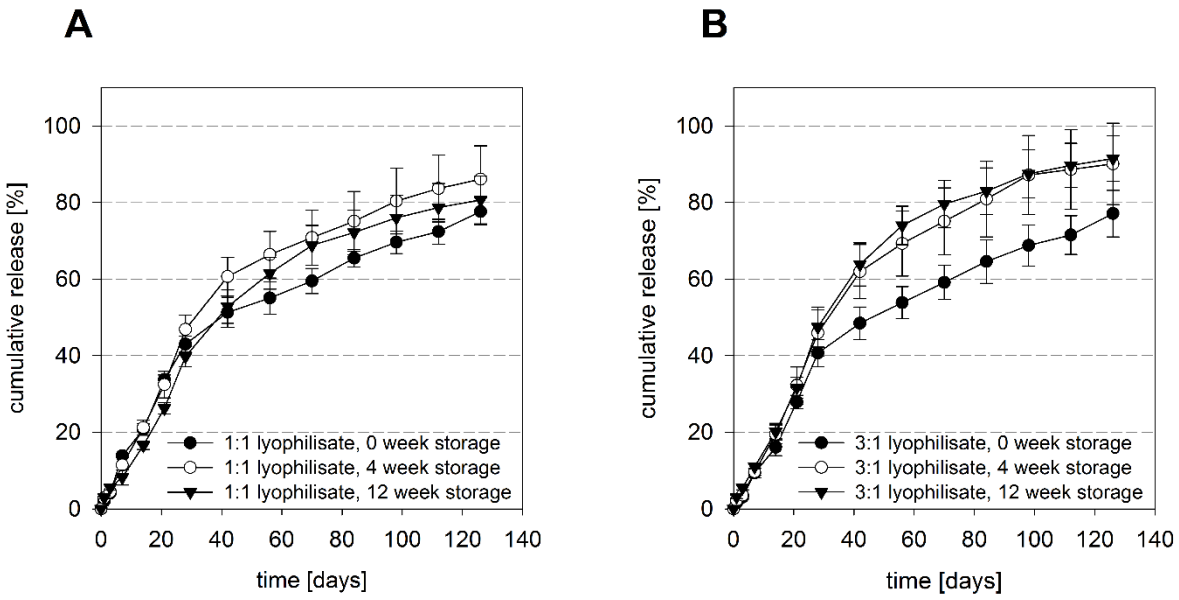

Figure IV-26: Cumulative release of Ranibizumab from SLIs extruded with pre-melted lipids and after a storage of 0, 4 and 12 weeks at 4°C. Lipid implants were produced with different protein lyophilisate compositions: either in a ratio of (A) 1:1 [w/w] or (B) 3:1 [w/w].

Interestingly, Ranibizumab release patterns were much less affected by storage: especially over the first 28 days, the characteristic release profile was retained for both lyophilisate compositions (Figure IV-26). Starting from day 28, release rates were accelerated from stored SLIs. A difference in release rates of 4-week stored and 12-week stored SLIs cannot be observed as it was the case for mAb described previously.

Therefore, not only the properties of the lipids affecting release patterns, also the proteins itself which are encapsulated within the depot. This is one of the most important aspects within this work and will also be addressed in chapter VIII.

IV.2.6.4 SUMMARY ON PRE-MELTING OF TRIGLYCERIDES AND THEIR IMPACT ON IMPLANT PROPERTIES

It can be summarised that the melting points, melting energies and crystallinity of the lipids was changed by the pre-melting technique. By a simultaneous pre-melting of both lipids prior to extrusion, it was demonstrated that release was prolonged for up to 200 days tested with mAb and Ranibizumab. However, when storing SLIs, differences between conventionally extruded SLIs and SLIs manufactured with pre-melted lipids can be observed (especially for melting energy). XRPD diffraction patterns stayed unchanged over time signifying no change in modifications for both extrusion techniques. Nevertheless, in terms of release patterns, major differences were apparent (even protein dependent). Thus, it seems that a straightforward correlation of thermal and physical characteristics and release patterns cannot be made probably due to the complexity of the system. Other parameters, e.g. extrusion temperature, extrusion pressure, screw speed, or other effects occurring during release (wettability) may affect the release more than expected. Since the only major difference of conventional extruded SLIs to those extruded with pre-melted lipids is the melting energy, the question raises if that might be the most crucial parameter for the different release behaviours observed.

The fact that also a protein dependent difference in release patterns was observed, points into the direction that this topic is much more complex than previously thought. In other words: the very promising release profiles obtained with this simple and straightforward technique, makes this topic even more attractive for further research. For instance, the process of melting both lipids simultaneously together offer great potential as the rate of heating, the final temperature or the cooling rate can be varied most likely impacting the properties of the lipids.

IV.2.7 PROTEIN RELEASE TESTS FROM PLGA MATRICES

This section describes the release of proteins from different PLGA matrices including Resomer® RG 502, RG 502 H and RG 755 S. It was aimed to evaluate how proteins are released from PLGA matrices and to compare those data with release profiles obtained from SLIs. PLGAs with different degradation time frames were used for two reasons: first, to evaluate the impact of depot erosion in addition to diffusion, and second, to determine the impact of different end groups on release profiles.

For this, PLGA implants were prepared by mixing 10 % protein lyophilisate (1:1 [w/w] protein:HP-β-CD) with 90 % Resomer® RG 502, Resomer® RG 502 H or Resomer® RG 755 S in a mortar to obtain a homogenous powder blend. The powder mixture (approximately 1.5 g) was fed manually to the ZE-5 mini-extruder from Three-Tec® (Seon, Switzerland) and extrusion was performed at 70°C at a screw speed of 60 rpm. *In-vitro* release was performed at 37°C.

The stability of released protein from PLGA matrices was assessed additionally and is described within chapter VII.

IV.2.7.1 RELEASE FROM RESOMER® RG 755 S MATRICES

Resomer® RG 755 S was chosen since the estimated degradation time frame of this PLGA (equipped with an ester as end group) is about 6 months. The polymer is characterised by a ratio of 75:25 and with a molecular weight of 76,000 to 116,000 Da (Table III-2). This rather long degradation time allows to exclude erosion as additional release mechanism because no considerable erosion was observed during *in-vitro* release experiments of SLIs.

For all proteins, no initial burst was observed. For mAb, a sustained released over approximately 98 days was observed delivering 9.8 % over this time (Figure IV-27). After this time, release stopped. For all other proteins, release rates were very slow delivering almost no protein (0.2 % to 3.1 % after 126 days). Due to the very low release rates and the beginning degradation of the PLGA matrix, the experiment was stopped after 126 days.

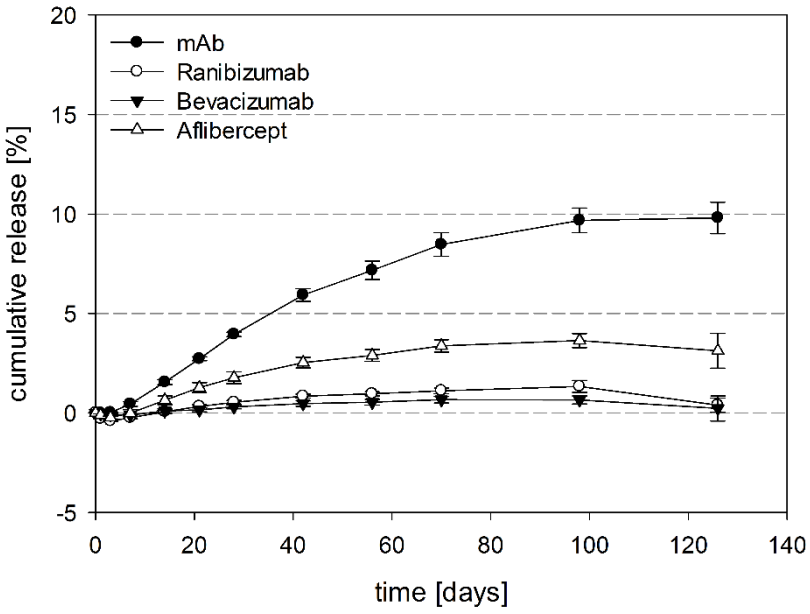

Figure IV-27: Cumulative release of (●) mAb, (○) Ranibizumab, (▼) Bevacizumab and (△) Aflibercept from a Resomer® RG 755 S matrix. Please note, that for better visualisation the y-axis is scaled from -5 % to 20 %.

The pH was monitored over the complete incubation time as erosion of the polymer would impact on the release kinetics. It was expected that a major decrease in pH value would indicate the erosion of the polymer because the PLGA is hydrolysed in its components lactic and glycolic acid creating an acidic pH. During this incubation of the PLGA extrudates, the incubation medium was not exchanged.

As Figure IV-28 Illustrates, the pH of all solutions stayed rather constant at pH 7.4 over the first 42 days and decreased slightly to approximately 6.5 after 98 days. A major drop in pH can be observed between day 98 and day 126 for all proteins down to pH 2.5 to 3.0 signifying the starting degradation of the PLGA matrix. After 98 days, the PLGA extrudates started to degrade but no release was seen (Figure IV-27). This leads to the assumption that the non-released protein (90 % to 100 % of incorporated protein) precipitated within the PLGA matrix.

Because generally no protein was released from this particular Resomer®, another Resomer® with a degradation time frame of approximately 3 months was chosen.

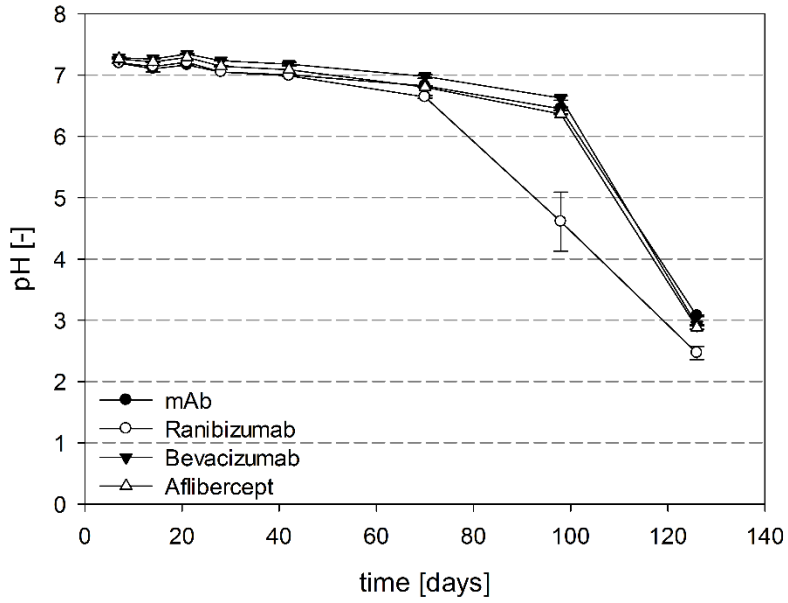

Figure IV-28: Overview of pH measured within the incubation medium in which PLGA extrudates were incubated. Extrudates were loaded with (●) mAb, (○) Ranibizumab, (▼) Bevacizumab and (△) Aflibercept lyophilisate.

IV.2.7.2 RELEASE FROM RESOMER® RG 502 AND RG 502 H MATRICES

In a next experiment, Resomer® RG 502 and Resomer® RG 502 H were used both with a ratio of 50:50 and a molecular weight of 7,000 to 17,000 Da. The estimated degradation time frame of those PLGAs is less than 3 months (Table III-2). Two different polymers were chosen to study the effect of different end groups on the release behaviour: Resomer® RG 502 comprises an esterified end group, Resomer® RG 502 H is equipped with a free carboxyl group.

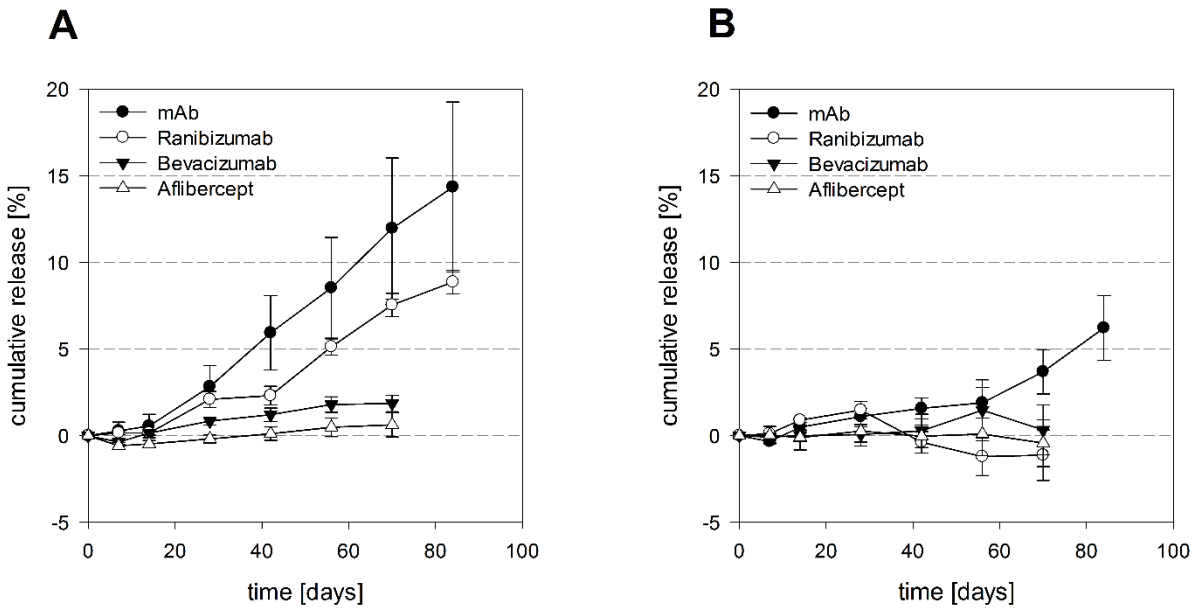

Figure IV-29: Cumulative release of (●) mAb, (○) Ranibizumab, (▼) Bevacizumab and (△) Aflibercept from (A) Resomer® RG 502 and (B) Resomer® RG 502 H matrices. Please note, that for better visualisation the y-axis is scaled from -5 % to 20 %.

Figure IV-29 provides an overview of sustained release of the proteins delivered from Resomer® RG 502 (Figure IV-29 A) and Resomer® RG 502 H (Figure IV-29 B). For Resomer® RG 502, a cumulative release of mAb and Ranibizumab can be observed. Both proteins were released without initial burst and release was almost linear over the complete incubation period of 84 days. In total, 14.4 % mAb and 8.9 % Ranibizumab was released after 84 days meaning that 85.6 % mAb and 91.1 % Ranibizumab remained within the polymer. A release of Bevacizumab and Aflibercept has not taken place. The release experiment was stopped after 84 days because the PLGA matrix totally disintegrated. This corresponds to the estimated degradation time frame of this polymer (< 3 months).

A sustained release from Resomer® RG 502 H depot was only noticed for mAb. After 84 days, 6.2 % mAb were released and 93.8 % remained within the PLGA matrix. The other proteins did not show any release (Figure IV-29 B).

A possible explanation that in some cases a sustained release was not noticed could be due to precipitation of the encapsulated protein already within the depot. The degradation of the

polymer creates a pH drop and an increase in osmotic pressure which results in aggregation of the encapsulated proteins [49, 253, 254] and incomplete release [54, 68, 242, 255]. This phenomenon is even more pronounced when the end group is a carboxylic acid which would correspond with our results (Figure IV-29). To prove this hypothesis, the pH was measured over the complete incubation time.

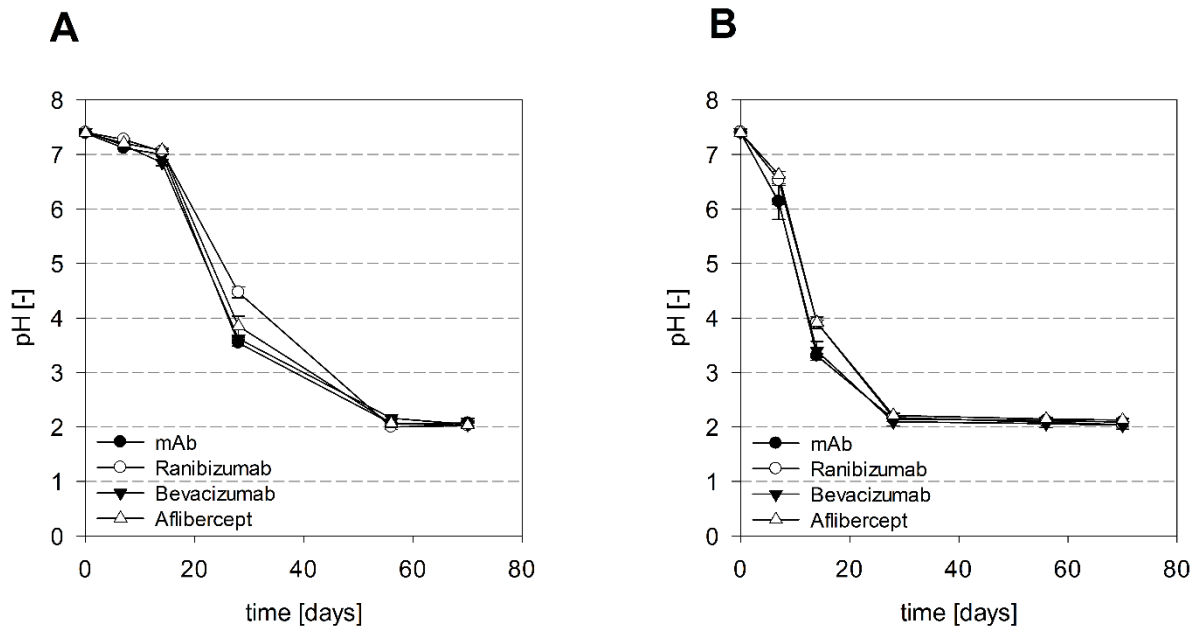

Figure IV-30: Overview of pH measured within the incubation medium in which PLGA extrudates were incubated. Extrudates were loaded with (●) mAb, (○) Ranibizumab, (▼) Bevacizumab and (△) Aflibercept lyophilisate and PLGA matrix consisted of either (A) Resomer® RG 502 or (B) Resomer® RG 502 H.

Measurements of pH confirm the hypothesis that pH dropped faster at the Resomer® RG 502 H based extrudates due to the free carboxylic group (Figure IV-30 B). It is important to note, that the incubation medium was not changed during pH measurements whereas the incubation medium has been exchanged when release was measured. Therefore, a direct correlation of release patterns (and their explanations) and the change of pH is not given.

It was further analysed if incomplete release (and the associated protein aggregation) was caused by the acidic microclimate within the PLGA matrix or by the acidic pH of the surrounding medium (chapter VII).

IV.2.7.3 COMPARISON OF OUR RESULTS TO CURRENT STATUS OF RESEARCH

The very incomplete release profiles observed during this study are corresponding to release profiles of proteins described in literature. For instance, the release of erythropoietin (EPO) from PLGA depots also showed incomplete release [45, 46, 242]. This is also true for different protein formats including BSA [255], insulin [49], recombinant human growth hormone (r-hGH) [47, 48] or insulin-like growth factor-I [50]. In most cases, the proteins encapsulated within PLGA depots showed poor release patterns namely incomplete release and/or substantial initial burst release. To overcome this problem, different strategies had been pursued, for instance PLGA composites such as PLGA-triacetin depots [72] or conjugates with amino cyclodextrine [66]. Also, the addition of excipients has been investigated like PEG-block-oligo(vinyl sulfadimethoxine) [69], PEG-poly(l-histidine) [43] or $Mg(OH)_2$ [52]. In some cases, protein release was improved which was reflected by a reduced burst release and a more continuous and complete release.

IV.3 CONCLUSION

The sustained long-term release of different protein formats from SLIs including therapeutically relevant proteins was successfully demonstrated. A controlled release over approximately 4 months of a mAb and the f_{ab}-fragment Ranibizumab was achieved. Both protein drugs were delivered in a sustained fashion without any initial burst release events for about 110 to 120 days. It is the first time that long-term release of two different molecules from SLIs have been reported. The formulation and extrusion settings previously developed within our group were further improved. The most appropriate formulation for the ZE-5 mini-extruder comprised 10 % protein lyophilisate and a lipid matrix consisting of 50 % H12 and 50 % D118; no PEG was added. An adequate extrusion temperature was determined at 35°C. This allows the production of SLIs which provided a constant and almost complete release (up to 95 %) of incorporated protein without any burst effects.

Several advantages in terms of the extrusion process were accomplished by an optimisation of the process: First, the avoidance of PEG as precipitant represents the most valuable improvement as it is known for its potential negative impact on protein integrity [262] and its allergic potential [263-265]. Also, the implant diameter was reduced by 25 % from 2.0 mm to 1.5 mm without negatively impacting the release duration. Furthermore, a manufacturing setup using extremely mild processing conditions and a most elegant excipient composition was established. By introducing the ZE-5 mini-extruder as new extruder, the minimum batch size was reduced by 80 %. Moreover, the protein load was increased to 3.00 mg protein per implant without negatively affecting the desired release time frame. It was also ensured that extruded SLIs can be stored for at least 3 months without impacting their properties considering release patterns, thermal properties and status of crystallinity, respectively.

Finally, it was possible to develop a depot releasing the f_{ab}-fragment Ranibizumab over 110 days *in-vitro* from SLIs being small enough for intravitreal use (the excellent stability profile

of released Ranibizumab will be discussed in chapter VII). Based on these very good results, an *in-vivo* study in rabbit eyes was performed (chapter V).

Beyond the principal scope of this chapter, the possibilities offered by triglycerides as depot were further investigated. Both triglycerides were pre-melted together prior to extrusion to change their properties and to study the effects on release patterns. By this, a prolongation of the release profiles of mAb and Ranibizumab was demonstrated. Release duration of mAb was prolonged by approximately 63 % up to 200 days and Ranibizumab release was extended to 160 days being 40 % longer compared to conventional extrusion. Additionally, the release was further linearised by this approach. However, it was not yet possible to associate the improved release profiles to individual lipid characteristics (e.g. melting points, melting energy or status of crystallinity) and release was substantially different when SLIs were stored prior to release. To systematically investigate those aspects, more research is necessary.

As a head to head comparison to lipid implants, PLGA implants having the same size and shape were manufactured using different Resomer® polymers. A sustained release of maximal 15 % and 10 % over 84 days was observed for the mAb and Ranibizumab, respectively, before the PLGA matrix completely degraded; no Bevacizumab or Aflibercept were released at all. As no burst release was seen when PLGA matrices degraded, incorporated protein most likely precipitated already within the depot.

V. *IN-VIVO* STUDY IN RABBIT EYES

V.1 INTRODUCTION

The intravitreal release of therapeutic peptides and proteins drugs is currently one of the most intensively investigated research areas. Table V-1 provides an overview of research which has been carried out in this field. Irrespective of the type of depot used within these studies, it is noteworthy that in most cases Bevacizumab was used. The depots already described in literature are highly diverse in terms of their size, method of production, and use of excipients. Reports can be found on implants [266], micro- and nanospheres [208, 209, 213], or hydrogels, which represent the most commonly used platforms including thermo-responsive hydrogels [206, 267], hydrogels prepared by Diels-Alder-reaction [112], or silk hydrogels [96]. In recent years, also more sophisticated depots have been investigated, for instance electrochemically prepared mesoporous silicon oxide [210], hexyl-substituted PLA [207], a capsule drug ring device [211, 212, 268], or stimuli-responsive nanomaterials [269, 270], just to name a few. If disclosed at all, Bevacizumab or a single-chain VEGF antibody fragment (most likely Ranibizumab) were used.

Also, new *in-vitro* models mimicking the vitreous have been described. Loch *et al.* introduced a vitreous model to obtain data on permeability coefficients of ophthalmic drugs, simulating the vitreous body or simulating drug distribution once administered into the eye [271-273]. Patel *et al.* reported on an *ex-vivo* vitreous humor model to evaluate or even predict protein stability after intravitreal administration [274, 275].

Table V-1: Literature overview of controlled release systems for intravitreal peptide and protein release.

LIPID BASED DELIVERY PLATFORMS					
Peptide or protein	**Analytical technique**	**Delivery platform**	***in-vitro* release**	**Reference**	**comment**
Bevacizumab	ELISA	Nanoliposomes	not available	Abrishami et al. (2009) [213]	• intravitreal injection of liposomes • encapsulated bevacizumab was well tolerated through 42 days in rabbits • clearance of this drug in vitreous from liposomal formulations was slower than soluble form.
OTHER DELIVERY PLATFORMS					
Peptide or protein	**Analytical technique**	**Delivery platform**	***in-vitro* release**	**reference**	**comment**
Bevacizumab	ELISA	Silk hydrogel	up to 90 days	Lovett *et al.* (2015) [96]	• concentrations in vitreous humor after 90 days equivalent to those levels for the positive control at 1 month
single-chain VEGF antibody fragment	SE-HPLC, SDS-PAGE	Semi-solid hexylsubstituted poly(lactic acid) (hexPLA)	up to 98 days	Asmus *et al.* (2015) [207]	• structure was kept intact during incorporation and release
connexin43 mimetic peptide	retinal ischaemia–reperfusion rat model	PLGA nano- and microparticles	up to 120 days	Chen *et al.* (2015) [208]	• promising results for Cx43 down-regulation and RGC rescue in acute injury mode
Bevacizumab	MTT, 3-D angiogenesis culture	Thermoresponsive hydrogel	up to 60 days	Hu *et al.* (2014) [267]	• after 1 month of intravitreal injection, the histomorphology of rabbit's retina was preserved • released bevacizumab inhibited anti-angiogenesis in 3-D cultures
Bevacizumab	ELISA	Nanostructured mesoporous silica (SiO_2) films	up to 30 days	Andrew *et al.* (2011) [210]	• antibody released in its active form over 1 month; approx. 98 % of drug released

Peptide or protein	Analytical technique	Delivery platform	*in-vitro* release	reference	Comment
Bevacizumab	induced choroidal neovascularization (CNV) in rat eyes	PLGA nanoparticles	not available	Pan *et al.* (2011) [276]	• reduction in CNV area suggests successful creation of formulations while retaining bevacizumab's active antiangiogenic properties

V.2 *IN-VIVO* STUDY IN RABBIT EYES WITH PLACEBO LIPID IMPLANTS

In 2012, a study using placebo SLIs was performed to assess the biocompatibility and biodegradability of SLIs inserted into rabbit eyes. SLIs were produced aseptically using a MiniLab® Micro Rheology Compounder (Thermo Haake GmbH Karlsruhe, Germany). The formulation consisted of 30 % H12 and 70 % D118, screw speed was set to 40 rpm and extrusion temperature was adjusted to 41°C. SLIs were inserted into rabbit eyes by a small incision, and biocompatibility and biodegradability were assessed over 84 days.

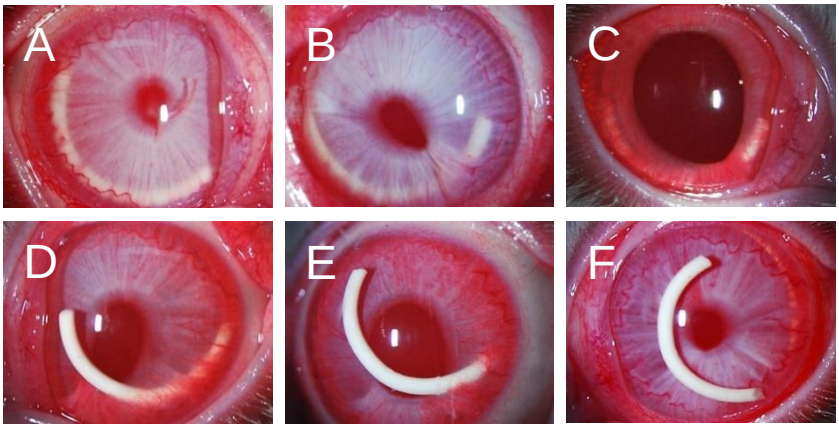

Figure V-1: SLIs inserted into the vitreous of rabbit eyes. The pictures were taken at pre-determined time points starting from (A) day 14 and then after (B) 28 days, (C) 42 days, (D) 56 days, (E) 70 days and (F) 84 days.

The pictures displayed in Figure V-1 show SLIs inserted into the vitreous of rabbit eyes. The macroscopic appearance was monitored over 84 days. Within this observation period, no adverse effects, e.g. inflammation, irritation or swelling occurred. It was therefore concluded that SLIs show very good biocompatibility in rabbit eyes, thereby underlining their potential for use as an intravitreal depot. After the SLIs were removed from rabbit eyes after 7, 30 and 90 days, the mass of explanted SLIs was assessed and compared to the original masses to monitor the implant degradation. After 90 days, SLIs were degraded by 25.6 % on average. The degradation profile was found to be linear (R^2 = 0.9766), which resulted in a theoretical

degradation time frame of approximately 1 year. The data of this study have not yet been published.

Based on the promising results obtained by the biocompatibility/biodegradability study, it was decided to perform a study with Ranibizumab loaded SLIs. Therefore, a formulation was developed (see chapter IV.2.3) which ensured the sustained release of Ranibizumab over approximately 110 days from SLIs being 1.5 mm in diameter, which is still a suitable diameter for intraocular use. Additionally, protein stability of released Ranibizumab was found to be excellent, making it to the most promising candidate (chapter VII.2.1) for this study.

The *in-vivo* study in rabbit eyes was performed by the Moran Eye Center, Salt Lake City, Utah, USA.

V.3 CHOROIDAL NEOVASCULARISATION (CNV) MODEL

Neovascularisation was induced as described in III.2.5.4. It was induced by an adeno-associated virus (AAV) mediated expression of vascular endothelial growth factor (VEGF) [243, 277]. AAV-VEGF was injected subretinally to induce neovascularisation in dutch-belted rabbit eyes. An increased expression of VEGF in the retina is sufficient to induce retinal neovascularisation [277].

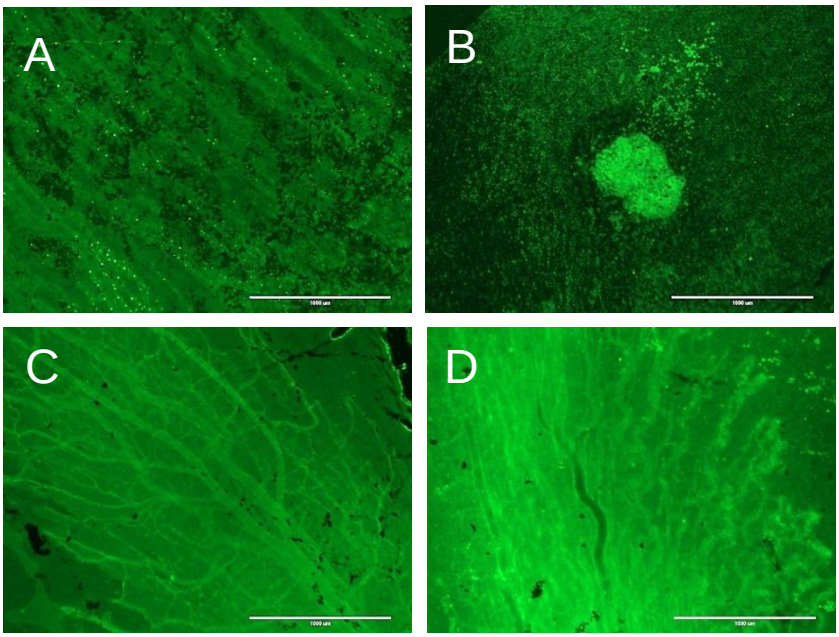

Figure V-2: Isolectin staining of flatmounts for choroidal neovascularisation lesions. Illustrated are the (A) choroid control, the (B) choroid lesions induced, (C) the control of retina, and the (D) increased retina vessel proliferation.

A fluorescein solution with 100 mg/ml was injected (100 µl) into the vitreous, enabling an imaging for up to 30 min. Figure V-2 illustrates that neovascularisation was successfully induced as choroidal lesions (Figure V-2 B) and an increased proliferation of retina vessels were observed (Figure V-2 D) compared to the controls (Figure V-2 A and Figure V-2 C). Although it was intended to induce choroidal neovascularisation, evidence suggested only retinal neovascularisation was achieved.

V.4 RESULTS AND DISCUSSION

V.4.1 *IN-VITRO* RELEASE OF RANIBIZUMAB

In-vitro release of Ranibizumab was evaluated additionally to *in-vivo* release. Thus, it was possible to perform an *in-vitro-in-vivo* correlation. Extrusion of aseptically SLIs was performed as described previously (III.2.5). The semicircle shaped SLIs had a final weight of 32.93 mg (±2.39 mg) and in average 1.65 mg (±0.12 mg) Ranibizumab were loaded onto an implant.

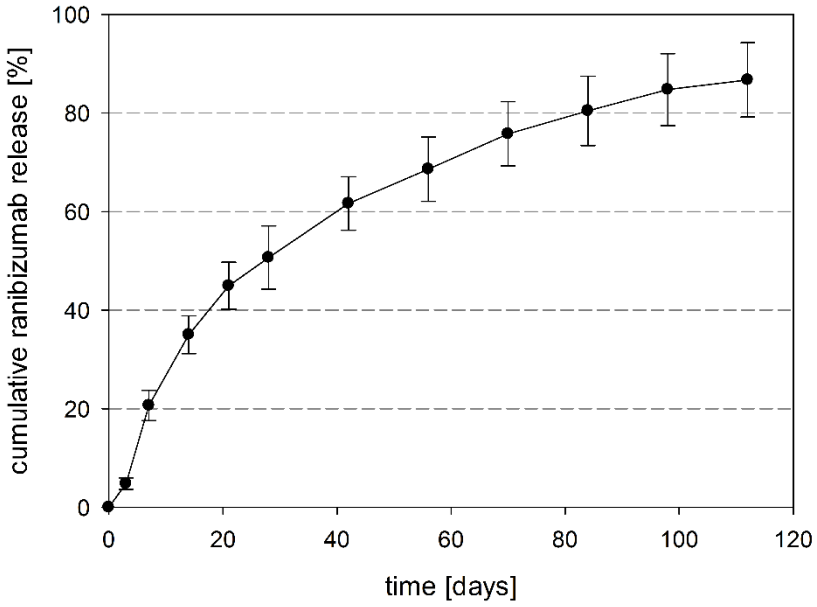

Figure V-3: *In-vitro* release of Ranibizumab from the same batch which was manufactured for the *in-vivo* study.

Results from Ranibizumab release study (Figure V-3) showed qualitatively comparable release behaviour as described before (chapter IV.2.3). During the first phase lasting for 4 weeks, 51 % of incorporated protein was released (30.1 µg/day), followed by a phase ranging from day 28 to day 112 in which approximately 36 % of incorporated protein equivalent to 7.1 µg protein per day was liberated. No burst release occurred, after 3 days of incubation only 4.8 % of Ranibizumab was released.

V.4.2 MACROSCOPIC OBSERVATIONS

SLIs were inserted into the vitreous of dutch-belted rabbits by a small incision. The vitreous was examined after 15, 22, 30, 51, 63 and 87 days after implantation of the SLI. Both placebo SLIs and Ranibizumab loaded SLIs were inserted.

Differences between placebo and Ranibizumab loaded SLIs were not observed, therefore the following descriptions do not distinguish between them.

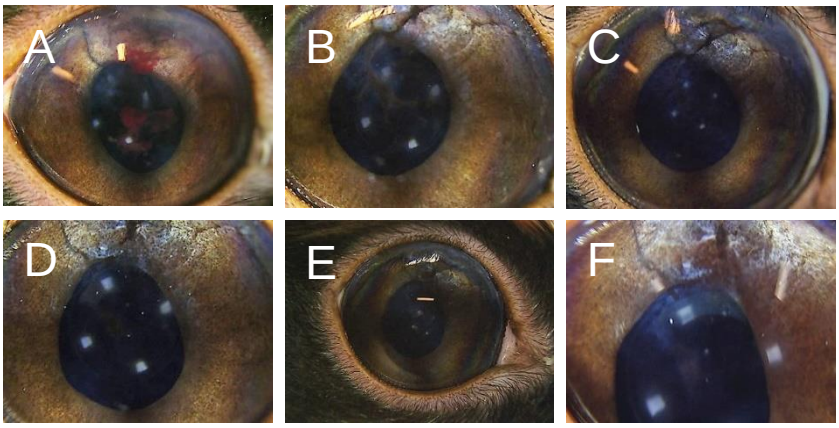

Figure V-4: Pictures of dutch-belted rabbit eyes where retinal neovascularisation was not induced (negative control). Ranibizumab loaded SLIs were inserted and the eyes examined after (A) day 6, (B) day 22, (C) day 30, (D) day 51, (E) day 63 and (F) day 87.

Within the observation period of 87 days, no adverse reactions or impairments like inflammation, encapsulation, swelling, or redness occurred. Also, the inserted SLIs stayed at the side of implantation (Figure V-4). Therefore, it can be concluded that the SLIs were well tolerable and biocompatible.

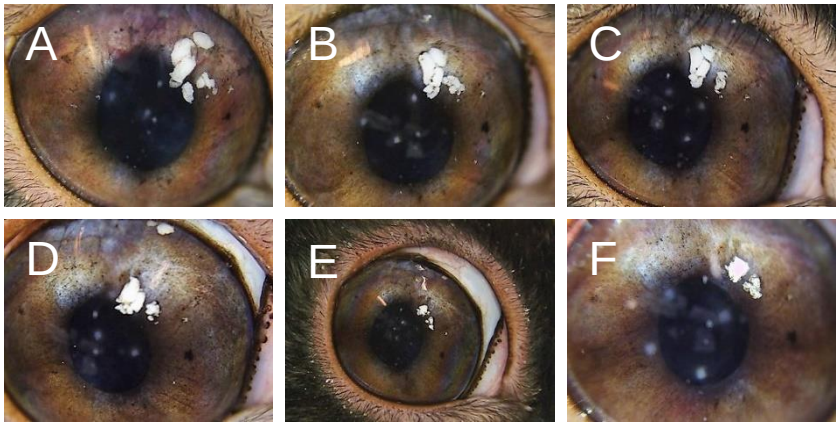

Figure V-5: Pictures of retinal neovascularisation induced dutch-belted rabbit eyes. SLIs were inserted and the eyes examined after (A) day 6, (B) day 22, (C) day 30, (D) day 51, (E) day 63 and (F) day 87.

Figure V-5 illustrates that also in some cases small pieces of SLIs floating in the vitreous were observed right from the beginning. This means that those small parts of the implant broke apart most likely already during to the incision procedure.

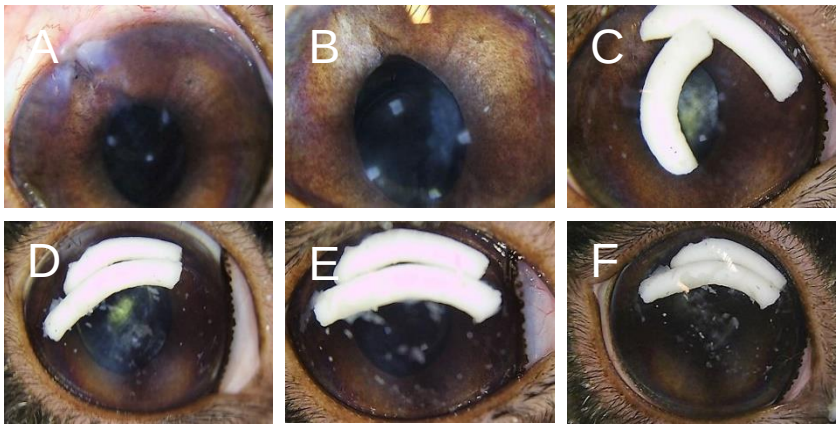

Figure V-6: Pictures of retinal neovascularisation induced dutch-belted rabbit eyes. SLIs were inserted and the eyes examined after (A) day 6, (B) day 22, (C) day 30, (D) day 51, (E) day 63 and (F) day 87.

Also, a breakage of the complete implant was noticed. As shown in Figure V-6, during the first 22 days of observation, no anomalies were observed, but at day 30 it was observed that the complete SLI broke apart into two pieces. This points into the direction that the breakage occurred during the incubation and was not caused by the incision as mentioned above.

In total, in 28.5 % of examined rabbit eyes a haze or debris of the cornea was observed after 1 month. The percentage increased over time ending up at 66.7 % where a haze/debris was noticed after 3 months. The migration of the SLI into the anterior chamber was observed for 25.0 % after 1 month and for 45.8 % after 2 months.

Compared to the biocompatibility/biodegradability study from 2012, SLIs used here were mechanically less stable. Breakage and disintegration observed within the present study (Figure V-6) had not been observed in 2012 (Figure V-1). There are several reasons for this observation: dutch-belted rabbit eyes are smaller than those of New Zealand rabbits used in 2012. Therefore, more force is required to place implants into the vitreous, possibly damaging the SLIs. Implants used here were smaller in diameter (1.5 mm) than the ones used previously (2.0 mm). Furthermore, a different formulation was used, comprising a higher percentage of H12 which could have possibly affected the mechanical stability of the SLIs. This aspect was further evaluated in detail and will be described below (V.4.5). As no difference was observed between placebo and Ranibizumab loaded implants in the current study, it is unlikely that the presence of Ranibizumab caused implant breakage.

Further reasons leading to the break-up of implants could be external/environmental factors. As published by Lorget *et al.* [278] and Schwartz *et al.* [279], the temperature within rabbit eyes is not exactly 37°C as it was the case for *in-vitro* conditions. It is known that the temperature ranges from 35.8°C to 38.2°C in rabbit eyes, and that temperatures within the vitreous of rabbits are higher in comparison to mini pig or monkey eyes. Furthermore, «significant regional differences […] particularly between the lateral and the medial locations where the delta was approximately 2.5°C in the rabbit» are described [278]. The average temperature in the lower vitreous is 37.5°C, which is the region were the implants were located. Based on our previous studies, it is known that the percentage of H12 substantially impacts mechanical stability of SLIs; at a very high percentage even causing complete disintegration at 37°C (IV.2.3.4). To determine, if a higher external temperature than 37°C could cause a mechanical weakening of the implants (and therefore causing a break-up), a study was performed discussed in V.4.5.

V.4.3 PHARMACOKINETIC STUDY

Released Ranibizumab was quantified according to III.2.5.5. In the following, the pharmacokinetic data from four different eyes are presented representing the pharmacokinetic profile of Ranibizumab within this study. Table V-2 provides an overview of Ranibizumab amounts in nanograms (ng) which was quantified within the different compartments of those eyes after the first months.

Table V-2: Overview of Ranibizumab amounts measured within the different rabbit eye compartments 1 month after implantation of SLIs. Amounts are given in ng.

Compartment	Eye 437 L	Eye 437 R	Eye 438 L	Eye 438 R
Cornea	53.13	35.59	72.90	4.85
Vitreous	8.52	0.72	22.91	1.21
Lens	137.29	106.07	483.63	41.68
Iris	3.89	2.30	46.94	3.77
Retina/choroid	1.21	3.77	5.35	2.67
Aqueous humor	31.21	90.60	189.74	15.72
Conjunctiva	0.60	0.48	1.21	0.84
Sclera	3.28	1.94	48.40	3.77
Total	**239.15**	**241.46**	**871.10**	**74.51**

The overall quantified amount of Ranibizumab varied between 871 ng (eye 438 L) and 75 ng (eye 438 R). Nonetheless, the overall amount of quantified Ranibizumab was very similar to each other regarding the other two eyes (239 ng and 241 ng). Most Ranibizumab was found in the lens (192.2 ng ±198.3 ng), cornea (41.6 ng ±28.9 ng), and aqueous humor (81.8 ng ±78.9 ng) in all examined eyes.

Table V-3: Overview of Ranibizumab amounts measured within the different rabbit eye compartments 2 month after implantation of SLIs. Amounts are given in ng.

Compartment	Eye 433 L	Eye 433 R	Eye 434 L	Eye 434 R
Cornea	0.00	0.00	7.65	46.75
Vitreous	0.00	0.00	0.00	0.06
Lens	0.85	0.00	97.76	103.50
Iris	282.35	347.06	260.21	262.21
Retina/choroid	0.00	0.00	2.46	27.75
Aqueous humor	0.20	0.77	83.47	222.79
Conjunctiva	0.00	0.00	8.31	0.00
Sclera	1.13	0.00	17.22	37.80
Total	**284.53**	**347.83**	**477.08**	**700.87**

The same results were observed for Ranibizumab quantified after 2 months (Table V-3): the overall amount of released Ranibizumab ranged from 285 ng (eye 433 L) to 701 ng (eye 434 R). The highest levels of Ranibizumab were measured within the lens (50.5 ng ±57.9 ng) and aqueous humor 102.3 ng (±112.2 ng). This time, also notable amounts were found in the iris (288.0 ng ±40.7 ng).

After 3 months, no noticeable amounts of Ranibizumab were quantified any more.

Ranibizumab concentrations were further measured within the retina/choroid after 1 month and 2 months as shown in Table V-4. The target concentration for total inhibition of proliferation was observed at Ranibizumab concentrations ≥ 1.3 nM which are 62 ng/g. The necessary Ranibizumab concentration to inhibit the biological activity of VEGF by 50 % (IC_{50}) was measured with 11 ng/g to 27 ng/g (data provided by Moran Eye Center, Salt Lake City, Utah, USA).

Table V-4: Overview of Ranibizumab concentrations in retina/choroid in ng/g after 1 and 2 months for all eyes.

	1 month [ng/g]	2 months [ng/g]	Target concentration for total inhibition [ng/g]
Eye 1	15.59	0.00	62
Eye 2	56.27	0.00	
Eye 3	50.66	27.81	
Eye 4	120.03	376.47	

The data presented in Table V-4 indicate, that after 1 month at all eyes the concentration reached the IC_{50} of VEGF. In the case of eye 4, the target concentration of 62 ng/g was exceeded as 120 ng/g Ranibizumab were measured. After 2 months, only for two eyes measurable concentrations were calculated with 28 ng/g and 376 ng/g Ranibizumab. As observed previously, concentrations were found to greatly vary from each other.

The *in-vivo* release of Ranibizumab was monitored over 3 months. Measurable amounts were found at the 1-month time point at all compartments and partly after 2 months. After 3 months, no noticeable amounts of Ranibizumab were quantified any more. Within the retina/choroid, especially after 1 month, concentrations were measured being above the IC_{50} of VEGF, partly even exceeded the concentration of total proliferation inhibition. However, *in-vivo* release was largely complete after 4 weeks and thus faster than measured *in-vitro*. Therefore, an *in-vitro-in-vivo* correlation could not be established.

V.4.4 COMPARISON OF OUR RESULTS TO CURRENT STATUS OF RESEARCH

Abrishami *et al.* [213] describes the encapsulation of Bevacizumab within phospholipid based liposomes using the well-known film method which was used previously to encapsulate versatile drugs into liposomes [231, 280-283]. The liposomes were further processed to reach the nanoscale. Liposomal encapsulated Bevacizumab was injected intravitreally into rat eyes and

concentration was determined over 42 days by ELISA. The authors stated, that the Bevacizumab concentration was measured up to five times higher in rat eyes which received liposomal encapsulated Bevacizumab compared to those where Bevacizumab was administered in an aqueous solution. This points into the direction that the encapsulated Bevacizumab was prevented from clearance better than the soluble drug showing the beneficial effects of liposomes as carrier. However, a disease model was not tested within this work.

A silk hydrogel as potential depot for intravitreal delivery of Bevacizumab was described by Lovett *et al.* in 2015 [96]. The concentration of Bevacizumab released from silk hydrogels was measured over 90 days within the vitreous humor of dutch-belted rabbit eyes. Bevacizumab concentrations measured at day 90 were equivalent or greater than those analysed at day 30 after administration of the positive (standard dose) control, which was a single injection of 1.25 mg Bevacizumab. Again, a disease model was not considered.

Nanostructured mesoporous silica films represent another option. Here, Bevacizumab was released in its active form over approximately 1 month, but was only measured *in-vitro* [210].

Hu *et al.* reports on the anti-angiogenetic effect of Bevacizumab released from thermo-responsive hydrogels [267]. Those gels consisted of block copolymers of methoxy-PEG-block-PLGA cross-linked with 2,2-bis (2-oxazoline) (BOX). This special polymer can reverse the sol-gel-sol phase transition. The mPEG-PLGA-BOX gel was injected intravitreally into rabbit eyes and released Bevacizumab was collected after 1 month. The bioactivity of released Bevacizumab was tested by different assays including the human umbilical vein endothelial cells (HUVECs) assay, Macaca mulatta retina epithelial cells (RF/6A) assay and 3-D angiogenesis assay. It was found that anti-angiogenesis took place, therefore demonstrating the bioactivity of released Bevacizumab.

The performance of Bevacizumab in a CNV rat model induced by laser photocoagulation has been reported by Pan *et al.* [276]. Within the study, different long-acting Bevacizumab formulations (PEG-bevacizumab conjugate and PLGA-encapsulated bevacizumab) were

compared to Bevacizumab as an aqueous solution. The authors reported on a reduction of CNV area for all long-acting Bevacizumab formulations compared to the aqueous Bevacizumab solution. The authors concluded that a reduction in CNV area suggests successful formulations while retaining bevacizumab's active antiangiogenic properties.

A study describing the *in-vivo* behaviour of Ranibizumab released from a depot in a disease model was not found in literature.

Biocompatibility issues were not reported in the studies described above. Also, within our study, biocompatibility of lipid implants was excellent since no adverse reactions or inflammation was observed over 3 months. Within our study, a sustained release of Ranibizumab over at least 28 days was measured. Partly, also after 42 days Ranibizumab was still released which corresponds to the deliver time frames described by Abrishami *et al.* [213] and Hu *et al.* [267]. Other references reported on longer release durations [96]. Since the breakage of SLIs occurred rather early within our *in-vivo* study, a further examination (e.g. histological examination) was not performed. By this, a comparison to published data is not possible.

V.4.5 MECHANICAL STABILITY OF IMPLANTS

During the *in-vivo* study, breakage of SLIs was observed, which did not occur during the biocompatibility study performed in 2012. A reason for this might be temperature gradients being present in rabbit eyes, which has been already reported [278, 279]. Those gradients are ranging from 35°C to 38°C and could therefore negatively impact mechanical properties of the implants, hence leading to breakage. Additionally, a higher percentage of the low melting lipid H12 was used within the study, which most likely influenced mechanical properties of the SLIs.

To verify these hypotheses, a study was performed focusing on the mechanical properties of SLIs. In a first experiment, implants of the same formulation used within the *in-vivo* study were incubated at different temperatures (35°C, 37°C, 39°C) and bending strength was measured

after 7 days and 28 days, respectively. Second, the composition of the lipid matrix of SLIs was varied (30 % to 50 % H12) and bending strength of implants was determined after an incubation at 37°C for 7 days and 28 days. All formulations tested here comprised 10 % protein lyophilisate. Implants were placed in 1.0 ml PBS pH 7.4 and were incubated in a Certomat IS (Sartorius BBI, Göttingen, Germany) horizontal shaker at 40 rpm. After 7 days and 28 days, SLIs were removed, dried in a vacuum chamber for 24 h at 25°C at 10 mbar (Memmert GmbH & Co KG, Schwabach, Germany) and bending strength was determined.

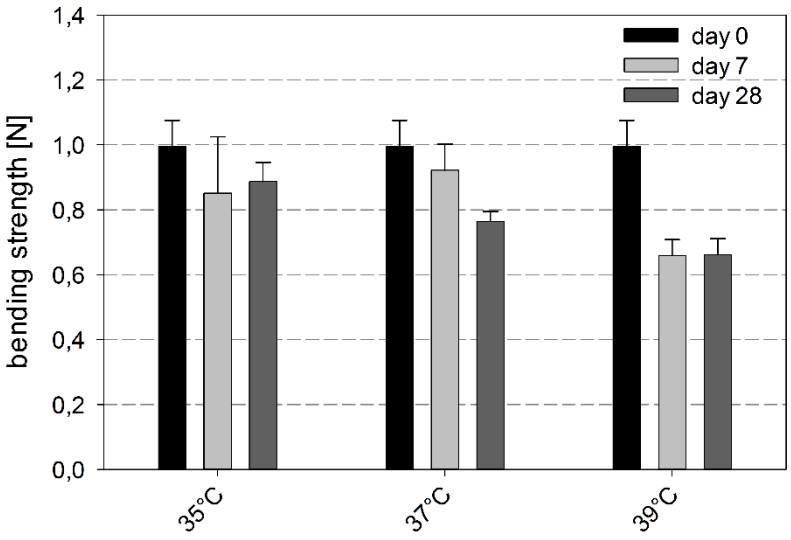

Figure V-7: Bending strength of lipid implants consisting of 10 % protein lyophilisate, 45 % H12 and 45 % D118 incubated at 35°C, 37°C and 39°C over 28 days. Bending strength was measured prior to release (day 0) and after 7 days and 28 days of release, respectively.

Figure V-7 displays the bending strength of SLIs incubated at 35°C, 37°C and 39°C. Irrespective of the incubation temperature, bending strength decreased upon incubation. Most importantly, mechanical stability was less the higher the incubation temperature was. After 28 days of incubation, bending strength was measured with 0.88 N (±0.06 N), 0.76 N (±0.03 N) and 0.66 N (±0.05 N) for the incubation temperatures 35°C, 37°C and 39°C, respectively. Thus, a correlation between mechanical stability and incubation temperature can be described.

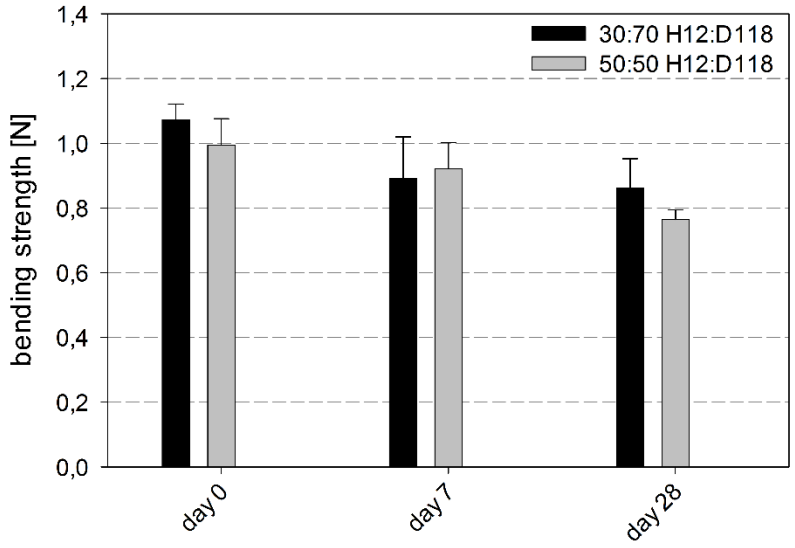

Figure V-8: Bending strength of lipid implants consisting of 10 % protein lyophilisate and different lipid matrices comprising 30 % and 50 % H12 were incubated at 37°C over 28 days. Bending strength was measured prior to release (day 0) and after 7 days and 28 days of release, respectively.

Second, SLIs were tested including both the exact lipid matrix used within the biocompatibility study from 2012 (30 % H12, 70 % D118) and the study described here (50 % H12, 50 % D118). The results of these experiments are displayed in Figure V-8. The formulation with 30 % H12 was mechanically more resistant than SLIs containing 50 % H12. As more mechanically stable SLIs were used for the biocompatibility study than used within the present study, the breakage which occurred within this study can be explained. Both aspects (temperature and implant composition) could be a possible explanation of SLI breakage occurring during the *in-vivo* study and the faster release *in-vivo* compared to *in-vitro* release.

V.5 CONCLUSION

Ranibizumab loaded SLIs were inserted into dutch-belted rabbit eyes and the *in-vivo* release was monitored over 3 months additionally to macroscopic observations.

In 2012, excellent biocompatibility of placebo lipid implants inserted into the vitreous of New Zealand rabbits was reported. Over 90 days, no inflammation, encapsulation or other adverse reactions and complications were observed, thereby highlighting the great potential of lipid implants for intravitreal applications.

Within our study, biocompatibility of lipid implants inserted into dutch-belted rabbit eyes was excellent, since no adverse reactions or inflammation was observed over the complete observation time of 3 months. After 2 months, in 45.8 % a break-up of implants occurred and in 2/3 of rabbit eyes a haze/debris was noticed after 3 months. Associated with the partial break-up of implants, *in-vivo* release was found to be faster than *in-vitro* going in line with high standard deviations. *In-vivo* release was tested over 3 months, but no more Ranibizumab was released after 8 weeks.

It was hypothesised that the formulation used here was mechanically more sensitive compared to the one used in 2012 for two reasons. First, the formulation used here, comprised a relatively high percentage of H12. Second, the temperature within dutch-belted rabbit eyes might be higher than 37°C possibly impacting mechanical properties of SLIs. We could confirm that both the relatively high percentage of H12 and slightly higher incubation temperatures (modelling elevated temperatures within the rabbit eye) than 37°C do negatively impact mechanical stability of SLIs. It is therefore likely that this was the reason for implant break-up and faster *in-vivo* release. Furthermore, another possible reason could be that due to the CNV induction the temperature within the rabbit eyes changed and hence influenced the mechanical stability of the implants additionally.

VI. BIOLOGICAL ACTIVITY OF RELEASED MINI-FH FROM LIPID IMPLANTS

VI.1 INTRODUCTION

This chapter describes the sustained release of the protein mini-Factor H (mini-FH) from SLIs and the determination of its biological activity following the release from the depot. Mini-FH is a protein having a molecular weight of 43.3 kDa and is a C3-opsonin targeted complement inhibitor for potential use against paroxysmal nocturnal hemoglobinuria (PNH) [240, 241]. PNH is characterised by haemolytic anaemia caused by the expansion of hematopoietic progenitor cells. In turn, PNH results in anaemia, hemoglobinuria, fatigue, and other hemolysis-related disabling symptoms [284-287]. Currently, Eculizumab is the only therapy available for patients suffering from PNH [288, 289]. Schmidt *et al.* recently described a novel therapeutic approach, which involves C3-opsonin targeted complement inhibitors, which are engineered from parts of the natural complement regulator Factor H (FH) or the complement receptor 2 (CR2) [240, 241]. The FH inhibitor class includes three variants of the so-called mini-FH which was used within this experiment. Schmidt *et al.* observed that mini-FH was more efficient in preventing complement activation on PNH erythrocytes which represents a promising therapeutic alternative [241].

PNH is a disease of the so-called alternative pathway (AP) [290-292] as it is also the case for wet AMD [293]. That is the reason why AP inhibitors (like mini-FH) are first tested in the «model disease» PNH before they are subsequently tested in other AP-mediated disease models as it is the case here. Currently, mini-FH is also being tested in canine and monkey eyes (not published). Meanwhile, other AP inhibitors than mini-FH have already been tested in AMD animal models. It is described that «Targeted complement inhibitors such as TT30 and its homologs have not only shown promising potential in PNH, but also in a variety of other AP-

mediated clinical conditions ranging from collagen induced arthritis and ischemia/reperfusion injury to AMD» [294, 295]. Further, Schmidt *et al.* stated that «in the case of AMD, mini-FH may have particular advantages» [240]. In the case of chronic and progressive eye diseases (as it is the case for AMD), the loss of vision and neovascularisation of the retinal tissue is strongly associated with the complement regulation by Factor H. Factor H was identified as a major binding protein for lipid peroxidation, which is a marker of oxidative stress accumulating under various diseases conditions including AMD as described by Weismann *et al.* [296, 297].

The aim of this chapter is to evaluate the potential of mini-FH loaded SLIs as depot for the treatment of AP-mediated diseases like wet AMD. The preparation of mini-FH loaded SLIs and their *in-vitro* release behaviour is described in the following. Additionally, the biological activity of released mini-FH was measured by a rabbit erythrocyte hemolysis assay. The assay was performed by the group of Dr. Christoph Schmidt at the Institute of Pharmacology and Natural Products and Clinical Pharmacology, University of Ulm, Germany.

VI.2 RESULTS AND DISCUSSION

VI.2.1 *IN-VITRO* RELEASE OF MINI-FH

Lipid implants were produced using a ZE-5 mini extruder. The lipid matrix consisted of 50 % H12 and 50 % D118, mini-FH load was adjusted to 5 %, resulting in a final protein load of 1.45 mg (± 0.03 mg) per implant. Mini-FH was available as freeze-dried powder without any further excipients. Extrusion temperature was set to 35°C and screw speed was adjusted to 40 rpm.

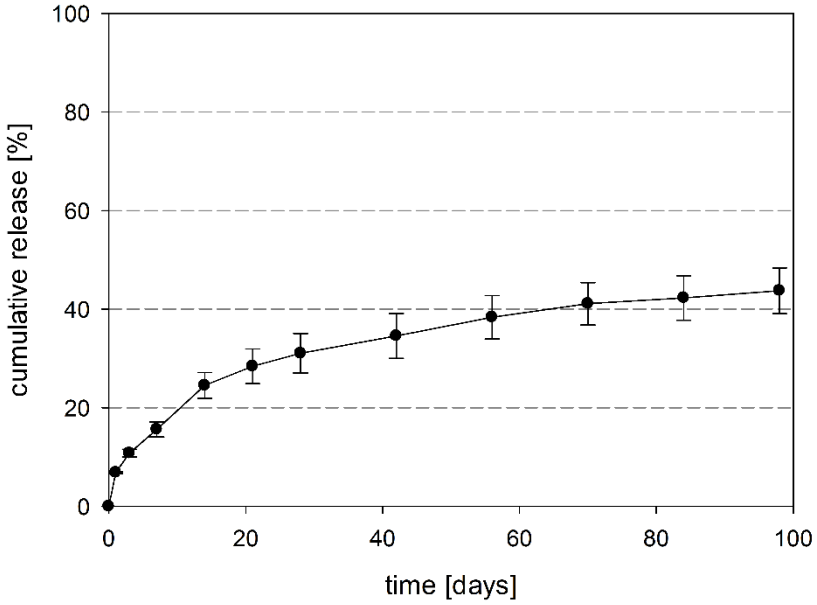

Figure VI-1: Cumulative release of mini-FH from SLIs being 1.5 mm x 15 mm in size. Protein load was set to 1.45 mg (± 0.03 mg) per implant.

According to the *in-vitro* incubation protocol described in chapter III.2.3, extrudates were placed into 2.0 ml micro centrifugation tubes, 1.0 ml PBS pH 7.4 was added and release was monitored at 37°C and 40 rpm using a Certomat IS (Sartorius BBI, Göttingen, Germany) horizontal shaker. Released mini-FH was measured spectrophotometrically at 280 nm applying an UV-VIS spectrometer (Agilent 8453, Böblingen, Germany). Linearity of measurements was established

for a concentration range of 0.001 mg/ml to 0.5 mg/ml (R^2 = 0.9997). The samples were stored at -80°C directly after protein concentration was measured.

Cumulative mini-FH release was monitored over 98 days. In total, 43.7 % of total incorporated mini-FH was released. The release curve did not show an initial burst, and the first phase was followed by a phase lasting until day 14 (25.4 µg mini-FH per day were delivered during this phase). Starting from day 14, release rate was slower (approximately 3.3 µg/day) lasting until day 98. After 98 days of release, the experiment was stopped because only minimal amounts of mini-FH were released. Those amounts would not be sufficient for biological activity determination. In contrast to the other proteins tested within this thesis (Figure IV-11), mini-FH was not completely released. In total, approximately 45 % of incorporated mini-FH were released. The non-recovered fraction of 55 % was probably still incorporated within the lipid matrix as this was already described for other proteins using triglyceride based SLIs [185]. As this phenomenon is more pronounced for hydrophobic proteins [185], it can be assumed that mini-FH is a rather hydrophobic protein. However, this was not evaluated within the present study and should be addressed in the future.

VI.2.2 BIOLOGICAL ACTIVITY OF RELEASED MINI-FH

Released mini-FH was collected at predetermined time points and frozen at -80°C prior to biological activity measurements. The biological activity of released mini-FH was determined as previously described [241]. In brief, 10 µl human serum containing Mg-EDTA was mixed with 20 µl sample in PBS pH 7.4 and 10 µl of a rabbit erythrocyte suspension in PBS/Mg-EDTA. The final serum concentration was 25 %. The mixture was incubated for 30 min at 37°C and reaction was stopped with 120 µl PBS/EDTA (5 mM) on an ice bath. Hemolysis was determined via optical density measurement of 100 µl of the supernatant at 405 nm using a spectrophotometer. Rabbit erythrocytes lyse in presence of active human serum due to the complement activation

and formation of membrane attack complexes on rabbit erythrocytes. Mini-FH inhibits the human complement system and therefore protects rabbit erythrocytes.

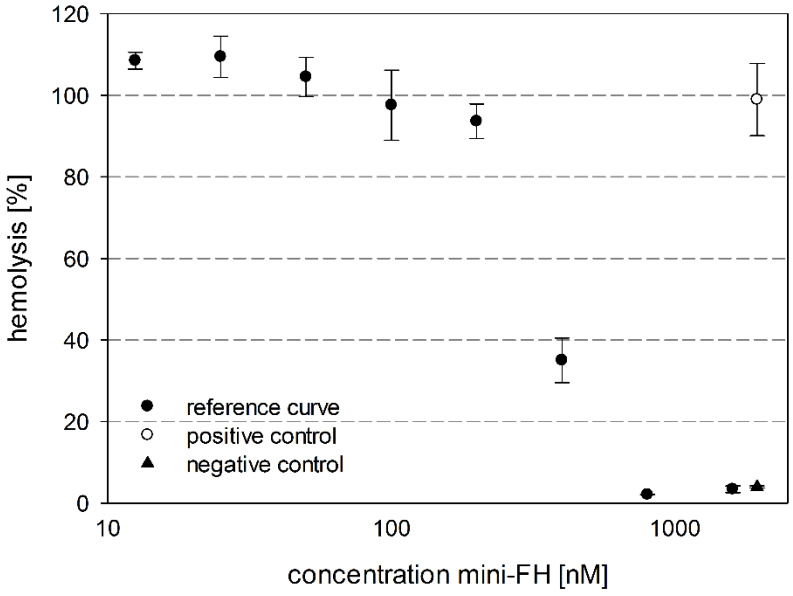

Figure VI-2: Hemolysis in dependence of mini-FH concentration. Positive and negative control in this experiment are displayed as open circles or filled triangles.

Figure VI-2 displays the mini-FH reference curve at a concentration range of 12.5 nM to 1600 nM and the controls (negative and positive). The reference of 100 % is defined by reagent red blood cells (rRBCs) in MQ water, having the same volume and ratio as the samples. The positive control (total hemolysis) consisted of rRBCs diluted with human serum without the addition of any inhibitors, e.g. mini-FH. The value of total hemolysis is slightly above 100 % (5 % to 9 %) which is within the error limit of the assay. The negative control was a dilution of the serum where 5 mM EDTA were added. In the absence of Mg^{2+} ions (present in EDTA), the AP of the cascade does not function, although all complement proteins are present.

Mini-FH data points were analysed in duplicates, whereas the positive and negative control were analysed in quadruplicates.

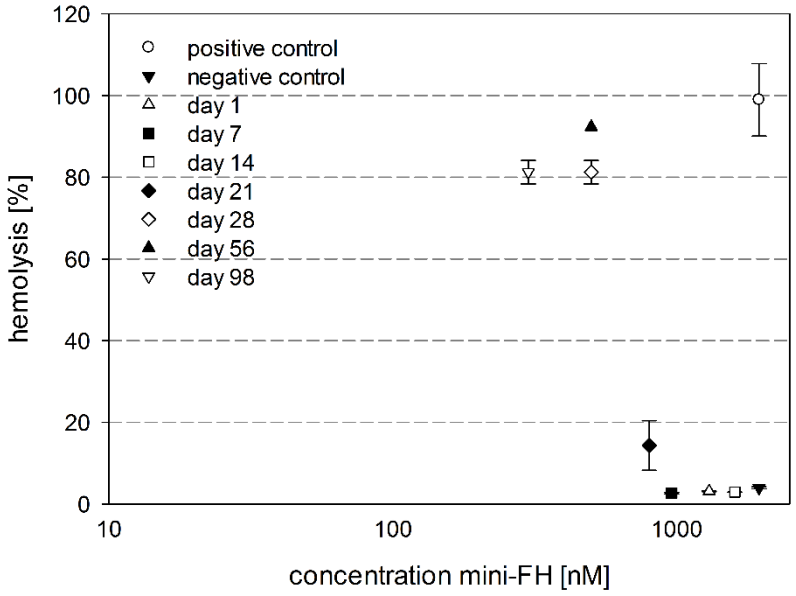

Figure VI-3: Hemolysis of mini-FH released from SLIs determined over 98 days.

The hemolysis percentage in dependence of mini-FH released from SLIs is illustrated in Figure VI-3. It can be observed that hemolysis was measured between 2.6 % and 3.1 % within the first 14 days of release meaning a complete inhibition of hemolysis occurred pointing into the direction of a strong biological activity of released mini-FH. Mini-FH released on day 21 still revealed clear biological activity (14.3 % inhibition of hemolysis). Samples taken between day 28 and day 98 showed a hemolysis of 92.3 % and 81.2 %. This leads to the conclusion that released mini-FH lost its biological activity upon release compared to the fractions released within the first 21 days. Nevertheless, still after 98 days of *in-vitro* release, mini-FH comprised biological activity.

The biological activity of proteins released from lipid based systems has been described in literature before. For instance, Koennings *et al.* described the biological activity of the brain-derived neurotrophic factor (BDNF), released *in-vitro* from compressed implants over 1 month. The biological activity of BDNF was measured with up to 60 % intact protein assessed by ELISA [175]. Also, the activity of released interleukin-18 (IL-18) from compressed lipid implants was

observed over 12 days, showing a progressive integrity loss down to 20 % to 40 % [174]. Even *et al.* demonstrated that the *in-vivo* release of the peptide TRP-2 delayed tumor growth for 3 days compared placebo groups, indicating that TRP-2 was biologically active [187].

Despite SLIs, solid lipid nanoparticles (SLNs) as delivery platform have been used as well. Human thymidylatesynthase inhibitor peptide, an octapeptide, was encapsulated within SLNs and apoptosis was measured using a cell culture model over 4 h once the SLNs were spiked to the cell media. The increase of apoptosis percentage observed indicated that SLNs could carry the peptide efficiently to its enzymatic target in its biologically active form [140]. In 2009, Abrishami *et al.* reported on the encapsulation of Bevacizumab within nanoliposomes [213]. Nanoliposomes were administrated intravitreally into rabbit eyes and Bevacizumab concentration was assessed by ELISA over 42 days, showing that the clearance of Bevacizumab from nanoliposomes was slower than from the soluble form and that Bevacizumab was still active.

VI.3 CONCLUSION

The protein mini-FH was encapsulated within SLIs and release was monitored over 98 days in a sustained fashion. Release started to level off after 70 days of incubation. However, even after 98 days, small amounts of mini-FH were still released from SLIs. The biological activity of released mini-FH was determined, showing a clear biological activity over the first 21 days. Furthermore, mini-FH released between day 56 and day 98 still exhibited biological activity.

In literature, lipid based systems have already been described for the sustained release of biologically active peptides and proteins [140, 187, 213]. To the best of our knowledge, none of those reports assessed the biological activity over a period of more than 42 days. Here, mini-FH biological activity was measured over a time frame of 98 days which is unique. These findings underline the great potential of lipid based implants, as they can ensure long-term release of proteins but at the same time preserve biological activity of encapsulated protein.

The present study demonstrated the feasibility of SLIs for long-term release of the complement factor mini-FH over several weeks. Based on these promising results, future work should progress with evaluating the source of incomplete mini-FH release, *in-vitro* release optimisation (further tailoring of release, more complete release) and consequently the *in-vivo* performance of the system, e.g. in rabbit eyes.

VII. STABILITY OF RELEASED PROTEIN FRACTIONS FROM LIPID AND PLGA MATRICES

PARTS OF THIS CHAPTER HAVE BEEN PUBLISHED IN THE *EUROPEAN JOURNAL OF PHARMACEUTICS AND BIOPHARMACEUTICS* AS:

Moritz Vollrath, Julia Engert, Gerhard Winter

Long-term release and stability of pharmaceutical proteins delivered from solid lipid implants, European Journal of Pharmaceutics and Biopharmaceutics 117 (2017) 244-255

VII.1 INTRODUCTION

Developing protein delivery systems ensuring the stability of the protein drug remains a challenge [215]. Extensively investigated delivery systems for protein delivery are PLGA based systems [45, 71, 242], PLGA composites [68, 298] or other polymers like chitosan [79] including different delivery platforms such as hydrogels [111], nanogels [88, 114] or silk [96]. Protein drugs investigated for controlled release include model proteins, for instance bovine serum albumin (BSA) [114], lysozyme [175] or pharmaceutical proteins, e.g. erythropoietin (EPO) [45, 242], insulin [68, 79, 298], goserelin (Zoladex®) or monoclonal antibodies like bevacizumab [96].

Table VII-1 and Table VII-2 display a review of controlled release systems for peptides and proteins delivered from lipidic and non-lipidic depots which address protein stability (Table VII-1) and bioactivity aspects (Table VII-2) of encapsulated and/or released protein. The references provided in the tables illustrate that significant research has been performed in this field within the last years, while the focus was mainly on PLGA based depots or hydrogels. Beyond «classical» analytical techniques to characterise proteins, e.g. SE-HPLC, SDS-PAGE or CD, also the bioactivity of released proteins (Table VII-2) have been investigated. Nonetheless, little research has been performed with respect to lipidic depots.

In the past, only a few studies have reported on protein stability after encapsulation into the matrix [68, 242], but stability of the released protein has often not been taken into account. But, protein stability and activity should be addressed more intensively in future, as a drug delivery system is useless when the delivered protein comprises no acceptable stability and biological activity, respectively.

More recently, several papers have been published also addressing protein stability and activity aspects of released protein for insulin [49] exenatide [217] or a f_{ab}-fragment [72] delivered from PLA/PLGA microspheres [49, 217] or PLGA-triacetin depots [72]. A major focus was on chemical degradation of insulin and exenatide during release from PLA/PLGA microspheres. The authors demonstrated deamidation of insulin [49] and acylation for exenatide [217] in the

time frame of 18 to 20 days upon release. Contrarily, stability of a f_{ab}-fragment released over approximately 80 days from a PLGA-triacetin based depot was described to be promising even though relative antigen binding capacity dropped to 80 % and peak area measured by IEX was found to be halved after 12 weeks of release [72].

Moreover, reports can be found on biological activity [63, 77, 84] and binding capacity [72] of released proteins of different size and structure, e.g. NEL-like molecule-1 (NELL-1), bone morphogenetic protein-2 (BMP-2), platelet-derived growth factor (PDGF-AA) or a f_{ab}-fragment from modified chitosan particles [77] or hydrogels [63, 84]. Irrespectively of the different delivery depots and proteins studied, biological activity and antigen binding capacity was found to be retained even after several weeks of release.

For lipid based (mainly triglycerides) depots, which have been investigated since the early 2000s, research has been focused on release profiles and underlying release mechanisms [155, 157, 158, 182, 299], the solid-state behaviour for the lipids [161, 163], effect of release modifiers [149, 160, 177, 178] or *in-vivo-in-vitro* correlations [168] of various drugs including small molecular drugs [163, 236, 299], model proteins [182] and pharmaceutical proteins [178]. However, protein stability aspects have not been investigated in depths until now. Analysis of encapsulated and released protein from lipidic systems has been described for the first time in 2004 [167]. The integrity of rh-interferon α-2a after incorporation into SLIs and after 28 days of *in-vitro* release was assessed by SDS-PAGE, showing no noticeable aggregation or fragmentation of the protein [167, 176]. The released fractions where further analysed by SE-HPLC for up to 60 days, confirming that the protein was mainly released in its monomeric form. (> 95 %) [167]. These promising results were underlined by a study by Sax *et al.* demonstrating that also a monoclonal antibody can be delivered over 150 days with a consistent monomer content [234]. Conversely, SDS-PAGE analysis of extracted brain-derived neurotropic factor (BDNF) from a glyceryl tripalmitate matrix revealed the formation of dimers upon incubation for 1 month [175]. On biological activity of extracted protein or liberated protein fractions was not reported.

In this chapter, the stability of released protein fractions is described. Three aspects were considered: First, released proteins were analysed over a period of 26 weeks (mAb), 18 weeks (Ranibizumab), 14 weeks (Aflibercept) and 3 weeks (Bevacizumab), respectively. Fractions were collected from *in-vitro* release experiments from SLIs (chapter IV). Second, fractions liberated from PLGA matrices (Resomer® RG 502 and RG 502 H) were collected and analysed over 14 weeks. In a third approach, protein released over the first week after a 1 or 3-month storage of SLIs at 4°C was performed. Analysing these three aspects assist to obtain information on protein stability during long-term release from triglyceride and PLGA matrices and on stability while the proteins are incorporated into a highly hydrophobic triglyceride matrix.

Table VII-1: Literature overview on controlled release systems for peptides and proteins from lipidic and non-lipidic depots including protein stability evaluations of encapsulated and/or released protein. The references provided in table are sorted by year of publication starting from 2015 to 1998.

LIPID BASED DEPOTS					
Peptide or protein	**Analytical technique**	**Delivery platform**	***in-vitro* release**	**Reference**	**Comment**
Ovalbumin	SE-HPLC	Tsc-extruded implants (Chol, lecithin, D114)	up to 14 days	Even *et al.* (2015) [233]	• 40 % monomer loss after 14 days of release due to aggregation
Interferon-α	SDS-PAGE, FT-IR	Tsc-extruded implants (H12, D118)	up to 60 days	Schulze *et al.* (2009) [181]	• preservation of the protein integrity after manufacturing
Brain-derived neurotrophic factor (BDNF), Lysozyme	SDS-PAGE	Compressed implants	up to 80 days	Koennings *et al.* (2007) [175]	• Lysozyme: tendency towards aggregation during preparation • BDNF: no change directly after preparation, after 1 month dimers detected
rh-interferon α-2a	SE-HPLC, RP-HPLC	Compressed tristearin implants	up to 30 days	Mohl *et al.* (2006) [176]	• formation of 15 % to 20 % aggregates and up to 16 % oxidised protein after 3 weeks of release after implant storage
rh-interferon α-2a	SDS-PAGE	Compressed tristearin implants	up to 30 days	Mohl *et al.* (2004) [167]	• slight aggregation during *in-vitro* release
NON-LIPIDIC DEPOTS					
Peptide or protein	**Analytical technique**	**Delivery platform**	***in-vitro* release**	**Reference**	**Comment**
Single-chain VEGF antibody fragment	SE-HPLC, SDS-PAGE	Semi-solid hexylsubstituted poly(lactic acid) (hexPLA)	up to 98 days	Asmus *et al.* (2015) [207]	• antibody structure was kept intact during incorporation and release
f_{ab}-fragment	IEX, SE-HPLC	PLGA-triacetin depot	up to 80 days	Chang *et al.* (2015) [72]	• 5 % monomer loss and 55 % loss in main peak area (IEX)

Peptide or protein	Analytical technique	Delivery platform	*in-vitro* release	Reference	Comment
Exenatide	RP-HPLC, HPLC-MS/MS	PLGA microspheres	20 days	Liang *et al.* (2013) [217]	• rapid acylation of exenatide dependent on water content
Exenatide	HPLC-MS/MS, optical rotation, UV	PLGA solution mimicking depot	incubation time: 5 days	Liang *et al.* (2013) [300]	• formation of non-native conformational changes • acylation as main degradation route
IgG_1 mAb	SE-HPLC, SDS-PAGE, IEF-PAGE, CD, peptide mapping	Silk hydrogels and lyogels	up to 80 days	Guziewicz *et al.* (2013) [98]	• slight fragmentation (SE-HPLC), not seen in SDS-PAGE • secondary and tertiary structure unchanged • elevated levels of oxidized mAb
Insulin	CD, DSC, SDS-PAGE, RP-HPLC, MALDI-TOF-MS, FT-IR	Chitosan-Zn-Insulin-Complex incorporated into PLA-PEG-PLA copolymer	up to 84 days	Oak *et al.* (2011) [81]	• formation of non-covalent aggregates upon release • FT-IR: significant depletion of α-helix and increase of random coils after 60 days of release • CD: changes in tertiary structure • DSC: dissociation of chitosan-Zn-insulin complex • RP-HPLC: complete degradation after 30 days • MALDI-TOF-MS: hydrolysis, deamidation; complete degradation after 30 days
Octreotide, modified with maleic anhydride (MA)	RP-HPLC, LC-MS	PLGA microspheres	42 – 56 days	Ahn *et al.* (2011) [301]	• 100 % acylation after 56 days of octreotide release • MA-octreotide: less acylation but faster release (42 days)
Recombinant human growth hormone (r-hGH)	SDS-PAGE	PLGA microparticles	up to 28 days	Rafi *et al.* (2010) [48]	• no aggregation or fragmentation over 1 month
insulin	SDS-PAGE	pH- and thermosensitive hydrogel	up to 3 days	Shi *et al.* (2010) [82]	• neither aggregation nor fragmentation of insulin upon 72 h of release
Growth hormone-releasing peptide-6 (GHRP-6)	RP-HPLC, MALDI-TOF-MS	PLGA microspheres	up to 30 days	Park *et al.* (2010) [229]	• acylation of GHRP-6 • after 30 days of release 21 % to 78 % intact peptide
Lysozyme	DSC	PLA in situ forming depot (triacetin)	up to 60 days	Al-Tahami *et al.* (2008) [54]	• better conformational stability than control (protein in buffer) after 2 weeks of release • increased polymer concentration stabilise protein

Peptide or protein	Analytical technique	Delivery platform	*in-vitro* release	Reference	Comment
Lysozyme, trypsin inhibitor	SE-HPLC	Recombinant gelatin hydrogel (HU4)	up to 5 days	Sutter *et al.* (2007) [302]	• formation of mainly aggregates upon release; slight increase in fragment percentage
BSA, ribonuclease A, avidin	CD	Sol-gel derived silica gels	up to 3.5 days	Teoli *et al.* (2006) [303]	• no modification of the tertiary structure after entrapment
Tetanus toxoid (TT), Ova, lysozyme	SDS-PAGE, CD, FL	Monomers of PLGA mimicking degradation	incubation time: 20 days	Determan *et al.* (2006) [304]	• TT: aggregation, formation of β-sheets, partial unfolding • Ovalbumin: no formation of aggregates, increase of α-helix content and tertiary structure • Lysozyme: no aggregate formation, increase of α-helix content, tertiary structure unchanged
BSA	SDS-PAGE, SE-HPLC, FT-IR	Release model for PLGA depots: acidic pH of 2	incubation time: 20 days	Estey *et al.* (2006) [253]	• Rapid aggregation and hydrolysis, secondary and tertiary changes
Insulin	RP-HPLC	Chitosan microspheres	up to 80 days	Wang *et al.* (2006) [79]	• In dependency of loading method, partially significant loss of insulin main peak
BSA	SDS-PAGE, CD	PLG-amino cyclodextrine conjugates	up to 28 days	Gao *et al.* (2006) [66]	• No aggregation of released BSA • Secondary structure unchanged over 21 days
Insulin	RP-HPLC, LC-MS	PLA and PLGA microspheres	6 h	Ibrahim *et al.* (2005) [49]	• Insulin mainly destabilized by deamidation rather than acylation • Observation time: 18 days
BSA	CD, FL,	PEG-poly(L-histidine) copolymer in PLGA microspheres	up to 60 days	Kim *et al.* (2005) [43]	• Rapid unfolding in secondary and tertiary structure
Diphteria toxoid (Dtxd)	SE-HPLC	Incubation with PLGA microspheres	incubation time: 56 days	Namur *et al.* (2004) [305]	• Monomer loss mainly caused by fragmentation
Recombinant human growth hormone (rHGH)	FT-IR	PLGA microspheres	up to 42 days	Capan *et al.* (2003) [47]	• Decrease in α-helix content and increase in β-sheet

Peptide or protein	Analytical technique	Delivery platform	*in-vitro* release	Reference	Comment
Atrial natriuretic peptide (ANP)	RP-HPLC, HPLC-MS	PLA and PLGA solutions mimicking PLGA matrix	incubation time: 60 days	Lucke *et al.* (2003) [61]	• Rapid acylation of ANP
BSA	Insoluble and soluble residue analysis	PLGA implants	up to 28 days	Kang *et al.* (2002) [52]	• BSA mostly released as insoluble form
Insulin-like growth factor-I (IGF-I)	RP-HPLC	PLGA microspheres	up to 21 days	Meinel *et al.* (2001) [50]	• Protective effect of various excipients after entrapment of IGF-I
Lysozyme, α-lactalbumin, BSA, VEGF	SE-HPLC, Heparin-affinity chromatography (HAC)	Semisolid, self-catalyzed poly(ortho ester)s (POEs)	up to 15 days	van de Weert *et al.* (2001) [306]	• BSA: increase of soluble aggregates up to 35 % over release time frame; occurred also for the other proteins (data were not shown)
Human erythropoietin (rhEPO)	SDS-PAGE	PLGA microspheres	1 to 2 days	Bittner *et al.* (1998) [45]	• Substantial aggregate formation after encapsulation
Erythropoietin	SDS-PAGE	LPLG-PEO-LPLG triblock copolymer microspheres	up to 15 days	Morlock *et al.* (1998) [44]	• Rapid and significant reduction in monomer content (up to 100 % aggregate formation)

Table VII-2: Literature overview on controlled release systems for peptides and proteins from lipidic and non-lipidic depots including protein bioactivity aspects of encapsulated and/or released protein. The references provided in the table are sorted by the year of publication starting from 2015 to 2000.

LIPID BASED DEPOTS

Peptide or protein	Analytical technique	Delivery platform	*in-vitro* release	Reference	Comment
Human thymidylatesynthase inhibitor peptide (octapeptide)	MTT	SLNs	up to 4 h	Sacchetti *et al.* (2015) [140]	• increase of apoptosis percentage observed indicating that SLNs were able to carry the peptide efficiently to its enzymatic target
Apolipoprotein E	MTT and LDH assays in human cerebral microvascular endothelial cells	SLNs functionalized with apolipoprotein E	not avaiable	Neves *et al.* (2015) [252]	• no toxicity and a 1.5-fold increment in the blood-brain-barrier permeability
Protamine, anionic polysaccarides	Cell viability (CCK-8 assay)	SLNs	not avaiable	Apaolaza *et al.* (2015) [148]	• partial recovery of retina • successful RS1 gene transfer to Rs1h-deficient animals using non-viral nanocarriers demonstrated
Ovalbumin	$CD4^+$ and $CD8^+$ T cell proliferation, IgG titer, IFN-γ and IL4 secretion	Tsc-extruded implants platform (Chol, lecithin, D114)	up to 7 days	Even *et al.* (2014) [186]	• generation of cellular and humoral immune responses
siRNA, antisense oligonucleotides	Transfection Assay	ketal nucleoside lipid (KNL) nanoparticles	not available	Luvino *et al.* (2013) [147]	• siRNA exhibits protein knockdown • suitable transfecting reagent for novel therapeutic approaches against prostate cancer
Bevacizumab	ELISA	Nanoliposomes	not available	Abrishami *et al.* (2009) [213]	• intravitreal injection of liposomes • encapsulated bevacizumab was well tolerated through 42 days in rabbits • clearance of this drug in vitreous from liposomal formulations was slower than soluble form

Peptide or protein	Analytical technique	Delivery platform	*in-vitro* release	Reference	Comment
Brain-derived neurotrophic factor (BDNF), Lysozyme	ELISA	Compressed implants	up to 80 days	Koennings *et al.* (2007) [175]	• Lysozyme: in the first 30 days, 60 % to 75 % were found in its enzymatically active form • BDNF: 20 % or 60 % intact protein over 1 month
Insulin	ELISA	Triglyceride based compressed implants	up to 14 days	Appel *et al.* (2006) [169]	• Preserved bioactivity of incorporated and released protein • strong dose-dependent effects on tissue engineered cartilage
Interleukin-18 (IL-18)	ELISA	Compressed implants	up to 12 days	Koennings *et al.* (2006) [174]	• progressive integrity loss (down to 20 % to 40 %) observed with ongoing release

NON-LIPIDIC DEPOTS

Peptide or protein	Analytical technique	Delivery platform	*in-vitro* release	Reference	Comment
Nel-like molecule-1 (Nell-1)	Alkaline phosphatase activity (ALP)	Chitosan/hydroxyapatite-modified tricalcium phosphate (TCP) particles	up to 28 days	Zhang *et al.* (2016) [77]	• About 78 % of the loaded protein's bioactivity was preserved over the period of investigation
Coumarin-6, fluocinolone acetonide (FA), BSA, BMP-2	Alkaline phosphatase activity (ALP), calcium deposition, gene expression	Chitosan-graft-poly(lactic acid) copolymers	up to 14 days	Niu *et al.* (2016) [70]	• Enhanced odontogenesis and significantly enhanced mineralized tissue regeneration • suppressed inflammation
Connexin43 mimetic peptide	retinal ischaemia–reperfusion rat model	PLGA nano- and microparticles	up to 120 days	Chen *et al.* (2015) [208]	• promising results on Cx43 down-regulation and RGC rescue in acute injury mode
Single-chain VEGF antibody fragment	Surface plasmon resonance analysis	Semi-solid hexylsubstituted poly(lactic acid) (hexPLA)	up to 98 days	Asmus *et al.* (2015) [207]	• released protein monomer maintained its high affinity to human VEGF-A
Bevacizumab	ELISA	Silk hydrogel	up to 90 days	Lovett *et al.* (2015) [96]	• concentrations in vitreous humor after 90 days equivalent to those levels for the positive control at 1 month

Peptide or protein	Analytical technique	Delivery platform	*in-vitro* release	Reference	Comment
Bone morphogenetic protein 2 (BMP-2)	Alkaline phosphatase activity (ALP)	Hydrogel embedded with alginate microspheres	up to 42 days	Zhu *et al.* (2015) [84]	• released BMP-2 retained bioactivity, maintaining of osteogenesis functions
Platelet-derived growth factor (PDGF-AA)	ELISA	Hydrogel/nanoparticle composite	up to 21 days	Elliott Donaghue *et al.* (2015) [63]	• Released PDGF-AA remained bioactive demonstrated by NSPC oligodendrocyte differentiation
f_{ab}-fragment	Antigen binding capacity	PLGA-triacetin depot	up to 80 days	Chang *et al.* (2015) [72]	• 80 % remaining binding capacity after 80 days of release
Fibroblast growth factor 2 (FGF-2), bone morphogenetic protein 2 (BMP-2)	Alkaline phosphatase activity (ALP), calcium accumulation	Core-shell PLGA microspheres	up to 30 days	Lei *et al.* (2014) [51]	• Accelerated differentiation of stem cells into osteogenic lineage • Higher calcium accumulation
Bevacizumab	MTT, 3-D angiogenesis culture	Thermoresponsive hydrogel	up to 60 days	Hu *et al.* (2014) [267]	• After 1 month of intravitreal injection, the histomorphology of a rabbit's retina was preserved • Released bevacizumab inhibited anti-angiogenesis in 3-D cultures
IgG_1	TGFβ induced release of IL-11	Silk hydrogels and lyogels	up to 80 days	Guziewicz *et al.* (2013) [98]	• No change in mAb potency represented by IL-11 inhibition
BSA, Lysozyme	Enzyme activity	dihydroxyacetone-based poly(carbonate ester) matrices	up to 80 days	Weiser *et al.* (2013) [107]	• Lysozyme: at least 50 % activity over the first month of release; 14 % to 16 % bioactivity after 60 days
Insulin	Glucose oxidase (GOD) assay	Multi-arm histidine copolymer-PLGA composite microspheres	up to 30 days	Park *et al.* (2012) [68]	• controlled blood-glucose levels and maintained lower glucose levels without a loss of body weight
Nel-like molecule-1 (Nell-1)	Alkaline phosphatase activity (ALP)	β-tricalcium phosphate (β-TCP) particles	up to 14 days	Hu *et al.* (2012) [307]	• Bioactivity preserved during loading • Bioactivity was preserved over 4 weeks in the lyophilized state
Nel-like molecule-1 (Nell-1)	Alkaline phosphatase activity (ALP)	Chitosan/tripolyphosphate/ Chondroitin sulfate nanoparticles	up to 14 days	Hou *et al.* (2012) [76]	• Bioactivity was preserved during encapsulating procedure

Peptide or protein	Analytical technique	Delivery platform	*in-vitro* release	Reference	Comment
Basic fibroblast growth factor (FGF-2)	ELISA	Polyelectrolyte multilayer microcapsules	up to 3 days	She *et al.* (2012) [308]	• Bioactive FGF-2 decreased from 0.6 ng to 0.4 to 0.1 ng
Bone morphogenetic protein-6 (BMP-6)	Alkaline phosphatase activity (ALP)	Chitosan scaffolds	up to 7 days	Soran *et al.* (2012) [78]	• Enhanced osteoblastic differentiation of bone marrow-derived rat mesenchymal stem cells
Bone morphogenetic protein-2 (BMP-2)	Alkaline phosphatase activity (ALP)	Core-shell PLLACL-collagen fibers	up to 21 days	Su *et al.* (2012) [92]	• Increased ALP activity, mineralization and osteoblast marker expression
Bevacizumab	ELISA	Nanostructured mesoporous silica (SiO_2) films	up to 30 days	Andrew *et al.* (2011) [210]	• antibody released in its active form over 1 month; approx. 98 % of drug released
Fibroplast growth factor (FGF)	Alkaline phosphatase activity (ALP)	Silica-chitosan hybrid coating on Ti	up to 35 days	Jun *et al.* (2011) [309]	• Improved osteoblast cell response
Bevacizumab	induced choroidal neovascularization (CNV) in rat eyes	PLGA nanoparticles	not available	Pan *et al.* (2011) [276]	• reduction in CNV area suggests successful creation of formulations while retaining bevacizumab's active antiangiogenic properties
Recombinant human growth hormone (r-hGH)	r-hGH bioactivity on rat lymphoma nB2 cell line	PLGA microparticles	up to 28 days	Rafi *et al.* (2010) [48]	• Bioactivity of release protein maintained over 4 weeks after single i.m. injection
Insulin sodium oleate	Diabetic rat model	PLGA nanoparticles	not available	Sun *et al.* (2010) [298]	• plasma glucose level reduced to 23.85 % from the initial one 12 h post-administration and this continued for 24 h in diabetic rats
Nel-like molecule-1 (Nell-1)	Rat spinal fusion model	Biomimetic apatite-coated alginate/chitosan microparticles	up to 30 days	Lee *et al.* (2009) [83]	• Enhanced spinal fusion rates measured by manual palpation, radiographs and µCT
Lysozyme	Enzyme activity	Thermosensitive mPEG–PLGA–mPEG copolymer	up to 28 days	Tang *et al.* (2009) [67]	• depot preserved lysozyme in its biologically active form
Lysozyme	Enzyme activity	PLA in-situ forming depot (triacetin)	up to 60 days	Al-Tahami *et al.* (2008) [54]	• Better enzyme activity than control (protein in buffer) after 2 weeks of release

Peptide or protein	Analytical technique	Delivery platform	*in-vitro* release	Reference	Comment
Lysozyme	Enzyme activity	PLGA microspheres	up to 28 days	Taluja *et al.* (2008) [69]	• Enzymatic activity decreased by approx. 10 % over 21 days of release
BSA and nerve growth factor (NGF)	ELISA	Nano-fibrous collagen microspheres	up to 28 days (only for BSA)	Chan *et al.* (2008) [310]	• Released NGF retained most of its bioactivity; but no comment on release duration of NGF and only 3 to 6 % delivered
Lysozyme	Enzyme activity	Electrospun poly(ε-caprolactone) and poly(ethylene oxide) fiber mesh	up to 12 days	Kim *et al.* (2007) [104]	• Released lysozyme retained sufficient bioactivity (90 % after 12 days)
Insulin	Glucose oxidase (GOD) assay	Insulin-phospholipid complex	up to 12 h	Cui *et al.* (2006) [311]	• Reduced plasma glucose levels in diabetic rats
Tetanus toxoid (TT), Ovalbumin, lysozyme	ELISA	Monomers of PLGA mimicking degradation	incubation time: 20 days	Determan *et al.* (2006) [304]	• TT: loss of antigenicity • Ovalbumin: increased antigenicity • Lysozyme: only little lost in enzymatic activity
Diphteria toxoid (Dtxd)	ELISA	Incubation with PLGA microspheres	incubation time: 56 days	Namur *et al.* (2004) [305]	• Complete loss of bioactivity after 56 days
Lysozyme	Enzyme activity	Poly(ether–ester) multiblock copolymers for macro-porous scaffolds	up to 70 days	Sohier *et al.* (2003) [312]	• Encapsulation of protein into depot did not reduced enzyme activity • 80 % – 90 % remaining bioactivity after 60 days of release
Tissue plasminogen activator (t-PA)	Serine protease activity	PLGA implants	up to 28 days	Kang *et al.* (2002) [52]	• No activity at all of t-PA after 4 weeks
Insulin-like growth factor-I (IGF-I)	Radioimmunoassay (RIA), fat cell assay (FCA)	PLGA microspheres	up to 21 days	Meinel *et al.* (2001) [50]	• Partially, up to 50 % less activity already after 0.2 days
Insulin, met-enkephalin, leuprolide, octreotide	Suppression of testosterone by Radioimmunoassay (RIA) for leuprolide	DepoFoam™	up to 25 days	Ye *et al.* (2000) [313]	• Prolonged suppression of testosterone levels in rats similar to Lupron® Depot after a single 1.m. injection

VII.2 Results and Discussion

VII.2.1 Stability of released protein fractions from lipid implants

VII.2.1.1 Analysis of soluble aggregates and fragments

Released proteins were collected, concentrated and analysed via SE-HPLC.

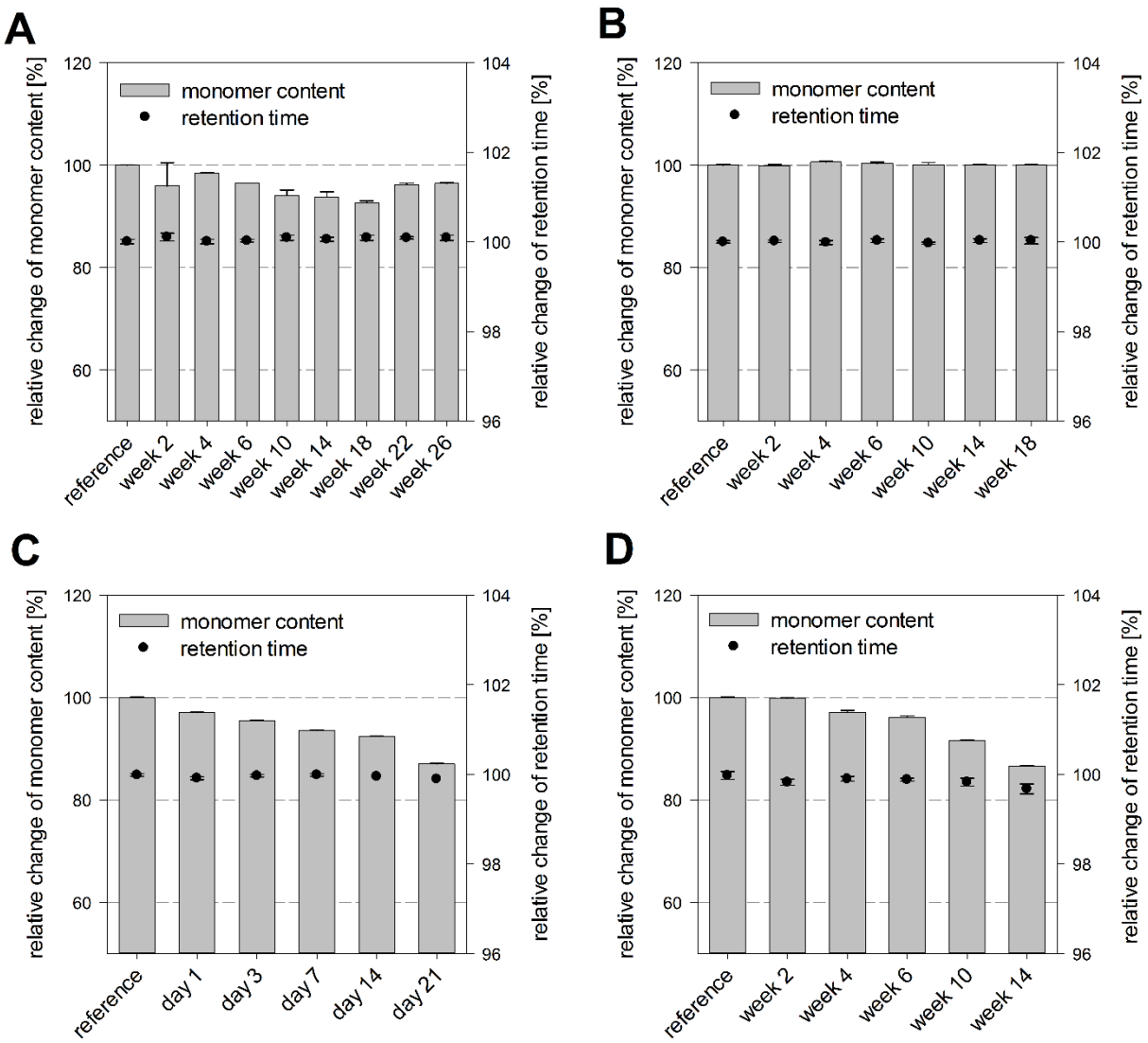

Figure VII-1: Monomer content of released (A) mAb, (B) Ranibizumab, (C) Bevacizumab and (D) Aflibercept monitored over 3 weeks to 26 weeks. Displayed are the relative percentages of monomer and the relative change of retention times compared to reference.

Figure VII-1 illustrates the monomer content over the period the proteins were released from the lipid matrix. If not otherwise noted, protein lyophilisate was formulated 1:1 [w/w] with HP-β-CD. Displayed are the relative percentages of the monomer content compared to the reference defined as 100 % (reference: protein solution after dialysis and prior to lyophilisation). The monomer content of released mAb fractions alternated between 93 % and 98 % over 26 weeks (Figure VII-1 A).

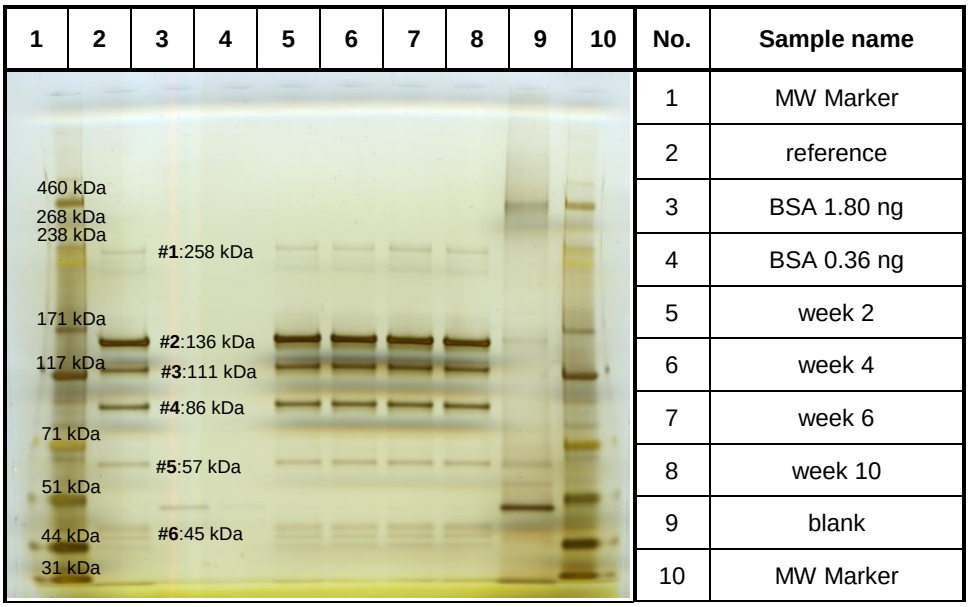

No.	Sample name
1	MW Marker
2	reference
3	BSA 1.80 ng
4	BSA 0.36 ng
5	week 2
6	week 4
7	week 6
8	week 10
9	blank
10	MW Marker

Figure VII-2: Non-reducing denaturating SDS-PAGE gels using NuPAGE® Novex® 3-8% Tris Acetate Protein Gels of released mAb fractions collected between week 2 and week 10.

The decrease in monomer content was caused by fragmentation rather than aggregation of the mAb, as observed by non-reducing denaturating SDS-PAGE using silver staining (Figure VII-2 and Figure VII-3).

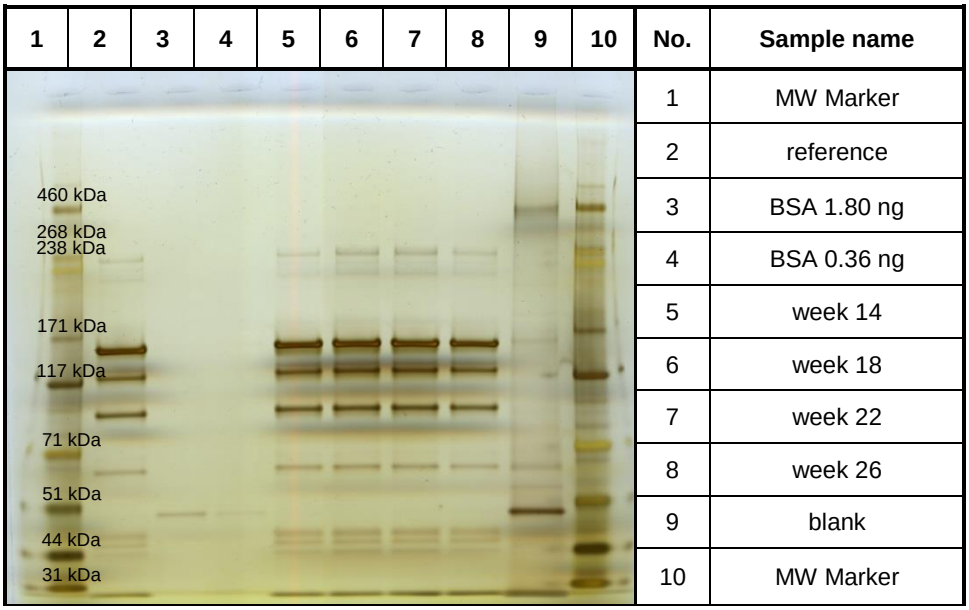

No.	Sample name
1	MW Marker
2	reference
3	BSA 1.80 ng
4	BSA 0.36 ng
5	week 14
6	week 18
7	week 22
8	week 26
9	blank
10	MW Marker

Figure VII-3: Released mAb fractions between 14 and 26 weeks of release analysed with non-reducing denaturating SDS-PAGE using NuPAGE® Novex® 3-8% Tris Acetate Protein Gels.

As indicated in Figure VII-2, a monomer band (#2, 136 kDa), and high molecular weight (HMW) species (#1, 258 kDa) were present in the released fractions. Compared to the reference, low molecular weight (LMW) species were particularly detectable, pointing into the direction of slight fragmentation, such as f_{ab}-fragments (#6, 45 kDa) or one-armed mAbs (#3, 111 kDa).

SE-HPLC of Ranibizumab revealed a monomer content of 100 % over the release duration (18 weeks) compared to the reference material (Figure VII-1 B). In addition, non-reducing SDS-PAGE was performed as an orthogonal method. Compared to the reference, additional bands were detected after 10 weeks, especially fragments ranging between 16 kDa to 18 kDa (Figure VII-4). Further, aggregates were identified having a size of approximately 151 kDa (#5) and 98 kDa to 109 kDa (#6) after 4 weeks.

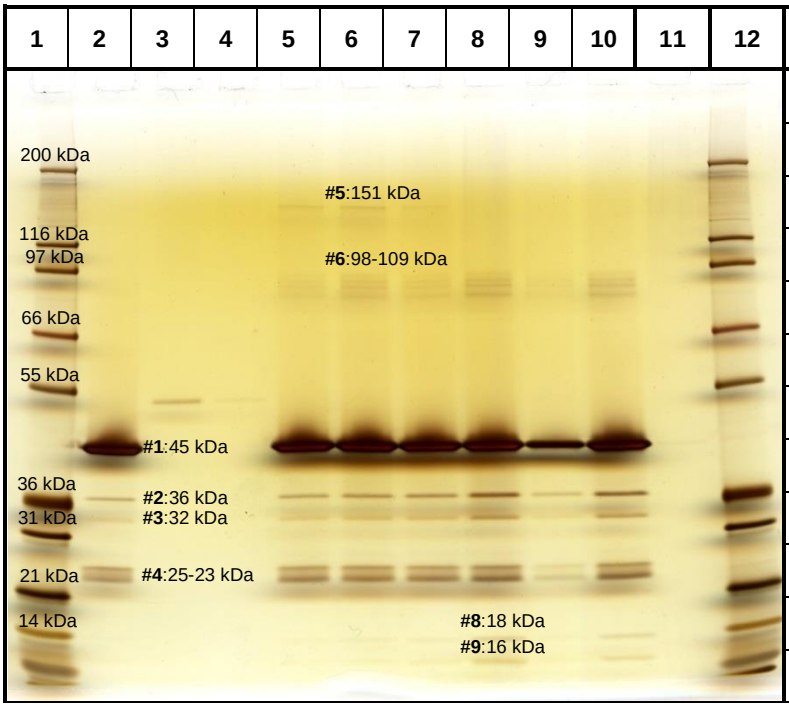

No.	Sample name
1	MW Marker
2	reference
3	BSA 1.80 ng
4	BSA 0.36 ng
5	week 2
6	week 4
7	week 6
8	week 10
9	week 14
10	week 18
11	blank
12	MW Marker

Figure VII-4: Non-reducing denaturating SDS-PAGE gels using NuPAGE® Novex® 4-12% Bis-Tris Protein Gels of released Ranibizumab fractions collected over 18 weeks.

These results were complemented by capillary gel electrophoresis, applying an Agilent 2100 Bioanalyzer. Capillary gel electrophoresis showed Ranibizumab monomer content ranging between 94 % to 96 % (Figure VII-5 A). Additionally, a slight increase in LMW species from 4 % to 6 % was identified, HMW species percentage remained constant at 0.2 % over time. Therefore, these results are qualitatively in line with SDS-PAGE results. A typical electropherogram is displayed in Figure VII-5 B.

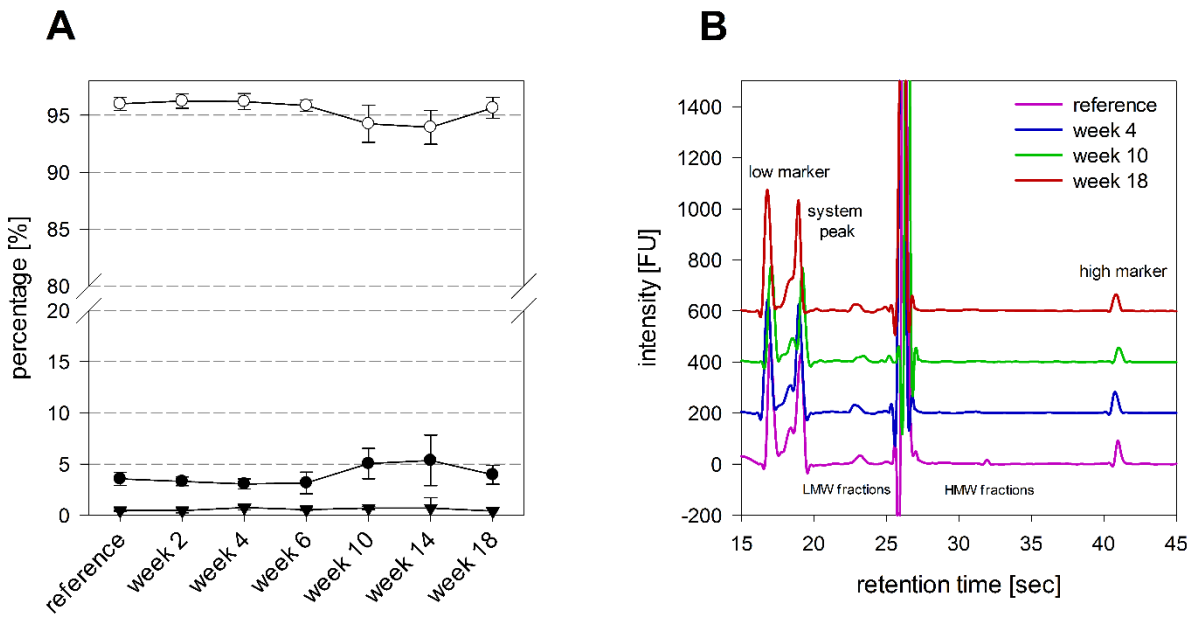

Figure VII-5: (A): Capillary gel electrophoresis of released Ranibizumab under non-reducing denaturating conditions. Shown are (○) monomer content, (●) low molecular weight (LMW) species and (▼) high molecular weight (HMW) species over the release period of 18 weeks. (B): typical electropherogram displaying markers, system peaks and signals of Ranibizumab.

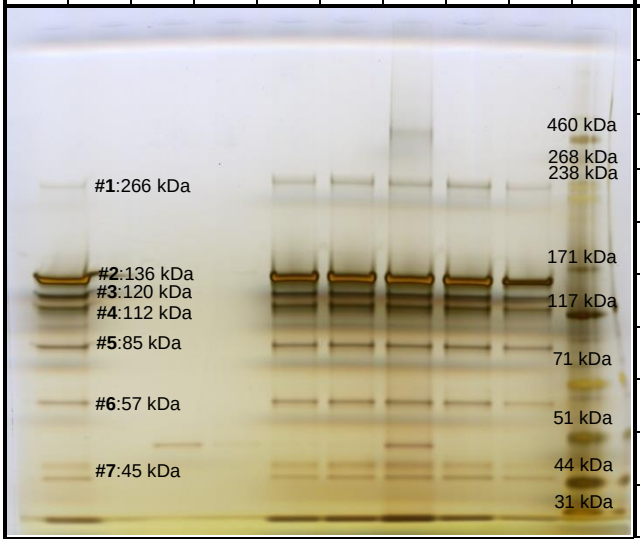

No.	Sample name
1	reference
2	blank
3	BSA 1.80 ng
4	BSA 0.36 ng
5	day 1
6	day 3
7	day 7
8	day 14
9	day 21
10	MW Marker

Figure VII-6: Non-reducing denaturating SDS-PAGE gels using NuPAGE® Novex® 3-8% Tris Acetate Protein Gels of released Bevacizumab fractions collected over 3 weeks of release.

The monomer content of Bevacizumab substantially dropped by 15 % within the first 3 weeks, highlighting the high sensitivity of Bevacizumab compared to the other proteins (Figure VII-1 C). Non-reducing SDS-PAGE underlined these results, pointing into the direction of aggregation (physical instability) and fragmentation (chemical instability) as displayed in Figure VII-6.

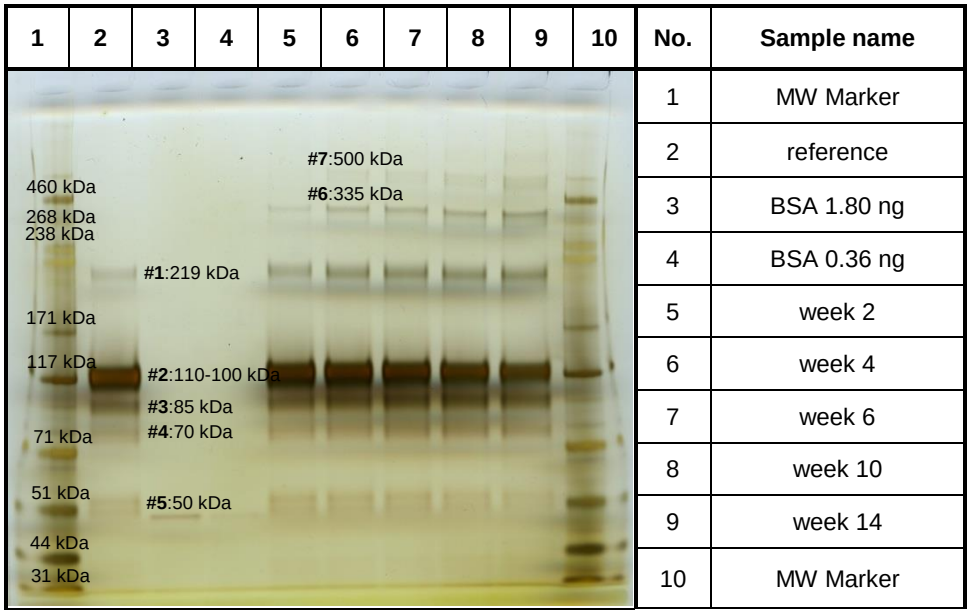

No.	Sample name
1	MW Marker
2	reference
3	BSA 1.80 ng
4	BSA 0.36 ng
5	week 2
6	week 4
7	week 6
8	week 10
9	week 14
10	MW Marker

Figure VII-7: Non-reducing denaturating SDS-PAGE gels using NuPAGE® Novex® 3-8% Tris Acetate Protein Gels of released Aflibercept fractions collected over 14 weeks.

Figure VII-1 D displays the monomer content of Aflibercept over 14 weeks, illustrating a continuous decrease from 100 % to nearly 85 % compared to the reference. The loss of monomer is caused by the formation of aggregates having a size of 219 kDa (#1), 335 kDa (#6) and 500 kDa (#7), respectively, which were already detectable at week 4 as indicated by non-reducing SDS-PAGE (Figure VII-7).

In literature, protein stability after incorporation into lipid matrices has already been discussed for smaller and less complex molecules like ovalbumin [233], rh-interferon α-2a [176, 181], lysozyme [175] or brain-derived neuropathic factor (BDNF) [175]. All references reported on no changes in the aggregation/fragmentation profile after incorporation and were assessed by SDS-PAGE. Used lipids were mainly triglycerides (C12 to C18) and additives like PEG or

trehalose processed within the protein lyophilisate were used. These observations are in line with our results, as no protein instabilities were observed after incorporation into the lipid matrix.

In terms of stability of released protein, Koennings *et al.* [175] described the dimerisation of BDNF during release from lipid depots measured after 1 month by SDS-PAGE. In contrast, Mohl *et al.* [176] observed only a minimal increase of rh-interferon α-2a aggregates (approximately 1 %) from compressed lipid implants comprising D118, PEG or trehalose over 20 days of release. Also, neither aggregation nor fragmentation of released rh-interferon α-2a after 28 days was observed. Rh-interferon α-2a was identified to be stable after 6-month storage of the SLIs when formulated with HP-β-CD as lyophilisate stabiliser. The aggregation level of released fractions over the first 3 weeks after 6 months remained constant at approximately 3 %. In addition, Schulze *et al.* reported that rh-interferon α-2a monomer content, delivered from a binary triglyceride matrix, stayed at 95 % over a release period of up to 60 days [181]. However, all studies mentioned reported on aggregation – if any - rather than fragmentation as main degradation pathway. This stands in contrast to our results most likely due to the different proteins used.

VII.2.1.2 CHEMICAL STABILITY OF PROTEINS

To determine possible chemical changes of the proteins, IEX methods for mAb and Bevacizumab were developed (III.2.6.5). Using this method, the separation of acidic and basic species from the main charge variant is possible by applying a salt or pH gradient for separation [247, 314-328]. Figure VII-8 A illustrates that the main charge variant of mAb decreased from initially 100 % (relative to reference) to 84 % over 26 weeks. Simultaneously, the percentage of acidic subspecies continuously increased whereas the level of basic residues stayed constant (Appendix, Figure XII-8 A). The retention time of the main charge variant stayed constant over 26 weeks pending between 98 % and 102 % compared to retention time of the reference.

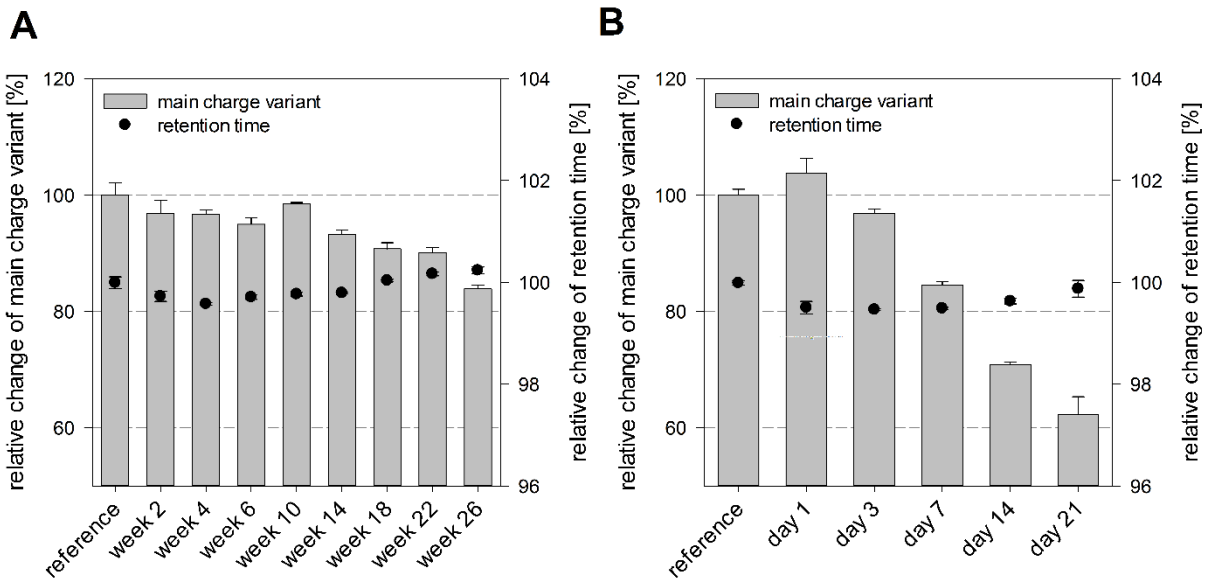

Figure VII-8: Relative change of the main charge variant area of (A) mAb and (B) Bevacizumab assessed by IEX. Retention time of the main peak eluting from the column relative to reference material is displayed as black dots.

As illustrated in Figure VII-8 B, the relative percentage of Bevacizumab's main charge variant decreased substantially and continuously over 3 weeks by 40 %. At once, more acidic subspecies eluting earlier than the main charge variant were identified (Appendix, Figure XII-8 B). Retention times did not change considerably throughout the 21 days of release.

Chemical degradation products from Ranibizumab and Aflibercept were identified and quantified by a HIC method (III.2.6.6) developed for each protein. HIC allows the separation of differently charged protein species and has already been described in literature [329-336]. As Figure VII-9 A demonstrates, the main charge variant of Ranibizumab decreased from 100 % to 90 %. The chromatograms of Ranibizumab did not change noteworthy during the first 6 weeks; a notable change occurred firstly after 10 weeks. Analysis of the chromatograms showed an increase of subspecies eluting later than the main peak, therefore signifying the formation of more hydrophobic residues. More hydrophilic residues (eluting faster than the main peak) were not detected (Appendix, Figure XII-9 A). Noticeably, the retention time of the main

charge variant shifted towards shorter elution times, highlighting that more hydrophilic subspecies were formed which were not separated by the gradient.

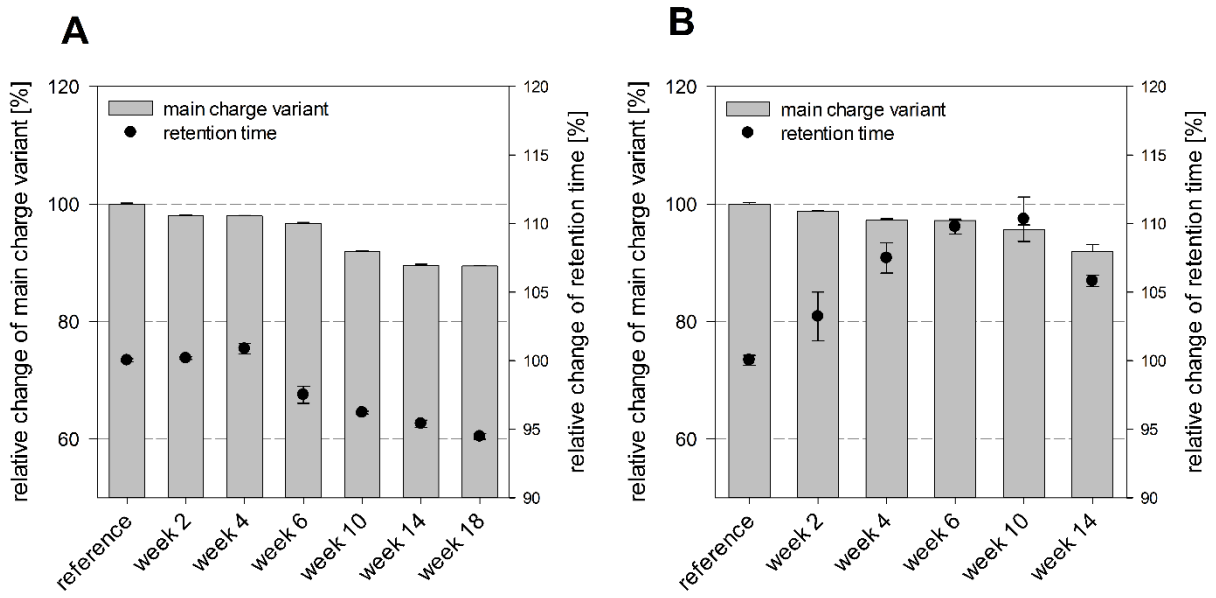

Figure VII-9: Relative change of the main charge variant area of (A) Ranibizumab and (B) Aflibercept as assessed by HIC.

The main charge variant of Aflibercept decreased by 8 % over 14 weeks as displayed in Figure VII-9 B. The formation of more hydrophobic rather than hydrophilic residues was detected. Additionally, the retention time of the main charge variant changed towards higher retention times, indicating that residues of slightly elevated hydrophobicity were formed.

To obtain more detailed information with respect to chemical stability, capillary gel electrophoresis was performed under reducing denaturating conditions to detect possible covalent bonds, e.g. disulfide bonds. Samples taken at each predetermined time point were compared to reference material as shown in Figure VII-10. For mAb, the percentage of heavy chain, light chain, LMW species and HMW species stayed rather constant over 26 weeks designating no formation of covalent bonds (Figure VII-10 A). In contrast, for Ranibizumab the heavy chain percentage slightly increased by 2 % over 18 weeks whereas the level of light chain decreased by 2.5 %. Levels of other sized fragments did not change (Figure VII-10 B). For

Bevacizumab, the percentage of the heavy chain declined from 69 % (day 1) to 58 % (day 21). In the same course, the percentages of the light chain, small sized and larger sized residues increased pointing into the direction of covalent bond formation (Figure VII-10 C).

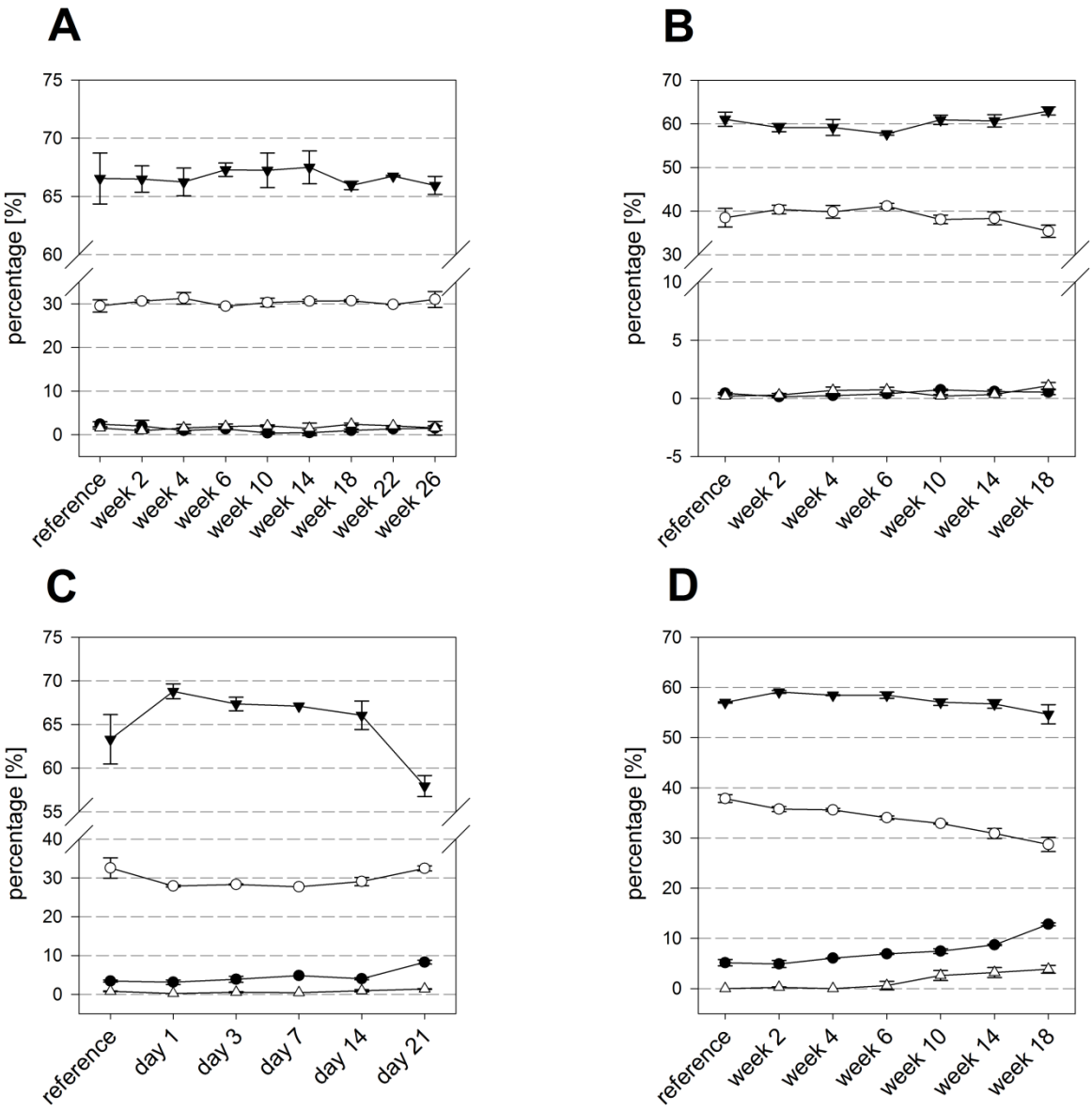

Figure VII-10: Capillary gel electrophoresis applying the 2100 Bioanalyzer under reducing denaturating conditions of (A) mAb, (B) Ranibizumab, (C) Bevacizumab and (D) Aflibercept released fractions. Shown are the (○) light chain and (▼) heavy chain percentages as well as the amount of (●) LMW and (△) HMW species over the specific release durations.

Figure VII-10 D displays the results obtained for Aflibercept: the percentage of heavy and light chain decreased by 5% and 10%, respectively. Concurrently, the formation of LMW and HMW species can be observed.

IEX and HIC analysis revealed formation of differently charged subspecies (IEX) or subspecies having a different hydrophobicity (HIC). Thus, more chemical degradation than physical degradation of proteins was observed when released from a hydrophobic matrix over time. Possible reactions forming acidic species are deamidation (asparagine, glutamine, c-terminal amides), cleavage of disulfide bonds, oxidation (proline, phenylalanine, o-tyrosine, tryptophan), conversation of arginine and hydrolysis [337]. Chemical subspecies of Ranibizumab and Aflibercept were measured by HIC, whereby exclusively subspecies were found being more hydrophobic than the main charge variant (Figure VII-9). This can be explained by the potential formation of disulfide bonds caused by oxidation, isomerisation of asparagine to succinimide [337] or unfolding of the protein. During partial unfolding of the protein, hydrophobic areas are turning to proteins` surface generating hydrophobic patches. While this happens, chemical reactions are not obligatory necessary.

In addition, a decrease in heavy chain percentage measured under reducing conditions (especially for Bevacizumab and Aflibercept) might have occurred due to the formation of covalent disulfide bonds. The disulfide bonds formed new linkers between protein helices where there were none before. The reducing agent DTT cleaved those bonds leading to more fractions being smaller in size than before.

In literature, little information is provided on chemical stability of proteins delivered from lipidic matrices. The chemical stability of released rh-interferon α-2a from compressed lipid matrices comprising the triglyceride D118 has already been discussed by Mohl *et al.* [176]. Oxidized species levels were measured using RP-HPLC taking also into account the storage of loaded implants prior to *in-vitro* release. For rh-interferon α-2a formulated with HP-β-CD, the level of

oxidized species did not change over release duration of 22 days. After 6-month storage prior to release, the level increased after 2 weeks of release from 1 % to 2 %.

VII.2.1.3 CONFORMATIONAL STABILITY OF PROTEINS

FT-IR is a well-established and widely used method to determine protein secondary structure [338-343] and was therefore used to obtain information on the conformational status of released protein. FT-IR spectra at every single predetermined time point were measured. For a better visualisation, only spectra of reference and selected samples, representing the progress upon release, are displayed in Figure VII-11. It should be noted, that the sample concentration of 1.0 mg/ml was at the lower end of instrument sensitivity. This fact may explain the not perfectly matching overlays.

Figure VII-11 A displays the FT-IR spectra of mAb between 1600 cm^{-1} and 1700 cm^{-1}. The amide I band, which is mainly generated by C=O stretching vibrations, represents the β-sheet band structure [340, 343] and can be identified between 1635 cm^{-1} and 1645 cm^{-1}. Apparently, the single peak present at the reference (1635 cm^{-1} to 1637 cm^{-1}) turned into a split peak with a left side shoulder at 1645 cm^{-1} starting at week 6. Additionally, an increase in band intensity at 1680 cm^{-1} and 1615 cm^{-1}can be observed, being characteristic for protein unfolding events [341]. Shifts towards higher wavenumbers represent unordered random coil like structures [341]. On the expense of regular structures, the formation of intermolecular hydrogen-bonded antiparallel β-sheet structures are pointing into the direction of partial unfolding of the mAb [344]. Changes in secondary structure of mAb might have arisen due to the hydrophobic environment (triglycerides) the antibody was exposed to.

Ranibizumab FT-IR spectra are shown in Figure VII-11 B, including the reference and the samples of week 4, 10 and 18, respectively. The spectra are characterised by a pronounced amide I band at 1636 cm^{-1}. Intensity of the amide I band slightly decreased over time whereas the band at 1678 cm^{-1} became more prominent. Overall, Ranibizumab is present in its native

state over the complete release period. Compared to mAb, the better conformational stability is most likely due to the less complex structure of the f_{ab}-fragment.

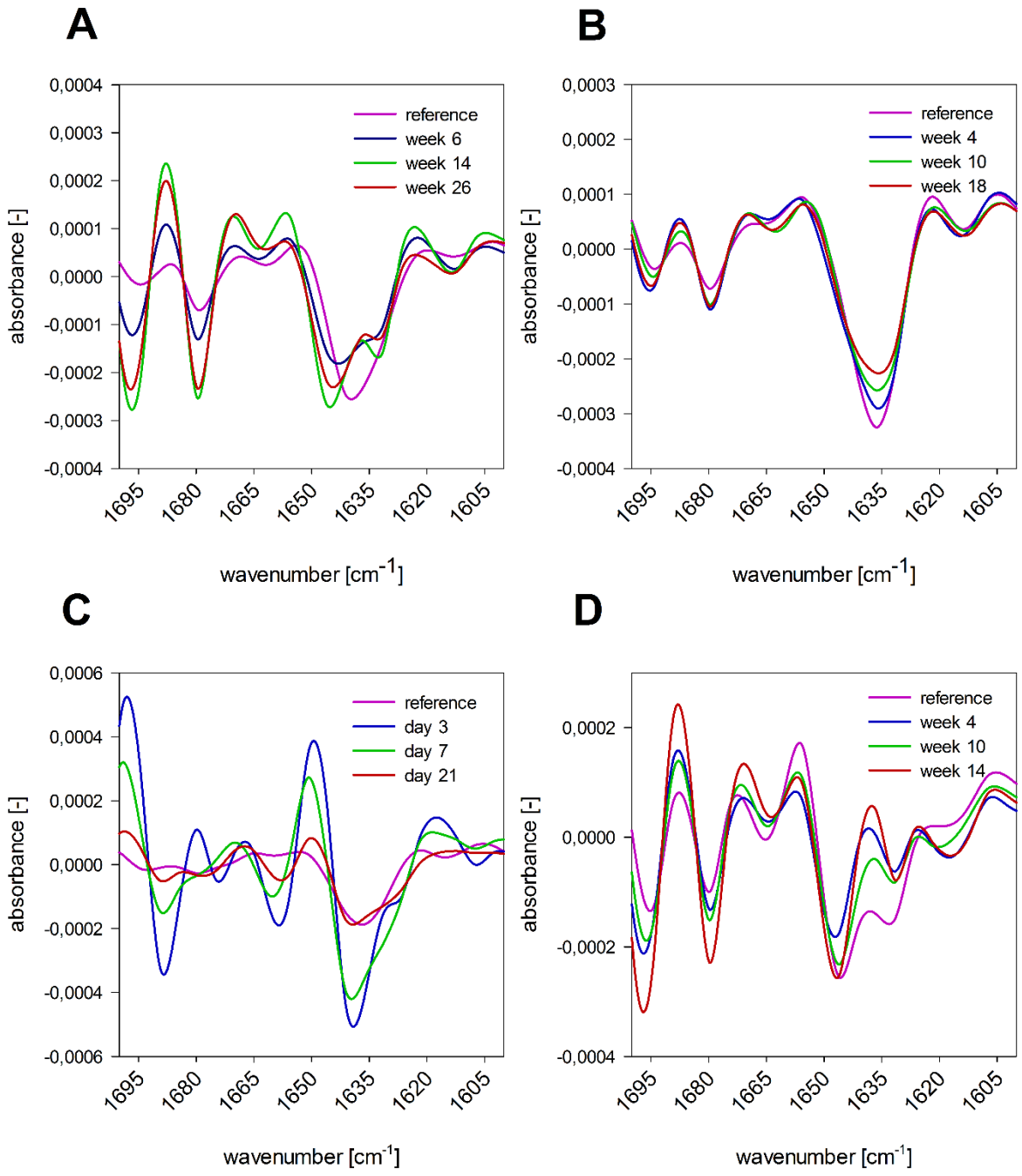

Figure VII-11: FT-IR spectra of collected released fractions from (A) mAb, (B) Ranibizumab, (C) Bevacizumab and (D) Aflibercept.

Figure VII-11 C shows the FT-IR spectra of Bevacizumab reference and released fractions collected over 21 days. The reference comprised a weak amide I single band at 1636 cm^{-1}. After

3 days, the spectra changed dramatically, pointing into the direction of substantial changes in secondary structure. The amide I band was shifted towards 1640 cm^{-1} (day 21), representing more unordered random coil like structures and band intensity at 1690 cm^{-1} increased (protein unfolding).

Aflibercept reference material is characterised by an amide I band consisting of two peaks: the main band having a maximum at 1640 cm^{-1} and a right-side shoulder band at 1630 cm^{-1} (Figure VII-11 D). While the protein was released, the band intensity of the amide I band at 1630 cm^{-1} declined considerably. Moreover, an increase in band intensities at 1680 cm^{-1} and 1697 cm^{-1} was observed.

Schulze *et al.* was the first assessing the conformational status of a protein after encapsulation into a lipid matrix, showing that the protein (lysozyme) was still in its native state [181]. To the best of our knowledge, our study is the first describing the conformational status of three different protein formats released from SLIs.

VII.2.2 STABILITY OF RELEASED PROTEIN FRACTIONS FROM PLGA MATRICES

PLA and PLGA polymers provide a biodegradable system for sustained release of protein drugs, but erosion/degradation of the polymer is associated with a drop in pH and an increase in osmotic pressure (particularly inside the matrix), which may result in degradation products caused by acylation, deamidation or aggregation [49, 253, 254].

Within our study, released protein from a PLGA matrix (Resomer® RG 502 or Resomer® RG 502 H) was collected over 12 weeks to investigate protein stability and compare these results to data obtained from SLIs (VII.2.1). The pH of the release medium was measured accordingly.

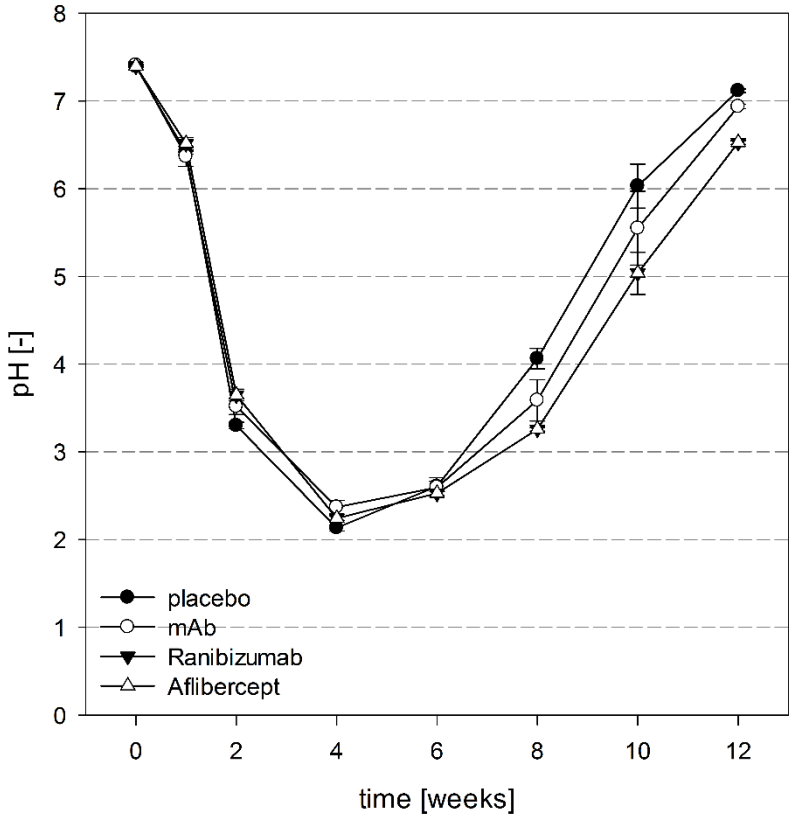

Figure VII-12: Displayed are the pH values of incubation medium in which protein loaded Resomer® RG 502 H matrices were incubated. The course of pH was monitored for extrudates containing (●) no protein, (○) mAb, (▼) Ranibizumab, and (△) Aflibercept.

When completely exchanging the release medium at predetermined time points (as it was performed for *in-vitro* release studies), the measured pH described a curve with a minimum of pH 2 after 4 weeks (Figure VII-12). Since the pH was around 3 from week 3 to week 7, an incubation study at pH 3 was performed to hedge that possible instabilities were due to the pH drop and osmotic pressure increase inside the PLGA matrix. Therefore, proteins were incubated in PBS pH 3.0 for 4 weeks at 37°C in a horizontal shaker (40 rpm). Samples were analysed after 2 weeks and 4 weeks.

VII.2.2.1 ANALYSIS OF SOLUBLE AGGREGATES AND FRAGMENTS

SE-HPLC data were obtained for released mAb and Ranibizumab over 12 weeks. The monomer content of reference, pH 3 incubated samples, released fractions from SLIs after 12 weeks and from a Resomer® matrix (Figure VII-13) were compared. Monomer content of mAb declined to 86 % after 4 weeks of incubation at pH 3. After 4 weeks of release from the PLGA matrix, monomer content was measured with 72 % (Figure VII-13 A). The lower value can be explained by the acidic microenvironment generated while PLGA eroded, namely a drastic change in pH and elevated osmotic pressure. Unfortunately, data from other time points were not available due to the very small amount of protein released within this time frame (IV.2.7).

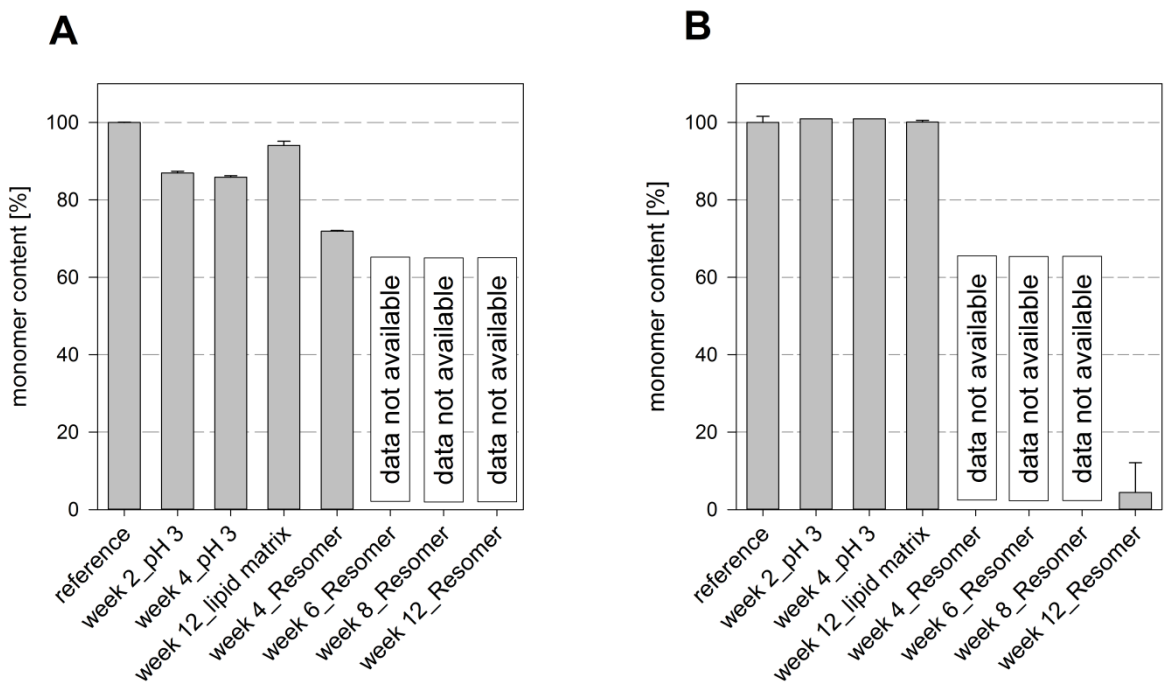

Figure VII-13: Monomer content of (A) mAb and (B) Ranibizumab of reference, pH 3 incubated samples, released fractions from SLIs after 12 weeks and released fractions from a Resomer® matrix.

The incubation at pH 3 did not affect the monomer content of Ranibizumab. Therefore, it can be assumed that incubation for even longer time would not negatively affect the monomer content. A head to head comparison of Ranibizumab released from SLIs after 12 weeks (100.1 %) and Resomer® RG 502 H (4.4 %) clearly showed that the PLGA matrix (and its

degradation products) degraded Ranibizumab dramatically. These results also highlight that SLIs provide an outstanding delivery matrix for proteins.

Additionally, non-reducing denaturating SDS-PAGE was performed for mAb, Bevacizumab and Aflibercept (for Ranibizumab capillary gel electrophoresis was performed and will be discussed in the following).

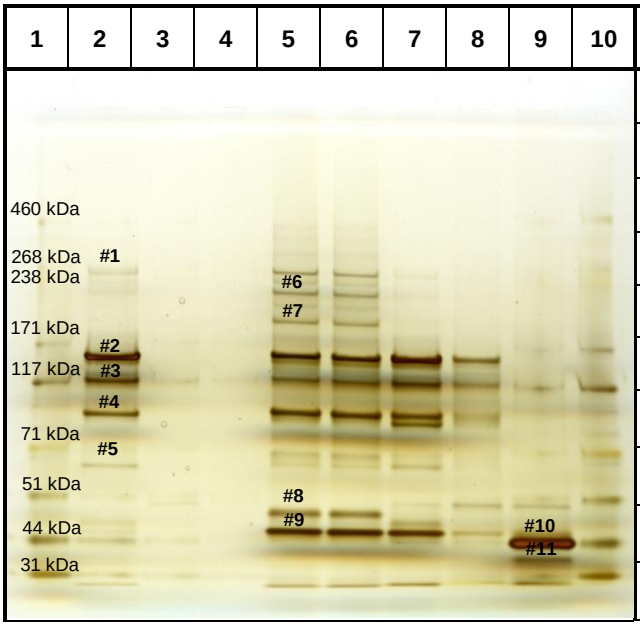

No.	Sample name
1	MW Marker
2	reference
3	BSA 1.80 ng
4	BSA 0.36 ng
5	pH3_week 2
6	pH3_week 4
7	Resomer® RG 502_week 4
8	Resomer® RG 502_week 6
9	Resomer® RG 502_week 12
10	MW Marker

Figure VII-14: Non-reducing denaturating SDS-PAGE of mAb. Shown is the head-to-head comparison of samples being incubated at pH 3 and those which were released from a PLGA matrix.

Illustrated in Figure VII-14, SDS-PAGE of mAb revealed a pH-induced degradation resulting in the formation of aggregates with a size of 250 kDa (#6) and 200 kDa (#7) and fragments being 51 kDa (#8) and 48 kDa (#9) in size compared to the reference (lane 2, 5 and 6). Interestingly, between week 2 and week 4 of incubation in the acidic solution, qualitatively no more degradation of mAb was observed leading to the conclusion that the pH-induced degradation was already complete after 2 weeks. Results for the released fractions of mAb from a Resomer® RG 502 matrix can be seen at lane 7 to 9. Comparable additional bands can be detected as it was the case for the pH 3 incubated samples. Moreover, intensity of fragment bands increased while the monomer band was less intense. After 12 weeks, the mAb was completely degraded and only bands with a MW of 37 kDa (#11) to 41 kDa (#10) were present pointing into the

direction of complete fragmentation. MAb fractions released from the PLGA matrix were much more degraded than the samples incubated at pH 3. Thus, it can be concluded that the instability of mAb was mainly caused by chemical interactions with PLGA and its degradation products.

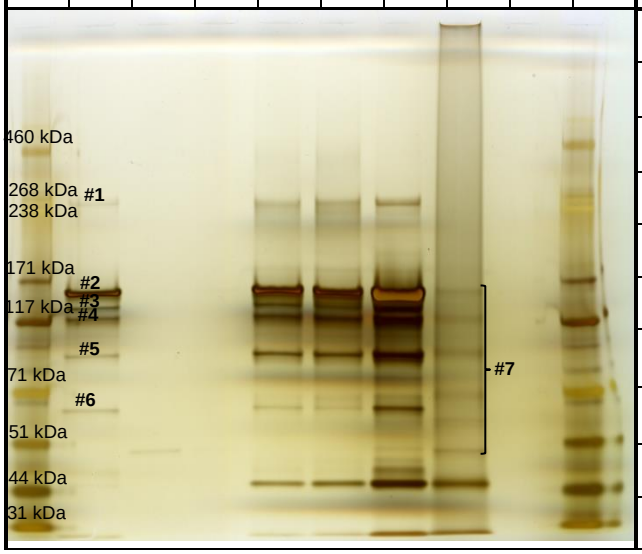

No.	Sample name
1	MW Marker
2	reference
3	BSA 1.80 ng
4	BSA 0.36 ng
5	pH3_week 2
6	pH3_week 4
7	Resomer® RG 502_week 4
8	Resomer® RG 502_week 12
9	blank
10	MW Marker

Figure VII-15: Non-reducing denaturating SDS-PAGE gel of released Bevacizumab fractions from a Resomer® RG 502 matrix. Due to the very incomplete release of Bevacizumab, only samples taken after 4 weeks and 12 weeks were accessible for analysis.

Figure VII-15 displays the results for separation of MW species of the pH 3 study (lane 5 and 6) and the released fractions of Bevacizumab from a Resomer® RG 502 matrix (lane 7 and 8). Due to the very incomplete release of Bevacizumab, only samples taken after week 4 and week 12 were accessible for analysis. Surprisingly, after a 2-week incubation at pH 3, no additional bands were detected; only slightly more intense HMW aggregates and fragment bands were observed. No obvious differences between the samples taken after 2 and 4 weeks of incubation at pH 3 were found. For the sample taken after 4 weeks of release from the PLGA matrix, no apparent differences in band patterns are noticeable (compared to the pH 3 samples), thereby demonstrating that Bevacizumab was not further degraded by the PLGA matrix. This result was surprising because in previous studies (VII.2.1) Bevacizumab was the most sensitive protein. After 12 weeks of release, a clear and distinct tendency towards fragmentation was observed: the monomer band almost completely disappeared and was replaced by a broad spectrum of

bands ranging in a size of 50 kDa to 150 kDa (#7). In addition, intense bands at 45 kDa and 30 kDa were present. In case of Bevacizumab, a concluding answer if the acidic pH of the incubation media or the acidic microclimate inside the PLGA matrix were responsible for its degradation, remains unanswered.

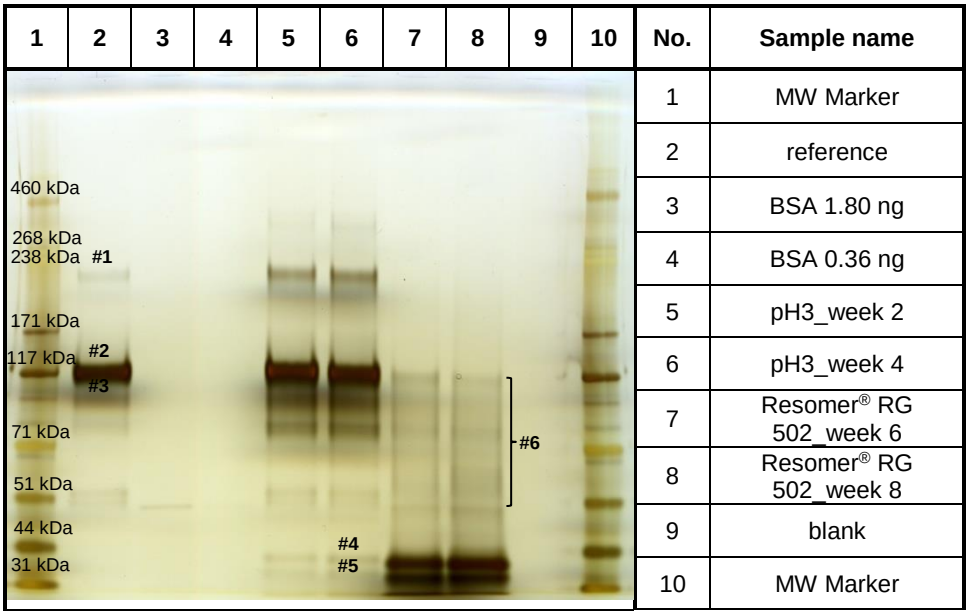

No.	Sample name
1	MW Marker
2	reference
3	BSA 1.80 ng
4	BSA 0.36 ng
5	pH3_week 2
6	pH3_week 4
7	Resomer® RG 502_week 6
8	Resomer® RG 502_week 8
9	blank
10	MW Marker

Figure VII-16: Non-reducing denaturating SDS-PAGE gel of Aflibercept samples incubated at pH 3 and of released fractions of Aflibercept from a Resomer® RG 502 matrix.

The results for the recombinant fusion protein Aflibercept are displayed in Figure VII-16. The reference material was characterised by weak bands at approximately 246 kDa (#1), most likely aggregates, whereas bands at 129 kDa (#2) represented the monomer in its glycosylated form; an additional band was identified at 106 kDa (#3) which was probably the deglycosylated form. After 2 weeks at pH 3 (lane 5), bands already seen for the reference became more intense; very weak bands around 37 kDa (#4) and 34 kDa (#5) were also identified. Qualitatively, the aggregation profile did not change between week 2 and week 4 upon incubation at pH 3, meaning that a further degradation of Aflibercept would be unlikely. Lane 7 and 8 are illustrating the degradation profile of released fractions taken after 6 and 8 weeks. The monomer band disappeared almost completely and was replaced by strong bands in the MW region of 20 kDa to 30 kDa. A similar profile can be seen after 8 weeks. These results proof, that Aflibercept was

mainly degraded by products formed due to the PLGA erosion. Degradation took also place upon incubation at pH 3, but the differences between the sample at lane 6 (4 weeks at pH 3) and lane 7 (6 weeks of release) were substantial. Consequently, the major degradation can be reduced to PLGA erosion.

Table VII-3: Non-reducing denaturating capillary gel electrophoresis of Ranibizumab samples.

	LMW species [%]	Monomer [%]	HMW species [%]
reference	2.05 (±0.49)	97.85 (±0.64)	1.10 (±0.14)
week 2_pH 3	1.47 (±0.15)	98.47 (±0.21)	0.06 (±0.12)
week 4_pH 3	1.60 (±0.36)	98.03 (±0.25)	0.03 (±0.06)
week 12_lipid matrix	2.10 (±0.14)	97.90 (±0.14)	0.00 (±0.00)
week 12_Resomer® RG 502	31.65 (±0.92)	65.85 (±2.05)	2.50 (±1.13)
week 12_ Resomer® RG 502 H	27.75 (±0.78)	64.05 (±3.04)	8.20 (±2.26)

Table VII-3 displays the results from non-reducing capillary gel electrophoresis of Ranibizumab. No difference can be observed between the reference and the samples incubated at pH 3 as the monomer content stays constant at 98 %. Released Ranibizumab from both Resomer® polymers (ester terminated and free COOH-group), showed 28 % to 32 % fragments and up to 8 % aggregates were formed. This clearly illustrates that not the low pH of the incubation medium predominantly caused protein degradation, rather the direct chemical interaction of Ranibizumab and PLGA/PLGA degradation products inside the matrix as reported previously [49, 253].

Finally, it was possible to confirm that the degradation of the proteins was mainly driven by the erosion of the PLGA matrix and the direct interaction of the proteins with PLGA and its degradation products rather than the acidic pH of the surrounding incubation medium. This statement holds true for mAb, Aflibercept and Ranibizumab whereby it was not possible to unequivocally answer this question for Bevacizumab.

VII.2.2.2 CHEMICAL STABILITY OF PROTEINS

Samples were further analysed towards chemical stability. IEX and HIC was not applicable due to the very little sample volume. Instead, capillary gel electrophoresis under reducing conditions was executed to detect possible covalent bonds potentially formed (Figure VII-17). Shown are the percentages of light and heavy chain as well as of LMW and HMW species for samples incubated at pH 3 for 2 weeks and 4 weeks and of released protein after 12 weeks from lipid implants and from Resomer® RG 502 and RG 502 H matrix as head-to-head comparison of both delivery platforms.

Figure VII-17 A illustrates the results for mAb. Upon incubation at pH 3, a significant increase in LMW species can be detected by a similarly decrease of the heavy chain percentage already after 2 weeks. The light chain percentage increased by 10 %. No major differences between samples taken after 2 weeks and after 4 weeks were detected, meaning that the chemical degradation of mAb took place rapidly and was complete already after 2 weeks of incubation. Interestingly, no significant differences were identified between the reference and the released mAb from SLIs after 12 weeks pointing out, that no additional covalent bonds were formed during release. Contrarily, released mAb from Resomer® RG 502 was characterised by a drastic increase in LMW species and light chain at the expense of heavy chain percentage. MAb released from Resomer® RG 502 H was almost exclusively present as LMW species in the range of molecular weight of the light chain (no single peaks were isolated; more a multi-peak region was observed). The difference in degradation profile of mAb between both PLGAs can be explained by the acidic end group Resomer® RG 502 H is equipped with promoting the cleavage of the peptide bonds.

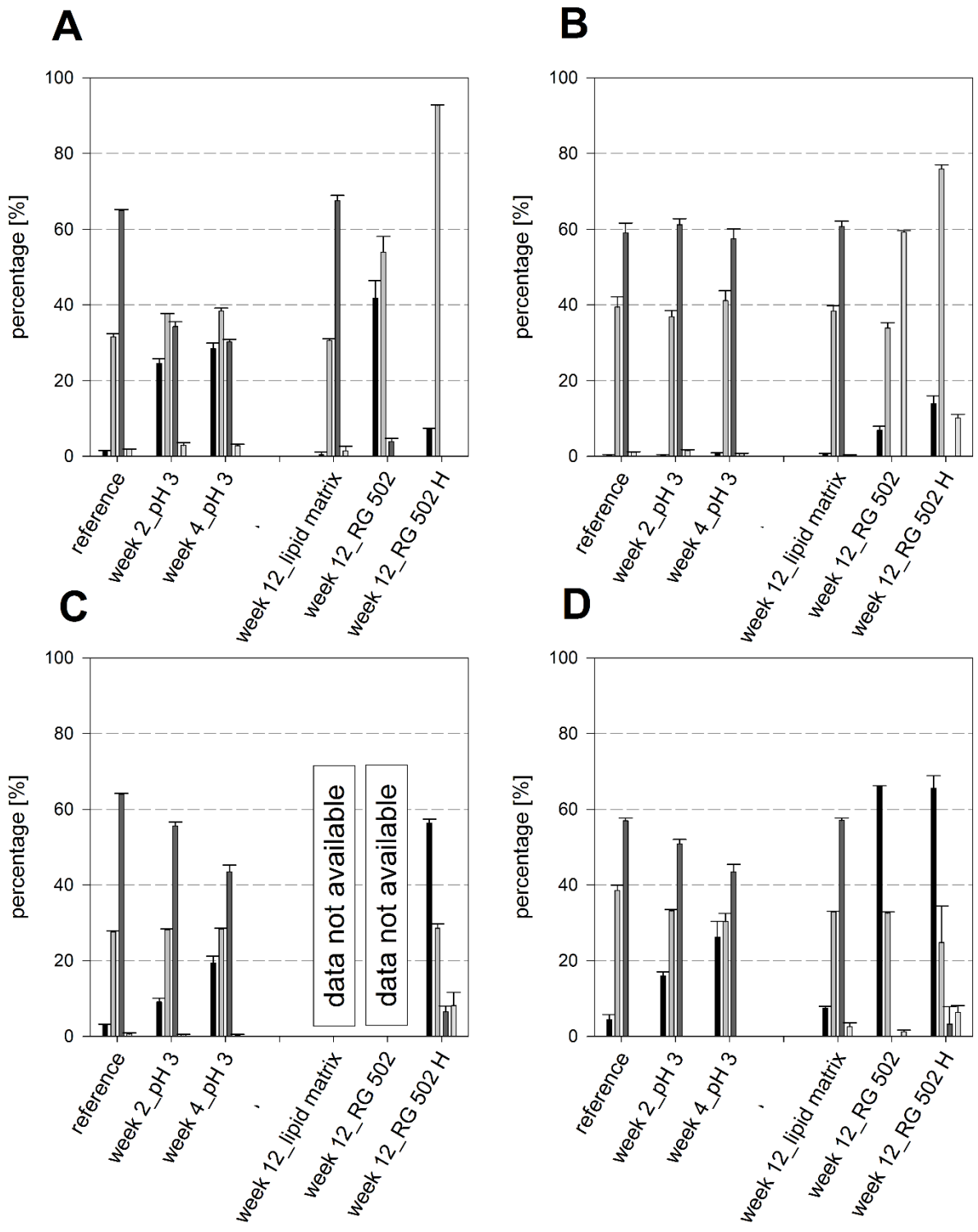

Figure VII-17: Reducing denaturating capillary gel electrophoresis of (A) mAb, (B) Ranibizumab, (C) Bevacizumab and (D) Aflibercept samples incubated at pH 3 for 2 and 4 weeks and of released fractions from both lipid and PLGA matrices after 12 weeks of release.

In case of Ranibizumab, the incubation in acidic PBS buffer did not lead to any alterations in light chain and heavy chain percentage, thereby showing the remarkable stability of Ranibizumab (Figure VII-17 B). The released Ranibizumab from SLIs did not revealed any changes, which indicates that no covalent bonds were formed during release. In contrast, no heavy chain was detected released from Resomer® RG 502, but instead an increase of about 60 % of smaller sized fragments was found. Even more (approximately 75 %) LMW species were measured for Ranibizumab samples released from Resomer® RG a carboxyl group). Both PLGAs heavily promoted the formation of additional covalent bonds whereas for the samples released from SLIs no differences compared to the reference were apparent.

As it was already the case for SE-HPLC analysis, Bevacizumab samples were not available for all time points due to the short release duration (for SLIs) of only 3 to 4 weeks or the very small amount released which was the case for the Resomer® matrices. Therefore, the data set presented at Figure VII-17 C gives no conclusive results and will not be further discussed.

Aflibercept samples are illustrated in Figure VII-17 D. Upon incubation in PBS at pH 3, the formation of LMW species was observed after 2 weeks; even more LMW species were formed after 4 weeks of incubation indicating that additional covalent bonds were formed also after a longer incubation period. Similarly, the heavy chain and light chain percentage dropped over the time. Collected and concentrated Aflibercept liberated from SLIs was distinguished by slight changes in the chain profile compared to the reference. In contrast, once released from both Resomer® matrices, the fraction of LMW species (approximately 60 % more compared to reference) increased dramatically whereas almost no heavy chain was detectable anymore.

In summary, it was demonstrated that the formation of additional covalent bonds was mainly driven by erosion of the PLGA matrix. But also, a shift in chain profile upon incubation at pH 3 was detectable, meaning that also the pH of the incubation medium promoted partially the formation of chemical alterations. However, proteins were chemically modified more intensively when released from PLGA, even differences between Resomer® RG 502 and RG 502 H were

observed, which can be explained by the different end groups the polymers are equipped with. Contrarily, only slight changes - if any - were noticed when proteins were released from SLIs highlighting the benefit of this delivery platform. For Bevacizumab, it was not possible to unmistakably answer this question due to the limited sample available.

Other reports in the literature also addressed the topic of chemical protein stability during release from PLGA based depots [44, 46]. Estey *et al.* [44] reported on BSA stability under acidic conditions (pH 2) by modelling the microclimate within PLGA matrices. BSA monomer dropped to 0 % within 14 days to 28 days due to the formation of aggregates and fragments measured by SE-HPLC and SDS-PAGE. The chemical degradation (mainly deamidation) of insulin from PLGA microspheres [49, 345] over 18 days [49] or the acylation of atrial natriuretic peptide (ANP) has been described. The acylation of ANP over 60 days has also been described by Lucke *et al.* modelling the microclimate within PLGA matrices by lactic acid solutions [254]. The same holds true for exenatide as reported by Liang *et al.* [217] with the additional background of water uptake onto PLGA microspheres. Chang *et al.* [72] measured the main peak area of a released f_{ab}-fragment by IEX from PLGA-triacetin depots over 80 days showing a continuous decrease from almost 100 % to approximately 50 %. In our study, for SLIs (Table VII-3) the main charge variant of Ranibizumab dropped only by 10 % over 18 weeks of release. All references reported on a fast and distinct chemical degradation, which was not the case in our study, highlighting the benefit of lipid based depots in terms of chemical protein stability.

VII.2.3 STABILITY OF RELEASED PROTEIN FRACTIONS AFTER STORAGE OF LIPID IMPLANTS

Besides the stability analysis performed with protein released from freshly prepared implants, it was also analysed if mAb and Ranibizumab show sufficient stability when stored for up to 3 months within the highly hydrophobic lipid matrix. SLIs were stored at 4°C after production for 4 weeks and 12 weeks prior to *in-vitro* release. The protein fraction released over the first 7 days

after storage was then collected, concentrated and analysed. For this study, the 3:1 protein:cyclodextrine [w/w] lyophilisate formulation was used.

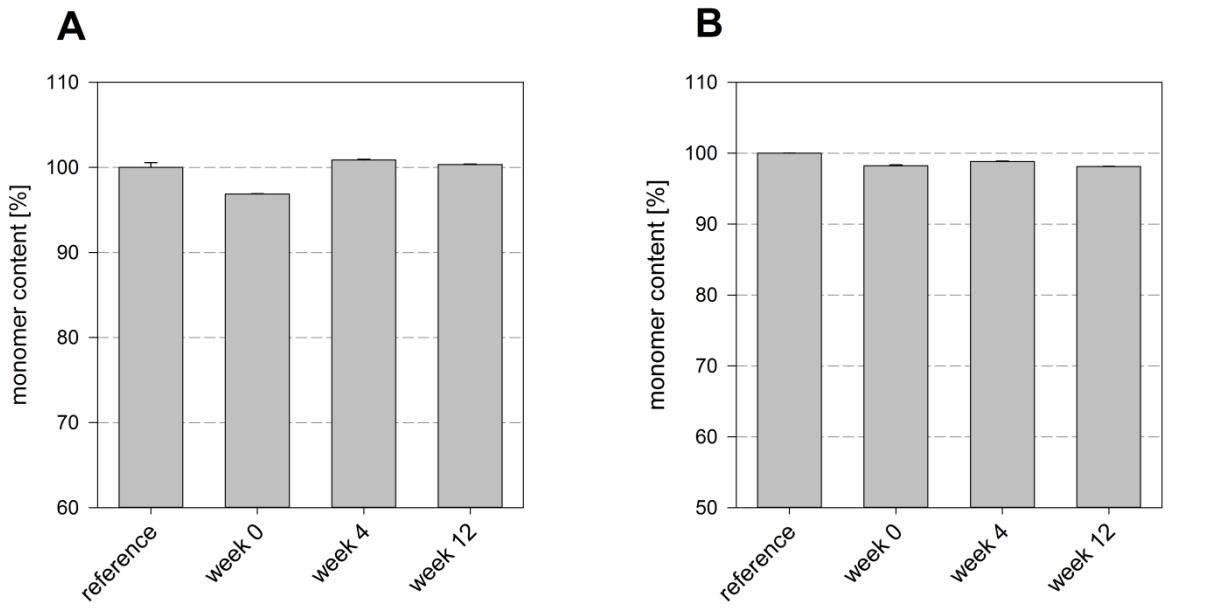

Figure VII-18: Monomer content of (A) mAb and (B) Ranibizumab released within the first 7 days after storage of lipid implants for 0, 4 and 12 weeks at 4°C. Displayed is the variation relative to the reference.

In Figure VII-18, SE-HPLC results are displayed showing the monomer content of the reference and samples directly after production (week 0) and after storage of 4 and 12 weeks, respectively. For mAb, the monomer content remained unchanged ranging from 96.9 % to 100.9 % relative to the reference also after a 12-week storage. Non-reducing denaturating SDS-PAGE was performed orthogonally showing slightly more intense bands of stored samples at 276 kDa (#6) and 178 kDa (#7) (aggregates) and bands of different sized fragments (45 kDa, 64 kDa) compared to reference (Appendix, Figure XII-10).

Ranibizumab monomer content was measured with 98.1 % to 98.9 % relatively to the reference, also showing no decrease after storage. Orthogonally, capillary gel electrophoresis was performed as illustrated in Table VII-4. The monomer content slightly decreased by 1 % between week 0 and week 12. A significant change in HMW and LMW upon storage was not detected.

Table VII-4: Results of non-reducing denaturating on-chip gel electrophoresis of Ranibizumab fractions stored for 12 weeks at 4°C prior to release compared to reference.

	Reference	Week 12
LMW species [%]	2.05 (±0.49)	1.90 (±0.00)
Monomer [%]	97.85 (±0.63)	97.00 (±0.00)
HMW species [%]	0.10 (±0.14)	0.10 (±0.00)

Regarding chemical stability, the percentage of mAb's main charge variant decreased by approximately 5 % upon storage while the percentages of acidic (+6 %) and basic species increased (+0.7 %) (Figure VII-19 A). For Ranibizumab, exclusively more hydrophobic subspecies were formed (+2 %) upon storage equivalent to a decrease in main charge variant by 2 % (Figure VII-19 B).

In addition to IEX and HIC, reducing denaturating capillary gel electrophoresis was performed (Table VII-5). The heavy chain percentage of mAb decreased by 3 % after a 12-week storage whereas slightly more LMW and HMW species were detected compared to the reference. The percentage of light chain stayed constant. Ranibizumab samples also showed a slight reduction in heavy chain percentage (1.5 %) as well as a minor increase of light chain and LMW species (together 1.5 %).

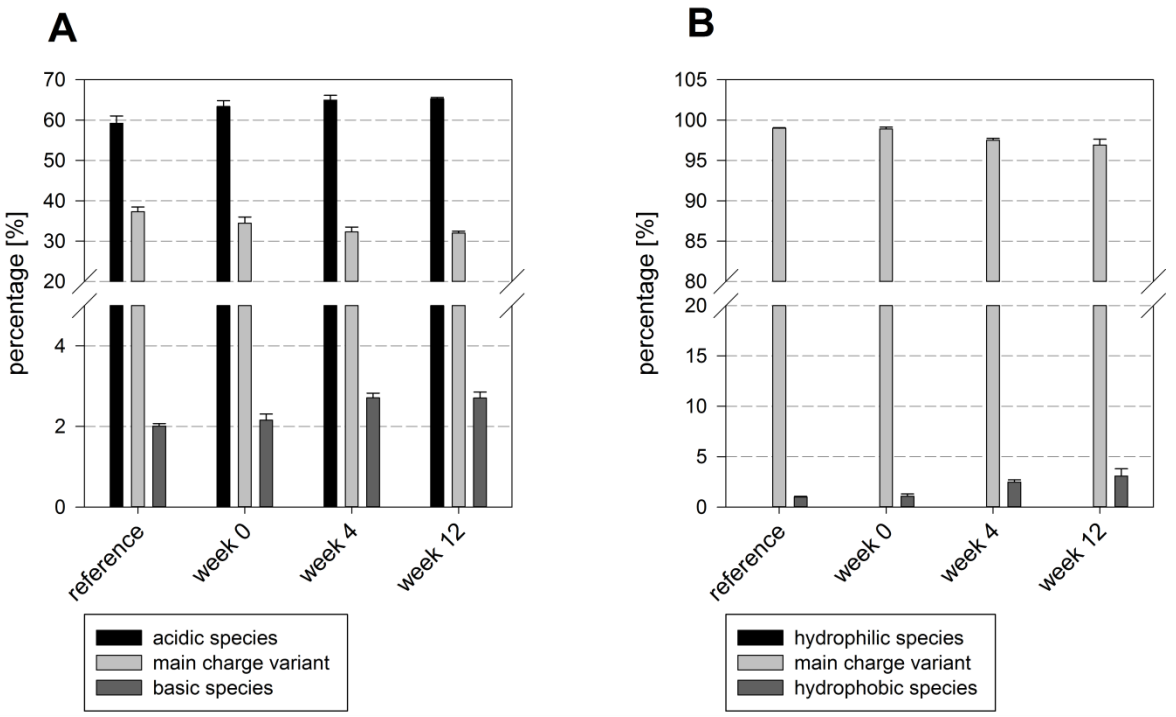

Figure VII-19: Chemical stability of (A) mAb and (B) Ranibizumab released within the first 7 days after storage of lipid implants for 0, 4 and 12 weeks at 4°C.

Table VII-5: Reducing denaturating capillary gel electrophoresis of mAb and Ranibizumab released fractions after a 12-week storage. Displayed are the light and heavy chain percentages as well as the amount of LMW and HMW species compared to reference.

	mAb		**Ranibizumab**	
	Reference	**Week 12**	**Reference**	**Week 12**
LMW species [%]	0.95 (±0.00)	1.80 (±0.14)	0.30 (±0.28)	1.15 (±0.35)
Light chain [%]	29.10 (±0.14)	28.85 (±0.92)	34.50 (±0.14)	34.66 (±1.98)
Heavy chain [%]	67.90 (±0.00)	64.75 (±0.49)	64.55 (±0.35)	63.00 (±1.41)
HMW species [%]	2.05 (±0.07)	2.70 (±0.14)	0.65 (±0.07)	1.40 (±0.00)

The FT-IR spectra of mAb and Ranibizumab samples are given in Figure VII-20. Spectra of the reference and of the released protein after 0, 4 and 12 weeks are illustrated. The amide I band region (1635 cm^{-1} to 1645 cm^{-1}) of mAb samples did not alter in band maxima but band intensity

differed. Furthermore, increasing band intensities were noticed at 1680 cm^{-1} and 1615 cm^{-1}, leading to the conclusion that unfolding events must have taken place. FT-IR spectra of Ranibizumab samples did not show any deviations including band intensity and wavenumber of band maxima (Figure VII-20 B). Compared to mAb, the better conformational stability was due to the less complex structure of the f_{ab}-fragment [346].

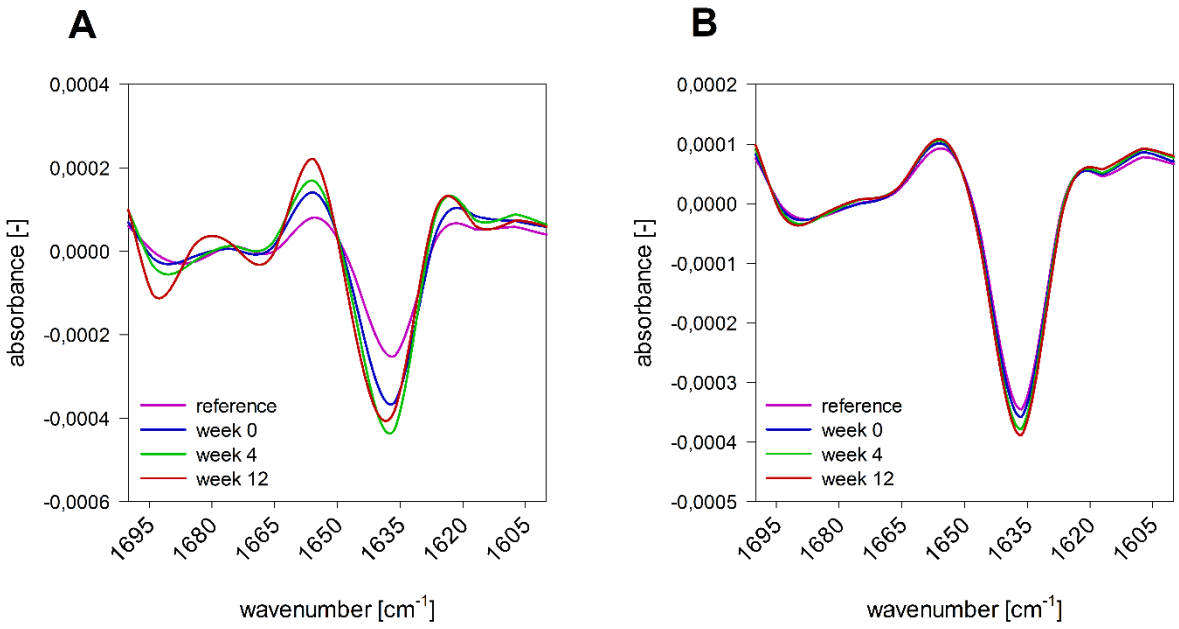

Figure VII-20: FT-IR spectra of released (A) mAb and (B) Ranibizumab samples collected over the first 7 days of release. Lipid implants were stored at 4°C for 0, 4 or 12 weeks prior to *in-vitro* release.

When stored in the dry state at 4°C, mAb and Ranibizumab showed very good stability even after a period of 3 months. Both proteins were more stable compared to the stability profile obtained after 12 weeks of release. This can easily be explained by the elevated temperatures during incubation and the aqueous environment which are well-known triggers for protein degradation [347-351].

VII.3 CONCLUSION

Within this chapter, the stability of four different proteins was analysed, including three commercial products.

The stability of the proteins was assessed released either from lipid or PLGA depots. As a model protein, an IgG_1 antibody (mAb) was used which was characterised by an adequate stability over more than 6 months (26 weeks) when released from SLIs. Monomer content stayed between 93 % and 98 % over the release duration, even though major chemical and conformational instabilities were detected. Ranibizumab was delivered over 18 weeks, showing excellent physical, chemical and conformational stability over the complete release period. Therefore, Ranibizumab was the most promising therapeutic. Aflibercept comprised an acceptable stability profile over 14 weeks, therefore being an additional candidate for further studies. Only Bevacizumab was characterised by poor stability and comparatively short release durations.

The stability of released protein from a PLGA matrix was assessed as well. All proteins showed a rapid and substantial degradation – physically and chemically – which was mainly caused by the micro environment within the PLGA matrix rather than the pH of the incubation medium. These results are in line with reports in the literature (Table VII-1).

For fractions released from SLIs, such promising protein stability data have - to the best of our knowledge - not yet been published (Table VII-1), neither regarding the period of release nor the variety of proteins, most of them being therapeutically relevant proteins. Various publications have already addressed this topic describing the stability of peptides [301], small sized proteins [43, 45, 49, 253] or f_{ab}-fragments [72], but none of them reported over such long release durations and comprehensive stability data, irrespective of the delivery platform. Compared to other delivery platforms described in literature such as PLGA [43, 49] or chitosan [79], the lipid based depot described here provides an adequate stability for at least the mAb and

Ranibizumab over a long-term release period of 18 weeks to 26 weeks as well as after storage of the implants.

Overall, the benefit of lipid based systems was demonstrated, as it can retain the stability of the incorporated protein during long-term release and storage. Especially the excellent stability profile of Ranibizumab is promising basis for future work.

VIII. TRIGLYCERIDE-PROTEIN-INTERACTION STUDIES

VIII.1 INTRODUCTION

Within chapter IV and chapter VII, release patterns and stability profiles of two IgG_1 antibodies, the f_{ab}-fragment Ranibizumab (Lucentis®) and the fusion protein Aflibercept (Eylea®) were described. However, the complexity of the lipid depot systems in particular with regard to lipid-protein interactions has not been studied. In this chapter, experiments were performed to study possible interactions between the proteins and triglycerides with the aim to identify if the lipids may potentially be accountable for the different release profiles and protein instability issues observed. Considering such interactions is crucial since lipid based depots are not considered to be inert. Even *et al.* already described the interactions between differently charged peptides and lipids including D114, soy lecithin and cholesterol [187]. The interactions between interferon β-1b and the triglycerides H12 and D118 has been addressed by Neuhofer [185].

Interactions between proteins and lipids have been studied extensively before, but exclusively phospholipids have been analysed. In such studies, the focus was mainly on interactions at a cellular level, for instance interactions of proteins with membranes [352-368], or between proteins and liposomes [185], or hexosomes [369] using methods like surface plasmon resonance (SPR), isothermal titration calorimetry (ITC), dynamic scanning calorimetry (DSC), dynamic light scattering (DLS) or flow cytometry.

However, triglycerides differ from phospholipids by structure, solubility, hydrophobicity and charge [125, 370]. To our knowledge, Neuhofer was the first describing interactions between a pharmaceutical protein and triglycerides, namely H12 and D118, which have also been used in this study [185]. Interactions have been studied by performing incubation studies with native and PEGylated interferon β-1b and the relevant triglycerides. Neuhofer described that in the

presence of lipids, interferon β-1b formed soluble aggregates and oxidized subspecies. Furthermore, the biological activity of the protein decreased in presence of triglycerides. At the same time, protein recovery was significant lower upon incubation with triglycerides. Triglyceride-protein-interactions were further investigated by using QCM to study adsorption and desorption events of interferon β-1b on tristearin coated chips. Additionally, Neuhofer observed substantial different release patterns of native and PEGylated interferon β-1b released from the same lipid depot. This raised the question, if such interactions may influence protein release from lipidic depots in addition to diffusion and erosion which are well-known release mechanisms.

The present chapter describes how two IgG_1 antibodies, the f_{ab}-fragment Ranibizumab and the fusion protein Aflibercept behave upon contact with H12, D118 or Resomer® RG 755 S, respectively. The aim was to identify possible interactions between the different compounds Therefore, rods consisting of pure H12, D118 or RG 755 S, respectively, were extruded and incubated with protein solutions to study possible interactions. After an 8-week incubation period at 35°C, the protein was analysed with regards to colloidal, chemical and conformational stability. Additionally, raw material and extruded rods were tested for the presence of heavy metals. Heavy metals could potentially be introduced into the lipid matrix during the manufacturing process and may be a cause for protein instabilities [371-373].

VIII.2 RESULTS AND DISCUSSION

VIII.2.1 INCUBATION STUDY OF PROTEIN SOLUTIONS WITH TRIGLYCERIDE AND PLGA RODS

To study possible interactions between proteins and the depot forming materials used within this work, lipid and PLGA rods were extruded and incubated with the proteins for 8 weeks at 35°C and 40 rpm in a horizontal shaker. Implants were extruded consisting of 100 % H12 (extrusion temperature 35°C), 100 % Dynasan® D118 (extrusion temperature 60°C) or 100 % Resomer® RG 755 S (extrusion temperature 70°C), respectively, using a ZE-5 mini-extruder. Resomer® RG 755 S was chosen, as it has a degradation time frame of approximately 6 months. Thereby, it was ensured that during an 8-week incubation study no erosion of the RG 755 S rod occurred, which could have caused elevated particle counts or could have otherwise interfered with protein analysis. Extruded implants had a size of 2.0 mm x 15 mm, resulting in a surface of approximately 100 mm^2. Rods were placed in 2.0 ml micro-centrifuge tubes (VWR, Radnor, PA, USA) and 1.0 ml protein solution was added at a concentration of 2.0 mg/ml (protein stock solutions comprising 10 mg/ml in 50 mM sodium phosphate buffer pH 6.2 were diluted with 0.22 µm filtered PBS pH 7.4). As a negative control, proteins were also incubated in PBS pH 7.4 for 8 weeks without any additives. After 2, 4 and 8 weeks, samples were taken for each incubation protocol (incubation protocol: the material the protein was exposed to) and analysed using the following techniques: Light obscuration (LO), turbidity, SE-HPLC, electrophoretic techniques (SDS-PAGE and capillary gel electrophoresis under reducing and non-reducing conditions), protein recovery, IEX, HIC, cIEF, extrinsic fluorescence and FT-IR.

In the following, the results of the incubation study will be discussed separately in terms of colloidal, chemical and conformational stability. Furthermore, the phenomena of possible protein absorption onto lipids/PLGA surfaces will be discussed. Therefore, it is clearly stated, that the behaviour of the proteins will be evaluated covering two completely different aspects (protein stability and adsorption phenomena) in the presence of lipids/PLGA.

VIII.2.1.1 COLLOIDAL STABILITY OF PROTEINS

The colloidal stability of incubated proteins was measured using different methods covering the formation of subvisible particles (LO, turbidity) and soluble aggregates (SE-HPLC, non-reducing denaturating electrophoresis). In previous studies, an incubation temperature of 37°C had been applied as it mimics the physiological temperature. Here, the incubation temperature was set to 35°C due to the low T_{onset} (36.8°C) of the extrudates consisting of 100 % H12 as it was expected that an incubation temperature of 37°C would lead to a complete disintegration of the H12 rods.

LIGHT OBSCURATION (LO) AND TURBIDITY

The results of LO measurements are displayed in Figure VIII-1. The particle count of the negative controls (rods incubated in PBS) after 8 weeks of incubation was well below 100 counts indicating that an elevated particle count at the protein containing samples was not due to disintegration (particle formation) of the rods. However, at the negative control of the H12 rods, about 500 particles were counted pointing into the direction of a slight disintegration of the H12 rod even though the incubation temperature was below its T_{onset}. Nevertheless, particle counts of protein solutions were higher. It can therefore be hypothesised that the elevated particle count measured was based on protein aggregates. The mechanism and kinetics of particle formation is highly relevant and would deliver additional information [348, 349, 351, 374-386], however, this aspect was not further investigated as it was beyond the scope of this work.

As a control, protein solutions were incubated without any lipids/PLGA rods (Figure VIII-1). Particle counts were found to comprise the lowest levels; in maximum 650 particles were measured for Bevacizumab after 8 weeks of incubation. Turbidity measurements confirming this observation as the values were found to be the lowest ones for each protein ranging between 0.73 (±0.07) and 1.07 (±0.08) (Table VIII-1).

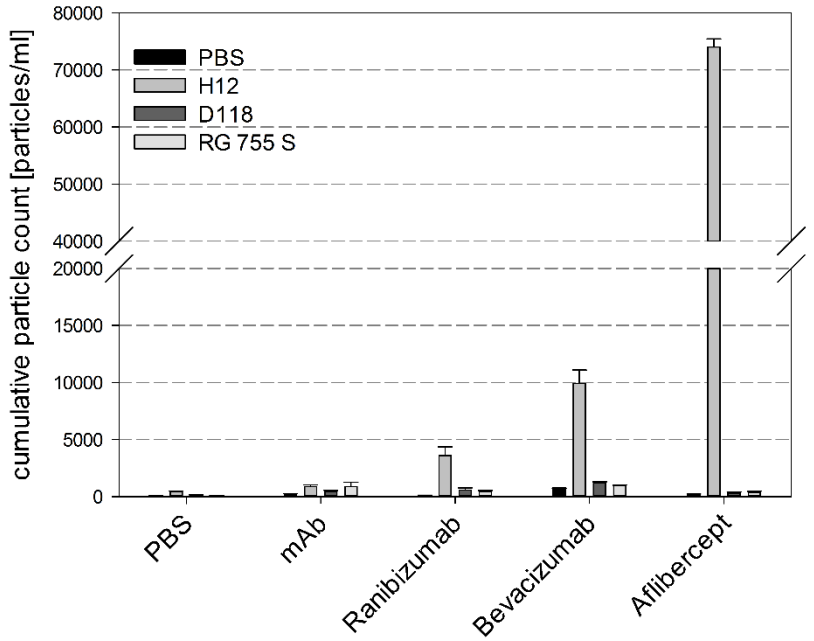

Figure VIII-1: Cumulative particle count (> 1 µm) of protein solutions incubated with H12, D118 and RG 755 S rods and without any additives (PBS, negative control) after 8 weeks at 35°C and 40 rpm.

Upon incubation with D118 and PLGA rods, both particle count and turbidity were very low for all proteins as illustrated by Figure VIII-1 and Table VIII-1. Merely, slightly elevated particle count and turbidity can be seen for Bevacizumab containing solutions.

The highest particle counts can be identified when proteins were incubated with H12 rods. Particle counts for the protein containing samples were between 850 particles/ml (mAb) up to 77.000 particles/ml for Aflibercept. Regarding the Aflibercept containing samples, the high particle count was caused by the complete disintegration of the H12 rods. Interestingly, disintegration of the H12 rod only occurred when Aflibercept was present. For mAb, Ranibizumab and Bevacizumab, H12 rods did not fully disintegrated although a partial «softening» and disintegration was observed. If incubated without any proteins (negative control), the H12 rods remained solid. Turbidity values were in line with particle measurements: for all proteins turbidity of protein solutions incubated with H12 showed the highest values ranging from 1.07 (±0.02) to 24.56 (±1.21). Again, the high value for Aflibercept samples

incubated with H12 rods (24.56 FNU ±1.21 FNU), was caused by the total disintegration of the H12 rod which was only observed for this protein.

Table VIII-1: Turbidity of samples incubated with H12, D118 and RG 755 S rods and without any additives (PBS, negative control) after 8 weeks at 35°C and 40 rpm. Results are given in FNU.

	PBS	mAb	Ranibizumab	Bevacizumab	Aflibercept
PBS	0.53 (±0.03)	0.73 (±0.07)	0.73 (±0.01)	0.74 (±0.05)	1.07 (±0.08)
H12	1.09 (±0.11)	1.07 (±0.02)	1.25 (±0.05)	2.36 (±0.14)	24.56 (±1.21)
D118	0.56 (±0.03)	0.79 (±0.13)	1.13 (±0.03)	0.91 (±0.08)	1.35 (±0.09)
RG 755 S	0.58 (±0.02)	0.89 (±0.05)	0.94 (±0.16)	1.01 (±0.12)	1.02 (±0.10)

Both particle count and turbidity for proteins incubated with PLGA rods were comparatively low. That signifies that PLGA is more inert than the triglycerides tested here from a colloidal stability perspective. However, it should not be forgotten that proteins were incubated with the lipids/PLGA rather than encapsulated within the matrix material.

When comparing H12 and D118 head-to-head, it is striking that both cumulative particle count and turbidity are clearly higher for H12 than for D118 for all proteins tested. As the particle count for H12 rods incubated in PBS (negative control) revealed less counts, a disintegration of the H12 rod due to the incubation close to T_{onset} was most likely not the cause for the elevated particles observed. In fact, it can be concluded that an interaction between proteins and H12 took place.

Based on these results, it can be assumed that even the protein itself might has an impact on lipid disintegration due to its amphiphilic character. For Aflibercept, even a complete disintegration of the H12 rods was observed.

As additional factors, pH and surface-active additives (residues from the marketed formulations which were not removed by the dialysis) can possibly lead to disintegration of the H12 rods. As

the pH represents a critical parameter, the pH was monitored over 8 weeks and is displayed in the Appendix, Table XII-1. For all proteins, the pH value stayed constant (a change of a maximum of 0.12 was observed) over the complete incubation time. Furthermore, the pH of the protein containing samples was measured between 6.79 (Bevacizumab) and 7.00 (Ranibizumab) at week 8. These results pointing into the direction that a different pH as possible source of H12 rod disintegration can be excluded. Since all proteins (except mAb) were originally formulated with PS 20 (III.1.1), the presence of surface-active additives should be considered. Although all marketed formulations were dialysed, small amounts of PS 20 were most likely still present within all formulations. Therefore, the disintegration of the H12 rods was probably not caused by surface-active additives. These theories were not further investigated and need to be thoroughly studied in future experiments. For instance, to distinguish between protein aggregates and particles with a lipidic origin, microflow imaging (MFI) would be a suitable method.

Elevated particle count and turbidity could be explained by a potential partial unfolding of the proteins in presence of the highly hydrophobic surfaces the proteins were exposed to [387]. It is known, that partially unfolded proteins can act as nuclei for protein aggregation [350, 380, 388] and therefore for the formation of small soluble and large insoluble aggregates. The surface charge distribution and presence of hydrophobic patches at proteins' surface are also factors influencing the propensity to unfold. For instance, that could be a reason for the comparable high particle count for Bevacizumab samples. It has the highest tendency to interact with hydrophobic surfaces probably due to its propensity to unfold. This is caused by hydrophobic patches present at Bevacizumab`s surface. HIC analysis revealed the longest retention time for Bevacizumab, signifying the highest hydrophobicity of this protein compared to the other proteins. This would also explain the incomplete release patterns of Bevacizumab observed during *in-vitro* release studies described in chapter IV.

SE-HPLC AND ELECTROPHORETIC ANALYSIS

The percentage of monomer content was monitored in samples collected after 0 (before incubation started), 2, 4 and 8 weeks. For the detailed course of monomer depletion upon incubation with lipid/PLGA rods, please see Appendix Figure XII-11. Protein recovery was assessed as well but will be discussed separately within VIII.2.1.4 as it is an indication for adsorption of proteins onto lipid/PLGA surfaces.

Table VIII-2: SE-HPLC results of mAb incubated with H12, D118 and RG 755 S rods and without any additives (PBS, negative control) after 0 weeks (reference) and 8 weeks at 35°C and 40 rpm. Results are given in %.

	Reference			**Week 8**		
	Aggregates	**Monomer**	**Fragments**	**Aggregates**	**Monomer**	**Fragments**
PBS				0.63 (±0.16)	95.05 (±0.39)	4.34 (±0.22)
H12				0.43 (±0.12)	89.88 (±0.29)	9.69 (±0.19)
	1.11 (±0.13)	98.19 (±0.06)	0.69 (±0.07)			
D118				0.45 (±0.16)	94.21 (±1.07)	5.34 (±0.98)
RG 755 S				0.46 (±0.10)	93.61 (±0.17)	5.93 (±0.20)

Table VIII-2 provides an overview of the monomer content of mAb upon incubation. Interestingly, the monomer content after 8 weeks of incubation with H12 rods dropped down to 90 % compared to 93 % to 95 % if incubated with D118 or PLGA rods, respectively. The monomer loss for all incubation protocols was due to fragmentation but approximately 5 % more fragments were observed upon incubation with H12 rods. Formation of soluble aggregates was not detected. However, these differences were not seen by non-reducing denaturating SDS-PAGE (Appendix, Figure XII-12).

Table VIII-3: SE-HPLC results of Bevacizumab incubated with H12, D118 and RG 755 S rods and without any additives (PBS, negative control) after 0 weeks (reference) and 8 weeks at 35°C and 40 rpm. Results are given in %.

	Reference			Week 8		
	Aggregates	**Monomer**	**Fragments**	**Aggregates**	**Monomer**	**Fragments**
PBS				4.25 (±0.16)	94.06 (±0.10)	1.69 (±0.06)
H12				3.79 (±0.03)	94.16 (±0.23)	2.04 (±0.24)
	2.90 (±0.04)	96.73 (±0.09)	0.38 (±0.11)			
D118				4.34 (±0.08)	93.91 (±0.14)	1.75 (±0.06)
RG 755 S				3.93 (±0.13)	94.26 (±0.11)	1.81 (±0.17)

For Bevacizumab, the monomer content ranged between 93.9 % to 94.3 % after an 8-week incubation without any differences between lipids, PLGA and PBS, respectively (Table VIII-3). In contrast to mAb, the monomer loss can be traced back to the formation of soluble aggregates rather than the formation of fragments. Again, major differences between the aggregation/fragmentation profile as a function of the incubation protocol was not noticed as it was also confirmed by SDS-PAGE (Appendix, Figure XII-13).

Table VIII-4: SE-HPLC results of Ranibizumab incubated with H12, D118 and RG 755 S rods and without any additives (PBS, negative control) after 0 weeks (reference) and 8 weeks at 35°C and 40 rpm. Results are displayed in %.

	Reference			Week 8		
	Aggregates	**Monomer**	**Fragments**	**Aggregates**	**Monomer**	**Fragments**
PBS				0.00 (±0.00)	97.93 (±0.35)	1.96 (±0.25)
H12				0.00 (±0.00)	98.40 (±0.05)	1.60 (±0.05)
	0.00 (±0.00)	98.66 (±0.31)	1.34 (±0.31)			
D118				0.00 (±0.00)	99.06 (±0.21)	0.94 (±0.21)
RG 755 S				0.00 (±0.00)	97.20 (±0.80)	2.80 (±0.80)

The monomer content of Ranibizumab after an incubation for 8 weeks in the presence of lipid or PLGA rods ranged between 97.2 % to 99.1 % meaning no differences were observed. If any, slightly more fragmentation might be observed (2.80 %) upon incubation with PLGA compared to the lipid rods (in maximum 1.60 %).

Table VIII-5: SE-HPLC results of Aflibercept incubated with H12, D118 and RG 755 S rods and without any additives (PBS, negative control) after 0 weeks (reference) and 8 weeks at 35°C and 40 rpm. Results are given in %.

	Reference			Week 8		
	Aggregates	**Monomer**	**Fragments**	**Aggregates**	**Monomer**	**Fragments**
PBS				0.52 (±0.02)	99.48 (±0.02)	0.00 (±0.00)
H12	0.71 (±0.02)	99.29 (±0.02)	0.00 (±0.00)	2.56 (±0.00)	97.44 (±0.06)	0.00 (±0.00)
D118				0.52 (±0.03)	99.48 (±0.03)	0.00 (±0.00)
RG 755 S				0.54 (±0.07)	99.46 (±0.07)	0.00 (±0.00)

The same scenario as described for mAb was also observed for Aflibercept: the monomer content stayed constant at 99.5 % for all incubation protocols except for samples incubated with H12 rods (decrease to 97.4 %), which was due to aggregation rather than fragmentation (Table VIII-5). These results were not confirmed by non-reducing denaturating SDS-PAGE (Appendix, Figure XII-14).

In conclusion, for two proteins – mAb and Aflibercept - a H12 promoted monomer loss was noticeable. Interestingly, for mAb the monomer loss was caused by an elevated formation of fragments (Table VIII-2) whereas for Aflibercept the formation of soluble aggregates was the reason for enhanced monomer loss (Table VIII-5). However, fragmentation and aggregation, respectively, could not be confirmed by non-reducing denaturating SDS-PAGE (Appendix, Figure XII-12 and Figure XII-14). The reason for the monomer loss promoted by H12 rods remains to be investigated further. Another possibility could be impurities or contaminations of the H12 raw material with heavy metals which are known for their potency to induce protein

aggregation [371-373, 389-394]. To answer this question, ICP-AES analysis of all raw materials and extruded implants were analysed towards their heavy metal impurities (VIII.2.1.4).

Neuhofer [185] already performed an incubation study with the same triglycerides used here but using another protein. He investigated native interferon (nIFN) and PEGylated interferon β-1b. In terms of aggregation, he stated that «The formation of aggregates is slightly more pronounced in the presence of lipids in comparison with the pure buffer […]. In PBS buffer pH 7.4 +0.1 % SDS a slight trend towards the formation of soluble aggregates is visible with increased incubation time. Also the presence of placebo extrudates slightly promotes the formation of aggregates […]» [185]. This is in accordance with our results even though interferon is different by molecular weight and structure compared to the proteins used within our study.

VIII.2.1.2 CHEMICAL STABILITY OF PROTEINS

In addition to physical stability analysis, proteins were also analysed towards chemical changes by IEX, HIC, reducing capillary gel electrophoresis, and cIEF.

ION EXCHANGE CHROMATOGRAPHY (IEX)

An IEX method was developed for the separation of the charge variants of mAb and Bevacizumab as described previously (III.2.6.5). As indicated in Figure VIII-2 A, the fingerprint of mAb was divided into 5 subspecies, whereas the signal of Bevacizumab was classified into 4 different charge variants (Figure VIII-2 B).

Table VIII-6 displays the results obtained after an 8-week incubation in PBS (negative control) or in presence of H12, D118, or RG 755 S rods, respectively. MAb`s main peak area was slightly more reduced upon incubation with the lipid/PLGA rods with lowest percentage upon incubation with D118 rods (approximately 2.5 % less compared to samples incubated for 8 weeks in PBS). The same was true for Bevacizumab: main charge variant showed the most decrease upon incubation with D118 rods (approximately 3 %).

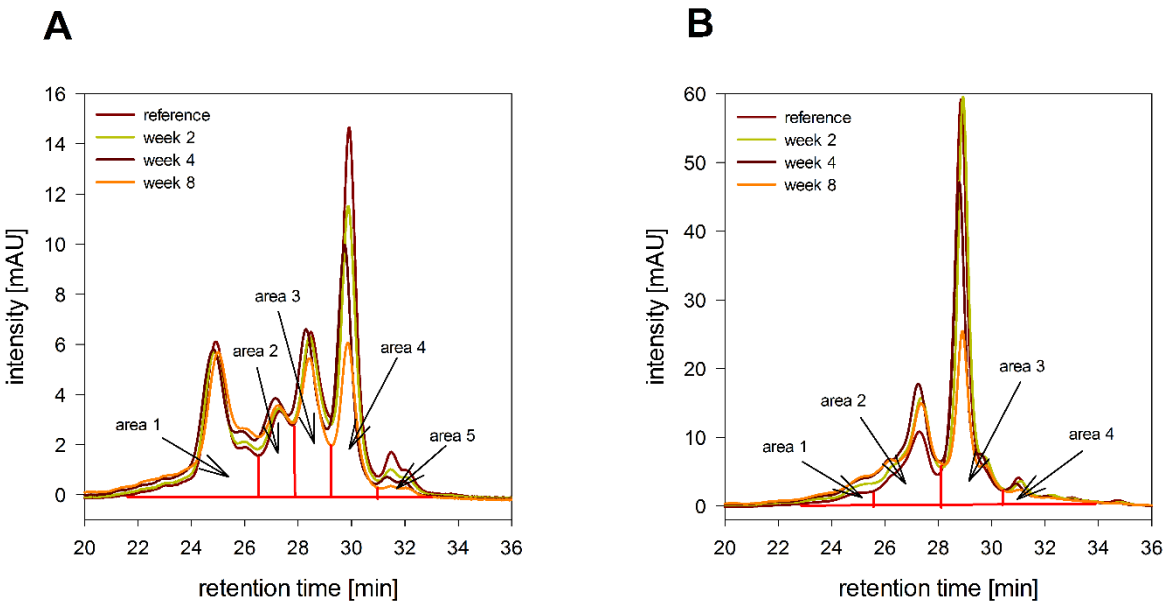

Figure VIII-2: Exemplary chromatographic profile of (A) mAb and (B) Bevacizumab using a WCX column for separation of charge variants upon incubation in PBS at 35°C over 8 weeks. As indicated, the fingerprint of mAb was divided into 5 subspecies whereas the signal of Bevacizumab was classified into 4 different charge variants.

The main charge variant of both proteins decreased distinctly upon incubation compared to the reference material: for mAb and Bevacizumab the percentage of main charge variant was halved after incubation. This result was expected, as an 8-week incubation at 35°C and 40 rpm represents relatively harsh environmental conditions leading to degradation [315, 395]. For both proteins, the retention time of the main peak was monitored additionally. A constant retention time underlines that the separation method was suitable to isolate differently charged subspecies which were formed during the incubation. Contrarily, a shift in retention time would point into the direction of differently charged subspecies which were not isolated by the separation method. In terms of mAb and Bevacizumab, the retention time of the main peak was found be to constant after 8 weeks of incubation irrespectively of the incubation protocol compared to the reference (Table VIII-6).

Table VIII-6: Area and retention time of the main charge variant of mAb and Bevacizumab after 8 weeks of incubation with H12, D118, or RG 755 S rods and in PBS (negative control) compared to the reference.

	mAb		Bevacizumab	
	Main charge variant [%]	**Retention time main peak [min]**	**Main charge variant [%]**	**Retention time main peak [min]**
Reference	37.44 (±0.69)	29.95 (±0.05)	62.77 (±0.29)	28.88 (±0.01)
PBS_week 8	20.36 (±0.05)	29.86 (±0.02)	39.40 (±0.70)	28.87 (±0.03)
H12_week 8	19.56 (±0.10)	29.80 (±0.00)	38.47 (±0.57)	28.92 (±0.01)
D118_week 8	17.86 (±0.20)	29.78 (±0.01)	36.45 (±0.12)	28.92 (±0.01)
RG 755 S_week 8	19.21 (±0.14)	29.80 (±0.00)	37.81 (±1.16)	28.88 (±0.01)

In general, both IgG_1 antibodies formed more acidic rather than basic subspecies as shown in the chromatographic fingerprint (Figure VIII-2). Those chemical alterations include deamidation (asparagine, glutamine, c-terminal amides), cleavage of disulfide bonds, oxidation of proline, oxidation of phenylalanine to o-tyrosine, oxidation of tryptophan (formation of oxindolyalanine, dioxindolyalanine, kynurenine, N-formylkynurenine), conversion of arginine to ornithine and/or citrulline or hydrolysis [337]. For both proteins, the formation of covalent bonds was not detected as measured by reducing capillary gel electrophoresis (Appendix, Figure XII-15 A and B). However, most degradation was seen at the D118 incubated samples.

HYDROPHOBIC INTERACTION CHROMATOGRAPHY (HIC)

Charge variants of Ranibizumab and Aflibercept were analysed applying HIC (III.2.6.6). The signal of Ranibizumab was sectioned into two areas (Figure VIII-3 A). Area 1, the area of the main charge variant, decreased marginally over the incubation time, whereas a minimal increase of area 2 was observable.

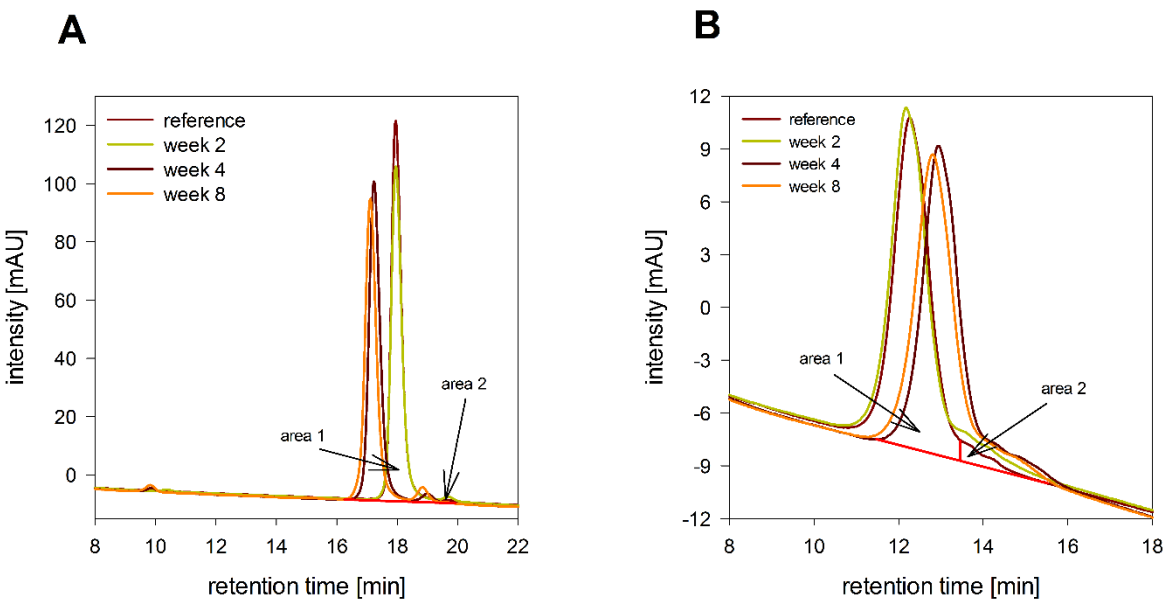

Figure VIII-3: Exemplary chromatographic profile of (A) Ranibizumab and (B) Aflibercept applying a MAbPac™ HIC-10 column for separation of charge variants upon incubation in PBS for 8 weeks at 35°C. As indicated, the fingerprint of Ranibizumab and Aflibercept was divided into 2 species.

The formation of hydrophilic isoforms eluting at approximately 9.5 min was noticeable. In addition, a shift of the main peak to shorter retention times pointed into the direction of more hydrophilic isoforms. The signal of Aflibercept featured by a shift to longer retention times, representing more hydrophobic variants arisen between week 2 and week 4 (Figure VIII-3 B).

Table VIII-7 displays the percentages of Ranibizumab`s main charge variant after the 8-week incubation. After 8 weeks, the main charge percentage decreased by 8 % in average compared to the reference. A difference upon incubation with lipids, PLGA or PBS was not detected as the percentage of the main charge differed less than 1 % from each other. However, the elution of the main peak shifted to shorter retention times from 18.48 min (reference) to 17.13 min and 17.89 min after incubation. The main peak eluted earliest upon incubation with D118 rods.

Table VIII-7: Area and retention time of the main charge variant of Ranibizumab and Aflibercept after 8 weeks of incubation with H12, D118, or RG 755 S rods and in PBS (negative control) compared to the reference.

	Ranibizumab		Aflibercept	
	Main charge variant [%]	**Retention time main peak [min]**	**Main charge variant [%]**	**Retention time main peak [min]**
Reference	99.26 (±0.11)	18.48 (±0.01)	96.89 (±0.44)	12.25 (±0.01)
PBS_week 8	92.18 (±0.10)	17.89 (±0.11)	93.78 (±0.43)	12.91 (±0.12)
H12_week 8	91.87 (±0.36)	17.74 (±0.02)	96.06 (±0.45)	12.73 (±0.01)
D118_week 8	91.41 (±0.47)	17.13 (±0.08)	96.16 (±0.80)	12.82 (±0.03)
RG 755 S_week 8	91.25 (±0.26)	17.58 (±0.13)	96.44 (±0.27)	12.71 (±0.03)

Conversely, the main charge percentage of Aflibercept had the lowest percentage when incubated in PBS without any additives - approximately 3 % less compared to the samples incubated with the lipid/PLGA rods (93 % versus 96 %). However, the retention time of the main peak shifted to longer retention times from 12.25 min (reference) to 12.8 min in average (Table VIII-7). This demonstrates the formation of more hydrophobic subspecies interacting more with the hydrophobic column material.

Interestingly, Ranibizumab and Aflibercept behaved completely different. The Ranibizumab chromatographic peak migrated to shorter retention times, especially for samples incubated with D118 (Figure VIII-3, Table VIII-7). This could be due to possible chemical reactions triggered by D118, for instance oxidation (tryptophan, methionine, proline, histidine, phenylalanine), isomerisation (e.g. aspartic acid isomerisation), N- and O-glycosylation, serine fucosylation, deamidation (e.g. asparagine, glutamine, C-terminal amides), hydrolysis or β-elimination [337]. Contrarily, the main peak of Aflibercept shifted to longer retention times, which is an indicator for the formation of more hydrophobic subspecies which can be possibly promoted by chemical alterations or partial unfolding. When the protein unfolds, hydrophobic patches arise at the surface of the protein, thereby changing its overall surface charge and making it more

hydrophobic [346, 350, 380, 396-403]. However, unfolding was not detected by FT-IR (see also VIII.2.1.3). Alternatively, chemical reactions like oxidation (formation of disulfide bonds) or isomerisation (e.g. asparagine to succinimide) [337] are conceivable. For Aflibercept, results from reducing denaturating capillary gel electrophoresis suggests the formation of disulfide bonds in presence of the PLGA rod: a higher percentage of LMW species and less heavy chain percentage was found (Appendix, Figure XII-15 D).

Finally, the question raises if the slight differences which were observed were caused by the different triglycerides/PLGA the proteins were exposed to. Interestingly, the main peak area for mAb, Bevacizumab and Ranibizumab decreased most in presence of D118.

CAPILLARY ISOELECTRIC FOCUSSING (CIEF)

The investigations towards chemical modifications using IEX and HIC revealed slightly more chemically modified subspecies when proteins were incubated with D118 rods. To verify the obtained data, cIEF was applied for Ranibizumab and Bevacizumab as an orthogonal method, as it is a more precise and more sensitive method than IEX and HIC and has been widely used in protein characterisation [404-408].

The Ranibizumab signal was classified into an acidic isoform, the main isoform (main peak) and a single basic isoform, whereas for Bevacizumab, two different acidic isoforms were identified. As Figure VIII-4 A illustrates, the 8-week incubation promoted the formation of mainly more acidic subspecies by a simultaneous depletion of the main peak. Addition of lipid/PLGA rods to the Ranibizumab containing solution resulted in more acidic isoforms upon incubation with D118 rods (approximately 5 %); all other results were comparable to each other. Consequently, it can be concluded that D118 promoted the formation of acidic isoforms. The percentage of basic isoforms was not affected. These data confirm the results obtained by HIC, where the shortest retention time of the main peak (more hydrophilic subspecies) was observed for samples incubated with D118 rods. It can be speculated that these changes were caused by deamidation or oxidation [337]. For Bevacizumab, Figure VIII-4 B illustrates that the area of the basic isoform

was more pronounced (approximately 4 %) in the presence of H12 rods. This finding contrasts with the obtained IEX results, where D118 was identified to promote most chemical alterations. Besides H12 and D118 rods, Ranibizumab and Bevacizumab were incubated with RG 755 S rods as well. For both proteins, levels of acidic and basic isoforms were in the same course as measured for both lipids and the negative control.

Overall, for both proteins differences in areas between the different incubation protocols are negligible. A decrease in main charge variant on account of more acidic isoforms compared to the reference was detected but differences between samples incubated with lipids/PLGA or PBS were not observed.

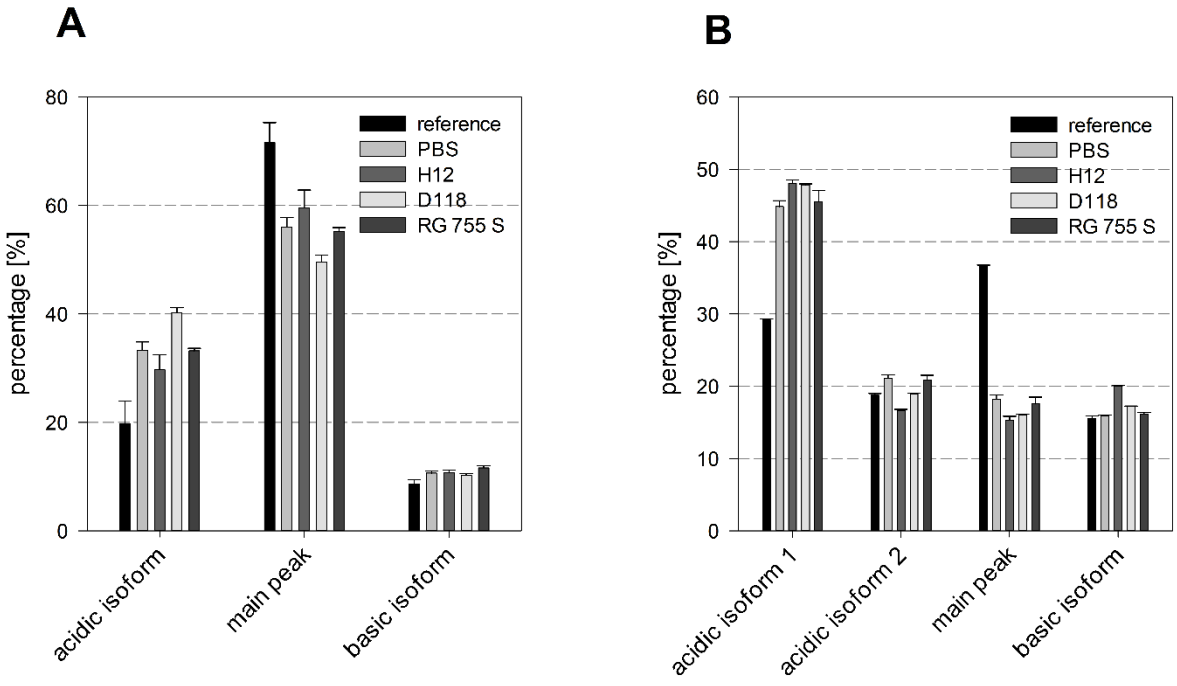

Figure VIII-4: Results of cIEF measurements of (A) Ranibizumab and (B) Bevacizumab. Protein containing solutions were incubated over 8 weeks in presence of H12, D118, or RG 755 S rods, respectively, or without any additives (PBS, negative control).

Neuhofer already addressed the chemical stability of proteins upon incubation with lipids. The level of oxidized IFN β-1b in presence of lipids was investigated applying RP-HPLC. Within his work, he demonstrated that up to 20 % more oxidized species were formed upon the incubation

with lipid rods consisting of H12 and D118 in comparison to PBS. To clarify the origin of the elevated oxidation levels, he incubated nIFN β-1b with H12, D118 and paraffin wax rods over 7 days. The highest oxidation levels were found upon incubation with D118 rods. This is in accordance with the results reported by us even though the proteins used were completely different by structure.

The lipid-induced oxidation of proteins has already been described in literature. During peroxidation of lipids, unsaturated lipid species can form peroxides or radicals which can react with proteins. For instance, lipoxidation [409] is an important factor in atherosclerosis [410, 411]. It is well known that lipoxidation is often catalysed by metal impurities, as described by Wills [412] where oxidized unsaturated fatty acids inhibited specific enzymes. The lipids used within the present work were all saturated C12 to C18 triglycerides and therefore not prone to oxidation or lipoxidation. It was proven that even at high temperatures, an oxidation of saturated fatty acids (and their corresponding esters) did not correlate with the chain length of the triglycerides [185]. This means that the chemical changes, which were observed upon incubation with D118 rods (consisting of tristearin), were not due to a preferred autoxidation of stearic acid. However, most chemical changes were observed in the presence of D118. In summary, it could be speculated that the presence of impurities was the reason for the increase in protein oxidation. As this is only speculative, it would be worth to invest more efforts to answer this question. As a follow-up study to the presented results, the presence of heavy metal was analysed as described in VIII.2.1.4.

VIII.2.1.3 CONFORMATIONAL STABILITY OF PROTEINS

Secondary structure analysis applying FT-IR was performed. Spectra were recorded of the bulk material (defined as reference) and of the samples after 8-week incubation in PBS (negative control) or in the presence of H12, D118, or RG 755 S rods, respectively.

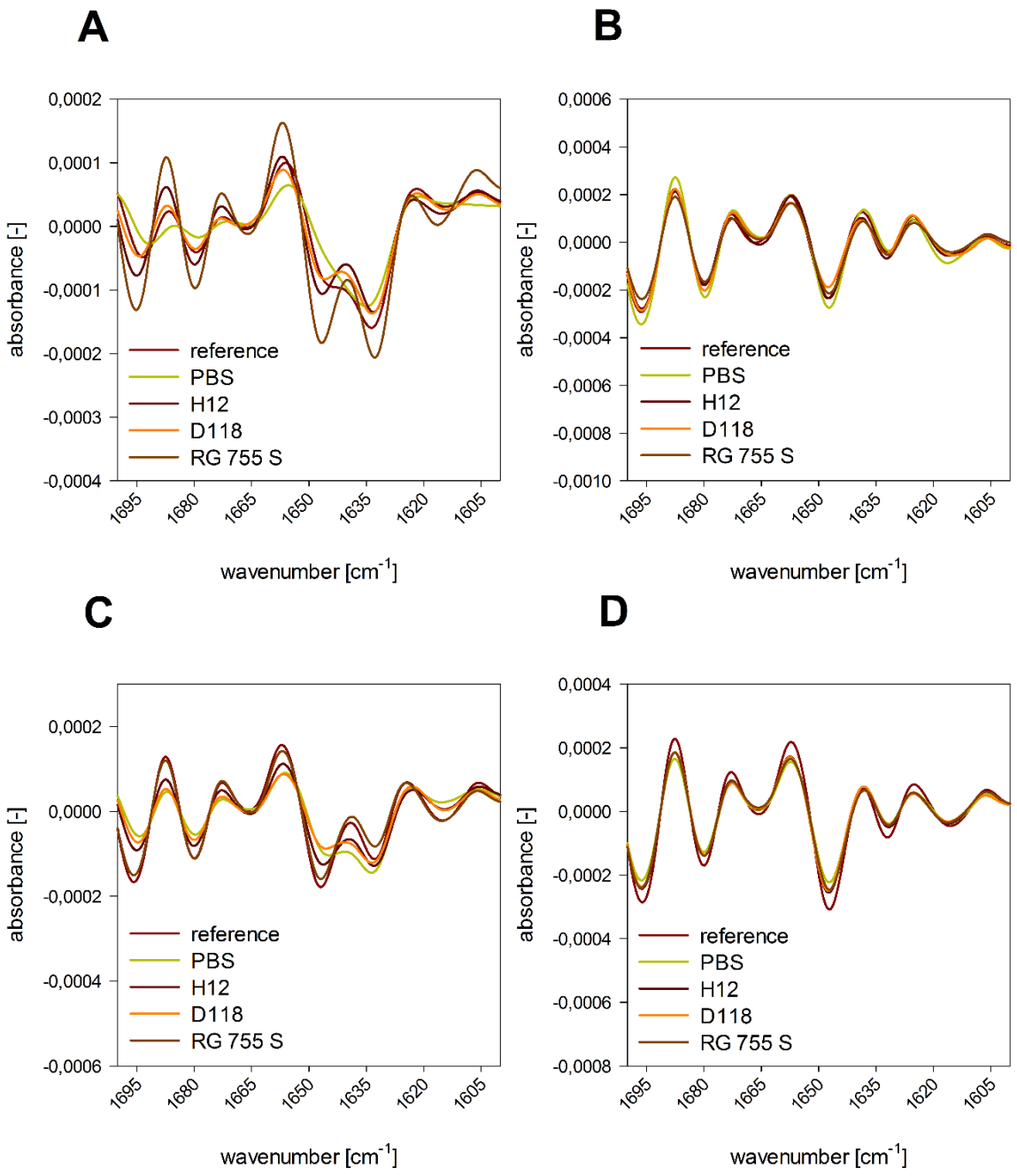

Figure VIII-5: FT-IR spectra of (A) mAb, (B) Ranibizumab, (C) Bevacizumab and (D) Aflibercept recorded after 8 weeks of incubation in PBS (negative control) or with H12, D118 or RG 755 S rods compared to reference.

FT-IR spectra of Ranibizumab and Aflibercept did not show any deviations, neither in band intensity nor in band wavenumber, therefore suggesting that the proteins were conformationally stable over the incubation period and that the presence of lipids or PLGA did not promoted unfolding (Figure VIII-5 B, Figure VIII-5 D).

Figure VIII-5 A shows the FT-IR spectra of mAb recorded between 1600 cm^{-1} and 1700 cm^{-1}. The amide I band, representing the β-sheet structure [340, 343], can be identified between 1635 cm^{-1} and 1645 cm^{-1}. The single peak present at the reference (1635 cm^{-1}) turned into a split peak with a left side shoulder at approximately 1645 cm^{-1} which was most pronounced for the samples which had been in contact with RG 755 S. Additionally, the band intensity at 1680 cm^{-1} and 1615 cm^{-1} indicated protein unfolding events [339]. Shifts towards higher wavenumbers represent unordered random coil like structures [338]. On the expense of regular structures, the formation of intermolecular hydrogen-bonded antiparallel β-sheet structures indicated partial unfolding of the mAb [342]. Changes in the secondary structure of mAb were also apparent when incubated with H12 and D118, but most pronounced for RG 755 S. In particular, an additional band at 1645 cm^{-1} was observed.

Conformational changes were also observed for Bevacizumab. In Figure VIII-5 C, the FT-IR spectra of Bevacizumab reference and samples measured after 8 weeks incubated with H12, D118 or RG 755 S rods are given. Bevacizumab`s secondary structure changed slightly but a difference between the differently incubated samples was not observed.

As an orthogonal method, extrinsic fluorescence was utilised using a Bis-ANS assay. In theory, Bis-ANS interacts with hydrophobic patches present at the protein surface, which leads to an increased fluorescence signal [380, 413-417]. If an enhanced signal is observed, it can be concluded that hydrophobic patches were formed upon partial unfolding. However, extrinsic fluorescence measurements did not confirm FT-IR results, as an enhanced signal was only measured for the positive control (proteins were exposed to 80°C and 400 rpm for 10 min) (Appendix, Figure XII-16).

VIII.2.1.4 ADSORPTION OF PROTEINS ONTO LIPID/PLGA SURFACES

To study absorptive effects of proteins on lipid/PLGA surfaces, protein recovery was measured via SE-HPLC assessing the AUC of the protein signal including the signal of soluble aggregates,

monomer and fragments. For the detailed course of protein recovery upon incubation with lipid/PLGA rods, please see Appendix Figure XII-17.

The recovery of mAb did not change during incubation irrespective of the material the protein was exposed to (Table VIII-8). Recovery was measured with 101 % in general, therefore, no absorption of the mAb to the lipid/PLGA rods was observed.

The protein recovery of Ranibizumab was characterised by a loss of recovery during incubation, especially if incubated with D118 rods (84.6 %). But also, protein recovery at the negative control decreased to 92 % within 8 weeks.

Table VIII-8: Protein recovery of mAb, Ranibizumab, Bevacizumab, and Aflibercept after an 8-week incubation in PBS (negative control) or with H12, D118 or RG 755 S rods, respectively, measured by SE-HPLC.

	PBS	H12 rods	D118 rods	RG 755 S rods
mAb	101.84 (±3.88)	101.75 (±1.80)	101.52 (±1.73)	102.83 (±0.13)
Ranibizumab	91.99 (±0.44)	98.99 (±1.49)	84.56 (±1.57)	96.27 (±1.27)
Bevacizumab	101.56 (±0.64)	94.08 (±0.82)	99.13 (±1.79)	100.59 (±1.53)
Aflibercept	96.36 (±2.53)	80.65 (±2.18)	95.40 (±1.37)	95.16 (±0.42)

Protein recovery for Bevacizumab and Aflibercept remained rather constant over 8 weeks regarding D118 and RG 755 S rods. More importantly, the recovery for both proteins was found to be 94 % (Bevacizumab) and 81 % (Aflibercept) when exposed to H12 rods.

Neuhofer also addressed protein recovery within his studies, showing a correlation between hydrophobicity of the protein (interferon β-1b in its native state and PEGylated interferon) and protein recovery. A loss of protein recovery of nIFN β-1b of 50 % already after 7 days of incubation with lipid rods was demonstrated [185]. He also measured protein recovery of nIFN β-1b after incubation with H12/D118 rods, and rods consisting of pure H12 and D118. After 7 days of incubation with H12/D118, recovery was only 50 % compared to the rods consisting of pure H12 (20 % loss) and D118 (25 % loss).

Lipid-protein-interactions were also studied by Even focussing on interactions of peptides (having different charges and hydrophobicity) and the lipids D114 (trimyristin), soybean lecithin and cholesterol [186]. Even concluded that neither the size nor the hydrophobicity of the peptides allows to predict the release behaviour or the interactions with the lipids, assuming that the three-dimensional protein structure should also be taken into account.

Especially for Bevacizumab and Aflibercept, distinct adsorptive phenomena were observed. As the same phenomenon can be observed for different protein formats described by Neuhofer and us, it can be speculated that adsorption of proteins to triglyceride surfaces might be a function of protein hydrophobicity. When considering adsorptive phenomena, the isoelectric point of the proteins is of special interest as it provides information on the surface charge of a protein at a given pH [418-421]. The theoretical isoelectric points of the studied proteins were given with 8.3 (mAb), 8.8 (Ranibizumab), 8.8 (Bevacizumab) and 8.2 (Aflibercept) according to Hirvonen *et al.* [422]. The authors calculated the theoretical values using ExPASy. For mAb, the isoelectric point was determined experimentally via isoelectric focusing. Since the isoelectric points of the proteins were very similar, it can be considered that they were all positively charged at the incubation pH of 7.4. Therefore, differences in the overall net charge of the surface were most likely not responsible for the different behaviour. Rather than the net charge of the overall surface, isolated hydrophobic areas on the protein surface (hydrophobic patches) might be a driving factor for protein adsorption. These «hydrophobic patches» have a higher density of hydrophobic amino acids (alanine, leucine, isoleucine, phenylalanine, tryptophane) than other regions of the protein and are not affected by the surrounding pH in their hydrophobicity. To verify this hypothesis, further experiments would be needed facing the three-dimensional structure of the proteins.

It should be stated that beyond diffusion and erosion, also the adsorption and desorption of the proteins to the highly hydrophobic lipid matrix should be considered also possibly explaining the different sustained release patterns observed (chapter IV). For instance, Ranibizumab is more hydrophobic than Aflibercept because it interacts more with the hydrophobic stationary phase

during HIC (Figure VIII-3, Table VIII-7). This might be a reason for a more sustained release of Ranibizumab compared to Aflibercept (Figure IV-11), even though Ranibizumab is smaller in size.

VIII.2.2 METAL IMPURITIES AND THEIR IMPACT ON PROTEIN STABILITY

During the preparation process of implants, many sources could theoretically act as an origin for possible contaminations of the material with traces of heavy metals. For instance, extruder parts, being in contact with the material during extrusion, are possible sources for metal abrasions. It is well-known that heavy metals can promote protein degradation [389, 390, 393]. In the present study, the level of diverse metals (Al, Co, Cr, Cu, Fe, Mn, Ni, Pb, Zn) was measured within the raw material (lipids, HP-β-CD), protein lyophilisates and extruded implants manufactured with both extruders (Table VIII-9). The samples were analysed according to III.2.6.12 using ICP-AES. Levels of titanium (serves as a catalyst during the bleaching step of triglyceride production) were not evaluated, as it is regularly monitored by Cremer Oleo. The certificates provided by Cremer Oleo showed that the titanium content was less than 1 ppm measured by a suitable method included in the European Pharmacopoeia (Ph. Eur. 2.2.23).

The results of the ICP-AES analysis are displayed in Table VIII-9 as milligram heavy metal per gram of sample. Levels for all elements were below the limit of detection (LOD) and are therefore not displayed in Table VIII-9, except for aluminium, were traces were identified. Within Ranibizumab, Bevacizumab and Aflibercept protein lyophilisates, aluminium was detected. Aluminium was also found in Witepsol H12. Consequently, aluminium was also found in all extruded implants, with the highest amount of 3 µg aluminium per implant.

To clarify if aluminium was a driving force for protein degradation within the lipid implants, protein solutions were incubated with highest aluminium content found (0.111 µg aluminium per mg protein).

Table VIII-9: Overview of samples analysed towards metal content with ICP-AES. Only results for aluminium content are displayed as for all other metals the level was below the LOD. Results are given in mg/g.

Sample code	Sample description	Concentration aluminium [mg/g]
#1	Lyophilisate mAb	< LOD
#2	Lyophilisate Ranibizumab	0.0348
#3	Lyophilisate Bevacizumab	0.0233
#4	Lyophilisate Aflibercept	0.2350
#5	HP-β-CD	< LOD
#6	H12	< LOD
#7	H12A	< LOD
#8	Witepsol H12	0.0051
#9	Dynasan® D118	< LOD
#10	SLI produced on a MiniLab® extruder (mAb)	0.0088
#11	SLI produced on a MiniLab® extruder (Ranibizumab)	0.0685
#12	SLI produced on a MiniLab® extruder (Bevacizumab)	0.0870
#13	SLI produced on a MiniLab® extruder (Aflibercept)	0.1045
#14	SLI produced on a ZE-5 mini-extruder (mAb)	0.1080
#15	SLI produced on a ZE-5 mini-extruder (Ranibizumab)	0.0585
#16	SLI produced on a ZE-5 mini-extruder (Bevacizumab)	0.0560
#17	SLI produced on a ZE-5 mini-extruder (Aflibercept)	0.0435

According to Table VIII-9, the highest aluminium content was found to be 0.1080 mg/g. Based on the average weight of an SLI (dimensions of 1.5 mm x 15 mm considered), which is 30.7 mg, in theory 3.2 µg aluminium per SLI were found. This amount aluminium is equal to 0.1 µg aluminium per mg protein (protein formulated 1:1 [w/w] with HP-β-CD). To evaluate, if an

aluminium content of 3.2 µg per SLI can cause protein degradation and therefore provide an explanation for protein instability observed during release (chapter VI), an incubation study with different aluminium concentrations was performed. Even though the study was performed in the liquid state, which cannot be transferred 1:1 to the dry state (protein lyophilisate incorporated into SLIs and not being released), it shall provide a first impression what could have happened within the SLIs. Protein solutions at a concentration of 1.0 mg/ml (diluted from stock solutions comprising 10 mg/ml in 50 mM sodium phosphate buffer pH 6.2 with PBS pH 7.4) were spiked with aluminium (as $AlCl_3*6H_20$) to obtain a final concentration of 0.1 µg/ml (maximum level found by ICP-AES) and 1.0 µg/ml (positive control). As negative control, non-spiked protein solutions were incubated. Samples were incubated for 4 weeks at 37°C in a horizontal shaker (40 rpm) and samples were analysed applying LO, SE-HPLC, IEX and HIC.

At a concentration of 0.1 µg/ml Al^{3+}, particle count was not elevated for all proteins compared to negative control (PBS). At the ten times higher concentration of Al^{3+} (positive control), particle count was higher for all proteins pointing towards metal induced formation of subvisible particles.

Table VIII-10: Cumulative particle count (> 1 µm) of protein solutions spiked with different concentrations of Al^{3+} incubated over 4 weeks at 37°C and 40 rpm.

	mAb	Ranibizumab	Bevacizumab	Aflibercept
PBS	380 (±203)	141 (±104)	806 (±175)	397 (±138)
0.1 µg/ml	241 (±42)	153 (±34)	607 (±110)	276 (±12)
1.0 µg/ml	489 (±110)	2134 (±189)	1899 (±240)	1166 (±168)

The monomer content of all tested proteins did not differ after 4 weeks upon incubation with Al^{3+}. Even in the positive control, no impact of aluminium to monomer content was observed.

Protein recovery of mAb and Ranibizumab were unaffected, whereas protein recovery of Bevacizumab and Aflibercept decreased to 77 % and 57 %, respectively, already at concentrations of 0.1 µg/ml Al^{3+}.

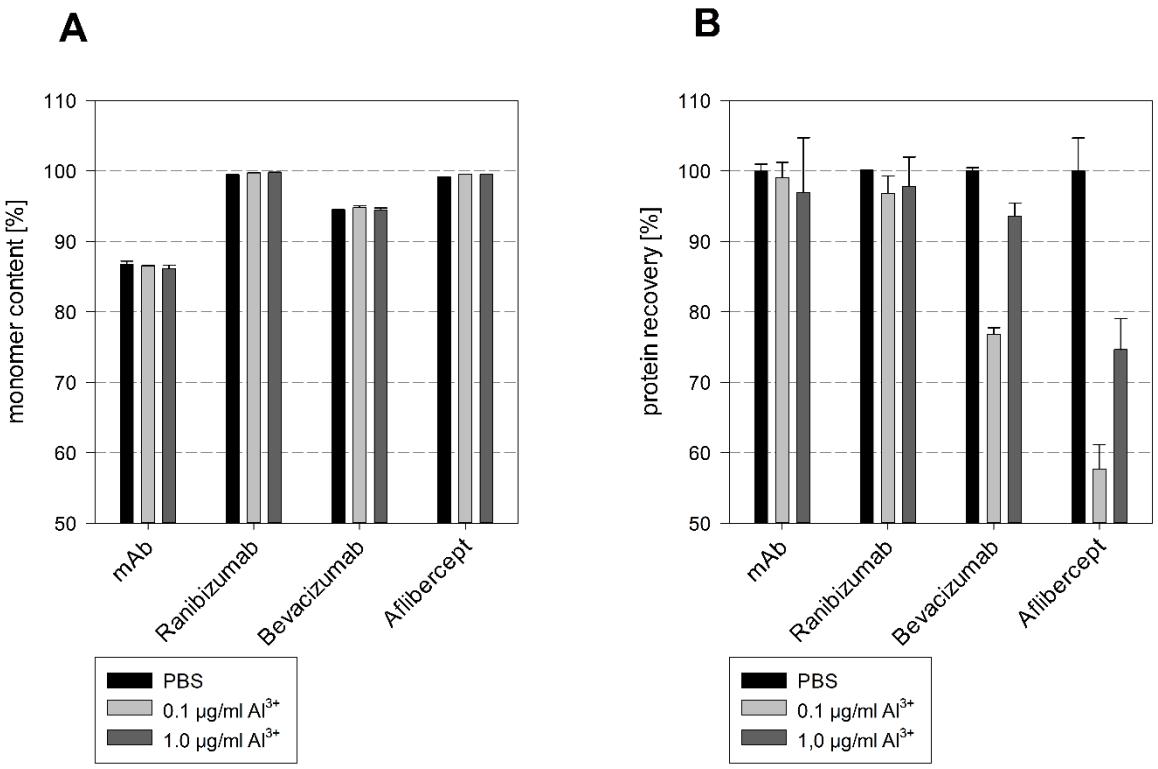

Figure VIII-6: (A) Monomer content and (B) protein recovery of proteins spiked with different concentrations of Al^{3+} incubated over 4 weeks at 37°C and 40 rpm.

Supplemental to particle count and SE-HPLC, IEX and HIC were applied to detect possible metal induced chemical alterations compared to the negative control (Table VIII-11). For all proteins, the percentage of main peak area was not negatively affected by the addition of Al^{3+}, not even for the positive control with the ten times higher aluminium concentration.

In summary, aluminium-induced protein degradation was not observed; neither elevated particle count, nor higher rates in monomer loss were detected. Likewise, more pronounced chemical degradation was not detected.

Table VIII-11: Main peak area in % of proteins spiked with different concentrations of Al^{3+} incubated over 4 weeks at 37°C and 40 rpm. As control, samples were incubated in PBS. For mAb and Bevacizumab, main peak percentage was assessed by IEX whereby main peak area for Ranibizumab and Aflibercept was assessed using HIC.

	mAb	Ranibizumab	Bevacizumab	Aflibercept
Reference	35.61 (±0.18)	99.26 (±0.11)	62.77 (±0.29)	96.89 (±0.44)
PBS	30.13 (±0.36)	94.46 (±0.08)	53.70 (±0.68)	98.63 (±0.12)
0.1 µg/ml	30.89 (±0.44)	95.47 (0.17)	54.79 (±1.61)	96.08 (±1.40)
1.0 µg/ml	33.35 (±0.35)	96.48 (±0.13)	53.28 (±0.35)	95.68 (±0.69)

On the contrary, protein recovery of Bevacizumab and Aflibercept decreased to 77 % (Bevacizumab) and 57 % (Aflibercept), respectively, compared to the negative control. As no elevated particle count was observed at this aluminium level, metal induced formation of large sized and insoluble aggregates forming precipitates was most likely. Those precipitates precipitated out of the solutions and were therefore not measured by LO. Metal induced aggregation (also forming large sized particles) has already been described in literature [373, 394], which supports our explanation. Our explanation was further confirmed by the observation of milky sediments.

VIII.3 CONCLUSION

Triglyceride-protein-interactions were studied within an incubation study, where extruded rods consisting of 100% H12, D118, or Resomer® RG 755 S were incubated with protein solutions over 8 weeks at 35°C and 40 rpm. Proteins were characterised towards colloidal, chemical and conformational stability as well as adsorptive effects upon incubation with either triglycerides or PLGA rods.

If incubated with H12 rods, elevated particle count and turbidity were observed for all proteins, especially for Aflibercept. H12 rods partially disintegrated upon incubation with proteins (total disintegration upon incubation with Aflibercept). It can be therefore speculated that the disintegration of the H12 rod could be due to the amphiphilic character of the proteins. For mAb and Aflibercept, monomer content decreased upon contact with H12, contrarily, monomer content of Ranibizumab and Bevacizumab stayed constant. For Bevacizumab and Aflibercept, protein recovery decreased over time, resulting in a recovery of 94 % (Bevacizumab) and 81 % (Aflibercept) after 8 weeks. This points into the direction of protein adsorption onto H12. Interestingly, for these two proteins highest particle count (suggesting the formation of subvisible particles) was observed. Regarding chemical and conformational stability, no differences were observed. Finally, it can be concluded that proteins partly interacted with H12 resulting in the formation of subvisible particles, the loss of monomer and adsorptive effects.

For D118 rods, another picture can be drawn. In terms of physical and conformational stability, no distinct differences between the proteins were noted. However, mAb and Ranibizumab comprised more chemical isoforms on the account of a loss of main charge variant in the presence of D118 (not seen upon contact with H12). It is noteworthy, that exclusively Ranibizumab recovery decreased (84.6 % after 8 weeks) compared to the other proteins. Since no elevated particle count or turbidity was observed, it can be assumed that the loss in protein recovery was due to adsorption onto D118 rather than formation of particles. Overall, interaction between D118 and proteins was less compared to H12.

Proteins were incubated with rods consisting of Resomer® RG 755 S. Overall, proteins revealed no reduced physical, chemical and conformational stability. Additionally, protein recovery was not affected. These results are in a strong contrast to the results described within chapter VII.2.2. There, substantial physical and chemical instabilities were observed when proteins were encapsulated within a PLGA matrix. Here, proteins were incubated with placebo PLGA rods for sure not fully mimicking the environment within a PLGA matrix.

Studies towards heavy metal impurities revealed detectable levels only of aluminium within the protein lyophilisates and H12 and consequently also in extruded SLIs. However, particle formation, monomer content and main charge variant were not negatively affected by the presence of Al^{3+} at a concentration of 3.2 µg per implant (highest Al^{3+} concentration found). However, protein recovery of Bevacizumab and Aflibercept decreased in the presence of Al^{3+}.

Finally, it can be concluded that proteins interacted most with H12 but also partly with D118. Thereby, the observed instabilities were not caused by heavy metal impurities of the raw materials. Other impurities possibly being present at the lipid raw material (peroxides or aldehydes) could be a further reason for protein degradation.

IX. PRESSURE MEASURMENT AS A NEW ANALYTICAL TOOL FOR TWIN-SCREW EXTRUSION OF SOLID LIPID IMPLANTS

IX.1 INTRODUCTION

This chapter is aimed to systematically investigate the extrusion process on a ZE-5 mini-extruder. The formulation comprising 10 % protein lyophilisate and a lipid matrix consisting of 50 % H12 and 50 % D118 (from now on referred to as 50:50 lipid composition) was used as starting point. The mAb as model protein for *in-vitro* release was used. The ZE-5 mini-extruder was equipped with a resistance strain gauge located at the outlet plate of the extruder barrel as an online pressure monitoring tool. This allows to measure extrusion forces in real time. The impact of process parameters such as extrusion speed, temperature, and lipid composition on implant properties was studied. Bending strength, true density and microscopic appearance of extruded implants was assessed. Extrusion temperature (33°C to 42°C), screw speed (40 rpm to 80 rpm) and the lipid composition (30 % to 70 % of each triglyceride) were modified. Furthermore, SLIs were double-extruded to evaluate this technique as a potential tool to further modify implant properties.

IX.2 DISTINCTION BETWEEN HOT MELT EXTRUSION (HME) AND SOLID LIPID EXTRUSION (SLE)

It is important to differentiate between HME and SLE. Generally, synthetic polymers such as EVA, PEO, PLA, or PLGA are used for HME, and processing takes place at temperatures far above 100°C [423]. This is normally performed at 15°C to 60°C above the T_m or T_g [424] of the used material. At these process temperatures, the material is completely molten and in a liquid-like state. For SLE, mainly fatty acids (myristic acid, stearic acid), polyoxylglycerides (Gelucire, Compritol) or acylated glycerides (Dynasan, Imwitor, Precirol ATO) [425] have been used. Irrespective of the lipid, the extrusion temperature is below the T_m of the components, which leads to a semi-solid state of the material.

Regarding HME, the process has been thoroughly characterised and the impact of process parameters – mixing [426], shape of screws [427], impact of degassing [428], screw speed, effect of plasticisers, process temperature - on product properties has been described within numerous publications [424, 429].

For SLE, research focused on release profiles and underlying release mechanisms [155, 157, 158, 182, 299, 430], the solid-state behaviour [161, 163], effect of release modifiers [149, 160, 177, 178] or *in-vivo-in-vitro* correlations [168] for various drugs [163, 182, 236, 299] including pharmaceutical relevant proteins such as rh-interferon-α [178] and interleukin-18 [174]. However, the extrusion process in pharmaceutical applications itself has not been investigated in depths until now.

IX.3 RESULTS AND DISCUSSION

IX.3.1 ANALYSIS OF PRESSURE-TIME CURVES DURING EXTRUSION

Pressure curves were recorded for each batch produced on the extruder. A representative pressure profile is displayed in Figure IX-1, illustrating the course of pressure during an extrusion run of a 50:50 composition at 35°C and 60 rpm. The pressure profile can be separated in four different phases, namely the feeding phase (I), compacting phase (II), implant formation phase (III) and termination of implant formation (IV). During section I, the material is fed via a feeding tube and pestle to the inlet of the barrel (Figure III-6 C). During this step, no pressure at the outlet plate is measured because the material did not yet reach the outlet plate. During this time, the components are merged, melted, admixed, and pre-compressed as a function of screw speed, extrusion temperature and extrudates' formulation.

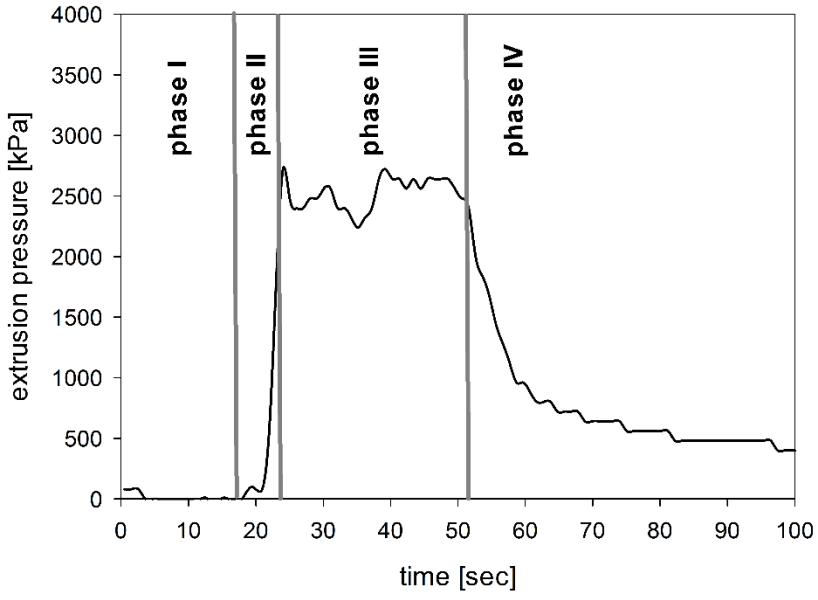

Figure IX-1: Representative extrusion pressure profile of a 50:50 lipid composition extruded at 35°C and 60 rpm. The extrusion run can be divided into four different phases, namely (I) feeding, (II) compacting, (III) implant formation and (IV) termination of implant formation.

In phase II, the material has reached the end of the extruder barrel. The material has been transported to the space between the end of the screws and the outlet plate. Due to this, first little pressure peaks can be observed (Figure IX-1, phase II). While the pressure is increasing, lipid strand formation already started.

During the plateau phase, lipid strand formation takes place (Figure IX-1, phase III). An initial pressure peak can be observed followed by a phase where the extrusion pressure reaches a steady-state plateau. When no further material is fed to the inlet of the barrel, the steady-state is no longer maintained, which is indicated by a continuous decrease in pressure until it reaches a plateau again. Once the pressure started to decrease, implant formation started to slow down and stopped subsequently. The low plateau represents the end of the extrusion run (Figure IX-1, phase IV). For calculation of the average extrusion pressure, the mean values measured during the steady-state plateau were taken. The comparatively low remaining pressure after the run has been completed (approximately 500 kPa for the run depicted in Figure IX-1) is generated by the remaining material left behind within the barrel.

IX.3.2 INVESTIGATION OF INNER-STRAND HOMOGENEITY

The inner-strand homogeneity was assessed by extruding a 50:50 lipid composition at 35°C and 40 rpm, which represents the standard extrusion settings within this study (Figure IX-2). The resulting lipid strand had a total length of approximately 130 cm to 140 cm. For this run, implant formation (phase III) started after approximately 40 sec and lasted for 40 sec which equates an extrusion speed of 3.4 cm/sec. The last 15 cm to 20 cm were discarded and not further analysed since the implant strand formed during this phase (phase IV) was inhomogeneous and lipid strand formation was non-continuous. Thus, the first 120 cm were divided into four sections, each 30 cm in length. From each section four replicates (15 mm in length) were taken randomly.

Each phase was analysed towards true density, mechanical properties, and *in-vitro* release of the mAb. The average extrusion pressure was calculated by taking all pressure values into consideration measured during the steady-state plateau. For this particular run, the average pressure was calculated between 50 sec and 80 sec (Figure IX-2) resulting in an average pressure of 975 kPa ±74 kPa. Even if the pressure reaches a constant level during the implant formation section, it is not self-evident that the characteristics of the implants formed during this period comprise the same properties, e.g. true density or release patterns. Importantly, it should be noted that the first section (0 cm to 30 cm) was produced while the extrusion pressure plateau was not yet reached (45 to 50 sec, Figure IX-2) whereas all other sections (30 cm to 120 cm) were extruded during the steady-state phase (between 50 sec and 80 sec of the run).

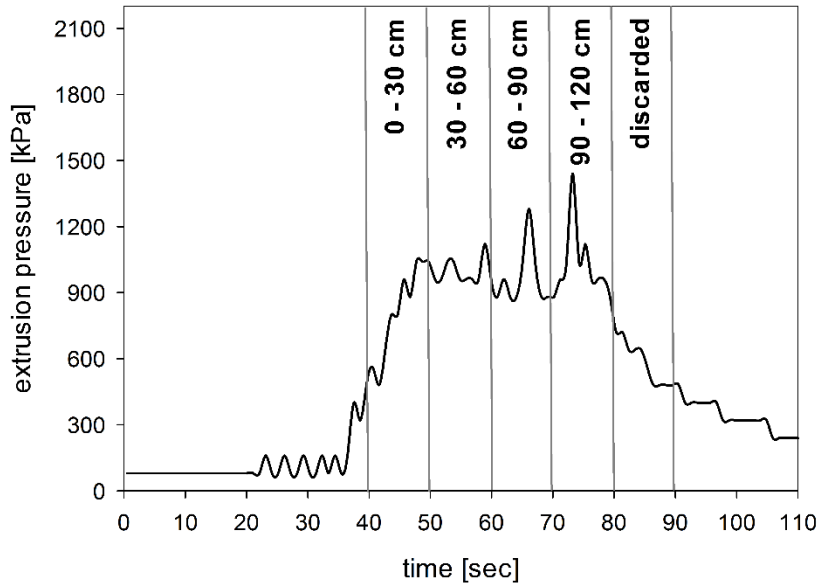

Figure IX-2: Representative extrusion pressure profile of a 50:50 lipid composition extruded at 35°C and 60 rpm.

As shown in Table IX-1, both true density and bending strength measurements had lower values for the first section (0 cm to 30 cm) compared to the following three sections. The sections taken between 30 cm to 120 cm were comparable in terms of true density and bending strength. Additionally, cumulative release of the mAb was monitored over 4 weeks. Release from SLIs

taken from section 30 cm to 120 cm was comparable ranging from 45.62 % to 46.21 % after 4 weeks. Release from the first section (0 cm to 30 cm) was faster (64.66 % after 4 weeks). Consequently, within the following experiments, the first 30 cm were discarded and not used for further analysis.

Table IX-1: Summary on true density, bending strength, and release of mAb for the different sections of the lipid strand.

Section	True density [g/cm^3]	Bending strength [N]	Cumulative release of mAb after 4 weeks [%]
0 cm to 30 cm	0.974 (±0.004)	0.757 (±0.169)	64.66 (±2.89)
30 cm to 60 cm	1.032 (±0.002)	1.967 (±0.220)	45.86 (±1.83)
60 cm to 90 cm	1.031 (±0.002)	2.090 (±0.381)	45.62 (±3.23)
90 cm to 120 cm	1.030 (±0.001)	2.064 (±0.387)	46.21 (±2.25)

The low standard deviation, especially with regards to the *in-vitro* release, indicated that the protein was homogenously distributed within the lipid matrix. This means that the preparation technique provides an adequate distribution of the individual components even though the screws are rather short and were not equipped with any special mixing and kneading zones. Additionally, a pre-melting or full melting of the lipids is not necessary either.

Generally, it is important to consider that implant formation already started during the compacting phase (phase II). Collecting the lipid strand therefore started approximately after 40 sec of the corresponding run (Figure IX-2). The differences between the first (0 cm to 30 cm) and the following sections (30 cm to 120 cm) can be explained by the fact that during the very first formation of the lipid strand, the pressure did not reach completely the steady-state plateau as illustrated in Figure IX-2 at phase II. Consequently, the lipid strand showed macroscopic irregularities, e.g. a very rough surface or even gaps and cut-outs. This goes in line with a more porous implant. By this, the faster release is plausible as well because incubation medium can penetrate faster into the micro-pores and channels running through the lipid matrix. After the

steady-state phase (phase III), extrusion pressure decreased and lipid strand formation subsequently ended.

Throughout all experiments, the standard deviations of average extrusion pressures between independent runs (triplicates) were low which indicates a good reproducibility of the extrusion runs and a low batch to batch variety of the resulting lipid implant. Especially at lower extrusion temperatures, standard deviations ranged between 2 % to 5 %. Nevertheless, within a single run, isolated pressure peaks were observed as it is displayed in Figure IX-2.

IX.3.3 IMPACT OF PROCESS PARAMETERS ON EXTRUDATE CHARACTERISTICS

IX.3.3.1 EXTRUSION TEMPERATURE

The impact of extrusion temperature was evaluated using the 50:50 lipid composition. Three different extrusion temperatures were chosen, covering the complete temperature range where this specific formulation is extrudable (33°C to 37°C).

Figure IX-3 illustrates the pressure profiles at extrusion temperatures of 33°C, 35°C and 37°C, respectively. The lower the extrusion temperature the higher the steady-state pressure is: at 33°C 2373 kPa (±48 kPa) was measured, whereas 975 kPa (±74 kPa) and 487 kPa (±240 kPa) were measured when extrusion was performed at 35°C and 37°C, respectively (Figure IX-4 A). At 37°C, the formulation was problematic to extrude, as the lipid melt resulted in implant irregularities and a non-constant implant formation. Moreover, isolated pressure peaks, a less constant steady-state, and relatively high standard deviations were observed.

In addition to measuring the steady-state extrusion pressure, also the time of implant formation varied substantially. The speed at which implants were formed was strongly dependent on extrusion temperature.

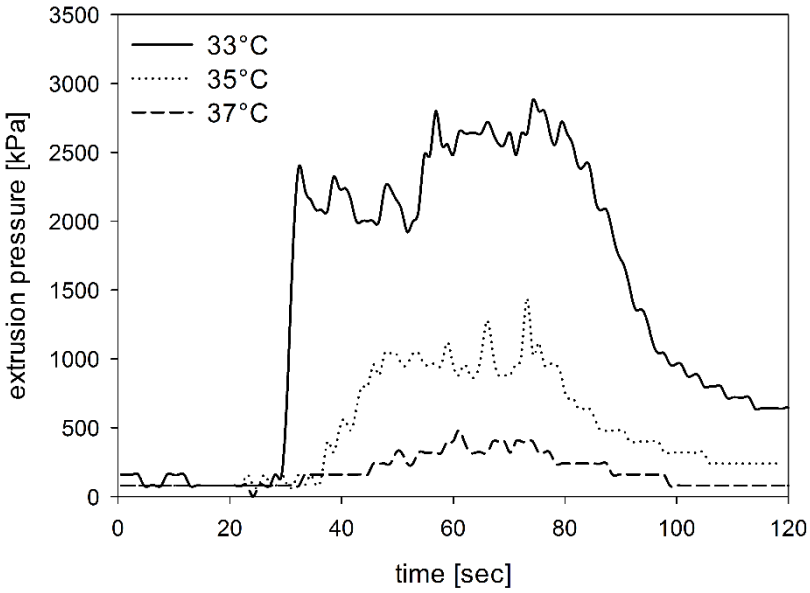

Figure IX-3: Representative extrusion pressure profiles of a 50:50 lipid composition extruded at 33°C, 35°C, and 37°C at 40 rpm.

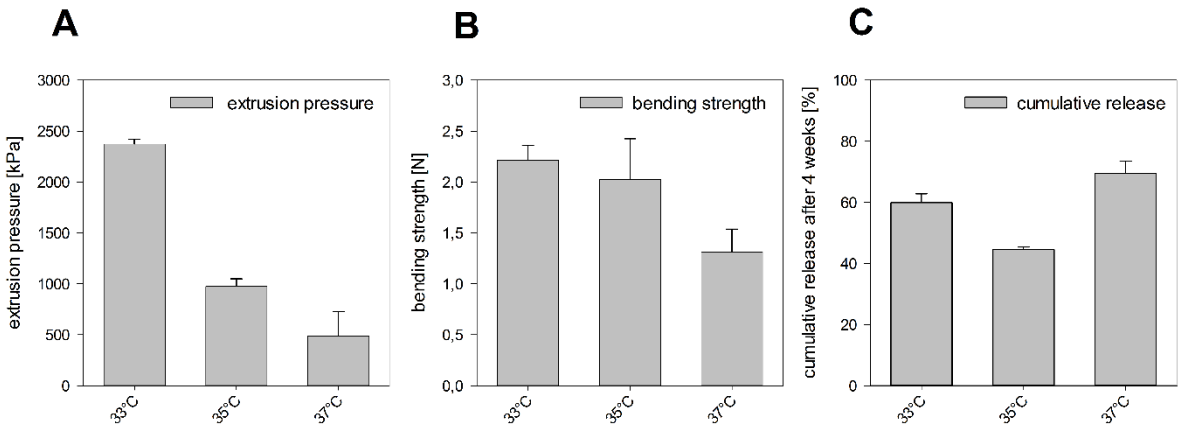

Figure IX-4: (A) Average extrusion pressure, (B) bending strength, and (C) cumulative release of mAb after 4 weeks of a 50:50 lipid composition as a function of extrusion temperature ranging from 33°C to 37°C extruded at 40 rpm.

As shown in Figure IX-3, at 33°C a steady-state plateau was present for approximately 50 sec, whereas this time was reduced to 30 sec at 37°C. Considering that the formed lipid strand had

a length of 120 cm, the extrusion speed can be calculated with 2.4 cm/sec at 33°C, 3.4 cm/sec at 35°C and 4.0 cm/sec at 37°C.

Mechanical properties of SLIs were highly dependent on the extrusion temperature as it can be seen in Figure IX-4. A strong correlation for extrusion pressure and bending strength can be observed: both decreasing with higher extrusion temperature.

In contrast to bending strength, release kinetics did not directly correlate with average extrusion pressure. Figure IX-4 C displays the cumulative released amount of mAb after 4 weeks as a function of the extrusion temperature. Compared to the standard extrusion temperature (35°C), release rates were comparably faster when extrusion temperature was either elevated (37°C) or reduced (33°C), as illustrated in Figure IX-4 C.

In Figure IX-5, microscopic appearance of SLIs in dependence of the extrusion temperature is depicted. At lower extrusion temperatures of 33°C (Figure IX-5 A) and 35°C (Figure IX-5 C), implants had a smooth surface with no irregularities (e.g. pores). At 37°C, a rather rough and uneven surface is noticeable (Figure IX-5 E). The micro-structure of the implants was affected by the extrusion temperature as well. At 33°C, needle-like structures are present with sharp edges and well-defined forms (Figure IX-5 B). In contrast, if 35°C or 37°C were applied, platelets-like structures instead of needles were observed (Figure IX-5 D and Figure IX-5 F), possibly due to the higher extrusion temperatures which were very close to the T_{onset} of H12 (36.8°C).

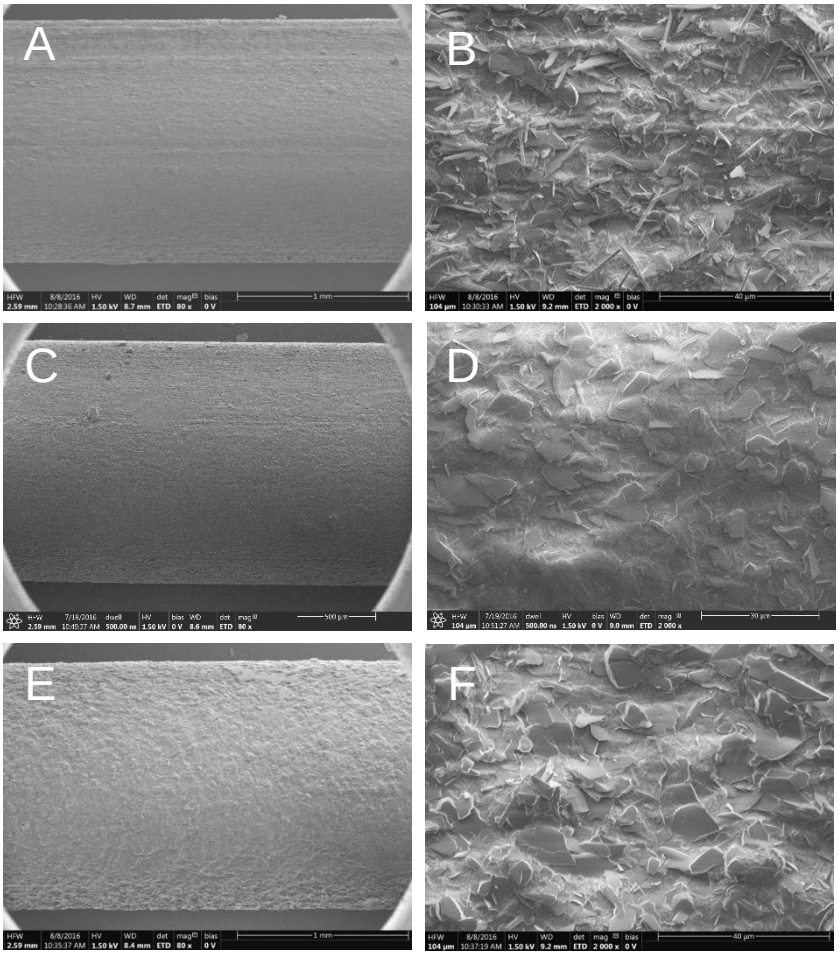

Figure IX-5: SEM micrographs of lipid implant surfaces consisting of a 50:50 lipid composition, which were extruded at (A, B) 33°C, (C, D) 35°C and (E, F) 37°C. Micrographs were taken at a magnification of (A, C, E) 80x, and (B, D, F) 2000x, respectively.

DISCUSSION

Within this experiment, the impact of extrusion temperature on implant properties was investigated for a 50:50 lipid composition which was extruded at 33°C, 35°C and 37°C at 40 rpm. At 33°C, the average extrusion pressure was nearly five times higher compared to pressure measured at 37°C (Figure IX-3 and Figure IX-4 A). Additionally, implant formation speed was practically doubled (2.4 cm/sec at 33°C versus 4.0 cm/sec at 37°C.). At temperatures close to the T_{onset} of H12 (36.8°C), the lipid is in a waxy condition rather than in a solid state, which creates a lower resistance and rigidity during feeding to the extruder inlet. For this reason, H12 is easier to compact because the waxy H12 is pressed between the interspace of non-molten

D118 particles more easily. Thus, the overall resistance and rigidity of the formulation generated less pressure, hence resulting in lower average extrusion pressure and a faster implant formation speed. Bending strength measurements support this explanation. Due to less compaction at higher extrusion temperatures, the material was less compacted resulting in a lower mechanical stability (2.21 N at 33°C compared to 1.31 N at 37°C).

At an extrusion temperature of 35°C, a perfect balance between waxy H12 and non-molten material (D118) resulted in the slowest release. The non-molten material (D118) acted as the solid phase; the waxy H12 served as a «kit» between the solid lipid platelets of the D118 during extrusion. Thereby, a tight and dense lipid matrix was formed. At lower extrusion temperatures than 35°C, less waxy H12 was present. Consequently, the solid lipid platelets of the D118 were less interconnected by molten H12. Thus, compression rather than melt extrusion might be the predominant implant formation process at this temperature. At higher extrusion temperatures than 35°C, no suitable implant was formed due to low compaction force.

No change in lipid modifications were observed neither due to the extrusion process nor upon incubation as monitored by differential scanning calorimetry (data not shown).

In conclusion, a correlation of extrusion pressure, mechanical stability and extrusion temperature was observed: the higher the extrusion temperature, the lower the average extrusion pressure associated with a faster implant formation. Mechanical stability decreased as a function of extrusion pressure. Contrarily, *in-vitro* release data did not correlate with extrusion temperature. The slowest release was observed for implants prepared at 35°C. In summary, both sufficient pressure and adequate molten material is needed to form a suitable implant.

IX.3.3.2 SCREW SPEED

In a next step, the impact of different screw speeds on implant properties was studied. For this approach, the lipid matrix consisted of the 50:50 lipid composition. Extrusion temperatures were

set to 33°C, 35°C, and 37°C. Additionally, screw speed was varied between 40 rpm and 80 rpm, respectively.

The resulting extrusion pressure profiles are given in Figure IX-6. At all extrusion temperatures, a strong relationship between extrusion pressure, duration of steady-state and screw speed can be observed. At 33°C, a steep onset and offset of pressure curves was noticeable. Further, at higher screw speeds the onset occurred earlier and consequently the steady-state plateau was reached faster. At 35°C, a steep onset and offset was observed for 60 rpm and 80 rpm, whereas the onset of the 40 rpm-pattern increased slower. Additionally, the steady-state plateau of the 40 rpm-pattern showed isolated peaks. Pressure curves recorded for 40 rpm and 60 rpm at 37°C were characterised by an even slower increase in pressure onset compared to 33°C and 37°C. Moreover, a higher degree of oscillation during the steady-state plateau was noticeable, especially at 40 rpm.

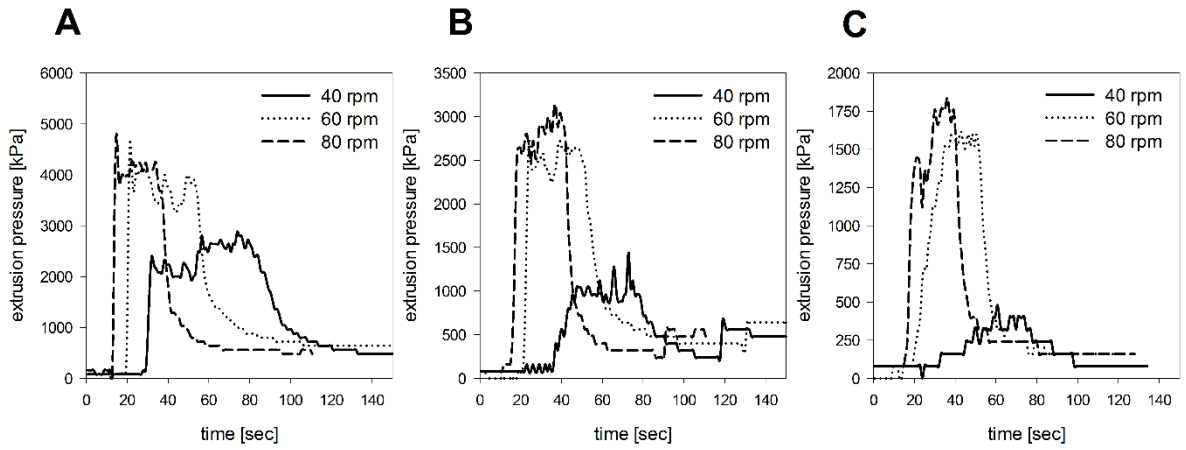

Figure IX-6: Representative extrusion pressure profiles of lipid implants consisting of a 50:50 lipid composition applying various screw speeds at an extrusion temperature of (A) 33°C, (B) 35°C, and (C) 37°C. Please note that the extrusion pressure axis is scaled differently.

Figure IX-7 A provides a summary of average extrusion pressures measured for all screw speeds at the different extrusion temperatures. For example, at 35°C, the average extrusion pressure increased from 975 kPa (±74 kPa) at 40 rpm to 2830 kPa (±539 kPa) at 80 rpm, which

represents a threefold increase by doubling the screw speed. This relationship was also valid for the other extrusion temperatures.

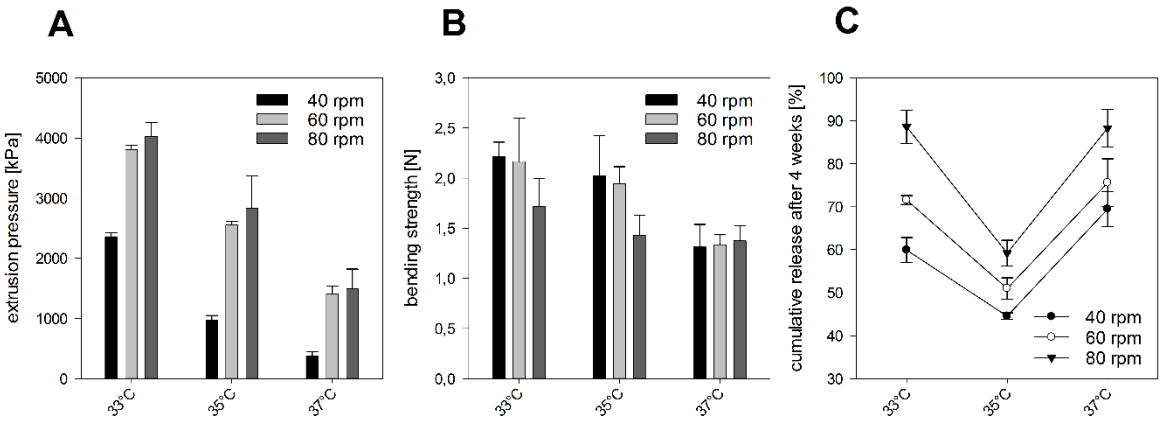

Figure IX-7: (A) Average extrusion pressures, (B) bending strength and (C) cumulative release after 4 weeks of a 50:50 lipid composition extruded at various screw speeds (40, 60 and 80 rpm) and different extrusion temperatures ranging from 33°C to 37°C.

Regarding the mechanical properties of SLIs, a tendency towards decreasing bending strength as a function of screw speed was observed (Figure IX-7 B). Moreover, slightly lower values can be detected for SLIs extruded at 35°C compared to 33°C. At 37°C, no differences in bending strength were observed between the applied screw speeds.

The cumulative release of the mAb was monitored over 4 weeks and is displayed in Figure IX-7 C as a function of extrusion temperature and screw speed. Release rates depended on the screw speed, although to a different extent. Generally, a slower screw speed resulted in slower release rates.

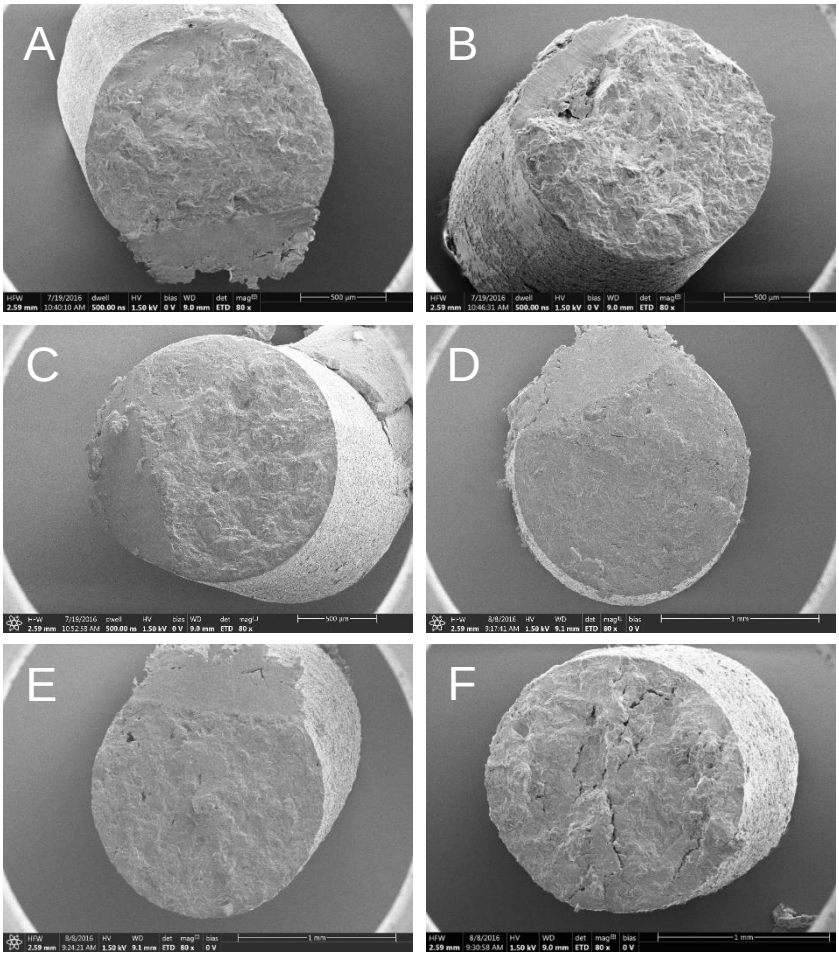

Figure IX-8: SEM micrographs of lipid implant cross sections taken at a magnification of 80x. Implants were composed of a 50:50 lipid composition and were extruded at (A, B) 33°C, (C, D) 35°C and (E, F) 37°C. Shown SLIs were manufactured with a screw speed of (A, C, E) 40 rpm or (B, D, F) 80 rpm.

SEM micrographs were acquired to determine the impact of different screw speeds on implant morphology (Figure IX-8). As demonstrated in Figure IX-8 A and Figure IX-8 B, at an extrusion temperature of 33°C implants contained more pores when extruded at 80 rpm compared to SLIs manufactured at 40 rpm, where a rather dense matrix can be noticed. At 35°C, only very small and isolated pores can be observed irrespectively of the applied screw speed (Figure IX-7 C). More pronounced pore formation was observed at 37°C. At 40 rpm, a few isolated pores were present, whereas at 80 rpm numerous pores and even channels running through the cross section can be noted. This is also in accordance with acquired *in-vitro* release data, since the fastest release was observed when implants were extruded at 80 rpm (Figure IX-7 C).

DISCUSSION

Within this experiment, the impact of screw speed on the implants´ mechanical stability and release patterns at three different extrusion temperatures was investigated. Higher screw speed resulted in higher extrusion pressure for all extrusion temperatures (Figure IX-7 A). Due to the higher screw speed, more material is transported per time interval. Therefore, at a constant implant diameter, the pressure during the compacting phase (phase II) of the extrusion process (where the sensor is located) is higher. Logically, once the compacting phase is completed, a faster screw speed results in faster lipid strand formation (Figure IX-6).

Interestingly, the higher pressures did not correlate with increased mechanical stability, as the bending strength decreased with increased screw speed for implants extruded at 33°C and 35°C. This can be explained by the retention period of the material within the barrel: faster transported material was less molten which resulted in lower bending strength. By this, the faster *in-vitro* release can be explained as well. Consequently, it can be concluded that the material requires a minimum time period to allow sufficient energy transfer from the barrel and screws. Only after this minimum retention time is reached, higher screw speed would lead to higher mechanical stability and lower release rates. This can easily be realized by a longer barrel during upscaling.

Additionally, it can be speculated that once the lipid strand is pressed through the outlet, it expands again (cavitation). This phenomenon has already been described during extrusion of PLGA-lipid blends using a RAM-extruder [431]. This effect might be more pronounced the faster the screws rotate, which is underlined by more porous implants (Figure IX-8) and a lower bending strength (Figure IX-7 B). This would also explain *in-vitro* release data, as the incubation medium can penetrate faster into more porous implants.

IX.3.3.3 LIPID COMPOSITION

Above, for the 50:50 lipid composition the impact of different screw speeds and extrusion temperatures on implant properties was described. Next, the impact of the lipid composition itself on implant properties was studied. The lipid composition was varied between 30 % (30:70 lipid composition) to 70 % of H12 (70:30 lipid composition) with the corresponding portions of D118 (70 % to 30 %); lyophilisate percentage was kept constant at 10 %. Implants were extruded at 33°C, 35°C and 37°C at a fixed screw speed of 40 rpm. The 30:70 lipid composition was additionally extruded at 39°C and 42°C.

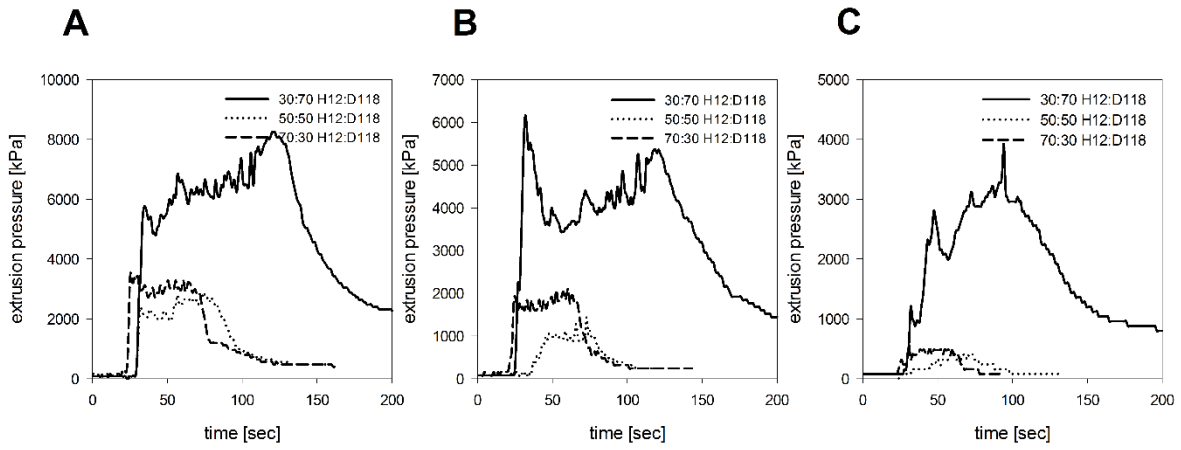

Figure IX-9: Representative extrusion pressure profiles of different lipid compositions extruded at (A) 33°C (B) 35°C and (C) 37°C. Lyophilisate percentage was kept constant at 10 %. Please note that the y-axis is scaled differently.

The pressure curves of the different compositions extruded at 33°C, 35°C and 37°C are displayed in Figure IX-9. For the 30:70 lipid composition, the average steady-state pressure was 2-3 times higher as the average steady-state pressure measured for the 50:50 and 70:30 lipid composition at all extrusion temperatures. The pressure patterns of the 50:50 and 70:30 lipid composition were comparable with respect to the duration of the plateau phase. However, the average steady state pressure (Figure IX-10 A) was lower for the 50:50 lipid composition compared to the 70:30 lipid composition for implants extruded at 33°C and 35°C. For the

implants extruded at 37°C, no difference in average steady-state pressure between the 50:50 and 70:30 lipid composition was detectable (Figure IX-10 A).

Furthermore, it should be noted that the plateau phase of the 30:70 lipid composition was almost twice as long and increased steadily, whereas a constant pressure was not reached (for all extrusion temperatures). Further, the pressure peak (most pronounced at 35°C) right at the beginning of the plateau phase and the irregular, oscillating course of the pattern was noticeably. For the 30:70 lipid composition, an approximately four times higher remaining pressure was determined compared to the other compositions for all extrusion temperatures (Figure IX-9).

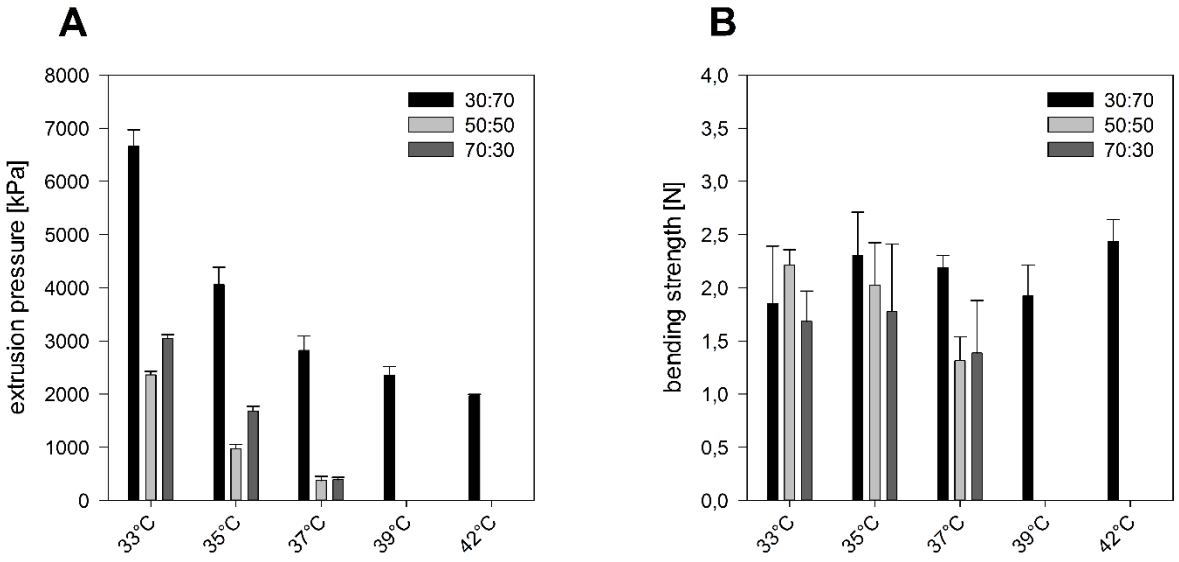

Figure IX-10: (A) Average extrusion pressure and (B) bending strength of implants consisting of different lipid compositions (30 % to 70 % H12) at various extrusion temperatures ranging from 33°C to 42°C.

Bending strength results are depicted in Figure IX-10 B. No noticeable trend with respect to the lipid composition at the different extrusion temperatures was determined.

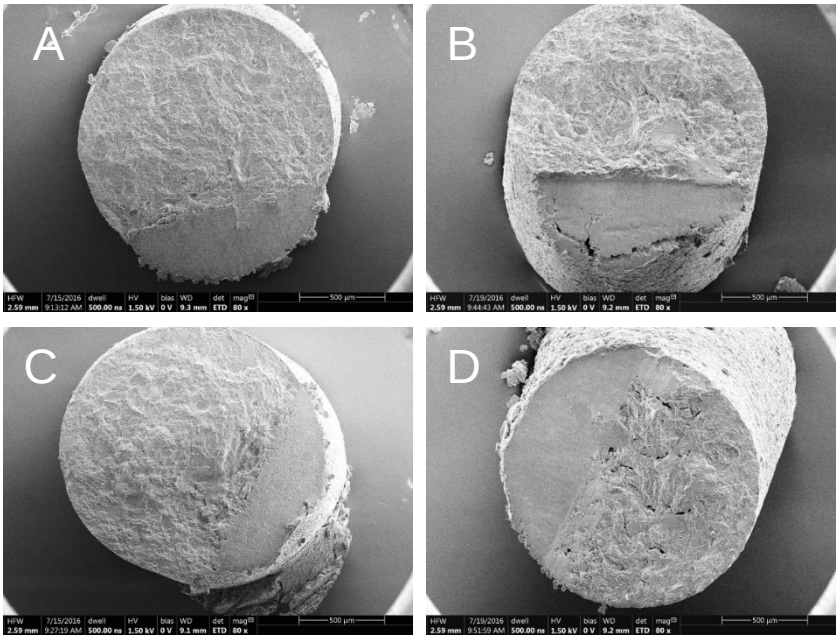

Figure IX-11: SEM micrographs of cross sections of lipid implants consisting of different lipid compositions. Micrographs (A) and (C) show implants consisting of the 30:70 lipid composition extruded at (A) 33°C and (C) 37°C. The right-hand side micrographs depict the 70:30 lipid composition extruded at (B) 33°C and (D) 37°C, respectively. The magnification was set to 80x.

The impact of lipid compositions on implant morphologies are illustrated in Figure IX-11. Exemplarily, micrographs of the 30:70 and 70:30 lipid compositions extruded at 33°C at 37°C are depicted, as they represent the «extreme cases» of this experiment. For the 30:70 lipid composition, the different extrusion temperatures did not impact implant microstructure as in both cases a dense matrix can be observed (Figure IX-11 A and Figure IX-11 C). Regarding the 70:30 lipid composition, differences in the microstructure were apparent: at an extrusion temperature of 33°C, tiny pores and channels were present (Figure IX-11 B). At 37°C, larger pores and channels running through the complete cross section were observed thereby generating an interconnected pore-network (Figure IX-11 D).

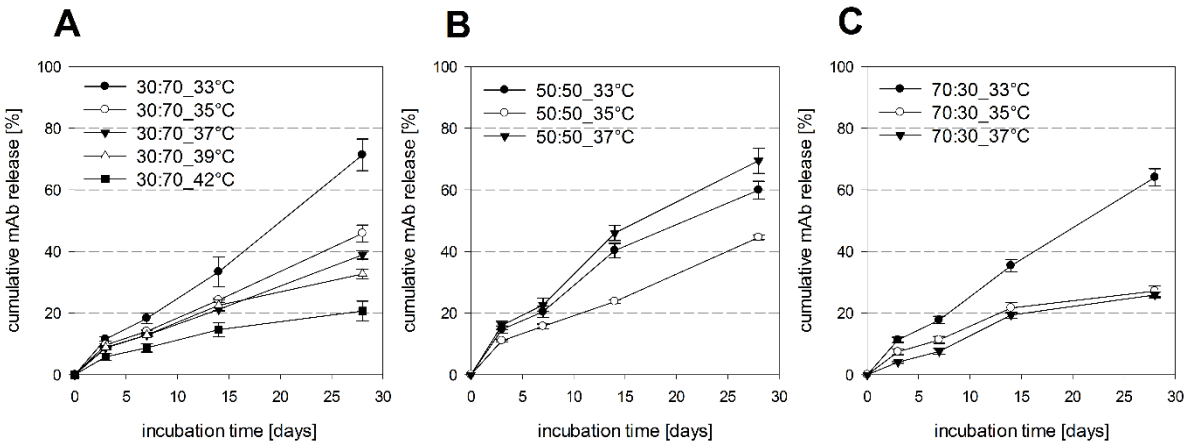

Figure IX-12: Cumulative release of mAb over 4 weeks in PBS pH 7.4 at 37°C. Lipid implants were prepared at different extrusion temperatures ranging from 33°C to 42°C. Additionally, lipid compositions were varied: (A) 30:70, (B) 50:50, (C) 70:30.

A detailed insight into *in-vitro* release is provided in Figure IX-12 illustrating the release profiles of all tested compositions over 4 weeks. For the 30:70 lipid composition, release was slower the higher the extrusion temperature. After 14 days, release of the implants extruded at 39°C and 42°C of the 30:70 lipid composition started to level off, already suggesting that release would stop rather early. SLIs prepared at 33°C, 35°C or 37°C provided a constant release. (Figure IX-12 A). The 70:30 lipid composition showed this trend after 14 days, even more considerably, also for the higher extrusion temperatures of 35°C and 37°C (Figure IX-12 C). Regarding the 50:50 lipid composition, Figure IX-12 B signifies that no levelling occurred at all extrusion temperatures.

In summary, formulations comprising slowest and most steady release were composed of 30:70 lipid composition extruded at 35°C and 37°C and 50:50 lipid composition extruded at 35°C (which was the lead formulation described earlier).

DISCUSSION

As expected, the highest extrusion pressures were observed for the 30:70 lipid composition comprising 70 % D118, because of the higher amount of solid D118. The higher pressure during

extrusion also resulted in more compact (less porous) implants, which was confirmed by SEM micrographs (Figure IX-11). According to this fact (higher solid D118 content leads to higher pressures), our findings of the higher extrusion pressure for the 70:30 lipid composition instead of the 50:50 lipid composition are controversy (for 33°C and 35°C). At this point of knowledge, it can only be speculated that dependent on the amount of molten lipid other effects, e.g. change from a laminar flow towards a more turbulent flow could have contributed to the extrusion pressure measured with our setup. Overall, more molten material within the 70:30 lipid composition caused more interaction and higher viscosity than a lower amount of molten material (30:70 lipid composition) with dispersed solid D118.

The detected differences in duration and course of the plateau phase between the 30:70 and 50:50 or 70:30 lipid composition, respectively, correlates with our observations during the extrusion process: the formation of the lipid strand of the 30:70 lipid composition took twice as long as for the other two lipid compositions (in all cases 3 g were processed) which was reflected by the longer plateau phase. The irregular, oscillating course of the pressure pattern during the «plateau phase» of the 30:70 lipid composition correlates to a non-continuous strand formation noticed during extrusion. This was true for all extrusion temperatures from 33° to 42°C.

With respect to the microstructure, it would have been expected, that at higher D118 percentages more pores were generated due to a lack of waxy H12 (as described in IX.3.3.1), therefore resulting in a faster release. However, SEM micrographs showed a dense matrix, most likely caused by compression rather than melt extrusion, which is in accordance with the comparatively high extrusion pressures. The dense matrix also explains the slow release rates. Further, the observed decrease in release for higher extrusion temperatures (less pressure) can be explained by a change from compression to melt extrusion as a function of extrusion temperature. It can be assumed that melt extrusion leads to a more permanent connection of the lipids compared to compression. Thus, melt extrusion could be the reason for the slower and levelling off release of implants produced at higher extrusion temperatures.

At percentages of 70 % H12, a dense and compact matrix was expected as the solid D118 would be completely surrounded by molten H12. In contrast, SEM micrographs showed a porous matrix. The micrographs indicated even more and larger pores for implants processed at higher extrusion temperatures. From the very low pressures measured using this setup, it can be assumed that not enough solid D118 was present to generate the minimum extrusion pressure, which is necessary to compact the material. Thus, no proper strand was formed (Figure IX-11 B and Figure IX-11 D). Having this in mind, it would have been expected that the release of the 70:30 lipid composition would have been faster compared to the non-porous matrix of the other composition. However, the measured slow release could be caused by a change in microstructure (from porous to dense) due to the incubation temperature of 37°C. This assumption was supported by the fact that the implant deformed upon incubation.

IX.3.4 DOUBLE TSC-EXTRUSION

Now, the aim was to study how extrusion pressure, implants´ mechanical properties and release patterns are changing when the same material was extruded twice. Lipid implants were extruded (first extrusion run), then ground and sieved (< 180 µm) prior to the second extrusion run. For all extrusions described in this section, the batch size was set to 3 g and screw speed was adjusted to 40 rpm.

Three different approaches were tested. First, extrudates comprising the 50:50 lipid composition (10 % lyophilisate) were extruded at 35°C and 40 rpm. The ground and sieved material was then extruded a second time at 33°C, 35°C, or 37°C, respectively. In a second approach, a formulation comprising 20 % lyophilisate and 80 % D118 was first extruded at 65°C (named «20% in 0:100» in Table IX-2). Afterwards, the strand was ground and sieved (< 180 µm), H12 was added to obtain a ratio of 50:50 and the second extrusion was performed at 35°C. Third, within the first extrusion run a formulation consisting of 20 % lyophilisate and 80 % H12 was extruded at 35°C (named «20% in 100:0» in Table IX-2). D118 was then added to the ground

and sieved (< 180 µm) material to obtain a 50:50 lipid composition which was then extruded at 35°C.

Table IX-2: Overview over formulations and settings applied for the different double tsc-extrusion experiments.

	First extrusion		Second extrusion	
	Formulation	**Settings**	**Formulation**	**Settings**
10% in 50:50/35°C_33°C	10% lyophilisate, 50:50 lipid matrix	35°C	10% lyophilisate, 50:50 lipid matrix	33°C
10% in 50:50/35°C_35°C		35°C		35°C
10% in 50:50/35°C_37°C		35°C		37°C
20% in 0:100/65°C_35°C	20% lyophilisate, D118 lipid matrix	65°C		35°C
20% in 100:0/35°C_35°C	20% lyophilisate, H12 lipid matrix	35°C		35°C

Figure IX-13 A provides a summary of the average extrusion pressures measured during the first and second extrusion runs. Within the first approach, the 50:50 lipid composition was extruded at 35°C providing an average pressure of 975 kPa (±74 kPa). Within the second extrusion run, temperature was set to 33°C, 35°C and 37°C which resulted in an average pressure of 3085 kPa (±251 kPa), 907 kPa (±115 kPa) and 334 kPa (±97 kPa), respectively. The pressure values measured were similar to those already observed previously (Figure IX-4 A).

An average pressure of 4438 kPa (±83 kPa) was measured for the extrusion of 20 % lyophilisate embedded within a pure D118 matrix (second approach). During this extrusion run, temperature was set to 65°C. This was the optimal extrusion temperature, as it is close to the T_{onset} of D118 (70.0°C). After H12 was added to give a lipid ratio of 50:50, a pressure of 1531 kPa (±168 kPa) was measured during the second extrusion. Throughout the third approach, both extrusion runs comprised comparable average extrusion pressures (1065 kPa and 1247 kPa).

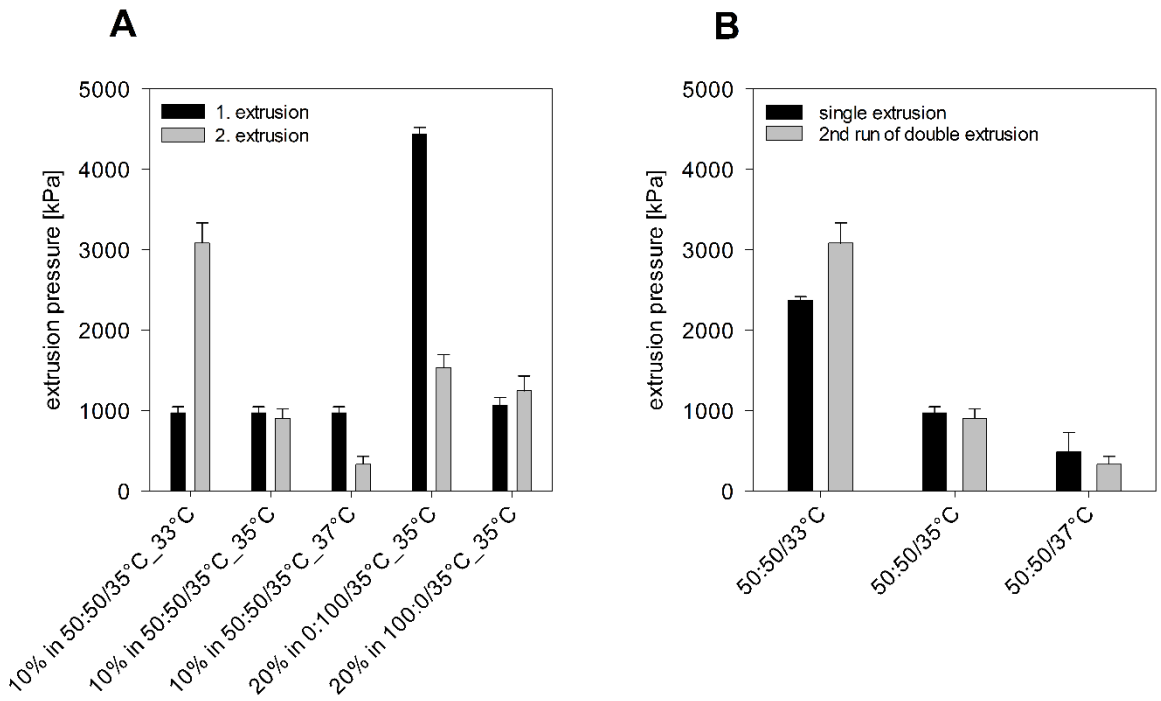

Figure IX-13: (A) Average extrusion pressure measured during the first and second extrusion run of the different approaches described above. (B) displays the average extrusion pressure only during the second extrusion run in comparison to the pressure values from the same formulations only extruded once.

Within Figure IX-13 B, the average extrusion pressures during the second extrusion run were compared to the pressure values of the same formulations only extruded once (single extrusion). Only at 33°C, different extrusion pressures can be observed. A 24 % higher extrusion pressure was recorded (2373 kPa compared to 3085 kPa) when the formulation was extruded twice compared to a single extrusion using the same settings. For extrusions performed at 35°C and 37°C, respectively, average extrusion pressures were comparable.

Mechanical properties were assessed by bending strength determination (Appendix, Table XII-2) and true density measurements (Appendix, Table XII-3). Regarding the first approach, bending strength stayed constant at approximately 2 N for all different approaches. True density values were found to correlate with average extrusion pressures as true density considerably decreased with decreasing temperature during the second run. This relation can also be described concerning the second approach. For lipid implants consisting of 100 % D118, true

density was measured at 1.086 g/cm^3. After H12 was added to a give a 50:50 lipid composition, true density decreased to 1.057 g/cm^3, which is in accordance with the reduced pressure. For the third approach, extruded implants consisting of 100 % H12 demonstrated a substantial softness indicated by the low bending strength of 0.87 N (±0.35 N). After D118 was added in a defined quantity, bending strength increased again to 1.42 N (±0.19 N), while true density reached the value as measured for the second approach.

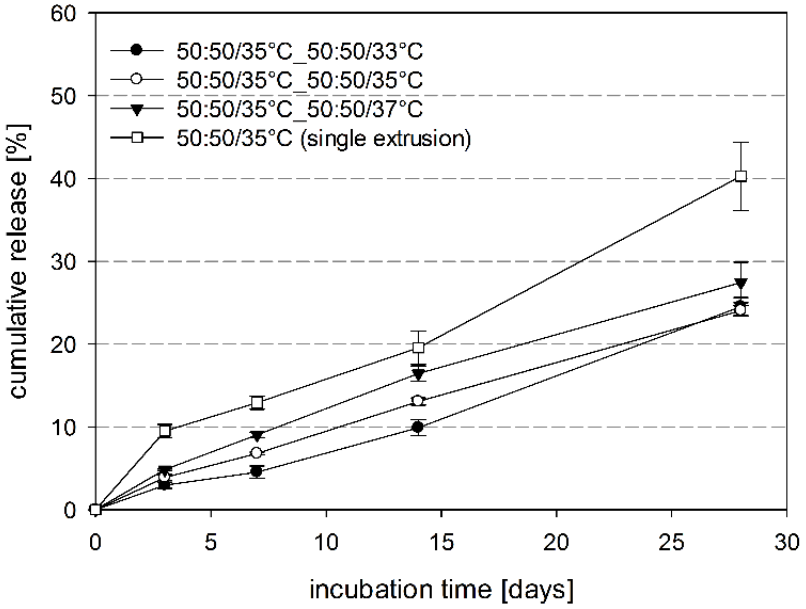

Figure IX-14: Cumulative release over the first 4 weeks of SLIs manufactured with the different double extrusion approaches compared to the lead formulation extruded only once. For a better visualisation, y-axis was scaled to 60 %.

As illustrated in Figure IX-14, cumulative release of mAb from double extruded implants was measured over 4 weeks. As a benchmark, release of mAb from the lead formulation (which was only extruded once) is shown additionally. When following the first approach, independent of the extrusion temperature during the second extrusion, release rates were slowed down clearly compared to the lead formulation: 40.3 % (±4.1 %) mAb was released from the lead formulation, compared to 24.0 % to 27.4 % released from double extruded SLIs after 4 weeks. Thus, release rates were almost halved.

Concerning the release patterns of SLIs prepared by the second and third approach, the release rates were comparable to the single extruded lead formulation (41.5 % compared to 47.6 %). Hence, a further retardation of release was not achieved.

DISCUSSION

The first approach of double extrusion did not influence average extrusion pressure much compared to a single extrusion run (Figure IX-13 B). The mechanical properties of double extruded SLIs were comparable to those only extruded once. Although, bending strength and true density were slightly higher, which is plausible because the material was extruded (and thereby compressed) twice (Appendix, Table XII-2 and Table XII-3).

Interestingly, release was slowed down almost by one half when the same formulation was extruded twice (Figure IX-14). This observation was most likely caused by changes within the microstructure of the lipid matrix. However, SEM micrographs showed comparable dense matrices in all cases and did not provide any additional information (data not shown). The protein was more thoroughly embedded within the lipid matrix by double extrusion, because the lipid material was compressed twice. True density measurements support this explanation (Appendix, Table XII-3). Consequently, this resulted in a slower release. To prove this assumption, a labelling of protein with fluorescence dyes might be beneficial. If a more effective encapsulation of the mAb was the reason for the slower release, it should be considered that the mAb could theoretically be encapsulated irreversibly into lipid cavities.

Release was not further slowed down by the second and third approach compared to the lead formulation (single extrusion), but release rates were within the same corridor. This leads to the conclusion that the double extrusion technique in general results in SLIs with very slow release rates.

In summary, very promising sustained release data were generated by a rather simple adjustment of the established extrusion process.

IX.4 CONCLUSION

Within this chapter we described the thorough investigation on process monitoring to understand solid lipid extrusion using a tsc-extruder for lipid protein depots.

A pressure measurement tool allowed us to monitor the process online. Thereby, we could describe and characterise an extrusion run in four different phases: feeding (I), compacting (II), implant formation (III) and end of implant formation (IV). Implant formation took place mainly during the steady-state phase (phase III). We would recommend discarding the first 30 cm of formed lipid strand and the parts which were formed during phase IV. In general, up to 100 cm product was manufactured utilising a batch size of 3 g.

Furthermore, the preparation process can ensure both a homogenous distribution of the protein encapsulated within the lipid matrix and consistent mechanical properties of SLIs (first 30 cm formed are not considered). Additionally, a low batch to batch variety demonstrated the good reproducibility and robustness of the extrusion process.

Insights into how a change of process parameters affects extrusion pressure, mechanical properties and release kinetics were gained. By changing process parameters, e.g. screw speed, mechanical properties of SLIs can be adjusted. Furthermore, it is now possible to estimate how and to which extent a change of a certain process parameter will impact mechanical properties or release patterns of SLIs. This allows us to assess if an extrusion process is either susceptible or robust against process parameter changes.

It should be pointed out, that an independent systematical investigation of extrusion temperature and screw speed could not completely be realized due to the short screws resulting in short retention times and incomplete heat transfer. The two parameters will be studies fully independent from each other with an elongated extruder barrel in the course of future scale up work.

The double extrusion technique slowed down mAb release by almost one half. This process reveals a great potential because versatile parameters can be adjusted creating a wide range of possible product features.

X. FINAL SUMMARY AND OUTLOOK

Within this thesis, solid lipid implants were manufactured by twin-screw extrusion and were evaluated with respect to their potential for intraocular use. The study included investigations on long-term release of different therapeutic protein formats (monoclonal antibody, f_{ab}-fragment, fusion protein), the *in-vivo* performance of SLIs which have been intravitreally administered in rabbit eyes, and the stability profile of both encapsulated and released protein. Also, the biological activity of released protein was evaluated. Triglyceride-protein interactions were further examined to study the influence of these interactions on the protein stability and release profile. Towards a better understanding of the extrusion process, a pressure measurement system was set up and the extrusion pressure was measured online. SLIs were analysed in terms of mechanical properties, morphology and release patterns to correlate those characteristics with extrusion parameters.

Chapter I and II include the general introduction and the objective of the thesis. In **chapter III**, the materials and methods are described.

In **chapter IV**, investigations on improving *in-vitro* release kinetics were described. *In-vitro* release for up to 120 days of different protein formats from implants being only 1.5 mm x 15 mm in size was achieved. The formulation developed ensured a constant release without any burst release by a load of 3.00 mg protein per implant. The avoidance of the precipitant PEG as a possible source for protein degradation represents a major improvement. The extrusion process was established on a ZE-5 mini-extruder, allowing to extrudate very small batch sizes (only 500 mg) at gentle temperatures of 35°C. It was also ensured that extruded lipid implants can be

stored for at least 3 months without any negative impact on the release patterns, thermal properties, and status of crystallinity, respectively.

To further prolong the release duration, triglycerides were pre-melted prior to extrusion. Release duration of mAb was prolonged to up to 200 days (increase of approximately 63 %) and Ranibizumab release was extended to circa 160 days (40 % longer release duration), compared to conventional extrusion. Since the release was substantially different after SLI storage in this case, more research is required to elucidate these aspects further.

For comparison, proteins were also incorporated into PLGA matrices by tsc-extrusion having the same dimensions as SLIs. In general, release was, if at all observed, very slow (maximum 15 % over 98 days). Even after matrix degradation no burst release was noticed, which underlines the problems with protein degradation when using PLGA.

The *in-vivo* performance of Ranibizumab (Lucentis®) loaded SLIs was evaluated within a 3-month *in-vivo* study in rabbit eyes using a choroidal neovascularisation model (CNV) and is reported in **chapter V**. We showed that biocompatibility was excellent throughout the 3 months of observation. Unfortunately, a partial break-up of implants was observed which was the reason for a faster *in-vivo* release compared to the release observed *in-vitro*. *In-vivo* release was measured over 3 months, but generally no more Ranibizumab was released after 8 weeks. It was identified that the formulation was mechanically sensitive, which was the cause for the break-up of implants. Possible reasons were: the relatively high percentage of H12 and the temperature within the rabbit eye. Even though the results did not fulfil the expectations, once the problem of mechanical stability can be solved, SLIs still represent an interesting depot for intravitreal delivery of pharmaceutical proteins.

The marketed products available for intravitreal applications should be taken into consideration as a benchmark. The depots Retisert® (5 mm x 2 mm x 1.5 mm), Ozurdex® (0.45 mm x 6.5 mm) and Iluvien® (0.37 mm x 3.5 mm) are all smaller in size compared to SLIs described here.

Therefore, investigating smaller sized SLIs by ensuring an adequate protein load should be considered for further work. Nevertheless, the size of SLIs used in this work was already suitable for intravitreal use.

Chapter VI was intended to extend our technology to other protein formats. For this, the *in-vitro* release of the complement factor H (mini-FH) and determination of its biological activity over a period of 98 days was reported. Even after 98 days, the mini-FH released from SLIs still exhibited biological activity.

The stability of both encapsulated and released proteins was reported in **chapter VII**. Moreover, the stability of proteins delivered from PLGA implants was assessed and compared to those of proteins delivered from SLIs. The IgG_1 monoclonal antibody was characterised by an adequate stability over more than 6 months, even though minor chemical and conformational instabilities were observed. This is a unique finding, since a delivery duration of 6 month of a protein therapeutic displaying such a good stability over the complete time frame can rarely be found in literature. Released Ranibizumab showed excellent physical, chemical and conformational stability over 4 months. Furthermore, Aflibercept stability was monitored over 3 months. Instabilities with respect to physical, chemical and conformational stability started approximately after 1 month and increased continuously. Bevacizumab instability was already observed after 1 week, and at the end of the observation time (1 month), the antibody was fully chemically and conformationally degraded.

In addition, the stability of mAb and Ranibizumab was assessed upon storage. For that, loaded SLIs were stored for 3 months at 4°C prior to *in-vitro* release in the dry state. MAb and Ranibizumab showed perfect stability after 3-month of storage.

The stability of released protein from a PLGA matrix was also assessed in **chapter VII**. For all proteins, a rapid and substantial degradation was observed, being in accordance with literature [49, 217, 300]. SE-HPLC and SDS-PAGE results revealed a distinct monomer loss of released proteins mainly caused by fragmentation (VII.2.2.1). For instance, comparing Ranibizumab monomer content released from SLIs after 12 weeks (100.1 %) and Resomer® RG 502 H implants (4.4 %) underlines this. Also, analysis towards chemical stability (IEX, HIC, reducing capillary gel electrophoresis) pointed into the direction of rapid degradation of all tested proteins in PLGA matrices. Especially higher percentages of LMW species and light chain were observed. These results highlight that SLIs provide an outstanding delivery matrix for proteins, as the stability of the incorporated protein during long-term release and storage was retained compared to the PLGA implants used here.

In **chapter VIII**, studies on triglyceride-protein-interactions are described. Incubation studies were performed, where extruded rods consisting of 100 % H12, D118, or Resomer® RG 755 S were incubated with solutions of mAb, Ranibizumab, Bevacizumab and Aflibercept over 8 weeks. Colloidal, chemical and conformational stability of proteins were assessed at predetermined time points. Elevated particle counts, monomer loss and less protein recovery upon incubation with H12 rods were observed. This was especially the case for Aflibercept and Bevacizumab, whereas for the other proteins the increase in particle counts was smaller. Neither H12 nor D118 were identified as trigger for inadequate release patterns or chemical degradation.

It was also tested if possible heavy metal impurities of the raw materials could cause protein degradation. Only aluminium was found by ICP-AES, which did not promote chemical instabilities. Other impurities possibly being present in the lipid raw material, e.g. peroxides or aldehydes, could be the reason for protein degradation. This should be further investigated. Lastly, it should be noted that adsorption phenomena play a major role affecting sustained

release of proteins form triglyceride based depots that should be more extensively examined in future.

Within **chapter IX**, the extrusion process was studied with regards to process parameters and how changing these parameters affected the properties of the lipid matrices. For this, a custom-made resistance strain gauge was designed and established to measure the pressure within the barrel during an extrusion run. The impact of process parameters such as extrusion speed, temperature, and lipid composition on implant properties was investigated systematically. Bending strength, true density and microscopic appearance of extruded implants was assessed. Furthermore, *in-vitro* release profiles were addressed using a monoclonal antibody. This allowed to characterise an extrusion run which can be defined into four different phases: feeding, compacting, implant formation, and end of implant formation. Additionally, the inner-strand homogeneity was investigated displaying a homogenous distribution of the protein within the lipid matrix. The batch to batch variation was very low, demonstrating good reproducibility and robustness of the extrusion process.

It was possible to correlate implant properties to the different process parameters (extrusion temperature, screw speed, lipid composition). In summary, we now know that both sufficient extrusion pressure and an appropriate ratio of molten to solid lipid is needed to form a suitable implant.

Furthermore, double extrusion was investigated as an additional preparation method. By this, the release rate of mAb was almost halved over the first 4 weeks by simply performing the extrusion twice with slightly different extrusion temperatures or even the same settings. Therefore, it reveals a great potential, because versatile parameters can be adjusted creating a great scope for further research. As lipids are exposed to extrusion temperatures twice, possible re-crystallisation of the triglycerides should be taken into consideration for further research.

XI. ADDENDUM

XI.1 LIST OF ABBREVIATIONS

AAV	adeno-associated virus
AMD	age related macular degeneration
ANP	atrial natriuretic peptide
AP	alternative pathway
AUC	area under the curve
BDNF	brain derived neurotropic factor
bFGF	basic fibroblast growth factor
BMP-2	bone morphogenetic protein-2
BSA	bovine serum albumin
CD	circular dichroism
CDR	capsule drug ring
cIEF	capillary isoelectric focussing
CNV	choroidal neovascularisation
CPP	central precocious puberty
DDS	drug delivery system
DLS	dynamic light scattering
DNA	deoxyribonucleic acid

DR	diabetic retinopathy
DSC	differential scanning calorimetry
DTT	dithiothreitol
EDTA	ethylene diamine tetra acetic acid
ELISA	enzyme-linked immunosorbent assay
EPO	erythropoietin
EVA	ethylene vinyl acetate
F_{ab}	fragment antigen binding
F_c region	fragment crystallisable region
FDA	food and drug administration
FFF	front face fluorescence
FNU	formazine nephelometric unit
FT-IR	fourier transform infrared spectroscopy
GLP	glucagon-like-peptide
GnRH	gonadotropin releasing hormone
HCl	hydrochloride
HEMA	hydroxyethyl methacrylate
HES	hydroxyethyl starch
HIC	hydrophobic interaction chromatography
HME	hot melt extrusion

HMW	high molecular weight
HNO_3	nitric acid
HP-β-CD	hydroxypropyl-beta-cyclodextrine
HRP	horseradish peroxidase
IC_{50}	half maximal inhibitory concentration
ICP-AES	inductively coupled plasma atomic emission spectroscopy
IEX	ion exchange chromatography
IgG	immunoglobulin G
ITC	isothermal titration calorimetry
KOH	potassium hydroxide
LMW	low molecular weight
LO	light obscuration
LOD	limit of detection
mAb	monoclonal antibody
MC	methylcellulose
MFI	microflow imaging
mPEG	monomethoxy polyethylene glycol
MQ water	milli-Q water
MW	molecular weight
MWCO	molecular weight cut off

NELL-1	NEL-like molecule-1
nIFN	native interferon
NIR	near-infrared
NMP	N-methyl-2-pyrrolidon
PBS	phosphate buffered saline
PCL	poly(ε-caprolactone)
PDGF	platelet-derived growth factor
PEG	polyethylene glycol
PEO	polyethylene oxide
pI	isoelectric point
PLA	poly-lactic acid
PLGA	poly-lactic-co-glycolic acid
PNH	paroxysmal nocturnal hemoglobinuria
PVA	poly vinyl acetate
QCM	quartz crystal microbalance
rRBCs	reagent red blood cells
RNA	ribonucleic acid
SDS	sodium dodecyl sulfate
SDS-PAGE	sodium dodecyl sulfate poly acryl gel electrophoresis
SE-HPLC	size exclusion high performance liquid chromatography

SEM	scanning electron microscopy
siRNA	small interfering ribonucleic acid
SLE	solid lipid extrusion
SLI	solid lipid implant
SLM	solid lipid microparticle
SLN	solid lipid nanoparticle
SPR	surface plasmon resonance
Tg`	glass transition temperature
TMPE-TL	trimethylopropane ethoxylated-ethyl 2-mercaptoproprionate
TMPE-TG	trimethylopropane ethoxylated ethyl thioglycolate
Tsc	twin screw
UV-VIS	ultraviolet-visible spectrophotometry
VEGF	vascular endothelial growth factor
WCX	weak cation exchange
XRPD	X-ray powder diffraction

XI.2 LIST OF FIGURES

XI.3 LIST OF TABLES

XI.4 PRESENTATIONS AND PUBLICATIONS

XI.4.1 PUBLICATIONS

Hayden RS, Vollrath M, Kaplan DL

Effects of clodronate and alendronate on osteoclast and osteoblast co-cultures on silk-hydroxyapatite films, Acta Biomaterialia, 2013

Vollrath M, Engert J, Winter G

Long-term release and stability of pharmaceutical proteins delivered from solid lipid implants, EJPB, 2017

XI.4.2 ORAL PRESENTATIONS

Vollrath M, Engert J, Winter G

Twin-screw extrusion of solid lipid implants for the intravitreal sustained delivery of pharmaceutical proteins. CRS Germany Local Chapter Meeting, 12th to 13th of February 2015, Muttenz, Switzerland

XI.4.3 POSTER PRESENTATIONS

Pöhlmann ML, Häusl AS, Hartmann J, Harbich D, Schmid B, Dedic N, Feng X, Breitsamer M, Vollrath M, Mederer A, Balsevich G1, Engelhardt C1, Hausch F, Deussing JM, Winter G, Chen A, Schmidt MV

Unraveling the functional contribution of FKBP51 in relevant brain areas to stress vulnerability. ECNP Workshop for Junior Scientists in Europe, 9th to12th March 2017, Nice, France,

Vollrath M, Engert J, Winter G

Long-term release of Ranibizumab from lipid based implants for intravitreal treatment of AMD. DPhG Annual Meeting 2016, 4th to 7th October, Munich, Germany

Vollrath M, Engert J, Winter G

Improving the long-term protein release profile from extruded lipid implants. 10th World Meeting on Pharmaceutics, Biopharmaceutics and Pharmaceutical Technology, 4th to 7th of April 2016, Glasgow, Scotland, UK

Vollrath M, Engert J, Winter G

Solid lipid implants for long-term release of pharmaceutical proteins for intravitreal treatment of AMD. AAPS Annual Meeting and Exposition 2015, 25th to 29th of October 2015, Orlando, FL, USA

XII. APPENDIX

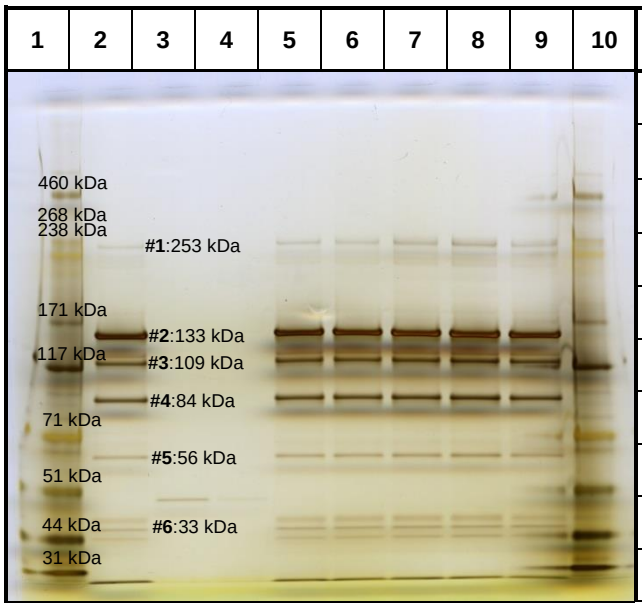

No.	Sample name
1	MW Marker
2	reference
3	BSA 1.80 ng
4	BSA 0.36 ng
5	week 0
6	week 4
7	week 8
8	week 12
9	week 24
10	MW Marker

Figure XII-1: Non-reducing denaturating SDS-PAGE of reconstituted mAb lyophilisates after a storage period of 0, 4, 8, 12 and 24 weeks at 4°C.

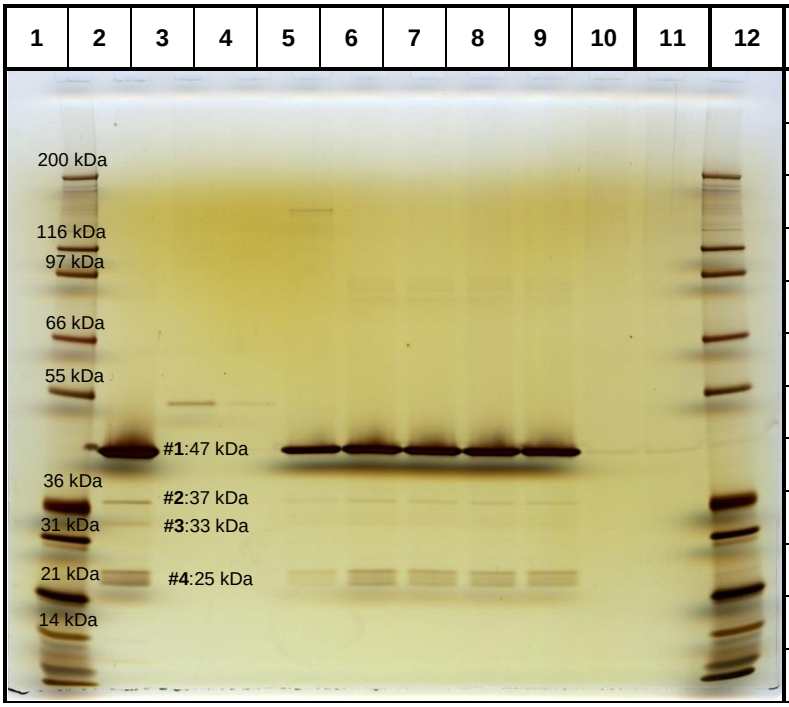

No.	Sample name
1	MW Marker
2	reference
3	BSA 1.80 ng
4	BSA 0.36 ng
5	week 0
6	week 4
7	week 8
8	week 12
9	week 24
10	blank
11	blank
12	MW Marker

Figure XII-2: Non-reducing denaturating SDS-PAGE of reconstituted Ranibizumab lyophilisates after a storage period of 0, 4, 8, 12 and 24 weeks at 4°C.

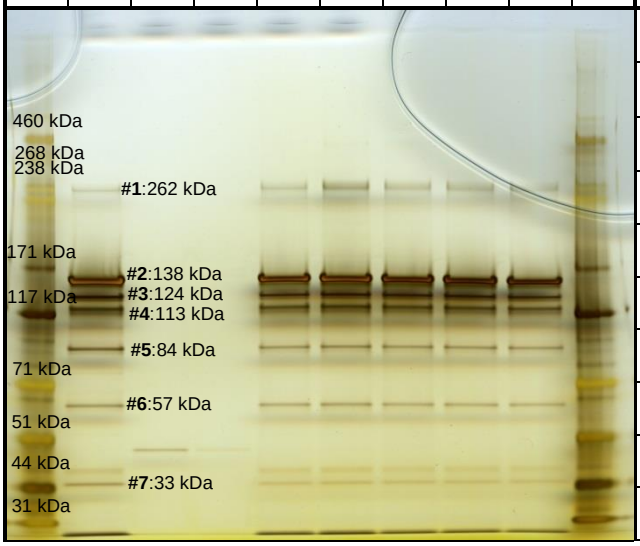

No.	Sample name
1	MW Marker
2	reference
3	BSA 1.80 ng
4	BSA 0.36 ng
5	week 0
6	week 4
7	week 8
8	week 12
9	week 24
10	MW Marker

Figure XII-3: Non-reducing denaturating SDS-PAGE of reconstituted Bevacizumab lyophilisates after a storage period of 0, 4, 8, 12 and 24 weeks at 4°C.

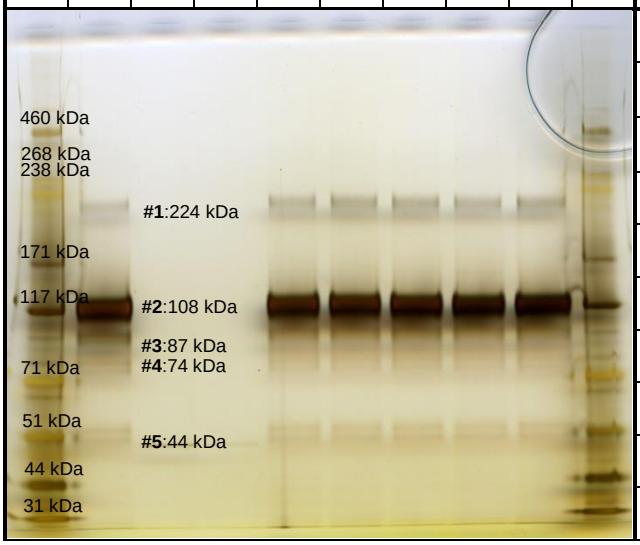

No.	Sample name
1	MW Marker
2	reference
3	BSA 1.80 ng
4	BSA 0.36 ng
5	week 0
6	week 4
7	week 8
8	week 12
9	week 24
10	MW Marker

Figure XII-4: Non-reducing denaturating SDS-PAGE of reconstituted Aflibercept lyophilisates after a storage period of 0, 4, 8, 12 and 24 weeks at 4°C.

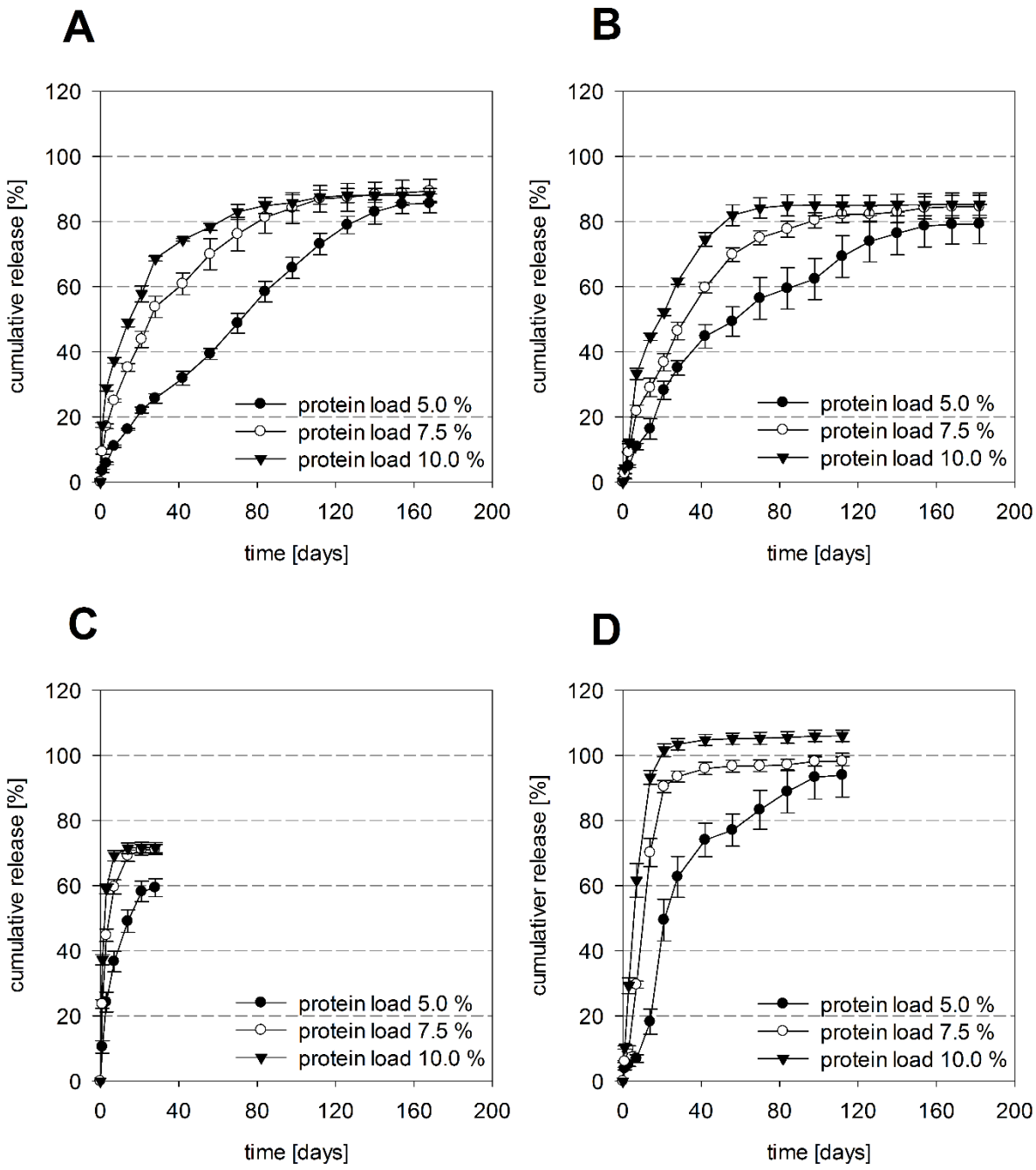

Figure XII-5: Cumulative release of (A) mAb, (B) Ranibizumab, (C) Bevacizumab and (D) Aflibercept from SLIs manufactured with pre-melted lipids. Lipid implants were produced with different percentages of protein lyophilisate in a 1:1 [w/w] formulation with HP-β-CD resulting in a final protein load of 5 %, 7.5 % and 10 % per implant.

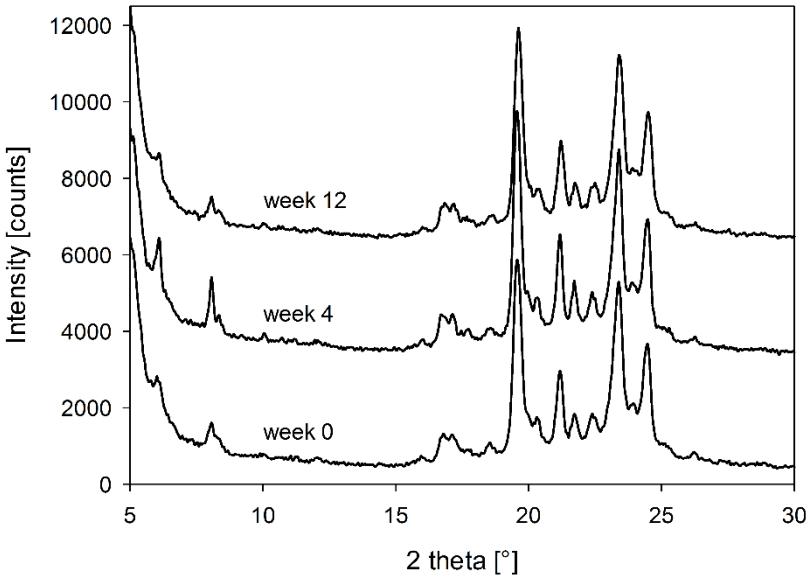

Figure XII-6: Diffraction patterns of SLIs produced with conventional extrusion technique. SLIs were stored for 0, 4 and 12 weeks at 4°C.

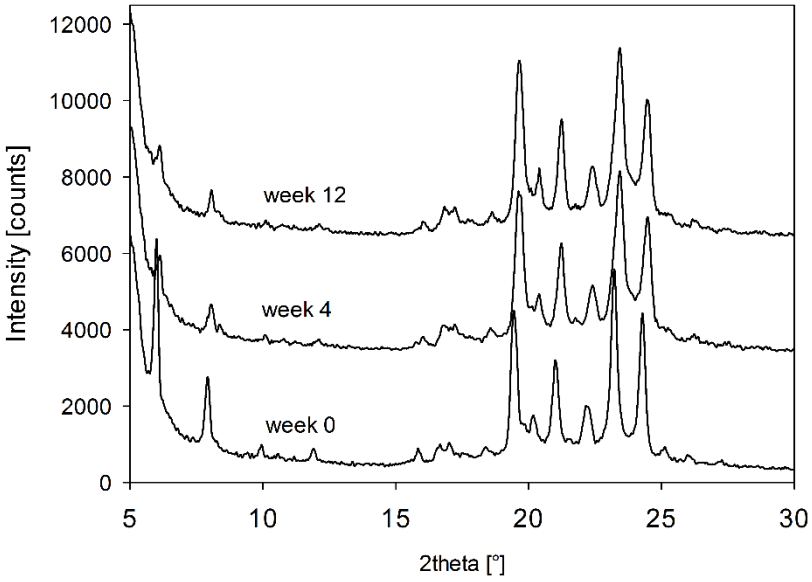

Figure XII-7: Diffraction patterns of SLIs extruded with pre-melted lipids. SLIs were stored for 0, 4 and 12 weeks at 4°C.

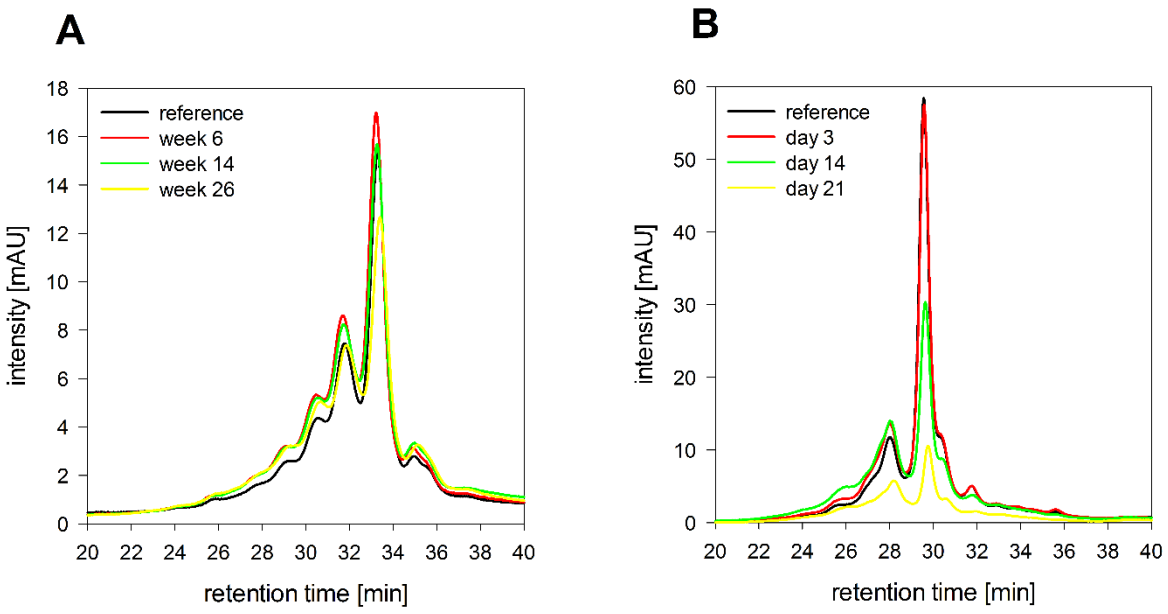

Figure XII-8: Chromatogram of (A) mAb and (B) Bevacizumab using a Dionex ProPac® WCX-10 column for separation of charge variants. For mAb, samples were analysed after 6, 14 and 26 weeks of release. Released Bevacizumab was analysed after 3, 14 and 21 days. For both proteins, the main charge variant decreased while the percentage of acidic subspecies increased.

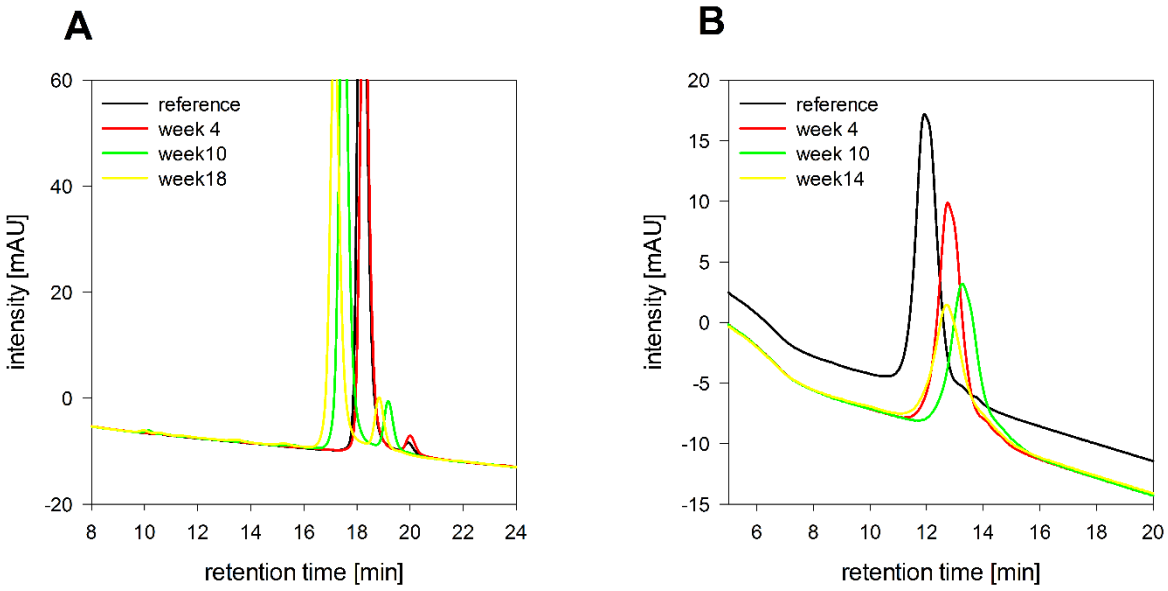

Figure XII-9: Chromatograms of (A) Ranibizumab and (B) Aflibercept using a Dionex MAbPac™ HIC-10 column for separation of charge variants. For Ranibizumab, samples were analysed after 4, 10 and 18 weeks of release. Released Aflibercept was analysed after 4, 10 and 14 weeks. For both proteins, the main charge variant shifted to shorter retention times upon incubation.

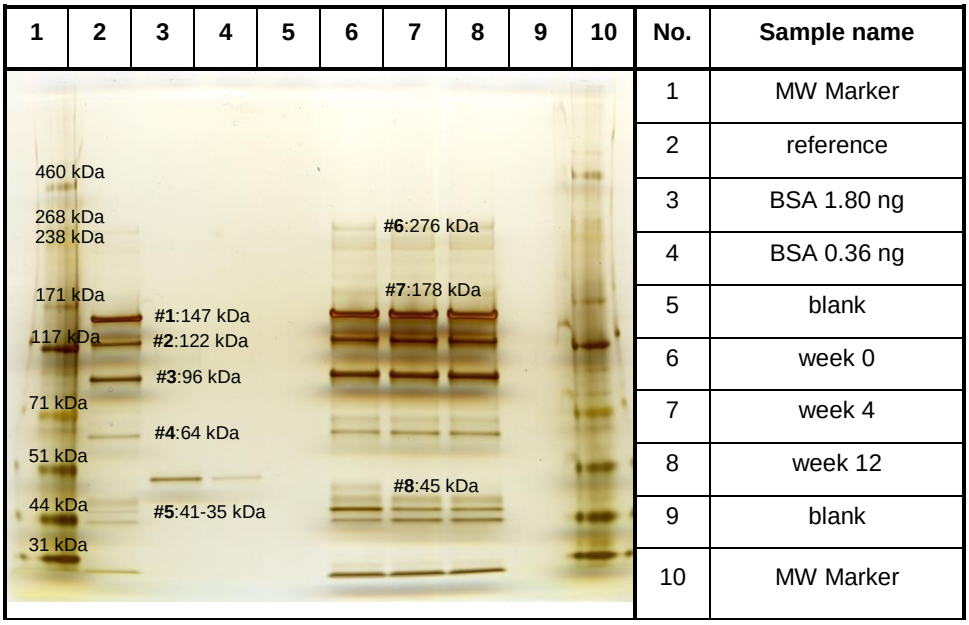

No.	Sample name
1	MW Marker
2	reference
3	BSA 1.80 ng
4	BSA 0.36 ng
5	blank
6	week 0
7	week 4
8	week 12
9	blank
10	MW Marker

Figure XII-10: Non-reducing denaturating SDS-PAGE gel of released mAb fractions from the first week of release after different storage times (0 weeks to 12 weeks). Only samples comprising the 3:1 [w/w] lyophilisate are displayed.

Table XII-1: Overview of pH of samples incubated with H12, D118 and RG 755 S rods and without any additives (PBS, negative control) after 0 weeks and 8 weeks at 35°C and 40 rpm.

	PBS		H12 rods		D118 rods		PLGA rods	
	week 0	**week 8**	**week 0**	**week 8**	**week 0**	**week 8**	**week 0**	**week 8**
PBS	7.40 (±0.02)	7.37 (±0.01)	7.40 (±0.02)	7.37 (±0.01)	7.40 (±0.02)	7.37 (±0.01)	7.40 (±0.02)	7.37 (±0.01)
mAb	6.89 (±0.11)	6.94 (±0.01)	6.94 (±0.05)	6.90 (±0.00)	6.96 (±0.07)	6.91 (±0.00)	6.88 (±0.03)	6.83 (±0.08)
Ranibizumab	6.99 (±0.02)	7.07 (±0.02)	6.98 (±0.07)	7.01 (±0.02)	6.99 (±0.04)	7.04 (±0.01)	7.00 (±0.03)	7.06 (±0.01)
Bevacizumab	6.78 (±0.02)	6.91 (±0.02)	6.84 (±0.06)	6.89 (±0.01)	6.87 (±0.05)	6.90 (±0.01)	6.79 (±0.03)	6.92 (±0.01)
Aflibercept	6.88 (±0.03)	6.89 (±0.01)	6.89 (±0.05)	6.87 (±0.02)	6.89 (±0.02)	6.89 (±0.02)	6.89 (±0.06)	6.89 (±0.01)

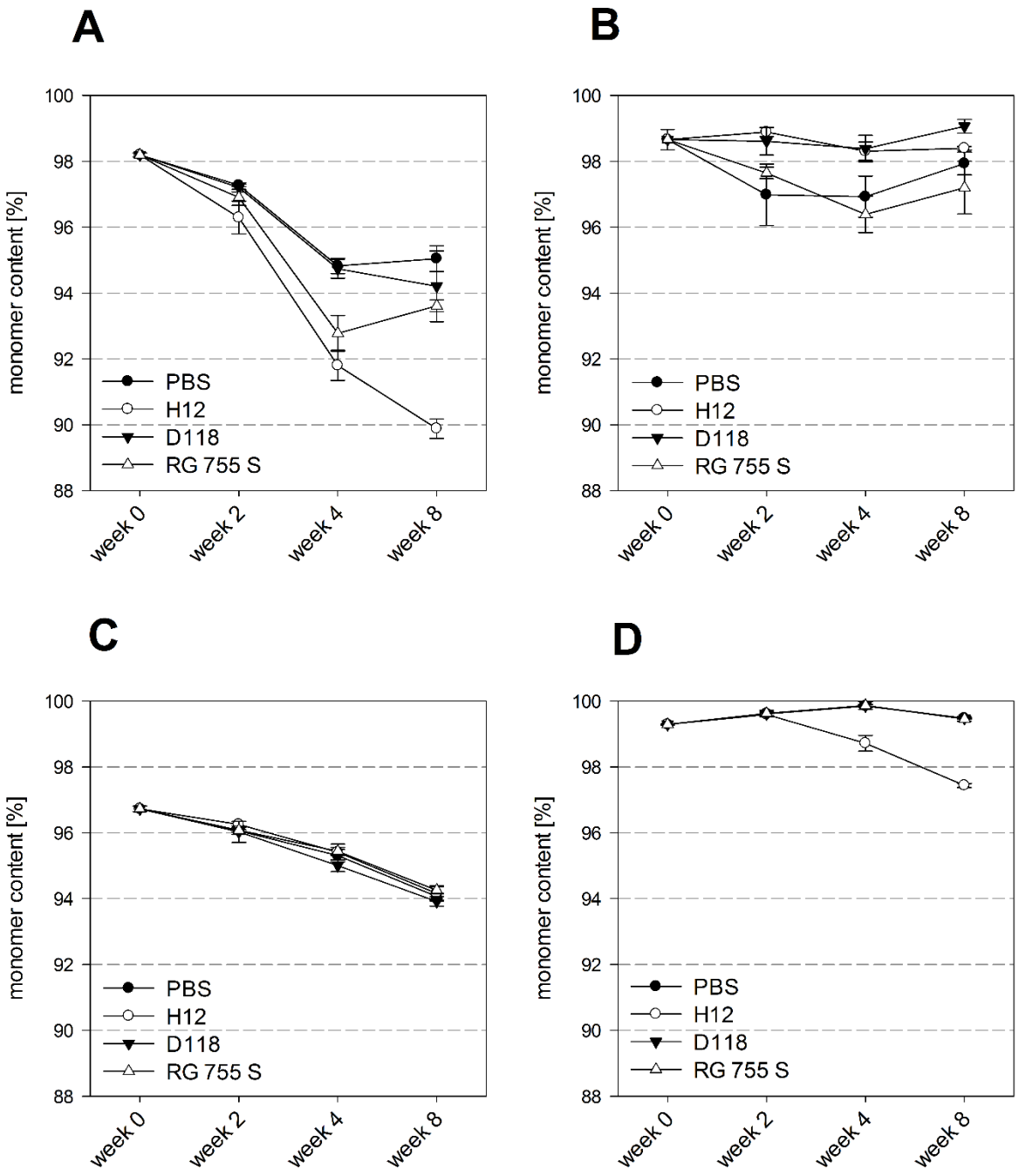

Figure XII-11: Monomer content of (A) mAb, (B) Ranibizumab, (C) Bevacizumab and (D) Aflibercept upon 8-week incubation in PBS (negative control) or with H12, D118 and RG 755 S rods.

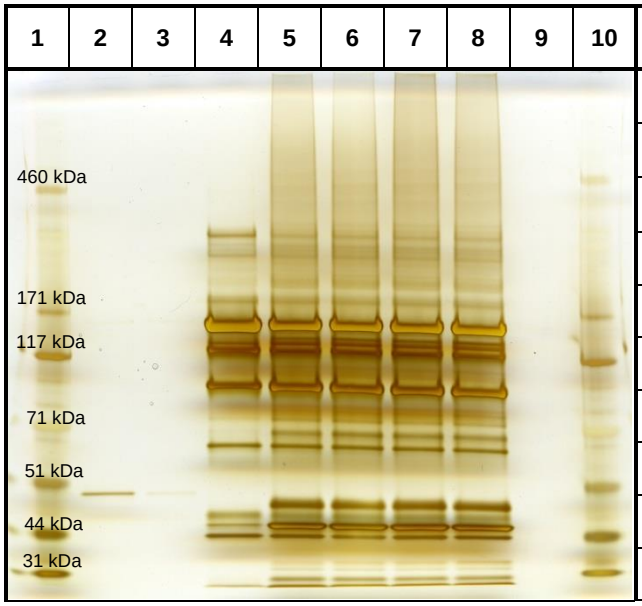

No.	Sample name
1	MW Marker
2	BSA 1.80 ng
3	BSA 0.36 ng
4	reference
5	PBS_week 8
6	H12_week 8
7	D118_week 8
8	RG 755 S_week 8
9	blank
10	MW Marker

Figure XII-12: Non-reducing denaturating SDS-PAGE gel of mAb incubated for 8 weeks with H12, D118 and RG 755 S rods or in PBS (negative control) at 35°C.

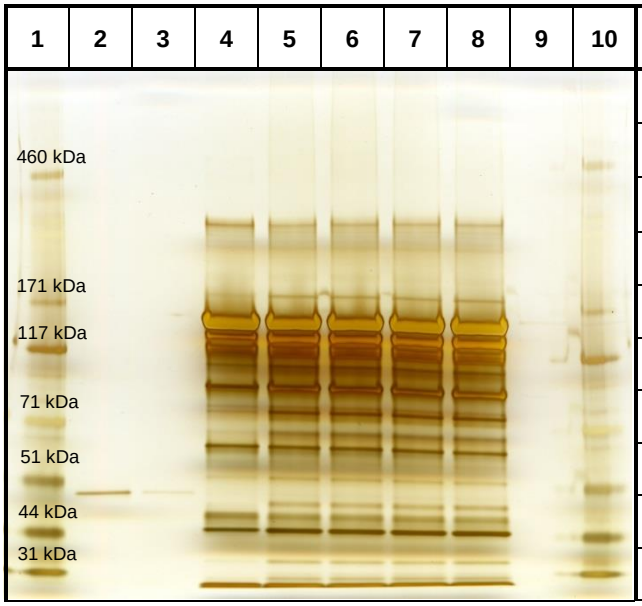

No.	Sample name
1	MW Marker
2	BSA 1.80 ng
3	BSA 0.36 ng
4	reference
5	PBS_week 8
6	H12_week 8
7	D118_week 8
8	RG 755 S_week 8
9	blank
10	MW Marker

Figure XII-13: Non-reducing denaturating SDS-PAGE gel of Bevacizumab incubated for 8 weeks with H12, D118 and RG 755 S rods or in PBS (negative control) at 35°C.

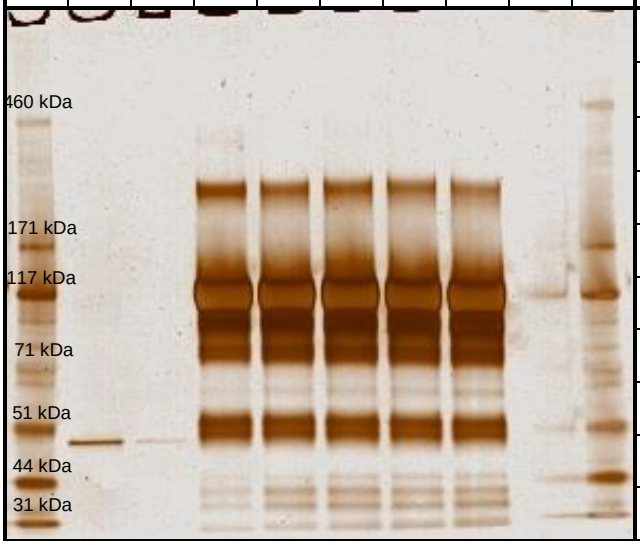

No.	Sample name
1	MW Marker
2	BSA 1.80 ng
3	BSA 0.36 ng
4	reference
5	PBS_week 8
6	H12_week 8
7	D118_week 8
8	RG 755 S_week 8
9	blank
10	MW Marker

Figure XII-14: Non-reducing denaturating SDS-PAGE gel of Aflibercept incubated for 8 weeks with H12, D118 and RG 755 S rods or in PBS (negative control) at 35°C.

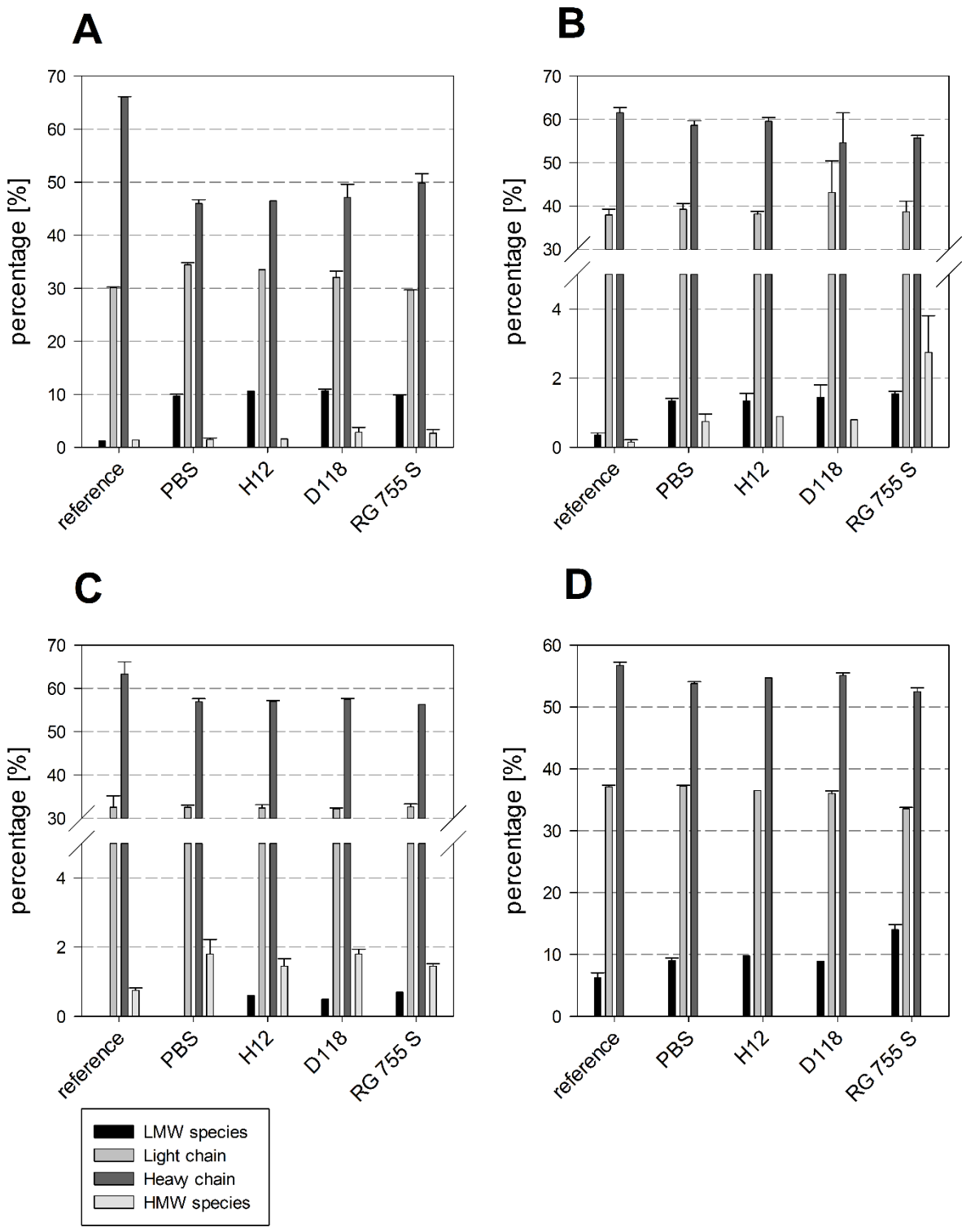

Figure XII-15: Capillary gel electrophoresis applying a 2100 Bioanalyzer under reducing denaturating conditions of (A) mAb, (B) Ranibizumab, (C) Bevacizumab, and (D) Aflibercept samples after an 8-week incubation with H12, D118 or RG 755 S rods. The protein bulk is defined as reference whereby incubation in PBS without any rods served as negative control.

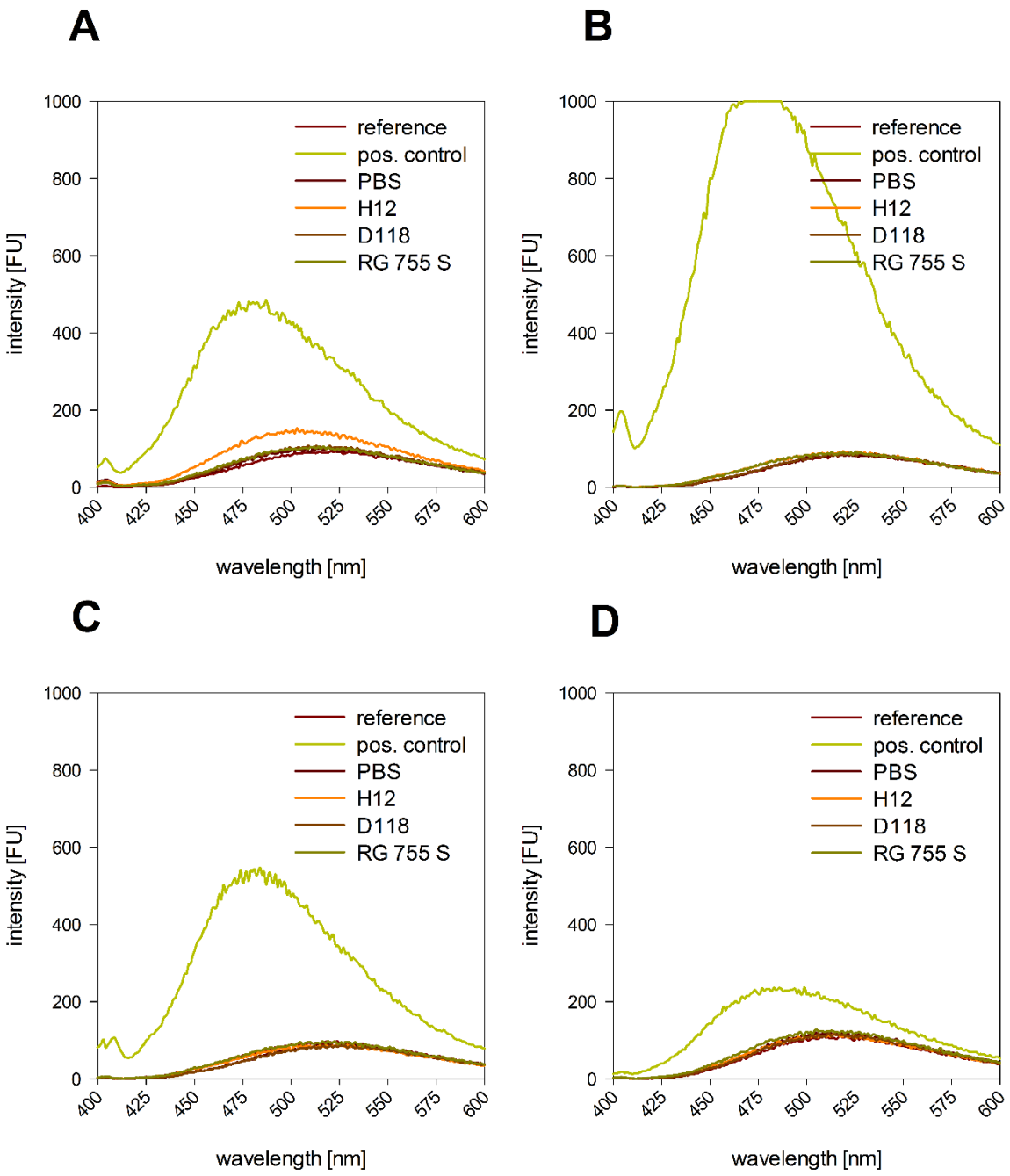

Figure XII-16: Extrinsic fluorescence measurements of (A) mAb, (B) Ranibizumab, (C) Bevacizumab and (D) Aflibercept samples after an 8-week incubation with H12, D118 or RG 755 S rods. The protein bulk is defined as reference whereby incubation in PBS without any rods served as negative control. As positive control, proteins were exposed to 80°C and 400 rpm for 10 min.

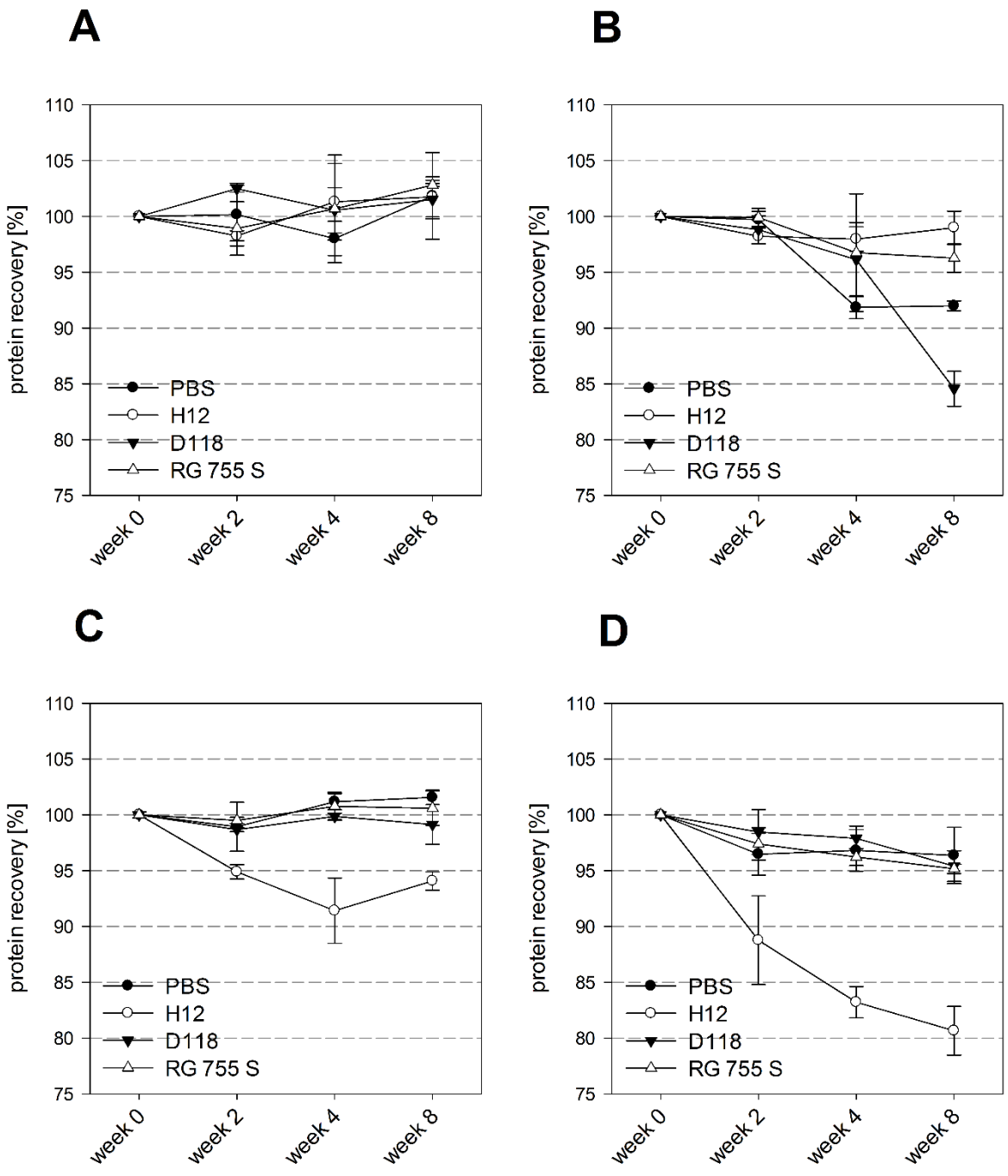

Figure XII-17: Protein recovery of (A) mAb, (B) Ranibizumab, (C) Bevacizumab and (D) Aflibercept upon 8-week incubation in PBS (negative control) or with H12, D118 or RG 755 S rods, respectively, measured by SE-HPLC.

Table XII-2: Overview of bending strength measured after the first and the second extrusion in comparison to single extrusion.

Extrusion settings	Bending strength [N]		
	First extrusion	**Second extrusion**	**Single extrusion**
10% in 50:50/35°C_33°C		1.978 (±0.43)	2.212 (±0.14)
10% in 50:50/35°C_35°C	2.025 (±0.39)	2.393 (±0.10)	2.025 (±0.39)
10% in 50:50/35°C_37°C		1.966 (±0.38)	1.312 (±0.22)
20% in 0:100/65°C_35°C	1.448 (±0.29)	1.458 (±0.33)	-
20% in 100:0/35°C_35°C	0.875 (±0.34)	1.424 (±0.19)	-

Table XII-3: True density of lipid implants measured after the first and second extrusion run applying different extrusion settings in comparison to single extrusion.

Extrusion settings	True density [g/cm^3]		
	First extrusion	**Second extrusion**	**Single extrusion**
10% in 50:50/35°C_33°C	1.031 (±0.002)	1.050 (±0.002)	1.049 (±0.002)
10% in 50:50/35°C_35°C	1.031 (±0.002)	1.048 (±0.002)	1.031 (±0.002)
10% in 50:50/35°C_37°C	1.031 (±0.002)	0.977 (±0.002)	1.008 (±0.005)
20% in 0:100/65°C_35°C	1.086 (±0.002)	1.057 (±0.004)	-
20% in 100:0/35°C_35°C	1.080 (±0.001)	1.056 (±0.002)	-

XIII. REFERENCES

[1] Evens, R. P., Pharma Success in Product Development-Does Biotechnology Change the Paradigm in Product Development and Attrition. AAPS J, 18 (2016): 281-285.
[2] Kinch, M. S., The rise (and decline?) of biotechnology. Drug Discov. Today, 19 (2014): 1686-1690.
[3] Walsh, G., Pharmaceutical biotechnology products approved within the European Union. Eur. J. Pharm. Biopharm., 55 (2003): 3-10.
[4] van de Weert, M., Jorgensen, L., Horn Moeller, E., Frokjaer, S., Factors of importance for a successful delivery system for proteins. Expert Opin Drug Deliv, 2 (2005): 1029-1037.
[5] Frokjaer, S., Otzen, D. E., Protein drug stability: a formulation challenge. Nat. Rev. Drug Discov., 4 (2005): 298-306.
[6] Serno, T.,Inhibition of therapeutic protein aggregation by cyclodextrins. Ludwig-Maximilians-University Munich, 2010.
[7] Serno, T., Carpenter, J. F., Randolph, T. W., Winter, G., Inhibition of agitation-induced aggregation of an IgG-antibody by hydroxypropyl-beta-cyclodextrin. J. Pharm. Sci., 99 (2010): 1193-1206.
[8] Serno, T., Geidobler, R., Winter, G., Protein stabilization by cyclodextrins in the liquid and dried state. Adv Drug Deliv Rev, 63 (2011): 1086-1106.
[9] Lee, J. C., Timasheff, S. N., The stabilization of proteins by sucrose. J. Biol. Chem., 256 (1981): 7193-7201.
[10] Ruan, K., Xu, C., Li, T., Li, J., Lange, R., Balny, C., The thermodynamic analysis of protein stabilization by sucrose and glycerol against pressure-induced unfolding. Eur. J. Biochem., 270 (2003): 1654-1661.
[11] Graziano, G., How does sucrose stabilize the native state of globular proteins? Int. J. Biol. Macromol., 50 (2012): 230-235.
[12] Serno, T., Hartl, E., Besheer, A., Miller, R., Winter, G., The role of polysorbate 80 and HPßCD at the air-water interface of IgG solutions. Pharm. Res., 30 (2013): 117-130.
[13] Hoffmann, C., Blume, A., Miller, I., Garidel, P., Insights into protein-polysorbate interactions analysed by means of isothermal titration and differential scanning calorimetry. Eur. Biophys. J., 38 (2009): 557-568.
[14] Lee, H. J., McAuley, A., Schilke, K. F., McGuire, J., Molecular origins of surfactant-mediated stabilization of protein drugs. Adv Drug Deliv Rev, 63 (2011): 1160-1171.
[15] Foldvari, M., Attah-Poku, S., Hu, J., Li, Q., Hughes, H., Babiuk, L. A., Kruger, S., Palmitoyl derivatives of interferon alpha: potential for cutaneous delivery. J. Pharm. Sci., 87 (1998): 1203-1208.
[16] Wang, J., Shen, D., Shen, W. C., Preparation, purification, and characterization of a reversibly lipidized desmopressin with potentiated anti-diuretic activity. Pharm. Res., 16 (1999): 1674-1679.
[17] Bhadra, D., Bhadra, S., Jain, P., Jain, N. K., Pegnology: a review of PEG-ylated systems. Pharmazie, 57 (2002): 5-29.
[18] Matthews, S. J., McCoy, C., Peginterferon alfa-2a: a review of approved and investigational uses. Clin. Ther., 26 (2004): 991-1025.
[19] Liebner, R., Meyer, M., Hey, T., Winter, G., Besheer, A., Head to head comparison of the formulation and stability of concentrated solutions of HESylated versus PEGylated anakinra. J. Pharm. Sci., 104 (2015): 515-526.
[20] Liebner, R., Mathaes, R., Meyer, M., Hey, T., Winter, G., Besheer, A., Protein HESylation for half-life extension: synthesis, characterization and pharmacokinetics of HESylated anakinra. Eur. J. Pharm. Biopharm., 87 (2014): 378-385.
[21] Moeller, E. H., Jorgensen, L., Alternative routes of administration for systemic delivery of protein pharmaceuticals. Drug Discov Today Technol, 5 (2008): 89-94.

[22] Degim, I. T., Celebi, N., Controlled delivery of peptides and proteins. Curr. Pharm. Des., 13 (2007): 99-117.
[23] Veuillez, F., Kalia, Y. N., Jacques, Y., Deshusses, J., Buri, P., Factors and strategies for improving buccal absorption of peptides. Eur. J. Pharm. Biopharm., 51 (2001): 93-109.
[24] du Plessis, L. H., Kotze, A. F., Junginger, H. E., Nasal and rectal delivery of insulin with chitosan and N-trimethyl chitosan chloride. Drug Deliv., 17 (2010): 399-407.
[25] Casettari, L., Illum, L., Chitosan in nasal delivery systems for therapeutic drugs. J. Control. Release, 190 (2014): 189-200.
[26] Nema, T., Jain, A., Jain, A., Shilpi, S., Gulbake, A., Hurkat, P., Jain, S. K., Insulin delivery through nasal route using thiolated microspheres. Drug Deliv., 20 (2013): 210-215.
[27] Germershaus, O., Schultz, I., Luhmann, T., Beck-Broichsitter, M., Hogger, P., Meinel, L., Insulin-like growth factor-I aerosol formulations for pulmonary delivery. Eur. J. Pharm. Biopharm., 85 (2013): 61-68.
[28] Hofer, M., Winter, G., Myschik, J., Recombinant spider silk particles for controlled delivery of protein drugs. Biomaterials, 33 (2012): 1554-1562.
[29] Schweizer, D., Serno, T., Goepferich, A., Controlled release of therapeutic antibody formats. Eur. J. Pharm. Biopharm., 88 (2014): 291-309.
[30] Steinbrook, R., The price of sight--ranibizumab, bevacizumab, and the treatment of macular degeneration. N. Engl. J. Med., 355 (2006): 1409-1412.
[31] Ahmann, F. R., Citrin, D. L., deHaan, H. A., Guinan, P., Jordan, V. C., Kreis, W., Scott, M., Trump, D. L., Zoladex: a sustained-release, monthly luteinizing hormone-releasing hormone analogue for the treatment of advanced prostate cancer. J. Clin. Oncol., 5 (1987): 912-917.
[32] Dlugi, A. M., Miller, J. D., Knittle, J., Lupron depot (leuprolide acetate for depot suspension) in the treatment of endometriosis: a randomized, placebo-controlled, double-blind study. Lupron Study Group. Fertil. Steril., 54 (1990): 419-427.
[33] Tunn, U. W., Gruca, D., Bacher, P., Six-month leuprorelin acetate depot formulations in advanced prostate cancer: a clinical evaluation. Clin. Interv. Aging, 8 (2013): 457-464.
[34] Lee, P. A., Klein, K., Mauras, N., Neely, E. K., Bloch, C. A., Larsen, L., Mattia-Goldberg, C., Chwalisz, K., Efficacy and safety of leuprolide acetate 3-month depot 11.25 milligrams or 30 milligrams for the treatment of central precocious puberty. J. Clin. Endocrinol. Metab., 97 (2012): 1572-1580.
[35] Kappy, M., Stuart, T., Perelman, A., Clemons, R., Suppression of gonadotropin secretion by a long-acting gonadotropin-releasing hormone analog (leuprolide acetate, Lupron Depot) in children with precocious puberty. J. Clin. Endocrinol. Metab., 69 (1989): 1087-1089.
[36] Sartor, O., Eligard: leuprolide acetate in a novel sustained-release delivery system. Urology, 61 (2003): 25-31.
[37] Braeckman, J., Michielsen, D., Efficacy and tolerability of 1- and 3-month leuprorelin acetate depot formulations (Eligard((R))/Depo-Eligard((R))) for advanced prostate cancer in daily practice: a Belgian prospective non-interventional study. Arch. Med. Sci., 10 (2014): 477-483.
[38] Kemp, S. F., Fielder, P. J., Attie, K. M., Blethen, S. L., Reiter, E. O., Ford, K. M., Marian, M., Dao, L. N., Lee, H. J., Saenger, P., Pharmacokinetic and pharmacodynamic characteristics of a long-acting growth hormone (GH) preparation (nutropin depot) in GH-deficient children. J. Clin. Endocrinol. Metab., 89 (2004): 3234-3240.
[39] DeYoung, M. B., MacConell, L., Sarin, V., Trautmann, M., Herbert, P., Encapsulation of exenatide in poly-(D,L-lactide-co-glycolide) microspheres produced an investigational long-acting once-weekly formulation for type 2 diabetes. Diabetes Technol. Ther., 13 (2011): 1145-1154.
[40] Scheen, A. J., [Bydureon: first once weekly GLP-1 receptor agonist (exenatide LAR)]. Rev. Med. Liege, 69 (2014): 214-219.
[41] Wysham, C. H., MacConell, L. A., Maggs, D. G., Zhou, M., Griffin, P. S., Trautmann, M. E., Five-year efficacy and safety data of exenatide once weekly: long-term results from the DURATION-1 randomized clinical trial. Mayo Clin. Proc., 90 (2015): 356-365.
[42] Diamant, M., Van Gaal, L., Guerci, B., Stranks, S., Han, J., Malloy, J., Boardman, M. K., Trautmann, M. E., Exenatide once weekly versus insulin glargine for type 2 diabetes

(DURATION-3): 3-year results of an open-label randomised trial. Lancet Diabetes Endocrinol, 2 (2014): 464-473.
[43] Kim, J. H., Taluja, A., Knutson, K., Han Bae, Y., Stability of bovine serum albumin complexed with PEG-poly(L-histidine) diblock copolymer in PLGA microspheres. J. Control. Release, 109 (2005): 86-100.
[44] Morlock, M., Kissel, T., Li, Y. X., Koll, H., Winter, G., Erythropoietin loaded microspheres prepared from biodegradable LPLG-PEO-LPLG triblock copolymers: protein stabilization and in-vitro release properties. J. Control. Release, 56 (1998): 105-115.
[45] Bittner, B., Morlock, M., Koll, H., Winter, G., Kissel, T., Recombinant human erythropoietin (rhEPO) loaded poly(lactide-co-glycolide) microspheres: influence of the encapsulation technique and polymer purity on microsphere characteristics. Eur. J. Pharm. Biopharm., 45 (1998): 295-305.
[46] Bittner, B., Witt, C., Mader, K., Kissel, T., Degradation and protein release properties of microspheres prepared from biodegradable poly(lactide-co-glycolide) and ABA triblock copolymers: influence of buffer media on polymer erosion and bovine serum albumin release. J. Control. Release, 60 (1999): 297-309.
[47] Capan, Y., Jiang, G., Giovagnoli, S., Na, K. H., DeLuca, P. P., Preparation and characterization of poly(D,L-lactide-co-glycolide) microspheres for controlled release of human growth hormone. AAPS PharmSciTech, 4 (2003): E28.
[48] Rafi, M., Singh, S. M., Kanchan, V., Anish, C. K., Panda, A. K., Controlled release of bioactive recombinant human growth hormone from PLGA microparticles. J. Microencapsul., 27 (2010): 552-560.
[49] Ibrahim, M. A., Ismail, A., Fetouh, M. I., Gopferich, A., Stability of insulin during the erosion of poly(lactic acid) and poly(lactic-co-glycolic acid) microspheres. J. Control. Release, 106 (2005): 241-252.
[50] Meinel, L., Illi, O. E., Zapf, J., Malfanti, M., Peter Merkle, H., Gander, B., Stabilizing insulin-like growth factor-I in poly(D,L-lactide-co-glycolide) microspheres. J. Control. Release, 70 (2001): 193-202.
[51] Lei, L., Wang, S., Wu, H., Ju, W., Peng, J., Qahtan, A. S., Chen, C., Lu, Y., Peng, J., Zhang, X., Nie, H., Optimization of release pattern of FGF-2 and BMP-2 for osteogenic differentiation of low-population density hMSCs. J. Biomed. Mater. Res. A, 103 (2015): 252-261.
[52] Kang, J., Schwendeman, S. P., Comparison of the effects of Mg(OH)2 and sucrose on the stability of bovine serum albumin encapsulated in injectable poly(D,L-lactide-co-glycolide) implants. Biomaterials, 23 (2002): 239-245.
[53] Zhu, G., Schwendeman, S. P., Stabilization of proteins encapsulated in cylindrical poly(lactide-co-glycolide) implants: mechanism of stabilization by basic additives. Pharm. Res., 17 (2000): 351-357.
[54] Al-Tahami, K., Meyer, A., Singh, J., Poly lactic acid based injectable delivery systems for controlled release of a model protein, lysozyme. Pharm. Dev. Technol., 11 (2006): 79-86.
[55] Matschke, C., Isele, U., van Hoogevest, P., Fahr, A., Sustained-release injectables formed in situ and their potential use for veterinary products. J. Control. Release, 85 (2002): 1-15.
[56] Arakawa, T., Kita, Y., Carpenter, J. F., Protein--solvent interactions in pharmaceutical formulations. Pharm. Res., 8 (1991): 285-291.
[57] Mahler, H. C., Senner, F., Maeder, K., Mueller, R., Surface activity of a monoclonal antibody. J. Pharm. Sci., 98 (2009): 4525-4533.
[58] Brunner, A., Mader, K., Gopferich, A., pH and osmotic pressure inside biodegradable microspheres during erosion. Pharm. Res., 16 (1999): 847-853.
[59] Li, L., Schwendeman, S. P., Mapping neutral microclimate pH in PLGA microspheres. J. Control. Release, 101 (2005): 163-173.
[60] van de Weert, M., Hennink, W. E., Jiskoot, W., Protein instability in poly(lactic-co-glycolic acid) microparticles. Pharm. Res., 17 (2000): 1159-1167.
[61] Lucke, A., Gopferich, A., Acylation of peptides by lactic acid solutions. Eur. J. Pharm. Biopharm., 55 (2003): 27-33.
[62] Crotts, G., Park, T. G., Protein delivery from poly(lactic-co-glycolic acid) biodegradable microspheres: release kinetics and stability issues. J. Microencapsul., 15 (1998): 699-713.

[63] Elliott Donaghue, I., Shoichet, M. S., Controlled release of bioactive PDGF-AA from a hydrogel/nanoparticle composite. Acta Biomater., 25 (2015): 35-42.
[64] Sah, H., Stabilization of proteins against methylene chloride/water interface-induced denaturation and aggregation. J. Control. Release, 58 (1999): 143-151.
[65] Zhu, G., Mallery, S. R., Schwendeman, S. P., Stabilization of proteins encapsulated in injectable poly (lactide- co-glycolide). Nat. Biotechnol., 18 (2000): 52-57.
[66] Gao, H., Wang, Y. N., Fan, Y. G., Ma, J. B., Conjugates of poly(DL-lactide-co-glycolide) on amino cyclodextrins and their nanoparticles as protein delivery system. J. Biomed. Mater. Res. A, 80 (2007): 111-122.
[67] Tang, Y., Singh, J., Biodegradable and biocompatible thermosensitive polymer based injectable implant for controlled release of protein. Int. J. Pharm., 365 (2009): 34-43.
[68] Park, W., Kim, D., Kang, H. C., Bae, Y. H., Na, K., Multi-arm histidine copolymer for controlled release of insulin from poly(lactide-co-glycolide) microsphere. Biomaterials, 33 (2012): 8848-8857.
[69] Taluja, A., Bae, Y. H., Role of a novel multifunctional excipient poly(ethylene glycol)-block-oligo(vinyl sulfadimethoxine) in controlled release of lysozyme from PLGA microspheres. Int. J. Pharm., 358 (2008): 50-59.
[70] Niu, X., Liu, Z., Hu, J., Rambhia, K. J., Fan, Y., Ma, P. X., Microspheres Assembled from Chitosan-Graft-Poly(lactic acid) Micelle-Like Core-Shell Nanospheres for Distinctly Controlled Release of Hydrophobic and Hydrophilic Biomolecules. Macromol. Biosci., 16 (2016): 1039-1047.
[71] Pakulska, M. M., Elliott Donaghue, I., Obermeyer, J. M., Tuladhar, A., McLaughlin, C. K., Shendruk, T. N., Shoichet, M. S., Encapsulation-free controlled release: Electrostatic adsorption eliminates the need for protein encapsulation in PLGA nanoparticles. Sci Adv, 2 (2016): e1600519.
[72] Chang, D. P., Garripelli, V. K., Rea, J., Kelley, R., Rajagopal, K., Investigation of Fragment Antibody Stability and Its Release Mechanism from Poly(Lactide-co-Glycolide)-Triacetin Depots for Sustained-Release Applications. J. Pharm. Sci., 104 (2015): 3404-3417.
[73] Ghalanbor, Z., Korber, M., Bodmeier, R., Interdependency of protein-release completeness and polymer degradation in PLGA-based implants. Eur. J. Pharm. Biopharm., 85 (2013): 624-630.
[74] Nagpal, K., Singh, S. K., Mishra, D. N., Chitosan nanoparticles: a promising system in novel drug delivery. Chem. Pharm. Bull. (Tokyo), 58 (2010): 1423-1430.
[75] Amidi, M., Mastrobattista, E., Jiskoot, W., Hennink, W. E., Chitosan-based delivery systems for protein therapeutics and antigens. Adv Drug Deliv Rev, 62 (2010): 59-82.
[76] Hou, Y., Hu, J., Park, H., Lee, M., Chitosan-based nanoparticles as a sustained protein release carrier for tissue engineering applications. J. Biomed. Mater. Res. A, 100 (2012): 939-947.
[77] Zhang, Y., Dong, R., Park, Y., Bohner, M., Zhang, X., Ting, K., Soo, C., Wu, B. M., Controlled release of NELL-1 protein from chitosan/hydroxyapatite-modified TCP particles. Int. J. Pharm., 511 (2016): 79-89.
[78] Soran, Z., Aydin, R. S., Gumusderelioglu, M., Chitosan scaffolds with BMP-6 loaded alginate microspheres for periodontal tissue engineering. J. Microencapsul., 29 (2012): 770-780.
[79] Wang, L. Y., Gu, Y. H., Su, Z. G., Ma, G. H., Preparation and improvement of release behavior of chitosan microspheres containing insulin. Int. J. Pharm., 311 (2006): 187-195.
[80] Khodaverdi, E., Tafaghodi, M., Ganji, F., Abnoos, K., Naghizadeh, H., In vitro insulin release from thermosensitive chitosan hydrogel. AAPS PharmSciTech, 13 (2012): 460-466.
[81] Oak, M., Singh, J., Controlled delivery of basal level of insulin from chitosan-zinc-insulin-complex-loaded thermosensitive copolymer. J. Pharm. Sci., 101 (2012): 1079-1096.
[82] Shi, W., Ji, Y., Zhang, X., Shu, S., Wu, Z., Characterization of pH- and thermosensitive hydrogel as a vehicle for controlled protein delivery. J. Pharm. Sci., 100 (2011): 886-895.
[83] Lee, M., Li, W., Siu, R. K., Whang, J., Zhang, X., Soo, C., Ting, K., Wu, B. M., Biomimetic apatite-coated alginate/chitosan microparticles as osteogenic protein carriers. Biomaterials, 30 (2009): 6094-6101.

[84] Zhu, Y., Wang, J., Wu, J., Zhang, J., Wan, Y., Wu, H., Injectable hydrogels embedded with alginate microspheres for controlled delivery of bone morphogenetic protein-2. Biomed Mater, 11 (2016): 025010.
[85] Zuo, Q., Guo, R., Liu, Q., Hong, A., Shi, Y., Kong, Q., Huang, Y., He, L., Xue, W., Heparin-conjugated alginate multilayered microspheres for controlled release of bFGF. Biomed Mater, 10 (2015): 035008.
[86] Zhai, P., Chen, X. B., Schreyer, D. J., Preparation and characterization of alginate microspheres for sustained protein delivery within tissue scaffolds. Biofabrication, 5 (2013): 015009.
[87] Schweizer, D., Schonhammer, K., Jahn, M., Gopferich, A., Protein-polyanion interactions for the controlled release of monoclonal antibodies. Biomacromolecules, 14 (2013): 75-83.
[88] Bazban-Shotorbani, S., Dashtimoghadam, E., Karkhaneh, A., Hasani-Sadrabadi, M. M., Jacob, K. I., Microfluidic Directed Synthesis of Alginate Nanogels with Tunable Pore Size for Efficient Protein Delivery. Langmuir, 32 (2016): 4996-5003.
[89] Marks, M. G., Doillon, C., Silver, F. H., Effects of fibroblasts and basic fibroblast growth factor on facilitation of dermal wound healing by type I collagen matrices. J. Biomed. Mater. Res., 25 (1991): 683-696.
[90] Friess, W., Uludag, H., Foskett, S., Biron, R., Sargeant, C., Characterization of absorbable collagen sponges as recombinant human bone morphogenetic protein-2 carriers. Int. J. Pharm., 185 (1999): 51-60.
[91] Friess, W., Uludag, H., Foskett, S., Biron, R., Sargeant, C., Characterization of absorbable collagen sponges as rhBMP-2 carriers. Int. J. Pharm., 187 (1999): 91-99.
[92] Su, Y., Su, Q., Liu, W., Lim, M., Venugopal, J. R., Mo, X., Ramakrishna, S., Al-Deyab, S. S., El-Newehy, M., Controlled release of bone morphogenetic protein 2 and dexamethasone loaded in core-shell PLLACL-collagen fibers for use in bone tissue engineering. Acta Biomater., 8 (2012): 763-771.
[93] Quinlan, E., Thompson, E. M., Matsiko, A., O'Brien, F. J., Lopez-Noriega, A., Long-term controlled delivery of rhBMP-2 from collagen-hydroxyapatite scaffolds for superior bone tissue regeneration. J. Control. Release, 207 (2015): 112-119.
[94] Sun, H., Wang, J., Deng, F., Liu, Y., Zhuang, X., Xu, J., Li, L., Codelivery and controlled release of stromal cellderived factor1alpha chemically conjugated on collagen scaffolds enhances bone morphogenetic protein2driven osteogenesis in rats. Mol Med Rep, 14 (2016): 737-745.
[95] Hayden, R. S., Vollrath, M., Kaplan, D. L., Effects of clodronate and alendronate on osteoclast and osteoblast co-cultures on silk-hydroxyapatite films. Acta Biomater., 10 (2014): 486-493.
[96] Lovett, M. L., Wang, X., Yucel, T., York, L., Keirstead, M., Haggerty, L., Kaplan, D. L., Silk hydrogels for sustained ocular delivery of anti-vascular endothelial growth factor (anti-VEGF) therapeutics. Eur. J. Pharm. Biopharm., 95 (2015): 271-278.
[97] Reeves, A. R., Spiller, K. L., Freytes, D. O., Vunjak-Novakovic, G., Kaplan, D. L., Controlled release of cytokines using silk-biomaterials for macrophage polarization. Biomaterials, 73 (2015): 272-283.
[98] Guziewicz, N. A., Massetti, A. J., Perez-Ramirez, B. J., Kaplan, D. L., Mechanisms of monoclonal antibody stabilization and release from silk biomaterials. Biomaterials, 34 (2013): 7766-7775.
[99] Dang, W., Saltzman, W. M., Controlled release of macromolecules from a degradable polyanhydride matrix. J. Biomater. Sci. Polym. Ed., 6 (1994): 297-311.
[100] Tabata, Y., Gutta, S., Langer, R., Controlled delivery systems for proteins using polyanhydride microspheres. Pharm. Res., 10 (1993): 487-496.
[101] Ron, E., Turek, T., Mathiowitz, E., Chasin, M., Hageman, M., Langer, R., Controlled release of polypeptides from polyanhydrides. Proc. Natl. Acad. Sci. U. S. A., 90 (1993): 4176-4180.
[102] Li, X., Petersen, L., Broderick, S., Narasimhan, B., Rajan, K., Identifying factors controlling protein release from combinatorial biomaterial libraries via hybrid data mining methods. ACS Comb Sci, 13 (2011): 50-58.

[103] Benoit, M. A., Baras, B., Gillard, J., Preparation and characterization of protein-loaded poly(epsilon-caprolactone) microparticles for oral vaccine delivery. Int. J. Pharm., 184 (1999): 73-84.
[104] Kim, T. G., Lee, D. S., Park, T. G., Controlled protein release from electrospun biodegradable fiber mesh composed of poly(epsilon-caprolactone) and poly(ethylene oxide). Int. J. Pharm., 338 (2007): 276-283.
[105] Rayaprolu, B. M., Strom, J. G., Design and evaluation of D-alpha tocopheryl polyethylene glycol 1000 succinate emulsified poly--caprolactone nanoparticles for protein/peptide drug delivery. Drug Dev. Ind. Pharm., 39 (2013): 1046-1052.
[106] Stankovic, M., Tomar, J., Hiemstra, C., Steendam, R., Frijlink, H. W., Hinrichs, W. L., Tailored protein release from biodegradable poly(epsilon-caprolactone-PEG)-b-poly(epsilon-caprolactone) multiblock-copolymer implants. Eur. J. Pharm. Biopharm., 87 (2014): 329-337.
[107] Weiser, J. R., Yueh, A., Putnam, D., Protein release from dihydroxyacetone-based poly(carbonate ester) matrices. Acta Biomater., 9 (2013): 8245-8253.
[108] O'Shea, T. M., Webber, M. J., Aimetti, A. A., Langer, R., Covalent Incorporation of Trehalose within Hydrogels for Enhanced Long-Term Functional Stability and Controlled Release of Biomacromolecules. Adv Healthc Mater, 4 (2015): 1802-1812.
[109] Chung, H. J., Lee, Y., Park, T. G., Thermo-sensitive and biodegradable hydrogels based on stereocomplexed Pluronic multi-block copolymers for controlled protein delivery. J. Control. Release, 127 (2008): 22-30.
[110] Chen, F. M., Zhao, Y. M., Sun, H. H., Jin, T., Wang, Q. T., Zhou, W., Wu, Z. F., Jin, Y., Novel glycidyl methacrylated dextran (Dex-GMA)/gelatin hydrogel scaffolds containing microspheres loaded with bone morphogenetic proteins: formulation and characteristics. J. Control. Release, 118 (2007): 65-77.
[111] Kirchhof, S., Abrami, M., Messmann, V., Hammer, N., Goepferich, A. M., Grassi, M., Brandl, F. P., Diels-Alder Hydrogels for Controlled Antibody Release: Correlation between Mesh Size and Release Rate. Mol. Pharm., 12 (2015): 3358-3368.
[112] Kirchhof, S., Gregoritza, M., Messmann, V., Hammer, N., Goepferich, A. M., Brandl, F. P., Diels-Alder hydrogels with enhanced stability: First step toward controlled release of bevacizumab. Eur. J. Pharm. Biopharm., 96 (2015): 217-225.
[113] Hammer, N., Brandl, F. P., Kirchhof, S., Messmann, V., Goepferich, A. M., Protein compatibility of selected cross-linking reactions for hydrogels. Macromol. Biosci., 15 (2015): 405-413.
[114] Qin, J., Zhong, Z., Ma, J., Biomimetic synthesis of hybrid hydroxyapatite nanoparticles using nanogel template for controlled release of bovine serum albumin. Mater. Sci. Eng. C Mater. Biol. Appl., 62 (2016): 377-383.
[115] Drinnan, C. T., Zhang, G., Alexander, M. A., Pulido, A. S., Suggs, L. J., Multimodal release of transforming growth factor-beta1 and the BB isoform of platelet derived growth factor from PEGylated fibrin gels. J. Control. Release, 147 (2010): 180-186.
[116] Das, P., Jana, N. R., Length-Controlled Synthesis of Calcium Phosphate Nanorod and Nanowire and Application in Intracellular Protein Delivery. ACS Appl Mater Interfaces, 8 (2016): 8710-8720.
[117] Jain, P. K., Karunakaran, D., Friedman, S. H., Construction of a photoactivated insulin depot. Angew. Chem. Int. Ed. Engl., 52 (2013): 1404-1409.
[118] Vaishya, R., Khurana, V., Patel, S., Mitra, A. K., Long-term delivery of protein therapeutics. Expert Opin Drug Deliv, 12 (2015): 415-440.
[119] Basu, S. K., Govardhan, C. P., Jung, C. W., Margolin, A. L., Protein crystals for the delivery of biopharmaceuticals. Expert Opin. Biol. Ther., 4 (2004): 301-317.
[120] Pechenov, S., Shenoy, B., Yang, M. X., Basu, S. K., Margolin, A. L., Injectable controlled release formulations incorporating protein crystals. J. Control. Release, 96 (2004): 149-158.
[121] Puhl, S., Li, L., Meinel, L., Germershaus, O., Controlled protein delivery from electrospun non-wovens: novel combination of protein crystals and a biodegradable release matrix. Mol. Pharm., 11 (2014): 2372-2380.
[122] Hildebrandt, C.,Crystalline Monoclonal Antibodies: Development of stable crystals for drying and sustained release formulations. Ludwig-Maximilians-University Munich, 2014.

[123] Smith, A., Oxford Dictionary of Biochemistry and Molecular Biology, Oxford University Press, Oxford, UK, 2000.
[124] Christie, W. W., Lipid Analysis, Oily Press, Bridgewater, UK, 2003.
[125] Fahy, E., Subramaniam, S., Brown, H. A., Glass, C. K., Merrill, A. H., Jr., Murphy, R. C., Raetz, C. R., Russell, D. W., Seyama, Y., Shaw, W., Shimizu, T., Spener, F., van Meer, G., VanNieuwenhze, M. S., White, S. H., Witztum, J. L., Dennis, E. A., A comprehensive classification system for lipids. J. Lipid Res., 46 (2005): 839-861.
[126] Wang, P. Y., Palmitic acid as an excipient in implants for sustained release of insulin. Biomaterials, 12 (1991): 57-62.
[127] Rawat, M., Singh, D., Saraf, S., Saraf, S., Lipid carriers: a versatile delivery vehicle for proteins and peptides. Yakugaku Zasshi, 128 (2008): 269-280.
[128] Li, P., Nielsen, H. M., Mullertz, A., Oral delivery of peptides and proteins using lipid-based drug delivery systems. Expert Opin Drug Deliv, 9 (2012): 1289-1304.
[129] Manjunath, K., Reddy, J. S., Venkateswarlu, V., Solid lipid nanoparticles as drug delivery systems. Methods Find. Exp. Clin. Pharmacol., 27 (2005): 127-144.
[130] Unger, E. C., Porter, T., Culp, W., Labell, R., Matsunaga, T., Zutshi, R., Therapeutic applications of lipid-coated microbubbles. Adv Drug Deliv Rev, 56 (2004): 1291-1314.
[131] Muller, R. H., Radtke, M., Wissing, S. A., Solid lipid nanoparticles (SLN) and nanostructured lipid carriers (NLC) in cosmetic and dermatological preparations. Adv Drug Deliv Rev, 54 Suppl 1 (2002): S131-155.
[132] Pardeike, J., Hommoss, A., Muller, R. H., Lipid nanoparticles (SLN, NLC) in cosmetic and pharmaceutical dermal products. Int. J. Pharm., 366 (2009): 170-184.
[133] Wissing, S. A., Kayser, O., Muller, R. H., Solid lipid nanoparticles for parenteral drug delivery. Adv Drug Deliv Rev, 56 (2004): 1257-1272.
[134] Ezzati Nazhad Dolatabadi, J., Valizadeh, H., Hamishehkar, H., Solid Lipid Nanoparticles as Efficient Drug and Gene Delivery Systems: Recent Breakthroughs. Adv Pharm Bull, 5 (2015): 151-159.
[135] Almeida, A. J., Souto, E., Solid lipid nanoparticles as a drug delivery system for peptides and proteins. Adv Drug Deliv Rev, 59 (2007): 478-490.
[136] Muller, R. H., Mader, K., Gohla, S., Solid lipid nanoparticles (SLN) for controlled drug delivery - a review of the state of the art. Eur. J. Pharm. Biopharm., 50 (2000): 161-177.
[137] Li, S., Zhao, B., Wang, F., Wang, M., Xie, S., Wang, S., Han, C., Zhu, L., Zhou, W., Yak interferon-alpha loaded solid lipid nanoparticles for controlled release. Res. Vet. Sci., 88 (2010): 148-153.
[138] Yang, R., Gao, R., Li, F., He, H., Tang, X., The influence of lipid characteristics on the formation, in vitro release, and in vivo absorption of protein-loaded SLN prepared by the double emulsion process. Drug Dev. Ind. Pharm., 37 (2011): 139-148.
[139] Pedersen, N., Hansen, S., Heydenreich, A. V., Kristensen, H. G., Poulsen, H. S., Solid lipid nanoparticles can effectively bind DNA, streptavidin and biotinylated ligands. Eur. J. Pharm. Biopharm., 62 (2006): 155-162.
[140] Sacchetti, F., Marraccini, C., D'Arca, D., Pela, M., Pinetti, D., Maretti, E., Hanuskova, M., Iannuccelli, V., Costi, M. P., Leo, E., Enhanced anti-hyperproliferative activity of human thymidylate synthase inhibitor peptide by solid lipid nanoparticle delivery. Colloids Surf. B. Biointerfaces, 136 (2015): 346-354.
[141] Xue, H. Y., Guo, P., Wen, W. C., Wong, H. L., Lipid-Based Nanocarriers for RNA Delivery. Curr. Pharm. Des., 21 (2015): 3140-3147.
[142] Bondi, M. L., Craparo, E. F., Solid lipid nanoparticles for applications in gene therapy: a review of the state of the art. Expert Opin Drug Deliv, 7 (2010): 7-18.
[143] Carrillo, C., Sanchez-Hernandez, N., Garcia-Montoya, E., Perez-Lozano, P., Sune-Negre, J. M., Tico, J. R., Sune, C., Minarro, M., DNA delivery via cationic solid lipid nanoparticles (SLNs). Eur. J. Pharm. Sci., 49 (2013): 157-165.
[144] Goncalves, C., Berchel, M., Gosselin, M. P., Malard, V., Cheradame, H., Jaffres, P. A., Guegan, P., Pichon, C., Midoux, P., Lipopolyplexes comprising imidazole/imidazolium lipophosphoramidate, histidinylated polyethyleneimine and siRNA as efficient formulation for siRNA transfection. Int. J. Pharm., 460 (2014): 264-272.

[145] Jin, J., Bae, K. H., Yang, H., Lee, S. J., Kim, H., Kim, Y., Joo, K. M., Seo, S. W., Park, T. G., Nam, D. H., In vivo specific delivery of c-Met siRNA to glioblastoma using cationic solid lipid nanoparticles. Bioconjug. Chem., 22 (2011): 2568-2572.
[146] Montana, G., Bondi, M. L., Carrotta, R., Picone, P., Craparo, E. F., San Biagio, P. L., Giammona, G., Di Carlo, M., Employment of cationic solid-lipid nanoparticles as RNA carriers. Bioconjug. Chem., 18 (2007): 302-308.
[147] Luvino, D., Khiati, S., Oumzil, K., Rocchi, P., Camplo, M., Barthelemy, P., Efficient delivery of therapeutic small nucleic acids to prostate cancer cells using ketal nucleoside lipid nanoparticles. J. Control. Release, 172 (2013): 954-961.
[148] Apaolaza, P. S., Del Pozo-Rodriguez, A., Torrecilla, J., Rodriguez-Gascon, A., Rodriguez, J. M., Friedrich, U., Weber, B. H., Solinis, M. A., Solid lipid nanoparticle-based vectors intended for the treatment of X-linked juvenile retinoschisis by gene therapy: In vivo approaches in Rs1h-deficient mouse model. J. Control. Release, 217 (2015): 273-283.
[149] Gures, S., Kleinebudde, P., Dissolution from solid lipid extrudates containing release modifiers. Int. J. Pharm., 412 (2011): 77-84.
[150] Windbergs, M., Haaser, M., McGoverin, C. M., Gordon, K. C., Kleinebudde, P., Strachan, C. J., Investigating the relationship between drug distribution in solid lipid matrices and dissolution behaviour using Raman spectroscopy and mapping. J. Pharm. Sci., 99 (2010): 1464-1475.
[151] Windbergs, M., Strachan, C. J., Kleinebudde, P., Tailor-made dissolution profiles by extruded matrices based on lipid polyethylene glycol mixtures. J. Control. Release, 137 (2009): 211-216.
[152] Windbergs, M., Gueres, S., Strachan, C. J., Kleinebudde, P., Two-step solid lipid extrusion as a process to modify dissolution behavior. AAPS PharmSciTech, 11 (2010): 2-8.
[153] Grassi, M., Voinovich, D., Franceschinis, E., Perissutti, B., Filipovic-Grcic, J., Theoretical and experimental study on theophylline release from stearic acid cylindrical delivery systems. J. Control. Release, 92 (2003): 275-289.
[154] Siepmann, F., Muschert, S., Flament, M. P., Leterme, P., Gayot, A., Siepmann, J., Controlled drug release from Gelucire-based matrix pellets: experiment and theory. Int. J. Pharm., 317 (2006): 136-143.
[155] Siepmann, J., Siepmann, F., Mathematical modeling of drug release from lipid dosage forms. Int. J. Pharm., 418 (2011): 42-53.
[156] Siepmann, F., Herrmann, S., Winter, G., Siepmann, J., A novel mathematical model quantifying drug release from lipid implants. J. Control. Release, 128 (2008): 233-240.
[157] Gures, S., Siepmann, F., Siepmann, J., Kleinebudde, P., Drug release from extruded solid lipid matrices: theoretical predictions and independent experiments. Eur. J. Pharm. Biopharm., 80 (2012): 122-129.
[158] Guse, C., Koennings, S., Kreye, F., Siepmann, F., Goepferich, A., Siepmann, J., Drug release from lipid-based implants: elucidation of the underlying mass transport mechanisms. Int. J. Pharm., 314 (2006): 137-144.
[159] Kreye, F., Siepmann, F., Siepmann, J., Drug release mechanisms of compressed lipid implants. Int. J. Pharm., 404 (2011): 27-35.
[160] Windbergs, M., Strachan, C. J., Kleinebudde, P., Influence of structural variations on drug release from lipid/polyethylene glycol matrices. Eur. J. Pharm. Sci., 37 (2009): 555-562.
[161] Windbergs, M., Strachan, C. J., Kleinebudde, P., Influence of the composition of glycerides on the solid-state behaviour and the dissolution profiles of solid lipid extrudates. Int. J. Pharm., 381 (2009): 184-191.
[162] Windbergs, M., Strachan, C. J., Kleinebudde, P., Investigating the principles of recrystallization from glyceride melts. AAPS PharmSciTech, 10 (2009): 1224-1233.
[163] Windbergs, M., Strachan, C. J., Kleinebudde, P., Understanding the solid-state behaviour of triglyceride solid lipid extrudates and its influence on dissolution. Eur. J. Pharm. Biopharm., 71 (2009): 80-87.
[164] Kreye, F., Siepmann, F., Zimmer, A., Willart, J. F., Descamps, M., Siepmann, J., Cast lipid implants for controlled drug delivery: importance of the tempering conditions. J. Pharm. Sci., 100 (2011): 3471-3481.

[165] Kreye, F., Siepmann, F., Zimmer, A., Willart, J. F., Descamps, M., Siepmann, J., Controlled release implants based on cast lipid blends. Eur. J. Pharm. Sci., 43 (2011): 78-83.
[166] Kreye, F., Siepmann, F., Willart, J. F., Descamps, M., Siepmann, J., Drug release mechanisms of cast lipid implants. Eur. J. Pharm. Biopharm., 78 (2011): 394-400.
[167] Mohl, S., Winter, G., Continuous release of rh-interferon alpha-2a from triglyceride matrices. J. Control. Release, 97 (2004): 67-78.
[168] Schwab, M., Kessler, B., Wolf, E., Jordan, G., Mohl, S., Winter, G., Correlation of in vivo and in vitro release data for rh-INFalpha lipid implants. Eur. J. Pharm. Biopharm., 70 (2008): 690-694.
[169] Appel, B., Maschke, A., Weiser, B., Sarhan, H., Englert, C., Angele, P., Blunk, T., Gopferich, A., Lipidic implants for controlled release of bioactive insulin: effects on cartilage engineered in vitro. Int. J. Pharm., 314 (2006): 170-178.
[170] Vogelhuber, W., Magni, E., Mouro, M., Spruss, T., Guse, C., Gazzaniga, A., Gopferich, A., Monolithic triglyceride matrices: a controlled-release system for proteins. Pharm. Dev. Technol., 8 (2003): 71-79.
[171] Wang, P. Y., Prolonged release of insulin by cholesterol-matrix implant. Diabetes, 36 (1987): 1068-1072.
[172] Vogelhuber, W., Magni, E., Gazzaniga, A., Gopferich, A., Monolithic glyceryl trimyristate matrices for parenteral drug release applications. Eur. J. Pharm. Biopharm., 55 (2003): 133-138.
[173] Guse, C., Koennings, S., Maschke, A., Hacker, M., Becker, C., Schreiner, S., Blunk, T., Spruss, T., Goepferich, A., Biocompatibility and erosion behavior of implants made of triglycerides and blends with cholesterol and phospholipids. Int. J. Pharm., 314 (2006): 153-160.
[174] Koennings, S., Garcion, E., Faisant, N., Menei, P., Benoit, J. P., Goepferich, A., In vitro investigation of lipid implants as a controlled release system for interleukin-18. Int. J. Pharm., 314 (2006): 145-152.
[175] Koennings, S., Sapin, A., Blunk, T., Menei, P., Goepferich, A., Towards controlled release of BDNF--manufacturing strategies for protein-loaded lipid implants and biocompatibility evaluation in the brain. J. Control. Release, 119 (2007): 163-172.
[176] Mohl, S., Winter, G., Continuous release of Rh-interferon (alpha-2a from triglyceride implants: storage stability of the dosage forms. Pharm. Dev. Technol., 11 (2006): 103-110.
[177] Herrmann, S., Winter, G., Mohl, S., Siepmann, F., Siepmann, J., Mechanisms controlling protein release from lipidic implants: effects of PEG addition. J. Control. Release, 118 (2007): 161-168.
[178] Herrmann, S., Mohl, S., Siepmann, F., Siepmann, J., Winter, G., New insight into the role of polyethylene glycol acting as protein release modifier in lipidic implants. Pharm. Res., 24 (2007): 1527-1537.
[179] Schwab, M., McGoverin, C. M., Gordon, K. C., Winter, G., Rades, T., Myschik, J., Strachan, C. J., Studies on the lipase-induced degradation of lipid-based drug delivery systems. Part II - Investigations on the mechanisms leading to collapse of the lipid structure. Eur. J. Pharm. Biopharm., 84 (2013): 456-463.
[180] Jensen, S. S., Jensen, H., Moller, E. H., Cornett, C., Siepmann, F., Siepmann, J., Ostergaard, J., In vitro release studies of insulin from lipid implants in solution and in a hydrogel matrix mimicking the subcutis. Eur. J. Pharm. Sci., 81 (2016): 103-112.
[181] Schulze, S., Winter, G., Lipid extrudates as novel sustained release systems for pharmaceutical proteins. J. Control. Release, 134 (2009): 177-185.
[182] Sax, G., Winter, G., Mechanistic studies on the release of lysozyme from twin-screw extruded lipid implants. J. Control. Release, 163 (2012): 187-194.
[183] Sax, G., Feil, F., Schulze, S., Jung, C., Brauchle, C., Winter, G., Release pathways of interferon alpha2a molecules from lipid twin screw extrudates revealed by single molecule fluorescence microscopy. J. Control. Release, 162 (2012): 295-302.
[184] Sax, G., Kessler, B., Wolf, E., Winter, G., In-vivo biodegradation of extruded lipid implants in rabbits. J. Control. Release, 163 (2012): 195-202.

[185] Neuhofer, C.,Development of lipid based depot formulations using interferon-beta-1b as model protein. Ludwig-Maximilians-University Munich, 2015.
[186] Even, M. P.,Twin-Screw Extruded Lipid Implants for Vaccine Delivery. Ludwig-Maximilians-University Munich, 2015.
[187] Even, M. P., Bobbala, S., Gibson, B., Hook, S., Winter, G., Engert, J., Twin-screw extruded lipid implants containing TRP2 peptide for tumour therapy. Eur. J. Pharm. Biopharm., (2017).
[188] Klein, R., Wang, Q., Klein, B. E., Moss, S. E., Meuer, S. M., The relationship of age-related maculopathy, cataract, and glaucoma to visual acuity. Invest. Ophthalmol. Vis. Sci., 36 (1995): 182-191.
[189] Christoforidis, J. B., Williams, M. M., Kothandaraman, S., Kumar, K., Epitropoulos, F. J., Knopp, M. V., Pharmacokinetic properties of intravitreal I-124-aflibercept in a rabbit model using PET/CT. Curr. Eye Res., 37 (2012): 1171-1174.
[190] Golik, P., Tonska, K., [Comparison of the biological principles underlying the action of monoclonal antibody (mAb) and decoy receptor anti-VEGF agents--on the example of ranibizumab (anti-VEGF-A mAb) and aflibercept (decoy VEGFR1-2 receptor)]. Klin. Oczna, 114 (2012): 79-83.
[191] Thomas, M., Mousa, S. S., Mousa, S. A., Comparative effectiveness of aflibercept for the treatment of patients with neovascular age-related macular degeneration. Clin. Ophthalmol., 7 (2013): 495-501.
[192] Nagineni, C. N., Kommineni, V. K., William, A., Detrick, B., Hooks, J. J., Regulation of VEGF expression in human retinal cells by cytokines: implications for the role of inflammation in age-related macular degeneration. J. Cell. Physiol., 227 (2012): 116-126.
[193] Rosenfeld, P. J., Bevacizumab versus ranibizumab for AMD. N. Engl. J. Med., 364 (2011): 1966-1967.
[194] Meyer, C. H., Holz, F. G., Preclinical aspects of anti-VEGF agents for the treatment of wet AMD: ranibizumab and bevacizumab. Eye (Lond.), 25 (2011): 661-672.
[195] Scott, A. W., Bressler, S. B., Long-term follow-up of vascular endothelial growth factor inhibitor therapy for neovascular age-related macular degeneration. Curr. Opin. Ophthalmol., 24 (2013): 190-196.
[196] Stewart, M. W., Rosenfeld, P. J., Penha, F. M., Wang, F., Yehoshua, Z., Bueno-Lopez, E., Lopez, P. F., Pharmacokinetic rationale for dosing every 2 weeks versus 4 weeks with intravitreal ranibizumab, bevacizumab, and aflibercept (vascular endothelial growth factor Trap-eye). Retina, 32 (2012): 434-457.
[197] Troutbeck, R., Al-Qureshi, S., Guymer, R. H., Therapeutic targeting of the complement system in age-related macular degeneration: a review. Clin Exp Ophthalmol, 40 (2012): 18-26.
[198] Kompella, U. B., Kadam, R. S., Lee, V. H., Recent advances in ophthalmic drug delivery. Ther. Deliv., 1 (2010): 435-456.
[199] Yasukawa, T., Ogura, Y., Kimura, H., Sakurai, E., Tabata, Y., Drug delivery from ocular implants. Expert Opin Drug Deliv, 3 (2006): 261-273.
[200] Kane, F. E., Burdan, J., Cutino, A., Green, K. E., Iluvien: a new sustained delivery technology for posterior eye disease. Expert Opin Drug Deliv, 5 (2008): 1039-1046.
[201] Scaramuzzi, M., Querques, G., Spina, C. L., Lattanzio, R., Bandello, F., Repeated intravitreal dexamethasone implant (Ozurdex) for diabetic macular edema. Retina, 35 (2015): 1216-1222.
[202] Wang, J., Jiang, A., Joshi, M., Christoforidis, J., Drug delivery implants in the treatment of vitreous inflammation. Mediators Inflamm., 2013 (2013): 780634.
[203] Patel, A., Cholkar, K., Agrahari, V., Mitra, A. K., Ocular drug delivery systems: An overview. World J Pharmacol, 2 (2013): 47-64.
[204] Pearce, W., Hsu, J., Yeh, S., Advances in drug delivery to the posterior segment. Curr. Opin. Ophthalmol., 26 (2015): 233-239.
[205] Mordenti, J., Thomsen, K., Licko, V., Berleau, L., Kahn, J. W., Cuthbertson, R. A., Duenas, E. T., Ryan, A. M., Schofield, C., Berger, T. W., Meng, Y. G., Cleland, J., Intraocular pharmacokinetics and safety of a humanized monoclonal antibody in rabbits after intravitreal administration of a solution or a PLGA microsphere formulation. Toxicol. Sci., 52 (1999): 101-106.

[206] Kang Derwent, J. J., Mieler, W. F., Thermoresponsive hydrogels as a new ocular drug delivery platform to the posterior segment of the eye. Trans. Am. Ophthalmol. Soc., 106 (2008): 206-213; discussion 213-204.
[207] Asmus, L. R., Grimshaw, J. P., Richle, P., Eicher, B., Urech, D. M., Gurny, R., Moller, M., Injectable formulations for an intravitreal sustained-release application of a novel single-chain VEGF antibody fragment. Eur. J. Pharm. Biopharm., 95 (2015): 250-260.
[208] Chen, Y. S., Green, C. R., Wang, K., Danesh-Meyer, H. V., Rupenthal, I. D., Sustained intravitreal delivery of connexin43 mimetic peptide by poly(D,L-lactide-co-glycolide) acid micro- and nanoparticles--Closing the gap in retinal ischaemia. Eur. J. Pharm. Biopharm., 95 (2015): 378-386.
[209] Li, F., Hurley, B., Liu, Y., Leonard, B., Griffith, M., Controlled release of bevacizumab through nanospheres for extended treatment of age-related macular degeneration. Open Ophthalmol J, 6 (2012): 54-58.
[210] Andrew, J. S., Anglin, E. J., Wu, E. C., Chen, M. Y., Cheng, L., Freeman, W. R., Sailor, M. J., Sustained Release of a Monoclonal Antibody from Electrochemically Prepared Mesoporous Silicon Oxide. Adv. Funct. Mater., 20 (2010): 4168-4174.
[211] Molokhia, S. A., Sant, H., Simonis, J., Bishop, C. J., Burr, R. M., Gale, B. K., Ambati, B. K., The capsule drug device: novel approach for drug delivery to the eye. Vision Res., 50 (2010): 680-685.
[212] Gooch, N., Burr, R. M., Holt, D. J., Gale, B., Ambati, B., Design and in vitro biocompatibility of a novel ocular drug delivery device. J Funct Biomater, 4 (2013): 14-26.
[213] Abrishami, M., Zarei-Ghanavati, S., Soroush, D., Rouhbakhsh, M., Jaafari, M. R., Malaekeh-Nikouei, B., Preparation, characterization, and in vivo evaluation of nanoliposomes-encapsulated bevacizumab (avastin) for intravitreal administration. Retina, 29 (2009): 699-703.
[214] Tamaddon, L., Mostafavi, A., Riazi-Esfahani, M., Karkhane, R., Aghazadeh, S., Rafiee-Tehrani, M., Abedin Dorkoosh, F., Asadi Amoli, F., Development, characterizations and biocompatibility evaluations of intravitreal lipid implants. Jundishapur J Nat Pharm Prod, 9 (2014): e16414.
[215] Brown, L. R., Commercial challenges of protein drug delivery. Expert Opin Drug Deliv, 2 (2005): 29-42.
[216] Jiskoot, W., Randolph, T. W., Volkin, D. B., Middaugh, C. R., Schoneich, C., Winter, G., Friess, W., Crommelin, D. J., Carpenter, J. F., Protein instability and immunogenicity: roadblocks to clinical application of injectable protein delivery systems for sustained release. J. Pharm. Sci., 101 (2012): 946-954.
[217] Liang, R., Li, X., Shi, Y., Wang, A., Sun, K., Liu, W., Li, Y., Effect of water on exenatide acylation in poly(lactide-co-glycolide) microspheres. Int. J. Pharm., 454 (2013): 344-353.
[218] Tan, M. L., Choong, P. F., Dass, C. R., Recent developments in liposomes, microparticles and nanoparticles for protein and peptide drug delivery. Peptides, 31 (2010): 184-193.
[219] Charman, S. A., Segrave, A. M., Edwards, G. A., Porter, C. J., Systemic availability and lymphatic transport of human growth hormone administered by subcutaneous injection. J. Pharm. Sci., 89 (2000): 168-177.
[220] Jiskoot, W., van Schie, R. M., Carstens, M. G., Schellekens, H., Immunological risk of injectable drug delivery systems. Pharm. Res., 26 (2009): 1303-1314.
[221] Schellekens, H., Immunogenicity of therapeutic proteins: clinical implications and future prospects. Clin. Ther., 24 (2002): 1720-1740; discussion 1719.
[222] Ratanji, K. D., Derrick, J. P., Dearman, R. J., Kimber, I., Immunogenicity of therapeutic proteins: influence of aggregation. J. Immunotoxicol., 11 (2014): 99-109.
[223] Freitag, A. J.,The Immunogenicity of Protein Aggregates: Studies on a Murine Monoclonal Antibody in Wild-Type Mice. Ludwig-Maximilians-University Munich, 2012.
[224] Freitag, A. J., Shomali, M., Michalakis, S., Biel, M., Siedler, M., Kaymakcalan, Z., Carpenter, J. F., Randolph, T. W., Winter, G., Engert, J., Investigation of the immunogenicity of different types of aggregates of a murine monoclonal antibody in mice. Pharm. Res., 32 (2015): 430-444.

[225] Bessa, J., Boeckle, S., Beck, H., Buckel, T., Schlicht, S., Ebeling, M., Kiialainen, A., Koulov, A., Boll, B., Weiser, T., Singer, T., Rolink, A. G., Iglesias, A., The immunogenicity of antibody aggregates in a novel transgenic mouse model. Pharm. Res., 32 (2015): 2344-2359.
[226] Filipe, V., Jiskoot, W., Basmeleh, A. H., Halim, A., Schellekens, H., Brinks, V., Immunogenicity of different stressed IgG monoclonal antibody formulations in immune tolerant transgenic mice. MAbs, 4 (2012): 740-752.
[227] Rojko, J. L., Evans, M. G., Price, S. A., Han, B., Waine, G., DeWitte, M., Haynes, J., Freimark, B., Martin, P., Raymond, J. T., Evering, W., Rebelatto, M. C., Schenck, E., Horvath, C., Formation, clearance, deposition, pathogenicity, and identification of biopharmaceutical-related immune complexes: review and case studies. Toxicol. Pathol., 42 (2014): 725-764.
[228] Elzoghby, A. O., El-Fotoh, W. S., Elgindy, N. A., Casein-based formulations as promising controlled release drug delivery systems. J. Control. Release, 153 (2011): 206-216.
[229] Park, E. J., Tak, T. H., Na, D. H., Lee, K. C., Effect of PEGylation on stability of peptide in poly(lactide-co-glycolide) microspheres. Arch. Pharm. Res., 33 (2010): 1111-1116.
[230] Herrmann, S.,Lipidic Implants for Pharmaceutical Proteins: Mechanisms of Release and Development of Extruded Devices. Ludwig-Maximilians-University Munich, 2007.
[231] Even, M. P., Young, K., Winter, G., Hook, S., Engert, J., In vivo investigation of twin-screw extruded lipid implants for vaccine delivery. Eur. J. Pharm. Biopharm., 87 (2014): 338-346.
[232] Sax, G. L.,Twin-screw extruded lipid implants for controlled protein drug delivery. Ludwig-Maximilians-University, Munich, 2012.
[233] Even, M. P., Bobbala, S., Kooi, K. L., Hook, S., Winter, G., Engert, J., Impact of implant composition of twin-screw extruded lipid implants on the release behavior. Int. J. Pharm., 493 (2015): 102-110.
[234] Sax, G., Twin-screw extruded lipid implants for controlled protein drug delivery. Dissertation LMU Munich, (2012).
[235] Schwab, M., Sax, G., Schulze, S., Winter, G., Studies on the lipase induced degradation of lipid based drug delivery systems. J. Control. Release, 140 (2009): 27-33.
[236] Reitz, C., Strachan, C., Kleinebudde, P., Solid lipid extrudates as sustained-release matrices: the effect of surface structure on drug release properties. Eur. J. Pharm. Sci., 35 (2008): 335-343.
[237] Witzleb, R., Kanikanti, V. R., Hamann, H. J., Kleinebudde, P., Solid lipid extrusion with small die diameters--electrostatic charging, taste masking and continuous production. Eur. J. Pharm. Biopharm., 77 (2011): 170-177.
[238] Bogusz, J., Majchrzak, A., Medra, A., Cebula-Obrzut, B., Robak, T., Smolewski, P., Mechanisms of action of the anti-VEGF monoclonal antibody bevacizumab on chronic lymphocytic leukemia cells. Postepy Hig Med Dosw (Online), 67 (2013): 107-118.
[239] Stewart, M. W., Predicted biologic activity of intravitreal bevacizumab. Retina, 27 (2007): 1196-1200.
[240] Schmidt, C. Q., Bai, H., Lin, Z., Risitano, A. M., Barlow, P. N., Ricklin, D., Lambris, J. D., Rational engineering of a minimized immune inhibitor with unique triple-targeting properties. J. Immunol., 190 (2013): 5712-5721.
[241] Schmidt, C. Q., Harder, M. J., Nichols, E. M., Hebecker, M., Anliker, M., Hochsmann, B., Simmet, T., Csincsi, A. I., Uzonyi, B., Pappworth, I. Y., Ricklin, D., Lambris, J. D., Schrezenmeier, H., Jozsi, M., Marchbank, K. J., Selectivity of C3-opsonin targeted complement inhibitors: A distinct advantage in the protection of erythrocytes from paroxysmal nocturnal hemoglobinuria patients. Immunobiology, 221 (2016): 503-511.
[242] Michael Morlock, T. K., *You Xin Li, Hans Koll, Gerhard Winter, Erythropoietin loaded microspheres prepared from biodegradable LPLG–PEO–LPLG triblock copolymers: protein stabilization and in-vitro release properties. Journal of Controlled Release, 56 (1998): 105-115.
[243] Wang, F., Rendahl, K. G., Manning, W. C., Quiroz, D., Coyne, M., Miller, S. S., AAV-mediated expression of vascular endothelial growth factor induces choroidal neovascularization in rat. Invest. Ophthalmol. Vis. Sci., 44 (2003): 781-790.
[244] Bennett, J., Maguire, A. M., Cideciyan, A. V., Schnell, M., Glover, E., Anand, V., Aleman, T. S., Chirmule, N., Gupta, A. R., Huang, Y., Gao, G. P., Nyberg, W. C., Tazelaar, J., Hughes, J., Wilson, J. M., Jacobson, S. G., Stable transgene expression in rod photoreceptors after

recombinant adeno-associated virus-mediated gene transfer to monkey retina. Proc. Natl. Acad. Sci. U. S. A., 96 (1999): 9920-9925.
[245] Bakri, S. J., Snyder, M. R., Reid, J. M., Pulido, J. S., Ezzat, M. K., Singh, R. J., Pharmacokinetics of intravitreal ranibizumab (Lucentis). Ophthalmology, 114 (2007): 2179-2182.
[246] Gaudreault, J., Fei, D., Rusit, J., Suboc, P., Shiu, V., Preclinical pharmacokinetics of Ranibizumab (rhuFabV2) after a single intravitreal administration. Invest. Ophthalmol. Vis. Sci., 46 (2005): 726-733.
[247] Farnan, D., Moreno, G. T., Multiproduct high-resolution monoclonal antibody charge variant separations by pH gradient ion-exchange chromatography. Anal. Chem., 81 (2009): 8846-8857.
[248] Volz, C., Pauly, D., Antibody therapies and their challenges in the treatment of age-related macular degeneration. Eur. J. Pharm. Biopharm., 95 (2015): 158-172.
[249] Kreye, F., Siepmann, F., Siepmann, J., Lipid implants as drug delivery systems. Expert Opin Drug Deliv, 5 (2008): 291-307.
[250] Vogelhuber, W., Monolithic glyceryl trimyristate matrices for parenteral drug release applications. European Journal of Pharmaceutics and Biopharmaceutics, 55 (2003): 133-138.
[251] Yasir, M., Sara, U. V., Solid lipid nanoparticles for nose to brain delivery of haloperidol: in vitro drug release and pharmacokinetics evaluation. Acta Pharm Sin B, 4 (2014): 454-463.
[252] Neves, A. R., Queiroz, J. F., Weksler, B., Romero, I. A., Couraud, P. O., Reis, S., Solid lipid nanoparticles as a vehicle for brain-targeted drug delivery: two new strategies of functionalization with apolipoprotein E. Nanotechnology, 26 (2015): 495103.
[253] Estey, T., Kang, J., Schwendeman, S. P., Carpenter, J. F., BSA degradation under acidic conditions: a model for protein instability during release from PLGA delivery systems. J. Pharm. Sci., 95 (2006): 1626-1639.
[254] Lucke, A., Acylation of peptides by lactic acid solutions. European Journal of Pharmaceutics and Biopharmaceutics, 55 (2003): 27-33.
[255] Cosse, A., Konig, C., Lamprecht, A., Wagner, K. G., Hot Melt Extrusion for Sustained Protein Release: Matrix Erosion and In Vitro Release of PLGA-Based Implants. AAPS PharmSciTech, 18 (2017): 15-26.
[256] Herrmann, S., Lipidic Implants for Pharmaceutical Proteins: Mechanisms of Release and Development of Extruded Devices. Dissertation LMU Munich, (2007).
[257] Ressing, M. E., Jiskoot, W., Talsma, H., van Ingen, C. W., Beuvery, E. C., Crommelin, D. J., The influence of sucrose, dextran, and hydroxypropyl-beta-cyclodextrin as lyoprotectants for a freeze-dried mouse IgG2a monoclonal antibody (MN12). Pharm. Res., 9 (1992): 266-270.
[258] Metz, B., Kersten, G. F., Hoogerhout, P., Brugghe, H. F., Timmermans, H. A., de Jong, A., Meiring, H., ten Hove, J., Hennink, W. E., Crommelin, D. J., Jiskoot, W., Identification of formaldehyde-induced modifications in proteins: reactions with model peptides. J. Biol. Chem., 279 (2004): 6235-6243.
[259] Johnson, D. M., Taylor, W. F., Degradation of fenprostalene in polyethylene glycol 400 solution. J. Pharm. Sci., 73 (1984): 1414-1417.
[260] Koennings, S., Tessmar, J., Blunk, T., Gopferich, A., Confocal microscopy for the elucidation of mass transport mechanisms involved in protein release from lipid-based matrices. Pharm. Res., 24 (2007): 1325-1335.
[261] Pattarino, F., Bettini, R., Foglio Bonda, A., Della Bella, A., Giovannelli, L., Polymorphism and kinetic behavior of binary mixtures of triglycerides. Int. J. Pharm., 473 (2014): 87-94.
[262] Hildebrandt, C., Joos, L., Saedler, R., Winter, G., The "New Polyethylene Glycol Dilemma": Polyethylene Glycol Impurities and Their Paradox Role in mAb Crystallization. J. Pharm. Sci., 104 (2015): 1938-1945.
[263] Wenande, E., Garvey, L. H., Immediate-type hypersensitivity to polyethylene glycols: a review. Clin. Exp. Allergy, 46 (2016): 907-922.
[264] Wenande, E., Kroigaard, M., Mosbech, H., Garvey, L. H., Polyethylene glycols (PEG) and related structures: overlooked allergens in the perioperative setting. A A Case Rep, 4 (2015): 61-64.

[265] Wylon, K., Dolle, S., Worm, M., Polyethylene glycol as a cause of anaphylaxis. Allergy Asthma Clin. Immunol., 12 (2016): 67.
[266] Lee, S. S., Hughes, P., Ross, A. D., Robinson, M. R., Biodegradable implants for sustained drug release in the eye. Pharm. Res., 27 (2010): 2043-2053.
[267] Hu, C. C., Chaw, J. R., Chen, C. F., Liu, H. W., Controlled release bevacizumab in thermoresponsive hydrogel found to inhibit angiogenesis. Biomed. Mater. Eng., 24 (2014): 1941-1950.
[268] Gooch, N., Molokhia, S. A., Condie, R., Burr, R. M., Archer, B., Ambati, B. K., Wirostko, B., Ocular drug delivery for glaucoma management. Pharmaceutics, 4 (2012): 197-211.
[269] Barar, J., Aghanejad, A., Fathi, M., Omidi, Y., Advanced drug delivery and targeting technologies for the ocular diseases. Bioimpacts, 6 (2016): 49-67.
[270] Yasin, M. N., Svirskis, D., Seyfoddin, A., Rupenthal, I. D., Implants for drug delivery to the posterior segment of the eye: a focus on stimuli-responsive and tunable release systems. J. Control. Release, 196 (2014): 208-221.
[271] Loch, C., Bogdahn, M., Stein, S., Nagel, S., Guthoff, R., Weitschies, W., Seidlitz, A., Simulation of drug distribution in the vitreous body after local drug application into intact vitreous body and in progress of posterior vitreous detachment. J. Pharm. Sci., 103 (2014): 517-526.
[272] Loch, C., Nagel, S., Guthoff, R., Seidlitz, A., Weitschies, W., The Vitreous Model - a new in vitro test method simulating the vitreous body. Biomed. Tech. (Berl.), 57 Suppl 1 (2012).
[273] Loch, C., Zakelj, S., Kristl, A., Nagel, S., Guthoff, R., Weitschies, W., Seidlitz, A., Determination of permeability coefficients of ophthalmic drugs through different layers of porcine, rabbit and bovine eyes. Eur. J. Pharm. Sci., 47 (2012): 131-138.
[274] Patel, S., Muller, G., Stracke, J. O., Altenburger, U., Mahler, H. C., Jere, D., Evaluation of protein drug stability with vitreous humor in a novel ex-vivo intraocular model. Eur. J. Pharm. Biopharm., 95 (2015): 407-417.
[275] Patel, S., Stracke, J. O., Altenburger, U., Mahler, H. C., Metzger, P., Shende, P., Jere, D., Prediction of intraocular antibody drug stability using ex-vivo ocular model. Eur. J. Pharm. Biopharm., (2016).
[276] Pan, C. K., Durairaj, C., Kompella, U. B., Agwu, O., Oliver, S. C., Quiroz-Mercado, H., Mandava, N., Olson, J. L., Comparison of long-acting bevacizumab formulations in the treatment of choroidal neovascularization in a rat model. J. Ocul. Pharmacol. Ther., 27 (2011): 219-224.
[277] Kinnunen, K., Korpisalo, P., Rissanen, T. T., Heikura, T., Viita, H., Uusitalo, H., Yla-Herttuala, S., Overexpression of VEGF-A induces neovascularization and increased vascular leakage in rabbit eye after intravitreal adenoviral gene transfer. Acta Physiol. (Oxf.), 187 (2006): 447-457.
[278] Lorget, F., Parenteau, A., Carrier, M., Lambert, D., Gueorguieva, A., Schuetz, C., Bantseev, V., Thackaberry, E., Characterization of the pH and Temperature in the Rabbit, Pig, and Monkey Eye: Key Parameters for the Development of Long-Acting Delivery Ocular Strategies. Mol. Pharm., 13 (2016): 2891-2896.
[279] Schwartz, B., Feller, M. R., Temperature gradients in the rabbit eye. Invest. Ophthalmol., 1 (1962): 513-521.
[280] Haeri, A., Sadeghian, S., Rabbani, S., Anvari, M. S., Boroumand, M. A., Dadashzadeh, S., Use of remote film loading methodology to entrap sirolimus into liposomes: preparation, characterization and in vivo efficacy for treatment of restenosis. Int. J. Pharm., 414 (2011): 16-27.
[281] Kiafar, F., Siahi Shadbad, M. R., Valizadeh, H., Filgrastim (G-CSF) loaded liposomes: mathematical modeling and optimization of encapsulation efficiency and particle size. Bioimpacts, 6 (2016): 195-201.
[282] Karn, P. R., Jin, S. E., Lee, B. J., Sun, B. K., Kim, M. S., Sung, J. H., Hwang, S. J., Preparation and evaluation of cyclosporin A-containing proliposomes: a comparison of the supercritical antisolvent process with the conventional film method. Int J Nanomedicine, 9 (2014): 5079-5091.

[283] Elhissi, A. M., O'Neill, M. A., Roberts, S. A., Taylor, K. M., A calorimetric study of dimyristoylphosphatidylcholine phase transitions and steroid-liposome interactions for liposomes prepared by thin film and proliposome methods. Int. J. Pharm., 320 (2006): 124-130.
[284] Mohammed, A. A., El-Tanni, H., Atiah, T. A., Atiah, A. A., Atiah, M. A., Rasmy, A. A., Paroxysmal Nocturnal Hemoglobinuria: From Bench to Bed. Indian J. Hematol. Blood Transfus., 32 (2016): 383-391.
[285] Mevorach, D., Paroxysmal nocturnal hemoglobinuria (PNH) and primary p.Cys89Tyr mutation in CD59: Differences and similarities. Mol. Immunol., 67 (2015): 51-55.
[286] Bessler, M., Hiken, J., The pathophysiology of disease in patients with paroxysmal nocturnal hemoglobinuria. Hematology Am. Soc. Hematol. Educ. Program, (2008): 104-110.
[287] Risitano, A. M., Paroxysmal nocturnal hemoglobinuria and the complement system: recent insights and novel anticomplement strategies. Adv. Exp. Med. Biol., 735 (2013): 155-172.
[288] Alashkar, F., Vance, C., Herich-Terhurne, D., Preising, N., Duhrsen, U., Roth, A., Serologic response to meningococcal vaccination in patients with paroxysmal nocturnal hemoglobinuria (PNH) chronically treated with the terminal complement inhibitor eculizumab. Ann. Hematol., (2017).
[289] Harder, M. J., Kuhn, N., Schrezenmeier, H., Hochsmann, B., von Zabern, I., Weinstock, C., Simmet, T., Ricklin, D., Lambris, J. D., Skerra, A., Anliker, M., Schmidt, C. Q., Incomplete inhibition by eculizumab: mechanistic evidence for residual C5 activity during strong complement activation. Blood, 129 (2017): 970-980.
[290] Angioi, A., Fervenza, F. C., Sethi, S., Zhang, Y., Smith, R. J., Murray, D., Van Praet, J., Pani, A., De Vriese, A. S., Diagnosis of complement alternative pathway disorders. Kidney Int., 89 (2016): 278-288.
[291] Ricklin, D., Manipulating the mediator: modulation of the alternative complement pathway C3 convertase in health, disease and therapy. Immunobiology, 217 (2012): 1057-1066.
[292] van der Maten, E., de Bont, C. M., de Groot, R., de Jonge, M. I., Langereis, J. D., van der Flier, M., Alternative pathway regulation by factor H modulates Streptococcus pneumoniae induced proinflammatory cytokine responses by decreasing C5a receptor crosstalk. Cytokine, 88 (2016): 281-286.
[293] Sweigard, J. H., Yanai, R., Gaissert, P., Saint-Geniez, M., Kataoka, K., Thanos, A., Stahl, G. L., Lambris, J. D., Connor, K. M., The alternative complement pathway regulates pathological angiogenesis in the retina. FASEB J., 28 (2014): 3171-3182.
[294] Holers, V. M., Rohrer, B., Tomlinson, S., CR2-mediated targeting of complement inhibitors: bench-to-bedside using a novel strategy for site-specific complement modulation. Adv. Exp. Med. Biol., 735 (2013): 137-154.
[295] Rohrer, B., Coughlin, B., Bandyopadhyay, M., Holers, V. M., Systemic human CR2-targeted complement alternative pathway inhibitor ameliorates mouse laser-induced choroidal neovascularization. J. Ocul. Pharmacol. Ther., 28 (2012): 402-409.
[296] Weismann, D., Binder, C. J., The innate immune response to products of phospholipid peroxidation. Biochim. Biophys. Acta, 1818 (2012): 2465-2475.
[297] Weismann, D., Hartvigsen, K., Lauer, N., Bennett, K. L., Scholl, H. P., Charbel Issa, P., Cano, M., Brandstatter, H., Tsimikas, S., Skerka, C., Superti-Furga, G., Handa, J. T., Zipfel, P. F., Witztum, J. L., Binder, C. J., Complement factor H binds malondialdehyde epitopes and protects from oxidative stress. Nature, 478 (2011): 76-81.
[298] Sun, S., Liang, N., Piao, H., Yamamoto, H., Kawashima, Y., Cui, F., Insulin-S.O (sodium oleate) complex-loaded PLGA nanoparticles: formulation, characterization and in vivo evaluation. J. Microencapsul., 27 (2010): 471-478.
[299] Reitz, C., Kleinebudde, P., Solid lipid extrusion of sustained release dosage forms. Eur. J. Pharm. Biopharm., 67 (2007): 440-448.
[300] Liang, R., Zhang, R., Li, X., Wang, A., Chen, D., Sun, K., Liu, W., Li, Y., Stability of exenatide in poly(D,L-lactide-co-glycolide) solutions: a simplified investigation on the peptide degradation by the polymer. Eur. J. Pharm. Sci., 50 (2013): 502-510.
[301] Ahn, J. H., Park, E. J., Lee, H. S., Lee, K. C., Na, D. H., Reversible blocking of amino groups of octreotide for the inhibition of formation of acylated peptide impurities in poly(lactide-co-glycolide) delivery systems. AAPS PharmSciTech, 12 (2011): 1220-1226.

[302] Sutter, M., Siepmann, J., Hennink, W. E., Jiskoot, W., Recombinant gelatin hydrogels for the sustained release of proteins. J. Control. Release, 119 (2007): 301-312.
[303] Teoli, D., Parisi, L., Realdon, N., Guglielmi, M., Rosato, A., Morpurgo, M., Wet sol-gel derived silica for controlled release of proteins. J. Control. Release, 116 (2006): 295-303.
[304] Determan, A. S., Wilson, J. H., Kipper, M. J., Wannemuehler, M. J., Narasimhan, B., Protein stability in the presence of polymer degradation products: consequences for controlled release formulations. Biomaterials, 27 (2006): 3312-3320.
[305] Namur, J. A., Takata, C. S., Moro, A. M., Politi, M. J., De Araujo, P. S., Cuccovia, I. M., Da Costa, M. H., Lactic acid triggers, in vitro, thiomersal to degrade protein in the presence of PLGA microspheres. Int. J. Pharm., 273 (2004): 1-8.
[306] van de Weert, M., van Steenbergen, M. J., Cleland, J. L., Heller, J., Hennink, W. E., Crommelin, D. J., Semisolid, self-catalyzed poly(ortho ester)s as controlled-release systems: protein release and protein stability issues. J. Pharm. Sci., 91 (2002): 1065-1074.
[307] Hu, J., Hou, Y., Park, H., Lee, M., Beta-tricalcium phosphate particles as a controlled release carrier of osteogenic proteins for bone tissue engineering. J. Biomed. Mater. Res. A, 100 (2012): 1680-1686.
[308] She, Z., Wang, C., Li, J., Sukhorukov, G. B., Antipina, M. N., Encapsulation of basic fibroblast growth factor by polyelectrolyte multilayer microcapsules and its controlled release for enhancing cell proliferation. Biomacromolecules, 13 (2012): 2174-2180.
[309] Jun, S. H., Lee, E. J., Kim, H. E., Jang, J. H., Koh, Y. H., Silica-chitosan hybrid coating on Ti for controlled release of growth factors. J. Mater. Sci. Mater. Med., 22 (2011): 2757-2764.
[310] Chan, O. C., So, K. F., Chan, B. P., Fabrication of nano-fibrous collagen microspheres for protein delivery and effects of photochemical crosslinking on release kinetics. J. Control. Release, 129 (2008): 135-143.
[311] Cui, F., Shi, K., Zhang, L., Tao, A., Kawashima, Y., Biodegradable nanoparticles loaded with insulin-phospholipid complex for oral delivery: preparation, in vitro characterization and in vivo evaluation. J. Control. Release, 114 (2006): 242-250.
[312] Sohier, J., Haan, R. E., de Groot, K., Bezemer, J. M., A novel method to obtain protein release from porous polymer scaffolds: emulsion coating. J. Control. Release, 87 (2003): 57-68.
[313] Ye, Q., Asherman, J., Stevenson, M., Brownson, E., Katre, N. V., DepoFoam technology: a vehicle for controlled delivery of protein and peptide drugs. J. Control. Release, 64 (2000): 155-166.
[314] Ahamed, T., Nfor, B. K., Verhaert, P. D., van Dedem, G. W., van der Wielen, L. A., Eppink, M. H., van de Sandt, E. J., Ottens, M., pH-gradient ion-exchange chromatography: an analytical tool for design and optimization of protein separations. J. Chromatogr. A, 1164 (2007): 181-188.
[315] Chumsae, C., Gaza-Bulseco, G., Sun, J., Liu, H., Comparison of methionine oxidation in thermal stability and chemically stressed samples of a fully human monoclonal antibody. J. Chromatogr. B Analyt. Technol. Biomed. Life Sci., 850 (2007): 285-294.
[316] Du, Y., Walsh, A., Ehrick, R., Xu, W., May, K., Liu, H., Chromatographic analysis of the acidic and basic species of recombinant monoclonal antibodies. MAbs, 4 (2012): 578-585.
[317] Fekete, S., Beck, A., Fekete, J., Guillarme, D., Method development for the separation of monoclonal antibody charge variants in cation exchange chromatography, Part I: salt gradient approach. J. Pharm. Biomed. Anal., 102 (2015): 33-44.
[318] Fekete, S., Beck, A., Fekete, J., Guillarme, D., Method development for the separation of monoclonal antibody charge variants in cation exchange chromatography, Part II: pH gradient approach. J Pharm Biomed Anal, 102 (2015): 282-289.
[319] Fekete, S., Beck, A., Veuthey, J. L., Guillarme, D., Ion-exchange chromatography for the characterization of biopharmaceuticals. J. Pharm. Biomed. Anal., 113 (2015): 43-55.
[320] Khawli, L. A., Goswami, S., Hutchinson, R., Kwong, Z. W., Yang, J., Wang, X., Yao, Z., Sreedhara, A., Cano, T., Tesar, D., Nijem, I., Allison, D. E., Wong, P. Y., Kao, Y. H., Quan, C., Joshi, A., Harris, R. J., Motchnik, P., Charge variants in IgG1: Isolation, characterization, in vitro binding properties and pharmacokinetics in rats. MAbs, 2 (2010): 613-624.

[321] Ljunglof, A., Lacki, K. M., Mueller, J., Harinarayan, C., van Reis, R., Fahrner, R., Van Alstine, J. M., Ion exchange chromatography of antibody fragments. Biotechnol. Bioeng., 96 (2007): 515-524.
[322] Rea, J. C., Moreno, G. T., Lou, Y., Farnan, D., Validation of a pH gradient-based ion-exchange chromatography method for high-resolution monoclonal antibody charge variant separations. J. Pharm. Biomed. Anal., 54 (2011): 317-323.
[323] Talebi, M., Nordborg, A., Gaspar, A., Lacher, N. A., Wang, Q., He, X. Z., Haddad, P. R., Hilder, E. F., Charge heterogeneity profiling of monoclonal antibodies using low ionic strength ion-exchange chromatography and well-controlled pH gradients on monolithic columns. J. Chromatogr. A, 1317 (2013): 148-154.
[324] Teshima, G., Li, M. X., Danishmand, R., Obi, C., To, R., Huang, C., Kung, J., Lahidji, V., Freeberg, J., Thorner, L., Tomic, M., Separation of oxidized variants of a monoclonal antibody by anion-exchange. J. Chromatogr. A, 1218 (2011): 2091-2097.
[325] Weisbjerg, P. L., Caspersen, M. B., Cook, K., Van De Weert, M., Serial coupling of ion-exchange and size-exclusion chromatography to determine aggregation levels in mAbs in the presence of a proteinaceous excipient, recombinant human serum albumin. J. Pharm. Sci., 104 (2015): 548-556.
[326] Zhang, T., Bourret, J., Cano, T., Isolation and characterization of therapeutic antibody charge variants using cation exchange displacement chromatography. J. Chromatogr. A, 1218 (2011): 5079-5086.
[327] Zhang, L., Patapoff, T., Farnan, D., Zhang, B., Improving pH gradient cation-exchange chromatography of monoclonal antibodies by controlling ionic strength. J. Chromatogr. A, 1272 (2013): 56-64.
[328] Zheng, J. Y., Janis, L. J., Influence of pH, buffer species, and storage temperature on physicochemical stability of a humanized monoclonal antibody LA298. Int. J. Pharm., 308 (2006): 46-51.
[329] Boschetti, E., Antibody separation by hydrophobic charge induction chromatography. Trends Biotechnol., 20 (2002): 333-337.
[330] Boyd, D., Kaschak, T., Yan, B., HIC resolution of an IgG1 with an oxidized Trp in a complementarity determining region. J. Chromatogr. B Analyt. Technol. Biomed. Life Sci., 879 (2011): 955-960.
[331] Haverick, M., Mengisen, S., Shameem, M., Ambrogelly, A., Separation of mAbs molecular variants by analytical hydrophobic interaction chromatography HPLC: overview and applications. MAbs, 6 (2014): 852-858.
[332] Lienqueo, M. E., Mahn, A., Salgado, J. C., Asenjo, J. A., Current insights on protein behaviour in hydrophobic interaction chromatography. J. Chromatogr. B Analyt. Technol. Biomed. Life Sci., 849 (2007): 53-68.
[333] Queiroz, J. A., Tomaz, C. T., Cabral, J. M., Hydrophobic interaction chromatography of proteins. J. Biotechnol., 87 (2001): 143-159.
[334] Valliere-Douglass, J., Jones, L., Shpektor, D., Kodama, P., Wallace, A., Balland, A., Bailey, R., Zhang, Y., Separation and characterization of an IgG2 antibody containing a cyclic imide in CDR1 of light chain by hydrophobic interaction chromatography and mass spectrometry. Anal. Chem., 80 (2008): 3168-3174.
[335] Valliere-Douglass, J., Wallace, A., Balland, A., Separation of populations of antibody variants by fine tuning of hydrophobic-interaction chromatography operating conditions. J. Chromatogr. A, 1214 (2008): 81-89.
[336] Valliere-Douglass, J. F., Brady, L. J., Farnsworth, C., Pace, D., Balland, A., Wallace, A., Wang, W., Treuheit, M. J., Yan, B., O-fucosylation of an antibody light chain: characterization of a modification occurring on an IgG1 molecule. Glycobiology, 19 (2009): 144-152.
[337] Reubsaet, J. L., Beijnen, J. H., Bult, A., van Maanen, R. J., Marchal, J. A., Underberg, W. J., Analytical techniques used to study the degradation of proteins and peptides: chemical instability. J. Pharm. Biomed. Anal., 17 (1998): 955-978.
[338] Barth, A., Infrared spectroscopy of proteins. Biochim. Biophys. Acta, 1767 (2007): 1073-1101.

[339] Jackson, M., Mantsch, H. H., The use and misuse of FTIR spectroscopy in the determination of protein structure. Crit. Rev. Biochem. Mol. Biol., 30 (1995): 95-120.
[340] Kong, J., Yu, S., Fourier transform infrared spectroscopic analysis of protein secondary structures. Acta Biochim Biophys Sin (Shanghai), 39 (2007): 549-559.
[341] Matheus, S., Friess, W., Mahler, H. C., FTIR and nDSC as analytical tools for high-concentration protein formulations. Pharm. Res., 23 (2006): 1350-1363.
[342] Pribic, R., van Stokkum, I. H., Chapman, D., Haris, P. I., Bloemendal, M., Protein secondary structure from Fourier transform infrared and/or circular dichroism spectra. Anal. Biochem., 214 (1993): 366-378.
[343] Yang, H., Yang, S., Kong, J., Dong, A., Yu, S., Obtaining information about protein secondary structures in aqueous solution using Fourier transform IR spectroscopy. Nat. Protoc., 10 (2015): 382-396.
[344] Pelton, J. T., McLean, L. R., Spectroscopic methods for analysis of protein secondary structure. Anal. Biochem., 277 (2000): 167-176.
[345] Uchida, T., Yagi, A., Oda, Y., Nakada, Y., Goto, S., Instability of bovine insulin in poly(lactide-co-glycolide) (PLGA) microspheres. Chemical & pharmaceutical bulletin, 44 (1996): 235-236.
[346] Welfle, K., Misselwitz, R., Hausdorf, G., Hohne, W., Welfle, H., Conformation, pH-induced conformational changes, and thermal unfolding of anti-p24 (HIV-1) monoclonal antibody CB4-1 and its Fab and Fc fragments. Biochim. Biophys. Acta, 1431 (1999): 120-131.
[347] Luo, Q., Joubert, M. K., Stevenson, R., Ketchem, R. R., Narhi, L. O., Wypych, J., Chemical modifications in therapeutic protein aggregates generated under different stress conditions. J. Biol. Chem., 286 (2011): 25134-25144.
[348] Roberts, C. J., Nesta, D. P., Kim, N., Effects of temperature and osmolytes on competing degradation routes for an IgG1 antibody. J. Pharm. Sci., 102 (2013): 3556-3566.
[349] Singla, A., Bansal, R., Joshi, V., Rathore, A. S., Aggregation Kinetics for IgG1-Based Monoclonal Antibody Therapeutics. AAPS J, 18 (2016): 689-702.
[350] Vermeer, A. W., Norde, W., The thermal stability of immunoglobulin: unfolding and aggregation of a multi-domain protein. Biophys. J., 78 (2000): 394-404.
[351] Zhang, A., Singh, S. K., Shirts, M. R., Kumar, S., Fernandez, E. J., Distinct aggregation mechanisms of monoclonal antibody under thermal and freeze-thaw stresses revealed by hydrogen exchange. Pharm. Res., 29 (2012): 236-250.
[352] Pali, T., Kota, Z., Studying lipid-protein interactions with electron paramagnetic resonance spectroscopy of spin-labeled lipids. Methods Mol. Biol., 974 (2013): 297-328.
[353] Peng, T., Yuan, X., Hang, H. C., Turning the spotlight on protein-lipid interactions in cells. Curr. Opin. Chem. Biol., 21 (2014): 144-153.
[354] Guler, G., Gartner, R. M., Ziegler, C., Mantele, W., Lipid-Protein Interactions in the Regulated Betaine Symporter BetP Probed by Infrared Spectroscopy. J. Biol. Chem., 291 (2016): 4295-4307.
[355] Baylon, J. L., Vermaas, J. V., Muller, M. P., Arcario, M. J., Pogorelov, T. V., Tajkhorshid, E., Atomic-level description of protein-lipid interactions using an accelerated membrane model. Biochim. Biophys. Acta, 1858 (2016): 1573-1583.
[356] Contreras, F. X., Ernst, A. M., Wieland, F., Brugger, B., Specificity of intramembrane protein-lipid interactions. Cold Spring Harb. Perspect. Biol., 3 (2011).
[357] Glatz, J. F., Lipids and lipid binding proteins: a perfect match. Prostaglandins Leukot. Essent. Fatty Acids, 93 (2015): 45-49.
[358] Saliba, A. E., Vonkova, I., Gavin, A. C., The systematic analysis of protein-lipid interactions comes of age. Nat. Rev. Mol. Cell Biol., 16 (2015): 753-761.
[359] Raguz, M., Mainali, L., O'Brien, W. J., Subczynski, W. K., Lipid-protein interactions in plasma membranes of fiber cells isolated from the human eye lens. Exp. Eye Res., 120 (2014): 138-151.
[360] Saita, E. A., de Mendoza, D., Thermosensing via transmembrane protein-lipid interactions. Biochim. Biophys. Acta, 1848 (2015): 1757-1764.
[361] Gilbert, R. J., Protein-lipid interactions and non-lamellar lipidic structures in membrane pore formation and membrane fusion. Biochim. Biophys. Acta, 1858 (2016): 487-499.

[362] Martfeld, A. N., Rajagopalan, V., Greathouse, D. V., Koeppe, R. E., 2nd, Dynamic regulation of lipid-protein interactions. Biochim. Biophys. Acta, 1848 (2015): 1849-1859.
[363] Vorobyov, I., Allen, T. W., On the role of anionic lipids in charged protein interactions with membranes. Biochim. Biophys. Acta, 1808 (2011): 1673-1683.
[364] Hite, R. K., Li, Z., Walz, T., Principles of membrane protein interactions with annular lipids deduced from aquaporin-0 2D crystals. EMBO J., 29 (2010): 1652-1658.
[365] Battle, A. R., Ridone, P., Bavi, N., Nakayama, Y., Nikolaev, Y. A., Martinac, B., Lipid-protein interactions: Lessons learned from stress. Biochim. Biophys. Acta, 1848 (2015): 1744-1756.
[366] Temmerman, K., Nickel, W., A novel flow cytometric assay to quantify interactions between proteins and membrane lipids. J. Lipid Res., 50 (2009): 1245-1254.
[367] Vitrac, H., Bogdanov, M., Heacock, P., Dowhan, W., Lipids and topological rules of membrane protein assembly: balance between long and short range lipid-protein interactions. J. Biol. Chem., 286 (2011): 15182-15194.
[368] Lee, A. G., Lipid-protein interactions. Biochem. Soc. Trans., 39 (2011): 761-766.
[369] Rodrigues, L., Kyriakos, K., Schneider, F., Dietz, H., Winter, G., Papadakis, C. M., Hubert, M., Characterization of Lipid-Based Hexosomes as Versatile Vaccine Carriers. Mol. Pharm., (2016).
[370] Fahy, E., Subramaniam, S., Murphy, R. C., Nishijima, M., Raetz, C. R., Shimizu, T., Spener, F., van Meer, G., Wakelam, M. J., Dennis, E. A., Update of the LIPID MAPS comprehensive classification system for lipids. J. Lipid Res., 50 Suppl (2009): S9-14.
[371] Stratton, A., Ericksen, M., Harris, T. V., Symmonds, N., Silverstein, T. P., Mercury(II) binds to both of chymotrypsin's histidines, causing inhibition followed by irreversible denaturation/aggregation. Protein Sci., (2016).
[372] Tamas, M. J., Sharma, S. K., Ibstedt, S., Jacobson, T., Christen, P., Heavy metals and metalloids as a cause for protein misfolding and aggregation. Biomolecules, 4 (2014): 252-267.
[373] Uversky, V. N., Li, J., Fink, A. L., Metal-triggered structural transformations, aggregation, and fibrillation of human alpha-synuclein. A possible molecular NK between Parkinson's disease and heavy metal exposure. J. Biol. Chem., 276 (2001): 44284-44296.
[374] Agrawal, N. J., Kumar, S., Wang, X., Helk, B., Singh, S. K., Trout, B. L., Aggregation in protein-based biotherapeutics: computational studies and tools to identify aggregation-prone regions. J. Pharm. Sci., 100 (2011): 5081-5095.
[375] Arosio, P., Rima, S., Morbidelli, M., Aggregation mechanism of an IgG2 and two IgG1 monoclonal antibodies at low pH: from oligomers to larger aggregates. Pharm. Res., 30 (2013): 641-654.
[376] Brummitt, R. K., Nesta, D. P., Chang, L., Kroetsch, A. M., Roberts, C. J., Nonnative aggregation of an IgG1 antibody in acidic conditions, part 2: nucleation and growth kinetics with competing growth mechanisms. J. Pharm. Sci., 100 (2011): 2104-2119.
[377] Brummitt, R. K., Nesta, D. P., Roberts, C. J., Predicting accelerated aggregation rates for monoclonal antibody formulations, and challenges for low-temperature predictions. J. Pharm. Sci., 100 (2011): 4234-4243.
[378] Gabrielson, J. P., Brader, M. L., Pekar, A. H., Mathis, K. B., Winter, G., Carpenter, J. F., Randolph, T. W., Quantitation of aggregate levels in a recombinant humanized monoclonal antibody formulation by size-exclusion chromatography, asymmetrical flow field flow fractionation, and sedimentation velocity. J. Pharm. Sci., 96 (2007): 268-279.
[379] Joubert, M. K., Luo, Q., Nashed-Samuel, Y., Wypych, J., Narhi, L. O., Classification and characterization of therapeutic antibody aggregates. J. Biol. Chem., 286 (2011): 25118-25133.
[380] Kayser, V., Chennamsetty, N., Voynov, V., Helk, B., Trout, B. L., Conformational stability and aggregation of therapeutic monoclonal antibodies studied with ANS and Thioflavin T binding. MAbs, 3 (2011): 408-411.
[381] Kiese, S., Papppenberger, A., Friess, W., Mahler, H. C., Shaken, not stirred: mechanical stress testing of an IgG1 antibody. J. Pharm. Sci., 97 (2008): 4347-4366.
[382] Mahler, H. C., Friess, W., Grauschopf, U., Kiese, S., Protein aggregation: pathways, induction factors and analysis. J. Pharm. Sci., 98 (2009): 2909-2934.

[383] Obrezanova, O., Arnell, A., de la Cuesta, R. G., Berthelot, M. E., Gallagher, T. R., Zurdo, J., Stallwood, Y., Aggregation risk prediction for antibodies and its application to biotherapeutic development. MAbs, 7 (2015): 352-363.
[384] Roberts, C. J., Non-native protein aggregation kinetics. Biotechnol. Bioeng., 98 (2007): 927-938.
[385] Wang, W., Protein aggregation and its inhibition in biopharmaceutics. Int. J. Pharm., 289 (2005): 1-30.
[386] Wang, W., Nema, S., Teagarden, D., Protein aggregation--pathways and influencing factors. Int. J. Pharm., 390 (2010): 89-99.
[387] Kapp, S. J., Larsson, I., Van De Weert, M., Cardenas, M., Jorgensen, L., Competitive adsorption of monoclonal antibodies and nonionic surfactants at solid hydrophobic surfaces. J. Pharm. Sci., 104 (2015): 593-601.
[388] Roque, C., Sheung, A., Rahman, N., Ausar, S. F., Effect of polyethylene glycol conjugation on conformational and colloidal stability of a monoclonal antibody antigen-binding fragment (Fab'). Mol. Pharm., 12 (2015): 562-575.
[389] Sharov, V. S., Pal, R., Dremina, E. S., Michaelis, E. K., Schoneich, C., Fluorogenic tagging of protein 3-nitrotyrosine with 4-(aminomethyl)benzene sulfonate in tissues: a useful alternative to Immunohistochemistry for fluorescence microscopy imaging of protein nitration. Free Radic. Biol. Med., 53 (2012): 1877-1885.
[390] Zhou, S., Mozziconacci, O., Kerwin, B. A., Schoneich, C., Fluorogenic tagging methodology applied to characterize oxidized tyrosine and phenylalanine in an immunoglobulin monoclonal antibody. Pharm. Res., 30 (2013): 1311-1327.
[391] Kryndushkin, D., Rao, V. A., Comparative Effects of Metal-Catalyzed Oxidizing Systems on Carbonylation and Integrity of Therapeutic Proteins. Pharm. Res., 33 (2016): 526-539.
[392] Tanaka, Y., Tsumoto, K., Nakanishi, T., Yasutake, Y., Sakai, N., Yao, M., Tanaka, I., Kumagai, I., Structural implications for heavy metal-induced reversible assembly and aggregation of a protein: the case of Pyrococcus horikoshii CutA. FEBS Lett., 556 (2004): 167-174.
[393] Ryu, J., Girigoswami, K., Ha, C., Ku, S. H., Park, C. B., Influence of multiple metal ions on beta-amyloid aggregation and dissociation on a solid surface. Biochemistry, 47 (2008): 5328-5335.
[394] Giese, A., Levin, J., Bertsch, U., Kretzschmar, H., Effect of metal ions on de novo aggregation of full-length prion protein. Biochem. Biophys. Res. Commun., 320 (2004): 1240-1246.
[395] Hu, D., Qin, Z., Xue, B., Fink, A. L., Uversky, V. N., Effect of methionine oxidation on the structural properties, conformational stability, and aggregation of immunoglobulin light chain LEN. Biochemistry, 47 (2008): 8665-8677.
[396] Su, J. G., Zhang, X., Han, X. M., Zhao, S. X., Li, C. H., The Intrinsic Dynamics and Unfolding Process of an Antibody Fab Fragment Revealed by Elastic Network Model. Int. J. Mol. Sci., 16 (2015): 29720-29731.
[397] Broom, A., Gosavi, S., Meiering, E. M., Protein unfolding rates correlate as strongly as folding rates with native structure. Protein Sci., 24 (2015): 580-587.
[398] Saluja, A., Sadineni, V., Mungikar, A., Nashine, V., Kroetsch, A., Dahlheim, C., Rao, V. M., Significance of unfolding thermodynamics for predicting aggregation kinetics: a case study on high concentration solutions of a multi-domain protein. Pharm. Res., 31 (2014): 1575-1587.
[399] McCully, M. E., Beck, D. A., Daggett, V., Multimolecule test-tube simulations of protein unfolding and aggregation. Proc. Natl. Acad. Sci. U. S. A., 109 (2012): 17851-17856.
[400] Brader, M. L., Estey, T., Bai, S., Alston, R. W., Lucas, K. K., Lantz, S., Landsman, P., Maloney, K. M., Examination of thermal unfolding and aggregation profiles of a series of developable therapeutic monoclonal antibodies. Mol. Pharm., 12 (2015): 1005-1017.
[401] Menzen, T.,Temperature-Induced Unfolding, Aggregation, and Interaction of Therapeutic Monoclonal Antibodies. Ludwig-Maximilians-University Munich, 2014.
[402] Sahin, E., Grillo, A. O., Perkins, M. D., Roberts, C. J., Comparative effects of pH and ionic strength on protein-protein interactions, unfolding, and aggregation for IgG1 antibodies. J. Pharm. Sci., 99 (2010): 4830-4848.

[403] Cirkovas, A., Sereikaite, J., Different effects of (L)-arginine on the heat-induced unfolding and aggregation of proteins. Biologicals, 39 (2011): 181-188.
[404] Kundu, S., Fenters, C., Isoelectric focusing of monoclonal antibodies by capillary electrophoresis. J. Capillary Electrophor., 2 (1995): 273-277.
[405] Kamoda, S., Kakehi, K., Evaluation of glycosylation for quality assurance of antibody pharmaceuticals by capillary electrophoresis. Electrophoresis, 29 (2008): 3595-3604.
[406] Shimura, K., Recent advances in IEF in capillary tubes and microchips. Electrophoresis, 30 (2009): 11-28.
[407] Silvertand, L. H., Torano, J. S., van Bennekom, W. P., de Jong, G. J., Recent developments in capillary isoelectric focusing. J. Chromatogr. A, 1204 (2008): 157-170.
[408] Wu, J., Wu, X. Z., Huang, T., Pawliszyn, J., Analysis of proteins by CE, CIEF, and microfluidic devices with whole-column-imaging detection. Methods Mol. Biol., 276 (2004): 229-252.
[409] Requena, J. R., Fu, M. X., Ahmed, M. U., Jenkins, A. J., Lyons, T. J., Thorpe, S. R., Lipoxidation products as biomarkers of oxidative damage to proteins during lipid peroxidation reactions. Nephrol. Dial. Transplant., 11 Suppl 5 (1996): 48-53.
[410] Negre-Salvayre, A., Coatrieux, C., Ingueneau, C., Salvayre, R., Advanced lipid peroxidation end products in oxidative damage to proteins. Potential role in diseases and therapeutic prospects for the inhibitors. Br. J. Pharmacol., 153 (2008): 6-20.
[411] Baynes, J. W., Thorpe, S. R., Glycoxidation and lipoxidation in atherogenesis. Free Radic. Biol. Med., 28 (2000): 1708-1716.
[412] Wills, E. D., Effect of unsaturated fatty acids and their peroxides on enzymes. Biochem. Pharmacol., 7 (1961): 7-16.
[413] Bhattacharya, M., Jain, N., Bhasne, K., Kumari, V., Mukhopadhyay, S., pH-Induced conformational isomerization of bovine serum albumin studied by extrinsic and intrinsic protein fluorescence. J Fluoresc, 21 (2011): 1083-1090.
[414] Koh, M., Lee, H., Lee, Y., Lee, M., Characterization of early-stage amyloid aggregates by incorporating extrinsic fluorescence and atomic force microscopy. J Nanosci Nanotechnol, 14 (2014): 8386-8389.
[415] Hawe, A., Sutter, M., Jiskoot, W., Extrinsic fluorescent dyes as tools for protein characterization. Pharm. Res., 25 (2008): 1487-1499.
[416] Schonbrunn, E., Eschenburg, S., Luger, K., Kabsch, W., Amrhein, N., Structural basis for the interaction of the fluorescence probe 8-anilino-1-naphthalene sulfonate (ANS) with the antibiotic target MurA. Proc. Natl. Acad. Sci. U. S. A., 97 (2000): 6345-6349.
[417] Jain, N., Bhattacharya, M., Mukhopadhyay, S., Kinetics of surfactant-induced aggregation of lysozyme studied by fluorescence spectroscopy. J Fluoresc, 21 (2011): 615-625.
[418] Santiago, P. S., Carvalho, F. A., Domingues, M. M., Carvalho, J. W., Santos, N. C., Tabak, M., Isoelectric point determination for Glossoscolex paulistus extracellular hemoglobin: oligomeric stability in acidic pH and relevance to protein-surfactant interactions. Langmuir, 26 (2010): 9794-9801.
[419] Kidman, G., Park, H., Northrop, D. B., Pressure stability of proteins at their isoelectric points. Protein Pept Lett, 11 (2004): 543-546.
[420] Talley, K., Alexov, E., On the pH-optimum of activity and stability of proteins. Proteins, 78 (2010): 2699-2706.
[421] Glomm, W. R., Halskau, O., Jr., Hanneseth, A. M., Volden, S., Adsorption behavior of acidic and basic proteins onto citrate-coated Au surfaces correlated to their native fold, stability, and pI. J. Phys. Chem. B, 111 (2007): 14329-14345.
[422] Hirvonen, L. M., Fruhwirth, G. O., Srikantha, N., Barber, M. J., Neffendorf, J. E., Suhling, K., Jackson, T. L., Hydrodynamic Radii of Ranibizumab, Aflibercept and Bevacizumab Measured by Time-Resolved Phosphorescence Anisotropy. Pharm. Res., 33 (2016): 2025-2032.
[423] Repka, M. A., Majumdar, S., Kumar Battu, S., Srirangam, R., Upadhye, S. B., Applications of hot-melt extrusion for drug delivery. Expert Opin Drug Deliv, 5 (2008): 1357-1376.

[424] Crowley, M. M., Zhang, F., Repka, M. A., Thumma, S., Upadhye, S. B., Battu, S. K., McGinity, J. W., Martin, C., Pharmaceutical applications of hot-melt extrusion: part I. Drug Dev. Ind. Pharm., 33 (2007): 909-926.
[425] Becker, K., Salar-Behzadi, S., Zimmer, A., Solvent-free melting techniques for the preparation of lipid-based solid oral formulations. Pharm. Res., 32 (2015): 1519-1545.
[426] Martin, C., Twin Screw Extruders as Continuous Mixers for Thermal Processing: a Technical and Historical Perspective. AAPS PharmSciTech, 17 (2016): 3-19.
[427] Lang, B., McGinity, J. W., Williams, R. O., 3rd, Hot-melt extrusion--basic principles and pharmaceutical applications. Drug Dev. Ind. Pharm., 40 (2014): 1133-1155.
[428] Alshahrani, S. M., Morott, J. T., Alshetaili, A. S., Tiwari, R. V., Majumdar, S., Repka, M. A., Influence of degassing on hot-melt extrusion process. Eur. J. Pharm. Sci., 80 (2015): 43-52.
[429] Repka, M. A., Battu, S. K., Upadhye, S. B., Thumma, S., Crowley, M. M., Zhang, F., Martin, C., McGinity, J. W., Pharmaceutical applications of hot-melt extrusion: Part II. Drug Dev. Ind. Pharm., 33 (2007): 1043-1057.
[430] Guse, C., Koennings, S., Blunk, T., Siepmann, J., Goepferich, A., Programmable implants--from pulsatile to controlled release. Int. J. Pharm., 314 (2006): 161-169.
[431] Sprengholz, M.,Industrial Ram Extrusion as Innovative Tool for the Developement of Biodegradable Sustained Release Implants. Ludwig-Maximilians-University Munich, 2014.